UNIVERSITÀ DEGLI STUDI
DI MODENA E REGGIO EMILIA

Dottorato di ricerca in Ingegneria Industriale e del Territorio/Industrial and Environmental Engineering

Ciclo XXXVI

SYNTHESIS OF GEOPOLYMERS WITH INDUSTRIAL WASTE, CHEMICAL AND MICROSTRUCTURAL CHARACTERIZATION

SINTESI DI GEOPOLIMERI CON SCARTI INDUSTRIALI,
CARATTERIZZAZIONE CHIMICA E MICROSTRUTTURALE

Candidato: Giovanni Dal Poggetto

Relatore (Tutor): Prof.ssa Cristina Leonelli

Correlatore (Co-Tutor): Prof.ssa Luisa Barbieri

Coordinatore del Corso di Dottorato: Prof. Alberto Muscio

Synthesis of Geopolymers with industrial waste, Chemical and Microstructural characterization

Abstract

This thesis project explores the innovative field of reusing industrial waste within a geopolymeric matrix. The research work begins with a thorough characterization of these waste powders, followed by an investigation to identify the optimal composition of metakaolin-based geopolymer. The incorporation of waste into geopolymers is a gradual process, as evidenced in the first part of the thesis, which characterizes post-abrasion corundum powders, post-erosion corundum, and waste cork. The comprehensive characterization underlines the potential harmlessness of these powders in the preparation of materials with future applications in construction. Through a series of tests on geopolymers with industrial waste, particular emphasis is placed on discerning the effects of incorporating these materials both before and after the alkaline activation of metakaolin. The exploration culminates in the evaluation of samples exposed to different acids, understanding their chemical properties for potential use in drainage systems, sewerage pipes, and as reinforcements in structures exposed to the corrosive effects of acid rains.

Sintesi di geopolimeri con scarti industriali, caratterizzazione chimica e microstrutturale

Riassunto

Questo progetto di tesi si concentra sull'innovativo campo del riutilizzo dei rifiuti industriali all'interno di una matrice geopolimerica. La ricerca inizia con una dettagliata caratterizzazione delle polveri di scarto, seguita da un'indagine per individuare la migliore composizione di geopolimero composto solo da metacaolino. L'incorporazione dei rifiuti nei geopolimeri è un processo graduale, come evidenziato nella prima parte della tesi, che coinvolge polveri di corindone post-abrasione, corindone post-erosione e sughero di scarto. La caratterizzazione chimica ha mostrato la non pericolosità nell'utilizzare tali polveri nella produzione di materiali destinati a future applicazioni nell'edilizia. Attraverso una serie di test sui geopolimeri contenenti rifiuti, viene posta particolare enfasi nella comprensione degli effetti dell'incorporazione di tali materiali sia prima che dopo l'attivazione alcalina del metacaolino. Infine, con la valutazione dei campioni esposti a diversi tipi di acidi si sono meglio comprese le loro proprietà chimiche per un potenziale impiego in sistemi di drenaggio, tubature fognarie e come rinforzi nelle strutture esposte agli effetti corrosivi delle piogge acide.

List of Abbreviations

OPC	Ordinary Portland Cement
GP	Geopolymer
MK	Metakaolin
M	Molarity
N	Normality
wt%	Weight percentage
RC	Recycled Corundum
CW	Waste Cork
AA	Alkali Activation
EDXRF	Energy Dispersive X-Ray Fluorescence
ICP-OES	Inductively Coupled Plasma Optical Emission Spectrometry
ICP-MS	Inductively Coupled Plasma-Mass Spectrometry
XRD	X-ray Diffraction
FTIR	Fourier Transform Infrared Spectroscopy
SEM	Scanning Electron Micrograph
EDS	Energy Dispersive X-ray Spectroscopy
MAS-NMR	Solid-State Magic Angle Spinning Nuclear Magnetic Resonance Spectroscopy
TGA/DTA	Differential Thermal Analysis-Thermo-Gravimetry
MPa	Mega Pascal
°C	Degree Centigrade

1. Introduction

1.1 Motivation

In the face of rapid industrialization and escalating environmental concerns, the quest for sustainable construction materials has intensified. Traditional cement production, a major contributor to greenhouse gas emissions, necessitates the exploration of alternative eco-friendly solutions. Geopolymer technology, heralded as a promising eco-friendly substitute for conventional Portland cement, has emerged as a beacon of sustainable construction practices. Geopolymers, synthesized through the alkali activation of aluminosilicate materials, offer several advantages over traditional cement. They exhibit lower carbon footprint, enhanced durability, and excellent mechanical properties, making them an ideal choice for sustainable construction. The innovative use of waste materials in geopolymer production not only addresses the challenge of waste management but also contributes significantly to the reduction of environmental impact associated with conventional construction practices.

As a novel binder, the performance of MK-based geopolymers is promising, especially in some aggressive situations where Portland cement concretes are vulnerable. An example is the case of acid attack as in sulphuric acid attack on sewer pipes.

1.2 Aim of the thesis

This thesis develops novel formulations of MK-based geopolymers, with a specific focus on their synthesis utilizing waste materials as recycled corundum and Waste cork. Subsequently, the thesis delves into the extensive research conducted to assess the performance of these geopolymers when exposed to various acid solutions. An examination of the microstructure of acid corroded geopolymers was undertaken, aiming to unravel the intricate processes through which these materials degrade in sulphuric, hydrochloric and nitric acid environments. This detailed analysis sheds light on the underlying mechanisms of geopolymer deterioration, providing insights into their behaviour under corrosive conditions.

Waste materials, often considered liabilities, can be transformed into valuable resources in the geopolymerization process, without affecting it. This thesis focuses on two specific waste materials; recycled

corundum, an inorganic material and waste cork, an organic natural material from the cork industry. The utilization of these wastes in geopolymer production not only repurposes waste but also enhances the material properties, making them suitable candidates for construction and fireproof applications.

Acid resistance is a critical parameter in assessing the durability of construction materials, particularly in environments where exposure to acidic substances is prevalent. In the final part of this thesis there is a special emphasis on evaluating the acid resistance of geopolymers incorporating recycled corundum and waste cork. Understanding the behaviour of these geopolymers under acidic conditions is essential for their practical application in real world scenario.

The primary objective of this research is to comprehensively investigate the synthesis process, mechanical properties and microstructural characteristics. The second goal is the investigation of acid resistance on geopolymers incorporating recycled corundum and waste cork.

Corundum, with its high hardness and abrasion resistance, can improve the mechanical properties of geopolymer matrices. This can result in improved strength, durability, and wear resistance.

Cork is known for its lightweight and insulating properties. When used in geopolymer matrices, it can impart these propertiess to the final material. The resulting geopolymer composite can have improved thermal insulation properties.

By addressing these key aspects, the study aims to contribute valuable insights to the field of sustainable construction materials, either if the dense form, as in the case of recycled corundum addition or in the lightweight composites panel, when waste cork is added. The findings of this research are expected to pave the way for the widespread adoption of geopolymers with waste materials, promoting environmental sustainability and fostering innovative approaches in the construction industry.

In the chapters that follow, this thesis will delve into the methodology, experimental results, and detailed analyses, providing a comprehensive understanding of the geopolymerization process using recycled corundum (RC) and waste cork (CW). Through this exploration, we endeavour to unravel the immense potential of these geopolymers, ushering in a new era of sustainable and durable construction materials.

Chapter 2 provides a detailed introduction on geopolymer science.

Chapter 3 is focused on the research plan and methodology/ experimental of this thesis project.

Chapter 4 provides a characterization of raw materials.

Chapter 5 concentrates on the choice of the best MK-based geopolymer formulation between three different processes.

Chapter 6 is divided in three big part and comprehensively examines the role of the recycled abrasive corundum powder added in the MK-based geopolymer matrix before and after the alkali activation. All the properties were thoroughly investigated by different techniques.

Chapter 7 concentrates on how the properties of the MK-based geopolymer change when corundum after erosion is added before and after the alkali activation.

Chapter 8 is focused on the MK-based geopolymer with the addition of the waste cork.

Chapter 9 is dedicated on the investigation on the change of the aluminosilicate structure and all the properties of the geopolymer with all waste material during acid exposure.

Chapter 10 shows the conlusions of this Ph.D. project and future applications.

2. Literature survey in geopolymer science

2.1 Definition and classification

In the 1970s, J. Davidovits, introduced the term "geopolymer" to describe a unique class of solid materials. These materials are created through a chemical reaction between an aluminosilicate powder and an alkaline solution [Davidovits, J. et al. 1995; Davidovits, J. et al 1982; Davidovits J. 2008]. The definition of geopolymer is still not well defined today. Geopolymer is a synthetic amorphous alkali aluminosilicate material, also known as alkali-activated aluminosilicates, low temperature aluminosilicate glass, alkali-activated cement, alkali-bonded ceramic, inorganic polymer concrete, or hydroceramic [Davidovits J. 2008.; Duxson et al. 2008.].

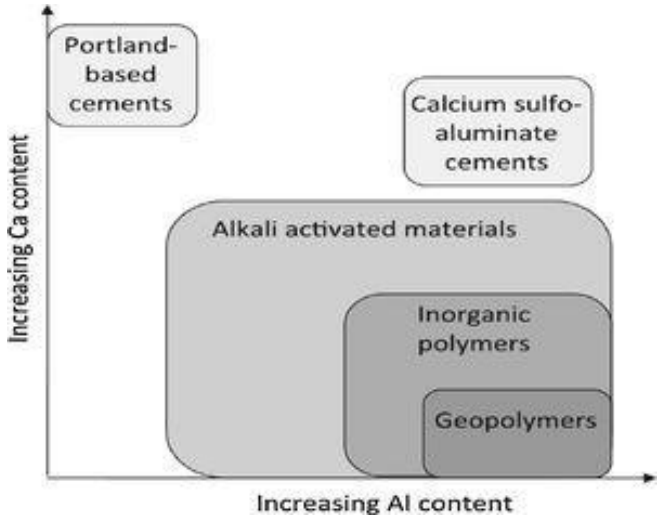

Fig.2-1 Classification of different subsets of alkali activated materials with comparisons to ordinary Portland cement OPC and calcium sulfoaluminate binder chemistry [van Deventer et al. 2010].

Geopolymer are produced through the activation of solid aluminosilicate sources using a highly concentrated alkaline solution at ambient temperatures [Davidovits, J. 2008]. Geopolymer chemical structure comprises amorphous to semicrystalline three-dimensional aluminosilicate tetrahedral networks.

Geopolymer and its chemistry have been much less explored, despite their enormous potential for the discovery and utilization of new aluminosilicate materials. Nevertheless, new advanced applications of geopolymer, including catalysis [Zhang et al. 2013.], drug delivery, and dye removal, have emerged. Given the significant importance of

aluminosilicate materials in modern science and technology, it is worth considering whether geopolymer-based aluminosilicates can be harnessed and tailored to exhibit nanostructures with useful functionalities for large-scale applications. The abundance of precursors and the facile synthetic conditions of geopolymer present great potential for its chemistry in synthesizing new nanostructured aluminosilicate materials. In this Ph.D. Thesis the term geopolymer is used to describe a solid material formed by the reaction of Metakaolin and NaOH + Na-silicate alkaline solutions.

2.2 Geopolymer starting materials

Geopolymer formulations have emerged as a promising alternative to traditional cement-based materials, offering a range of advantages such as reduced carbon emissions, enhanced chemical resistance, and improved mechanical properties. Over the years, extensive research and development efforts have focused on advancing geopolymer technology, exploring novel precursor materials, optimizing activators, incorporating modifiers and additives, and fine-tuning curing conditions. This section provides a comprehensive overview on geopolymer formulations, highlighting key aspects and recent trends in this rapidly evolving field. The points to take into consideration when talking about geopolymers are different, as precursor, alkaline activators, modifiers and additives and curing conditions.

2.2.1 Aluminosilicate precursor

The choice of precursor materials significantly influences the properties and performance of geopolymers. Metakaolin, a thermally activated form of kaolinite clay, has been widely utilized due to its reactivity and consistent composition. However, researchers have been exploring alternative aluminosilicate precursors, including fly ash and slag, to develop sustainable geopolymer formulations. These waste materials not only reduce environmental impact but also offer economic benefits. By understanding the composition and reactivity of various precursors, researchers aim to tailor geopolymer formulations for specific applications. Kaolinite is a clay mineral, with the chemical composition $Al_2Si_2O_5(OH)_4$. It is an important industrial mineral. It is a layered silicate mineral, with a tetrahedral sheet of silica (SiO_4) bonded via oxygen atoms to an octahedral sheet of

alumina (AlO_6) octahedra. Rocks rich in kaolinite are known as kaolin or China clay. Kaolinite has low shrinkage and swelling capacity and low cation exchange capacity. It is a soft, earthy, usually white mineral (dioctahedral phyllosilicate clay), produced by the chemical erosion of aluminium silicate minerals such as feldspar. In many parts of the world, it is coloured pink-orange-red by iron oxide, which gives it a distinct rusty hue. Lighter concentrations produce white, yellow, or light orange colours. Sometimes alternating layers are found, such as at Providence Canyon State Park in Georgia, USA. Commercial grades of kaolin are supplied and transported as dry powder, semi-dry paste or slurry. In its natural state kaolin is a white (Fig.2-2) and soft powder consisting mainly of the mineral kaolinite, which, under the electron microscope, consists of roughly hexagonal crystals ranging in size from about 0.1 micrometres to 10 micrometres or even bigger. These crystals can take on vermicular and book-like shapes, and macroscopic forms approaching millimetres size are occasionally found. Kaolin as found in nature usually contains varying amounts of other minerals such as muscovite, quartz, feldspar and anatase. Additionally, raw kaolin is often coloured yellow by iron hydroxide pigments. It is often necessary to chemically bleach the clay to remove the iron pigment and wash it with water to remove the other minerals to prepare kaolin for commercial use.

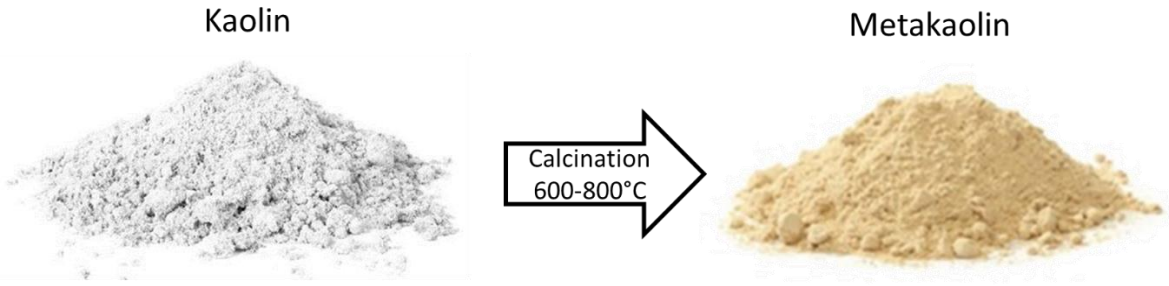

Fig.2-2 Formation of Metakaolin.

In the production of geopolymers, kaolin can be used as such or after calcination at temperatures higher than the dehydroxylation temperature, with a clear predominance of the second case. In fact, in the absence of a heat treatment, the reactivity of the powder is so low as to require the joint use of other raw materials, generally calcined, such as fly ash [Hua et al.2003]. Calcination of kaolin leads to the transformation of kaolinite into meta-kaolinite, an amorphous

phase with a high reactivity, which justifies the use of calcined kaolin in the production of geopolymers [Zhang et al. 2009].
The use of calcined clays as pozzolanic additives for cements has been known since Roman times, while the use of calcined kaolin as additives for cements and concretes has become very popular in more recent times, generating an interest in the meta- kaolinization of clays, still not fully clarified [Shvarzman et al. 2003].
Metakaolin (MK) (Fig.2.2) is a type of calcined clay and comes from the calcination of kaolin clay, and there has been some interest in the use of MK in recent years [Siddiqui et al. 2007]. For example, in the UK, the coal power industry will shut down in the next 10 years and fly ash will cease to be generated. To do this it is necessary to use alternative pozzolanic materials, improve concrete properties such as durability and reduce the amount of cement used in concrete production. The mechanical, physical and durability properties of the cementitious systems will be reported on the basis of the available literature. The use of other pozzolanic materials such as fly ash or blast furnace ground granules. Slag in combination with MK and the use of alkaline materials in the presence of materials are also examined.
MK differs from other cement substitute materials in that it is not a waste product from industrial activities nor is it completely natural. It originates from the clay mineral kaolinite and is worked for various uses and applications including the cement one [Kakali et al. 2001] and to the loss of zeolitic water, i.e. the one present in the kaolinite interlayers [Kong et al. 2008]. The decomposition of hydroxides such as gibbsite (aluminium hydroxide) according to the reaction:

$$1) \quad 2Al(OH)_3 \rightarrow Al_2O_3 + 3H_2O$$

The presence of this endothermic reaction depends on the purity of the clay, consequently this transformation may not be present in all samples. The dehydroxylation of the kaolinite with the formation of metakaolin according to the reaction:

$$2) \quad Al_2O_3 \cdot 2SiO_2 \cdot 2H_2O \rightarrow Al_2O_3 \cdot 2SiO_2 + 2H_2O$$

This reaction generally occurs in the range of 450-700°C; [Chandrasekhar et al. 2002] or to the presence of illite (clayey mineral of the subgroup of phyllosilicates). In the case of mullite formation

the reaction is [Ch. Bich et al. 2009; Ptácek et al. 2010; de Souza Santos et al. 2005]:

$$3) \qquad 2(Al_2O_3 \cdot 2SiO_2) \rightarrow 2Al_2O_3 \cdot 3SiO_2 + SiO_{2\ amorphus}$$

The phase obtained is a function of the starting kaolin and can be identified by XRD analysis. Starting from a kaolin, it is therefore possible to obtain the corresponding meta-kaolin, i.e. the active phase in the geopolymerization process, by calcination. The temperature interval between the end of the dihydroxylation reaction of the kaolinite and the beginning of the exothermic reaction of formation of a new non-reactive crystalline phase is that of existence of metakaolin powders, and within this interval it must be identified the optimal temperature to maximize the reactivity of the powder [Glukhovsky et al.1965; Kakali et al. 2001]. During calcination, the Si-O bonds remain essentially intact while the Al-O bonds are rearranged.
Dehydroxylation can occur in two ways:

1. Intra-dehydroxylation: it is the loss of –OH linked to the same Al atom: It produces the formation of the alumoxyl group -Al=O, (in analogy to the carboxyl group of organic chemistry).

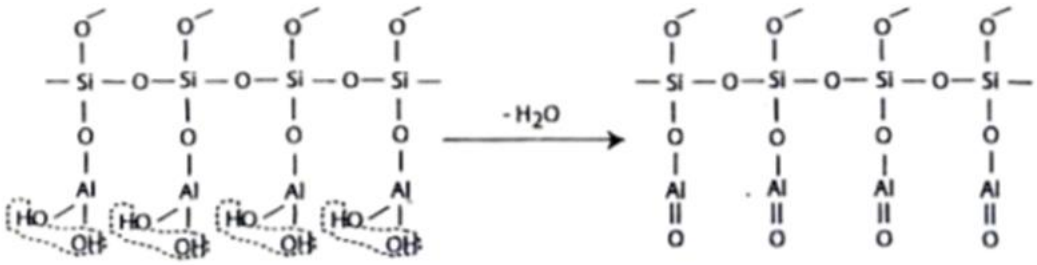

Fig.2-3 Intra-dehydroxylation, loss of -OH.

The formation of the alumoxyl (Fig.2-4) group provides a satisfactory explanation of the formation mechanism of the alpha-coordinated.
The oxygens involved in the formation of this coordination are those from 1 to 5.

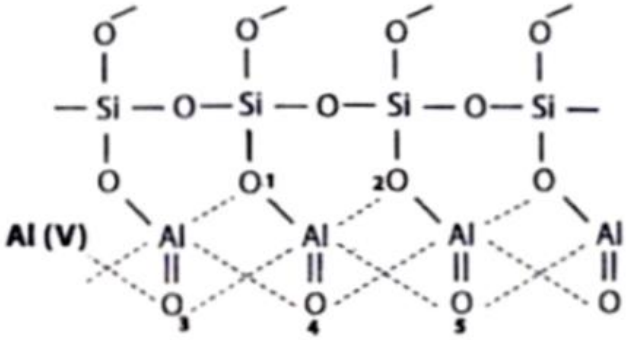

Fig.2-4 Intra-dehydroxylation, Formation of the alumoxyl group.

The configuration has two covalent bonds between Al and oxygens 1 and 4 and three Van der Waals bonds with oxygens 2, 3 and 5.

2. Inter-dehydroxylation (Fig.2-5): it is the loss of water involving the –OH of two neighbouring -$Al(OH)_2$ groups and sees the formation of a sequence of the Al-O-Al-O type.

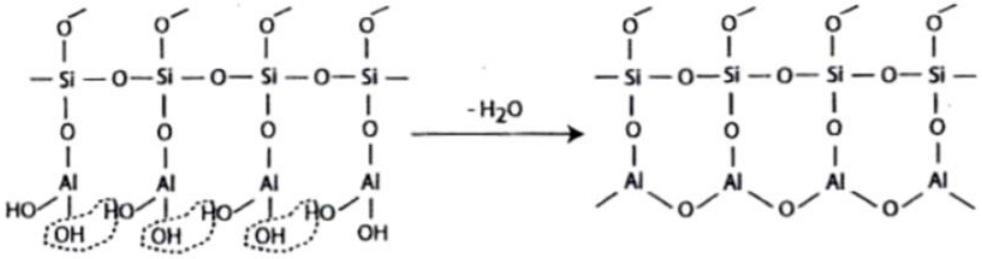

Fig.2-5 Inter-dehydroxylation, loss of H_2O.

Al is therefore in (IV) coordination (Fig.2-6), being covalently bonded with oxygens 1, 3 and 4 and exhibiting a van der Waals bond to oxygen 2 [Davidovits et al. 2008; Davidovits et al. 2020].

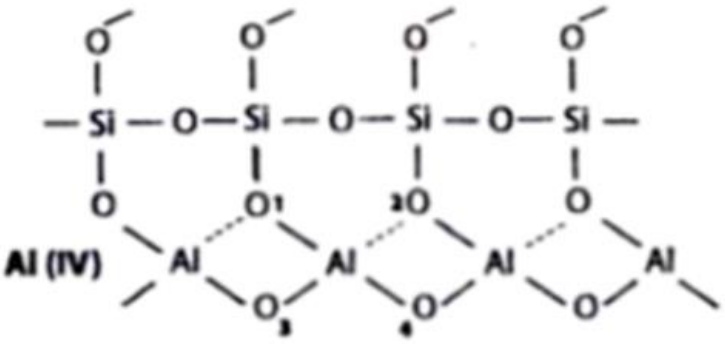

Fig.2-6 Inter-dehydroxylation, formation of Al(IV).

It was found that the main parameters significantly influencing the dehydroxylation process are heating temperature, heating duration and rate, cooling rate, and environmental conditions. The mass loss resulting from the dehydroxylation of pure kaolinite (39.5% Al_2O_3, 46.5% SiO_2 and 14% H_2O) in ambient atmosphere is about 14%. The calcination interval of the kaolin to obtain the reactive phase varies according to the secondary mineralogical phases present, the degree of crystallinity and the size of the particles of the starting kaolin [Kakali et al. 2001; Kong et al. 2008]. In almost all cases, products calcined at 500°C show kaolinite residues [Chandrasekhar et al. 2002], while at 1000°C crystalline phases form. The most used calcination temperature in the literature is 750°C, probably as it is intermediate in the range of existence of metakaolinite. The optimum temperature can be evaluated both as mechanical strength of the geopolymer obtained, and as pozzolanic capacity, i.e. as the quantity of calcium hydroxide consumed by the metakaolin in the pozzolanic reaction of formation of silicates and hydrated calcium aluminates. It has been reported that also the permanence time at the maximum calcination temperature influences the pozzolanic activity of the powder obtained. A cooking period that is too short does not allow complete dehydrolysis, regardless of the temperature reached; on the other hand, a too long calcination leads to the total dehydroxylation of the kaolinite phase, but also to the sintering of the particles [Bich et al. 2009].

Metakaolin (MK) is one of the building materials classified as a new generation and can be used in its finely ground form as a partial substitute for cement in concrete mix. Direct characterization includes thermogravimetry (TG), Fourier transform infrared radiation (FTIR), and X-ray diffraction (XRD) techniques.

The mineralogical composition of the clay can be determined by X-ray diffractometer before and after heat treatment. The XRD patterns of the calcined clay and the original one can be compared to confirm the characteristics of the kaolinite banding in the crude sample and its absence in the samples after they have been heat treated. The results are shown in Fig.2-7. It is evident that the main mineral constituents of the original clay are quartz and kaolinite.

The mineralogical composition and, consequently, the X-ray diffraction (XRD) spectra and Nuclear Magnetic Resonance (NMR)

characteristics of metakaolin can vary significantly depending on the type of kaolin clay used and the specific calcination process employed.

When kaolin from different sources undergoes calcination to form metakaolin, the resulting metakaolin will inherit the mineralogical composition of its precursor kaolin. Therefore, the XRD spectra and NMR signals will reflect the presence of these mineral phases. The temperature and duration of the calcination process play a crucial role in the transformation of kaolin to metakaolin. At lower temperatures, some of the kaolinite may not fully transform into metakaolin, leading to the presence of residual kaolinite in the final product. As the calcination temperature increases, the extent of metakaolin formation increases, and the XRD peaks corresponding to kaolinite will decrease in intensity or disappear, while new peaks attributed to metakaolin may appear. NMR signals will also change as the atomic environment of the metakaolin differs from that of kaolinite. Kaolin deposits may contain various impurities, such as quartz, feldspar, iron oxides, and organic matter. During the calcination process, some impurities may be eliminated, while others may remain or transform into new compounds.

In some cases, the transformation from kaolin to metakaolin may not be straightforward. Intermediary phases might form during the calcination process, and these phases could impact the mineralogical composition of the final product.

XRD and NMR can detect the presence of these intermediary phases.

In summary, the mineralogical composition, and analytical data (XRD spectra and NMR signals) of metakaolin can be significantly affected by the type of kaolin clay used, the calcination temperature and time, the presence of impurities and additives, and any phase transitions occurring during the process. Analysing these changes is essential for understanding the properties and potential applications of different types of metakaolin in various industries, such as construction, ceramics, and geopolymer production.

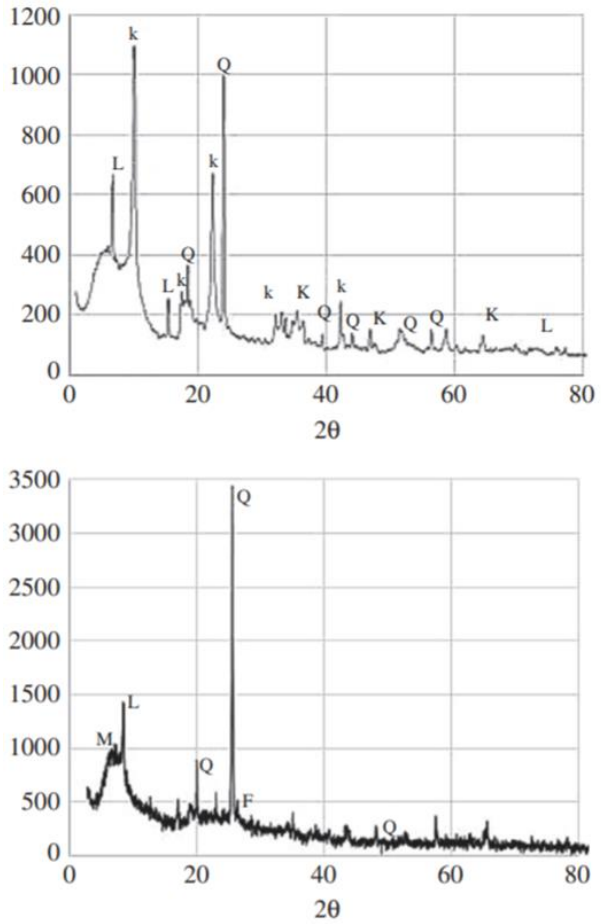

Fig.2-7 XRD patterns of the calcined clay and the original one can be compared to confirm the characteristics of the kaolinite banding in the crude sample and its absence in the samples after they have been heat treated [Bich et al. 2009].

FTIR spectrophotometer, can be used to confirm the disappearance of kaolinite peaks, after heat treatment. IR spectroscopy can be used to confirm the transformation of kaolinite during calcination. The IR spectroscopy results of the original clay (Fig.2-8) indicate that the characteristic kaolinite bands of kaolinite disappeared in the calcined clay due to the appearance of the amorphous SiO_2 phase. The FTIR spectra of the kaolin treated at different temperatures and duration times indicate the transformation of the kaolinite into an amorphous reactant due to the heat treatment. At 800°C calcination temperature and a duration of 30 min, bands of amorphous phase were obtained [Biljana et al.2010].

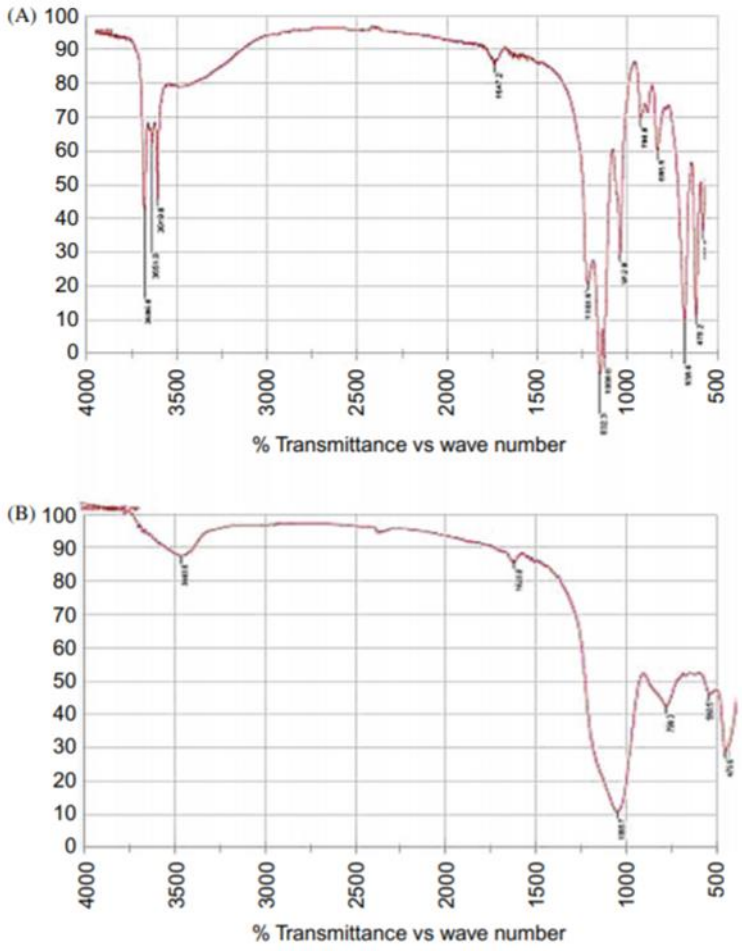

Fig.2-8 IR spectroscopy results of the original clay [Biljana R. 2010].

Solid-state magic angle spinning nuclear magnetic resonance spectroscopy (MAS-NMR) has emerged as a valuable technique for studying metakaolin geopolymers. NMR was one of the pioneering advanced analytical methods used to investigate metakaolin geopolymers [Davidovits J. 2008¸ Davidovits J. 2020]. Since then, it has consistently provided valuable insights [Rahier et al. 1996a; Duxson et al. 2008; Rowles et al. 2003]. Although the spectra may appear featureless at first glance, a detailed analysis of peak positions and widths enables the assessment of ordering and Si/Al substitution within the geopolymer frameworks. Introducing aluminium into the silicate network leads to a less negative chemical shift [Engelhardt et al. 1974; Engelhardt et al. 1984]. Consequently, geopolymers synthesized with higher Si/Al ratios exhibit greater Al substitution and lower distributions of connectivity types Q4 (nAl) (where tetrahedral Si is surrounded by 4 -O-Al bonds and (4-n) –O-Si bonds). Deconvolution of these spectra into individual component peaks (one

peak for each value of n) allows for comparison with the expected connectivity distribution computed from statistical thermodynamics [Duxson et al. 2008]. These comparisons revealed that the extent of framework disorder (Si/Al ordering violation) was higher in K-aluminosilicate geopolymers compared to Na-aluminosilicate geopolymers. It is worth noting that the deconvolution process requires the Si/Al ratio to match the known ratio of the samples, and precise sub-peak positions and widths must be employed. Deconvolution also assumes that all sites within the geopolymer framework are Q4 (fully connected to other framework species). The accuracy of this assumption was verified by ^{2}H MAS-NMR, specifically for the stoichiometrically formulated samples (Na/Al = 1.0) that were well-cured (20 hours at 40°C followed by 2 weeks at room temperature) in this study [Duxson et al.2008]. However, this limitation restricts the use of similar methods for partially-cured or non-stoichiometric geopolymer mixes, although attempts are sometimes made regardless [Zhang et al. 2013].

In addition to ^{29}Si MAS NMR, other nuclei provide valuable insights into the study of metakaolin geopolymers. The ^{27}Al MAS-NMR indicates the extent of metakaolin conversion to geopolymer gel, as residual Al (VI) is distinguishable from the tetrahedral Al in the geopolymer gel. Although the percentage of residual Al (VI) among all the Al present does not precisely represent the quantity of unreacted metakaolin, it serves as a useful measure for comparing a series of samples [Duxson et al. 2007].

Comparison of ^{23}Na and ^{39}K MAS NMR spectra of mixed-alkali geopolymers at low Si/Al ratios and early stages of formation has shown that K^{+} preferentially incorporates into the gel, while Na^{+} remains solvated for a longer duration [Duxson et al. 2007]. Two-dimensional triple-quantum MAS NMR has also been employed to differentiate various sites that would otherwise overlap in a simple MAS spectrum. This technique utilizes quadrupolar nuclei such as ^{17}O [Duxson, 2006] and ^{23}Na [Rowles et al.2003]. As previously mentioned, the starting MK powders can be different in the geopolymers, as shown in Fig.2-9 and 2-10. It is possible to notice how the spectra are slightly different.

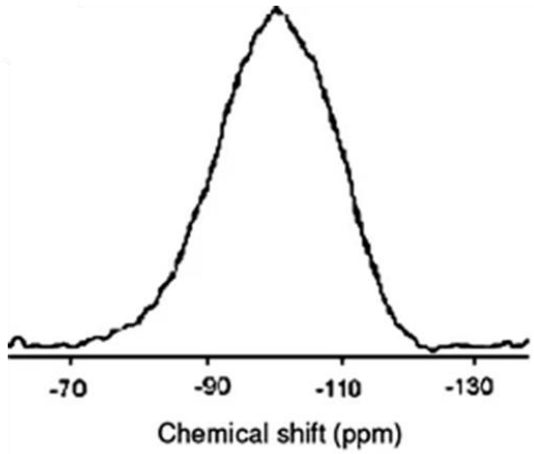

Fig.2-9 ^{29}Si MAS-NMR spectra of MK [Duxson et al. 2007].

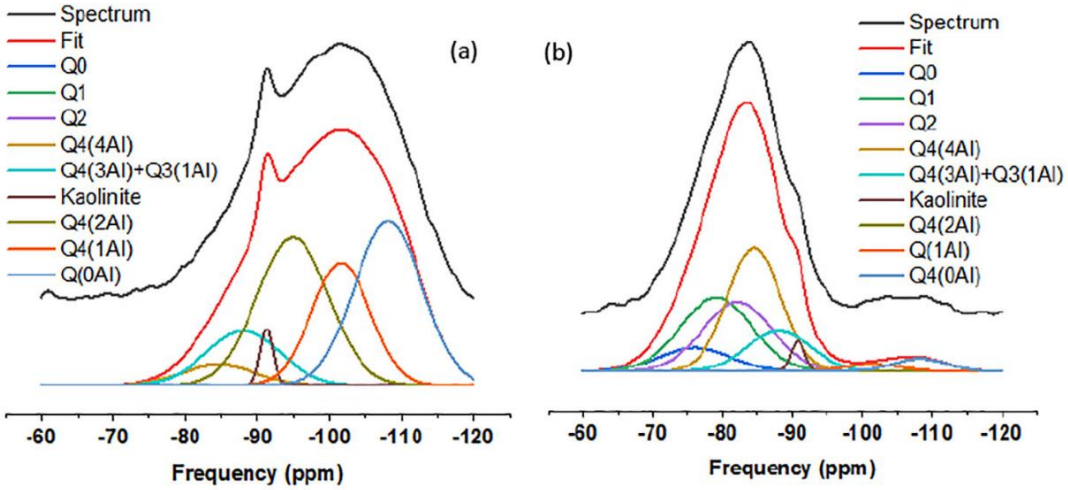

Fig.2-10 Deconvolution results for 29Si NMR spectra of (a) MK and (b) MKG paste [Zhenming Li et al. 2019].

In Figure 2-11, two ^{27}Al MAS-NMR spectra are shown, one representing the classic amorphous MK and the other the geopolymer based on that MK. It can be observed that after geopolymerization, the disappearance of Al(V) and Al(VI) occurs.

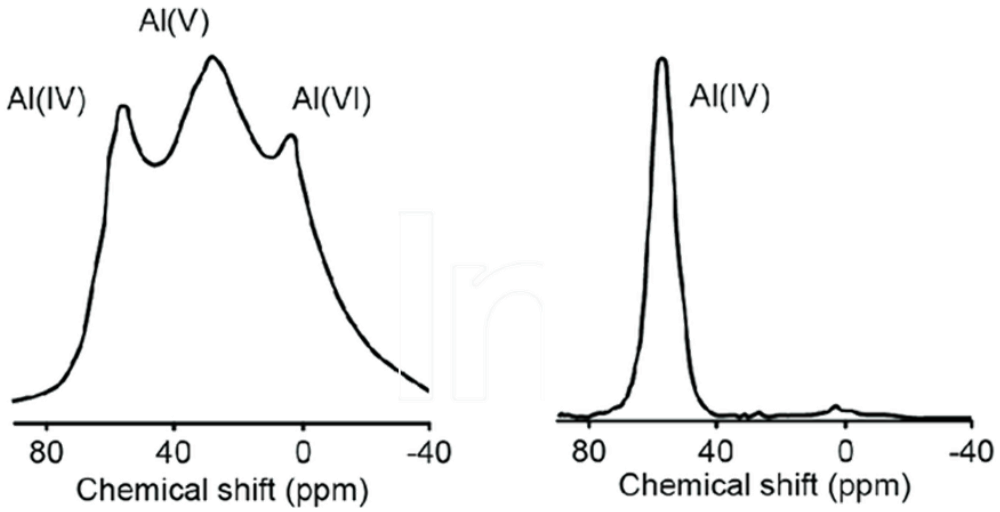

Fig.2-11 ^{27}Al MAS-NMR of MK (left) and of MK-based Geopolymer (right) [Duxson et al. 2007].

Though many macroscopic characteristics of geopolymers prepared from different aluminosilicate sources may appear similar, their microstructure and physical, mechanical, chemical and thermal properties change depending predominantly on the raw material from which they are derived. Typical images illustrating the microstructures of geopolymers synthesized from metakaolin and Class F fly ash are presented in Fig. 2-12 large differences can be observed between the microstructures of these geopolymers. The microstructure of metakaolin derived geopolymers, for example, has been investigated by systematic variation of activator composition and related to mechanical strength [Duxson et al. 2005; Duxson et al. 2006; Rowles et al. 2003]. It was observed that the microstructure changed from containing large pores to being more homogenous with small pores as the Si/Al ratio was increased.

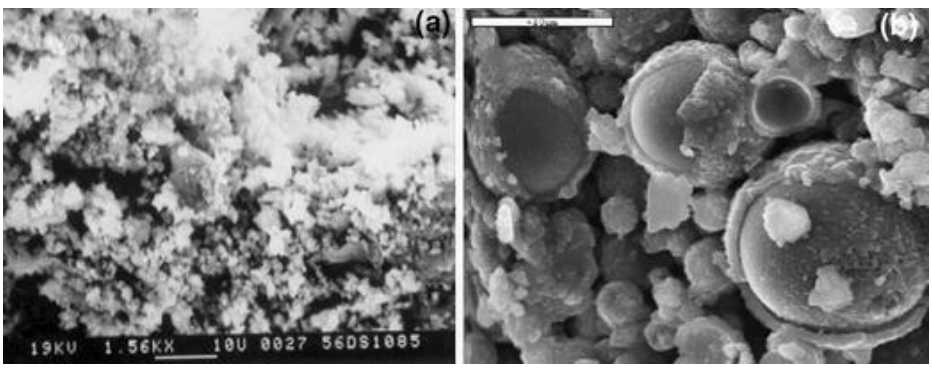

Fig.2-12 MK powder compared with Fly ash powder [Duxson et al. 2007].

2.2.2 Alkali activator

Strong alkaline solutions are required for the activation of the Si and Al present in the reactive powder: the common activators used are NaOH, Na_2SO_4, sodium and/or potassium silicate, Na_2CO_3, K_2CO_3, KOH and K_2SO_4. The choice depends on the nature of the reactive powder and the ratios characterizing the geopolymers to be prepared [Davidovits et al. 2008; Nodehi et al. 2022; Blaszcynski et al. 2017]. The silicate is used to increase the Si/Al ratio in the reactive powder and reach the desired value, which strongly influences the product properties. The hydroxide is instead used to modify the M_2O/Al_2O_3 and M_2O/H_2O ratios: the first is important to balance the negative charge that is generated on the Al, the second to increase the pH to the values required for the dissolution of the aluminosilicate powder in the first step of the geopolymerization reaction. To obtain the required ratios it is therefore possible to use both silicate and hydroxide, remembering that the ratio between the two plays a key role in the development of the mechanical properties of the geopolymer [Davidovits J. 2008; Davidovits J. 2020; Blaszcynski et al. 2017]. Excess sodium silicate inhibits water evaporation and the formation of the geopolymeric structure, resulting in a decrease in compressive strength. However, an excessive concentration of OH^- ions leads to a decrease in the strength of the material.

In general, it can be stated that the total amount of hydroxide added as a function of the amount of reactive powder leads to materials with different characteristics:

- from 0.5 to 1.0% (w/w): the powder is stabilized and has good resistance to water;
- from 1.0 to 2.5% (w/w): the product is stable in water and has a compressive strength between 4 and 6 MPa;
- from 2.5 to 5.0% (w/w): the product is comparable to a traditional ceramic, with a compressive strength between 8 and 60 MPa.

- Sodium Hydroxide (NaOH)

Sodium hydroxide, also known as caustic soda, [Blaszcynski et al.2017; Jacobs, et al. 1985] is an inorganic compound with the formula NaOH. It is a white solid ionic compound consisting of sodium cations Na^+ and hydroxide anions OH^-. Sodium hydroxide is a highly

caustic, alkaline base that decomposes proteins at ordinary room temperatures and can cause severe chemical burns. It is highly soluble in water and quickly absorbs moisture and carbon dioxide from the air. It forms a series of hydrates $NaOH \cdot nH_2O \cdot NaOH \cdot H_2O$ monohydrate crystallizes from aqueous solutions between 12.3 and 61.8°C. Commercially available "sodium hydroxide" is often this monohydrate, and published data may refer to it instead of the anhydrous compound. As one of the simplest hydroxides, sodium hydroxide is often used in conjunction with neutral water and hydrochloric acid to demonstrate the pH scale. Sodium hydroxide is used in many industries: in pulp and paper manufacturing, textiles, drinking water, soaps, detergents and as a drain cleaner. World production in 2004 was about 60 million tons, while demand was 51 million tons.

Fig.2-13 Pellets of NaOH.

Pure sodium hydroxide is a colorless crystalline solid that melts at 318°C without decomposition and with a boiling point of 1,388 °C. It is highly soluble in water, with lower solubility in polar solvents such as ethanol and methanol. NaOH is insoluble in ether and other non-polar solvents. The dissolution of solid sodium hydroxide in water is a highly exothermic reaction in which a large amount of heat is released, which poses a safety threat due to the possibility of splashing. The resulting solution is usually colourless and odourless.
However, solutions of NaOH can easily be supercooled by many degrees, which allows for the formation of hydrates (including metastable ones) from solutions with different concentrations.

A hot water solution containing 73.1% (mass) NaOH is a eutectic that solidifies at about 62.63°C as an intimate mixture of anhydrous crystals and monohydrates. A second stable eutectic composition is 45.4% (mass) NaOH, which solidifies at about 4.9°C to a mixture of crystals of the dihydrate and 3,5-hydrate.
The third stable eutectic contains 18.4% (mass) NaOH. Solidifies at about -28.7°C as a mixture of ice water and $NaOH \bullet 7H_2O$.
The α form of the tetrahydrate has a density of 1.33 g/cm^3. It dissolves congruously at 7.55°C in a liquid with 35.7% NaOH and density of 1.392 g/cm^3, and then floats on it like ice on water.
Commercially available "sodium hydroxide" is often the monohydrate (density 1.829 g/cm^3). Physical data in the technical literature may refer to this form, rather than the anhydrous compound.
Glass reacts slowly with aqueous solutions of sodium hydroxide at room temperature to form soluble silicates. For this reason, glass joints and stopcocks exposed to sodium hydroxide tend to "freeze up". Glass-lined flasks and chemical reactors are damaged by long exposure to hot sodium hydroxide, which also freezes the glass. Sodium hydroxide does not attack iron at room temperature, since iron does not have amphoteric properties (i.e., it only dissolves in acid, not base).
Like other corrosive acids and alkalis, drops of sodium hydroxide solution can readily decompose proteins and lipids in living tissue through amide hydrolysis and ester hydrolysis, which consequently cause chemical burns and can lead to permanent blindness to the eye contact. Solid alkalis can also express their corrosive nature if there is water, such as water vapor. Therefore, protective equipment, such as rubber gloves, safety clothing, and eye protection, should always be used when handling this chemical or its solutions.
When it comes to geopolymer composites, the highly alkaline nature of the mixture can react with and degrade molds at high Temperature. Silicone molds are commonly used for casting various materials at room Temperature due to their flexibility, non-stick properties, and ease of demolding.

- Sodium silicate solution

An alternative alkaline activator that can be utilized in geopolymer synthesis is alkali silicate solution, which is also known as soluble

glasses in the case of sodium-based solutions. These solutions consist of a mixture of Si_2O, Na_2O or K_2O, and H_2O. When present in solution, silica undergoes polymerization, forming various species that are challenging to differentiate. Analyzing these species is typically done using ^{29}Si NMR spectroscopy. The viscosity of alkali silicate solutions increases exponentially as the Si/Na ratio rises.

Studies by Criado et al. [Criado et al. 2007] have demonstrated that the formation of zeolitic phases decreases as the Si/M^+ ratio increases. Their research explored the phases present in geopolymer samples with different SiO_2/Na_2O ratios, namely N = 0, W15 = 0.19, W50 = 0.69, and W84 = 1.17. The results indicated a reduction in the glassy phase, which aligns with the dissolution of fly ash and the subsequent delivery of silicates and aluminates for geopolymer formation. In mixtures with higher soluble silica content, slower dissolution was observed due to the saturation of silica species in the mixture. Provis presented precipitation isotherms of hydrated sodium silicates based on the proportion of silica and sodium base (Na_2O) in his work. The majority of commercial SS solutions were found to precipitate as $Na_2SiO_3 \cdot 9H_2O$. The SS/NaOH ratio is a critical parameter influencing strength development.

2.2.3 Additives

While the basic components of a geopolymer matrix are the aluminosilicate powders and the activator, various additives can be incorporated to enhance specific properties or improve the performance of the material. Here are some common additives used in geopolymer matrices:

Silica Fume: byproduct of silicon and ferrosilicon alloy production. Adding silica fume to a geopolymer mix can increase its compressive strength, density, and chemical resistance.

Fibers: reinforcements such as glass fibers, carbon fibers, or polymeric fibers can be added to geopolymer matrices to enhance their tensile strength, toughness, and crack resistance.

Retarders/Accelerators: are additives used to slow down the setting time of geopolymers, allowing for better workability and longer application times. Conversely, accelerators are used to speed up the setting time, which can be beneficial in certain construction scenarios.

In addition to the primary source material, supplementary pozzolanic materials such as rice husk ash or ground granulated blast furnace slag can be incorporated to improve the geopolymer's performance and reduce the environmental impact.

Anti-Cracking Agents: Cracking is a common concern in geopolymer applications. Additives like shrinkage-reducing agents or crack control fibers can be employed to minimize the potential for cracking and improve the overall durability of the material.

Geopolymers can be susceptible to corrosion in certain environments. Corrosion inhibitors can be added to the mix to protect embedded steel reinforcement and enhance the geopolymer resistance to corrosive substances.

It's worth noting that the selection and proportion of additives may vary depending on the desired properties and specific application requirements. The use of additives in geopolymer matrices allows for customization and optimization of the material to meet different project needs.

2.3 Design of metakaolin-based geopolymer

By considering these design parameters, such as the type of metakaolin, concentration of alkali activators, SS/SH ratio, Si/Al ratio, mixing techniques, and curing time and Temperature it is possible to tailor the composition and processing parameters of metakaolin-based geopolymer materials. This optimization process aims to achieve the desired performance characteristics suitable for various applications, including construction materials, advanced composites, and sustainable infrastructure development. Through careful design, metakaolin-based geopolymers can offer improved mechanical properties, reduced environmental impact, and enhanced durability, paving the way for their broader utilization in diverse industrial sectors.

2.3.1 Type of metakaolin

The selection of the appropriate type of metakaolin is a crucial aspect in the design of geopolymer materials. Metakaolin is derived through the calcination of kaolinite clay at temperatures ranging from 500-800°C, and the choice of precursor clay, as well as its purity and crystallinity, determines the properties and reactivity of the resulting metakaolin. Particle size, purity, and crystallinity variations in

different metakaolin sources can significantly impact the final geopolymer's performance.

2.3.2 Concentration of alkali activators

In the design of metakaolin-based geopolymers, the concentration of alkali activators is a crucial factor that significantly impacts the overall performance and properties of the geopolymer material. Alkali activators, commonly highly concentrated alkaline solutions, are essential for activating metakaolin and initiating the geopolymerization process [Davidovits J. 2008; Davidovits J. 2020].

The concentration of alkali activators must be carefully determined to achieve the desired reactivity and strength development in the resulting geopolymer. The choice of the specific type of alkali activators also plays a significant role in the overall performance of the geopolymer material. Different alkali activators, such as sodium hydroxide (NaOH) or potassium hydroxide (KOH), may exhibit variations in reactivity and performance characteristics.

Optimizing the concentration of alkali activators involves finding the right balance between the amount of alkali required for effective activation of the metakaolin and the potential negative effects of excessive alkali content. Insufficient alkali concentration may result in incomplete activation and limited geopolymer formation, leading to reduced strength and suboptimal properties. On the other hand, excessive alkali concentration can lead to undesired side reactions, increased shrinkage, and reduced durability.

The selection of the appropriate concentration of alkali activators is typically determined through experimental investigations and optimization processes. Researchers and engineers analyze the reactivity of metakaolin with varying concentrations of alkali activators, assessing the resulting geopolymer's mechanical properties, chemical stability, and other relevant characteristics.

Furthermore, the concentration of alkali activators can be tailored for specific applications and desired performance requirements. For instance, high-strength geopolymer composites may require higher concentrations of alkali activators to promote extensive geopolymerization and enhance bond formation between metakaolin particles. Conversely, in applications where reduced shrinkage or

improved durability is crucial, lower concentrations of alkali activators may be preferred.

In summary, the concentration of alkali activators plays a critical role in the design of metakaolin-based geopolymers. It must be carefully adjusted to achieve optimal reactivity and strength development, while considering the specific application and desired performance requirements. By understanding the influence of alkali concentration on the geopolymerization process, researchers and engineers can effectively optimize the design of metakaolin-based geopolymers for a wide range of applications in construction, infrastructure, and other industries.

2.3.3 SS/SH ratio

In the design of geopolymer materials, the ratio of sodium silicate (SS) to sodium hydroxide (SH) plays a significant role in determining the properties and performance of the resulting geopolymer gel structure [Davidovits J. 2008; Leong et al. 2016]. This ratio is an essential consideration in geopolymer design as it directly influences the formation and stability of the geopolymer matrix.

By controlling the SS/SH ratio, engineers and researchers can customize the properties of the geopolymer to meet specific requirements. The ratio has a direct impact on various characteristics of the geopolymer, including mechanical strength, chemical resistance, and thermal stability.

A higher SS/SH ratio tends to promote the formation of a denser and more cross-linked geopolymer gel structure. This can lead to enhanced mechanical strength, as the increased network connectivity improves load-bearing capacity and resistance to deformation. Geopolymers with higher SS/SH ratios also tend to exhibit improved chemical resistance, making them suitable for applications in aggressive environments where corrosion or chemical attack is a concern.

Conversely, a lower SS/SH ratio can result in a more open and porous geopolymer structure. This may be desirable in certain applications where increased porosity is advantageous, such as in lightweight materials or when considering permeability for specific functionalities. Additionally, a lower SS/SH ratio can influence the

thermal stability of the geopolymer, making it more resistant to thermal stress or high-temperature exposure.

The SS/SH ratio can be adjusted by varying the composition and concentration of the alkali activators used in the geopolymer formulation. Different combinations of alkali sources, such as sodium silicate (Na_2SiO_3) and sodium aluminate ($NaAlO_2$), can be utilized to achieve the desired SS/SH ratio.

Optimizing the SS/SH ratio requires careful experimentation and analysis of the resulting geopolymer's properties. Researchers and engineers conduct tests to assess the mechanical strength, chemical resistance, thermal stability, and other relevant characteristics of geopolymer samples with different SS/SH ratios. Based on the desired performance requirements, the SS/SH ratio can be fine-tuned to achieve the desired balance of properties.

The SS/SH ratio is a crucial parameter in geopolymer design, as it directly influences the formation and stability of the geopolymer gel structure. By controlling this ratio, engineers and researchers can tailor the properties and performance of geopolymer materials to meet specific application requirements, including mechanical strength, chemical resistance, and thermal stability.

2.3.4 Si/Al ratio

The Si/Al ratio plays a pivotal role in determining the properties and composition of the geopolymer system, exerting a profound influence on its overall behavior. The Si/Al ratio stands as a paramount factor in determining the properties and composition of the geopolymer system, exerting a profound and far-reaching influence on its overall behavior. Through careful adjustments to the Si/Al ratio, a fine-tuning and optimization of the geopolymer's essential characteristics become achievable, encompassing crucial aspects such as strength, porosity, and reactivity [Davidovits J. 2020]. This critical parameter, the Si/Al ratio, can be effectively modified utilizing two primary methods: altering the composition of the metakaolin precursor or adjusting the formulation of the alkali activators. These techniques present a versatile approach that allows for precise control over the Si/Al ratio, ultimately enabling engineers and researchers to tailor the geopolymer's performance to meet specific application requirements with precision and efficacy. By varying the composition of the

metakaolin precursor, engineers can manipulate the Si/Al ratio, thereby customizing the geopolymer's behavior and properties. This can be achieved by utilizing metakaolin from different sources or implementing specific treatments to modify the precursor's composition. Adjusting the formulation of alkali activators offers another avenue for Si/Al ratio manipulation. The careful selection and adjustment of the alkali activators' components and concentrations enable engineers to finely control the Si/Al ratio within the geopolymer system, resulting in desired outcomes in terms of composition and properties.

The ability to manipulate the Si/Al ratio provides a powerful tool for engineers and researchers to achieve specific goals and meet diverse application requirements. Whether through variations in the metakaolin precursor or adjustments in the formulation of alkali activators, the Si/Al ratio acts as a fundamental parameter that empowers precise control over the geopolymer's behavior and performance. By leveraging this control, engineers can optimize the geopolymer's characteristics to deliver tailored solutions for a wide range of applications, ensuring the utmost effectiveness and efficiency in meeting project objectives.

2.3.5 SiO_2/Na_2O ratio

The SiO_2/Na_2O ratio is an essential parameter in geopolymer chemistry that significantly influences the properties and performance of geopolymers. The SiO_2/ Na_2O ratio refers to the molar ratio of silicon dioxide (SiO_2) to sodium oxide (Na_2O) in the geopolymer system. Here are some key aspects highlighting the importance of the SiO_2/Na_2O ratio in geopolymer chemistry:

The SiO_2/Na_2O ratio plays a crucial role in determining the formation and structure of the geopolymer gel network. A high SiO_2/Na_2O ratio promotes the formation of a more cross-linked and three-dimensional network structure. This results in a denser and more rigid geopolymer matrix, which generally exhibits improved mechanical strength and chemical resistance.

Geopolymers are formed by the alkali activation of aluminosilicate precursors, such as metakaolin or fly ash. The SiO_2/Na_2O ratio affects the dissolution and reactivity of these precursors. A higher SiO_2/Na_2O ratio provides a greater availability of silicon (Si) species, facilitating

the dissolution of aluminosilicate precursors and promoting the geopolymerization reaction [Leong et al. 2016].

The SiO_2/Na_2O ratio influences the rheological properties and workability of the geopolymer paste or slurry. A lower SiO_2/Na_2O ratio tends to result in a more fluid and workable paste, while a higher ratio leads to a stiffer and less flowable mixture. The appropriate SiO_2/Na_2O ratio needs to be considered to achieve the desired workability for casting, molding, or other processing techniques.

The SiO_2/Na_2O ratio influences the mechanical properties and durability of geopolymers. Geopolymers with a higher SiO_2/Na_2O ratio often exhibit higher compressive strength, flexural strength, and toughness. They also tend to have improved resistance to chemical attack, abrasion, and thermal stress. It is important to note that the optimal SiO_2/Na_2O ratio may vary depending on the specific application and desired properties of the geopolymer. Different ratios can be explored to achieve the desired balance of workability, mechanical strength, and durability for a particular application. Moreover, other factors such as curing conditions, activator composition, and precursor characteristics should also be considered in conjunction with the SiO_2/Na_2O ratio to optimize geopolymer performance.

An example of how the chemistry of bonds in a geopolymer can vary depending on the SiO_2/ Na_2O ratio is shown in figure 2-14.

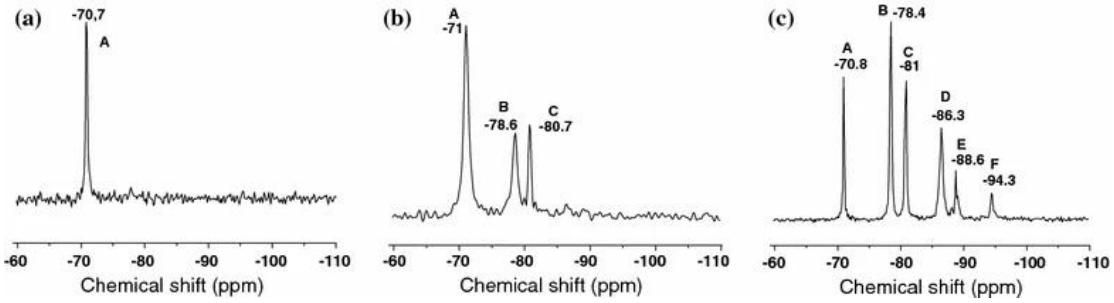

Fig.2-14 ^{29}Si MAS-NMR spectra of sodium silicate solutions, SiO_2/Na_2O ratio equal to (a) 0.19, (b) 0.69 and (c) 1.17 [Duxson et al. 2007].

2.3.6 Mixing

In the design of metakaolin-based geopolymer, the mixing process assumes a critical role, exerting a significant influence on the overall outcome. It becomes imperative to establish homogeneity and a uniform distribution of metakaolin particles within the activator

solution. To accomplish this, the utilization of proper mixing techniques, such as mechanical mixing or blending, becomes essential [Duxson et al. 2007]. These techniques are employed to ensure a consistent and well-dispersed geopolymer mixture, allowing for optimal results. Adequate mixing serves to facilitate the effective reaction between metakaolin and alkali activators, thereby promoting the formation of a uniform geopolymer structure and enhancing the material's properties. By ensuring thorough mixing, the metakaolin particles are intimately and evenly exposed to the activator solution, enabling efficient chemical reactions and bond formation. This, in turn, leads to improved structural integrity, enhanced strength, and desirable properties in the resulting geopolymer material.

By employing appropriate mixing techniques, engineers and researchers can maximize the potential of metakaolin-based geopolymer systems, optimizing their performance and achieving desired material characteristics. The careful consideration and implementation of effective mixing methods significantly contribute to the successful design and development of high-quality geopolymer materials for various applications.

2.3.7 Curing time and temperature

The curing time of a geopolymer is a crucial period in its development, encompassing the duration during which the material undergoes essential chemical reactions and gradually acquires strength and stability. During this curing process, various factors, including temperature and humidity, exert a significant influence on the evolution of the geopolymer's properties over time [Duxson et al. 2007]. The selection of optimal curing conditions becomes paramount in attaining the desired strength, durability, and long-term performance of the geopolymer material. By carefully controlling and manipulating the curing environment, engineers and researchers can effectively steer the development of the geopolymer's properties and enhance its overall performance.

Temperature plays a critical role in the curing process, as it directly affects the rate of chemical reactions and the kinetics of geopolymer formation. Higher temperatures can expedite the curing reactions, leading to accelerated strength gain. Conversely, lower temperatures

may extend the curing time but can also contribute to the development of desired material characteristics.

Humidity, on the other hand, influences the moisture content within the geopolymer matrix, impacting the reaction kinetics and moisture availability for hydration. Maintaining adequate humidity levels ensures that the geopolymer is not excessively dried out, allowing for optimal reaction progress and the development of desired properties. By carefully evaluating and adjusting the curing conditions, engineers can achieve the desired strength, durability, and long-term performance of the geopolymer. This involves finding the appropriate balance of temperature and humidity that promotes efficient curing reactions while minimizing potential detrimental effects such as cracking or inadequate hydration. The optimization of curing conditions is a vital aspect of geopolymer design, enabling the production of high-quality materials with tailored properties for specific applications.

Temperature plays a significant role in geopolymer chemistry, affecting various aspects of the geopolymerization process and the resulting properties of geopolymers.

Higher temperatures can accelerate the geopolymerization reaction, leading to faster setting and hardening of geopolymers. The increased kinetic energy of molecules at higher temperatures enhances the mobility and reactivity of the reactants, facilitating the formation of geopolymer bonds. Elevated temperatures promote the formation and growth of the geopolymer gel network. As the temperature rises, the reaction rate increases, allowing the aluminosilicate precursors (such as metakaolin) to dissolve and react more readily with the alkaline activator solution. This leads to the formation of a denser and more interconnected geopolymer matrix. Temperature influences the development of the geopolymer structure and the arrangement of its constituents. Higher temperatures can promote the formation of ordered and crystalline structures within the geopolymer matrix. This can result in improved mechanical properties and increased resistance to environmental factors. Temperature affects the evaporation rate of water and the curing process of geopolymers. Elevated temperatures can accelerate the evaporation of water, potentially leading to faster drying and curing. However, excessively high temperatures may cause rapid evaporation, leading to

shrinkage, cracking, and reduced strength. Proper temperature control during curing is crucial to achieve optimal geopolymer properties.

Geopolymers exhibit good thermal stability, and their performance at high temperatures is of interest for various applications. Higher curing temperatures can contribute to the development of a more thermally stable geopolymer structure, enabling geopolymers to withstand elevated temperatures without significant structural degradation.

In Figure 2-15, the effect of curing time on different geopolymers can be observed.

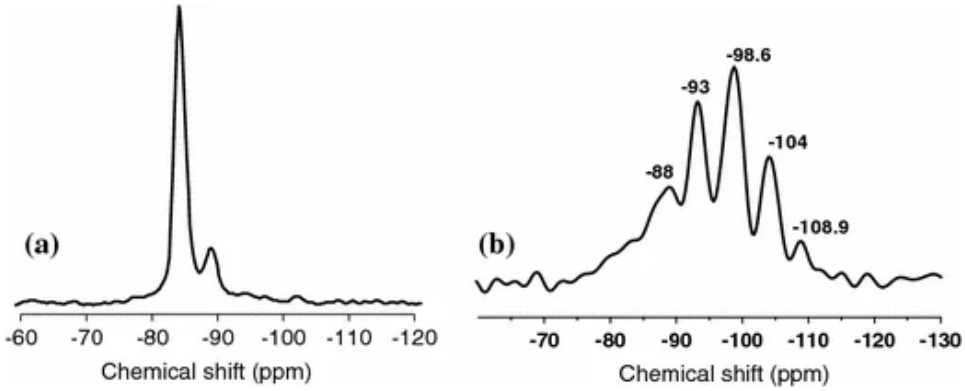

Fig.2-15 ^{29}Si MAS-NMR spectrum of (a) of Na-geopolymer with Si/Al ratio of 1.15 after 6 months of aging from alkali activated metakaolin (spectrum resembles faujasite); (b) alkaline aluminosilicate from alkali activated fly ash. 3 months at 85 °C (spectrum resembles Na-Chabazite) [Duxson et al. 2007].

2.4 Geopolymerization: dissolution and condensation

The interaction between alkali and aluminosilicates, such as clays, has been extensively studied for over a century. It has been scientifically demonstrated that when exposed to alkaline solutions, clays undergo a breakdown process, releasing dissolved silicates and aluminates. The extent of dissolution varies depending on the alkali concentration and type. For instance, clays are highly soluble in sodium hydroxide, insoluble in calcium hydroxide, and exhibit intermediate solubility with barium and potassium hydroxides. Among the clay minerals, sodium hydroxide has a stronger effect on kaolin-group minerals compared to montmorillonite, metabentonite, or illite. Additionally, metakaolin is more soluble than kaolin in alkaline environments. In alkaline solutions, various chemical reactions occur when aluminosilicate powders are immersed.

The mechanism is based on the thought of involvement of major three steps proposed by Davidovits for synthesis of geopolymer from

metakaolin MK-750 that takes place in seven steps [Davidovits J. 2020; Duxon et al. 2007]:

Step 1: Alkalination and formation of tetravalent Al in the side group sialate -Si-O-Al- $(OH)_3^-$ Na^+.

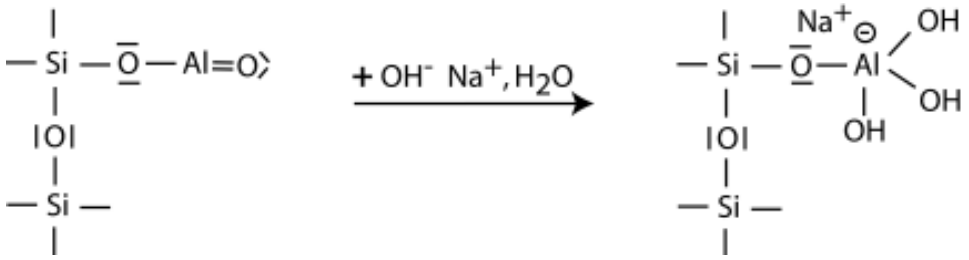

Fig.2-16 The nucleophilic attack of OH^- on Al^{3+}.

The nucleophilic attack of OH^- on Al^{3+} atom with the formation of a tetrahedral Al in the sialate group with a Na^+ in the role of charge balancing cation. The alkalination takes place in the first step of the mechanism which results in the tetravalent aluminum group formation.
Step 2: Alkaline dissolution starts with the attachment of the base OH- to the silicon atom, which is thus able to extend its valence sphere to the penta-covalent state.

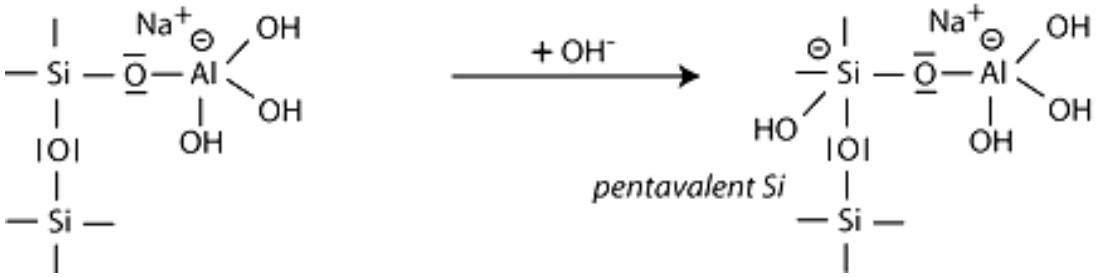

Fig.2-17 Attack of OH^- on Si to form pentavalent Si.

The hydroxide then attacks the attached silicon in the second step, taking it to a Pentacovalent state and a negatively charged central Si atom. This leads to the cleavage of the second Si as a silanol (Si-OH) group.

Step 3: The subsequent course of the reaction [Davidovits J. 2020; Duxon et al. 2007] can be explained by the cleavage of the siloxane oxygen in Si-O-Si through transfer of the electron from Si to O, formation of

intermediate silanol Si-OH on the one hand, and basic siloxo Si-O- on the other hand.

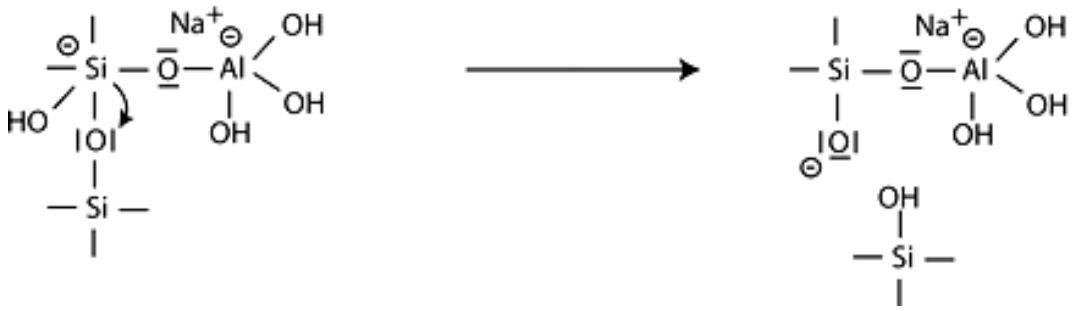

Fig.2-18 Formation of silanol (-Si-OH) and siloxo ($Si-O^-$) groups.

The third step of the mechanism leads eventually to the production of the ortho-sialate molecule.

Step 4: Further formation of silanol Si-OH groups and isolation of the ortho-sialate molecule, the primary unit in geopolymerisation.

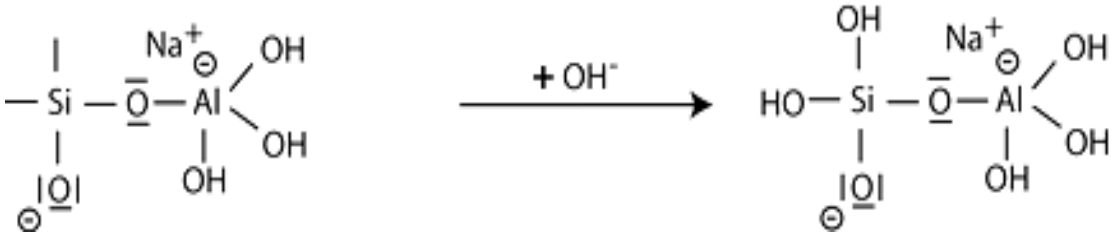

Fig.2-19 Attack of OH^- on -Si-O.

The ortho-sialate molecule shown as the product in the fourth step of the mechanism is the major subunit of geopolymerisation.

Step 5: Reaction of the basic siloxo Si-O- with the sodium cation Na^+ and formation of Si-O-Na terminal bond [Davidovits, 2008; Davidovits, 2020; Duxon et al. 2007].

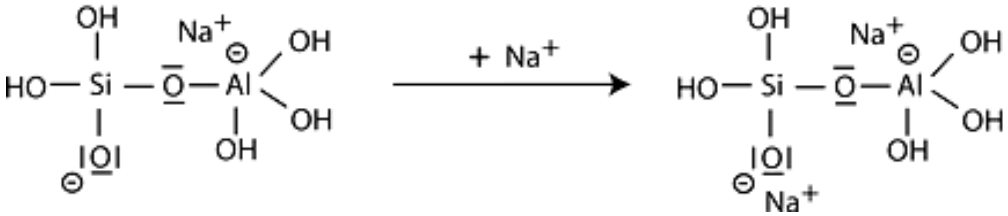

Fig.2-20 Formation of $Si-O^-$ - Na^+.

In the fifth step, the cation bonds with the basic siloxo, Si-O-, to form a terminal bond.

These steps show the polymerization of these subunits into the larger amorphous units that make up the final structure of the Na-poly(sialate-disiloxo).

Step 6a: Condensation between ortho-sialate molecules, reactive groups Si-O-Na and aluminum hydroxyl OH-Al, with production of NaOH, creation of cyclo-tri-sialate structure, whereby the alkali NaOH is liberated and reacts again and further polycondensation into Na-poly(sialate) nepheline framework.

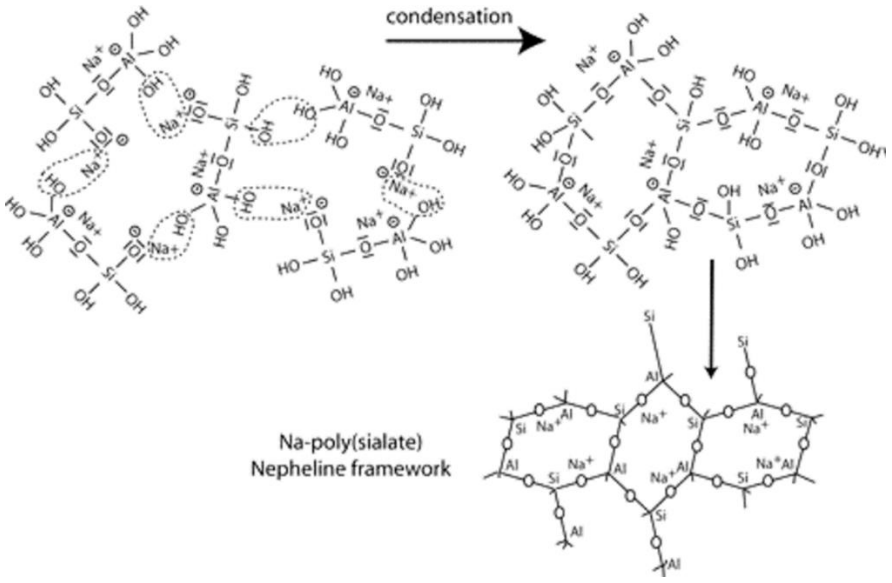

Fig.2-21 Polycondensation.

Step 6b: In the presence of waterglass (soluble Na- polysiloxonate) one gets condensation between di-siloxonate Q1 and ortho-sialate molecules, reactive groups Si-ONa, Si-OH and aluminum hydroxyl OH-Al, creation of ortho-sialate-disiloxo cyclic structure, whereby the alkali sodium hydroxide is liberated and reacts again [Davidovits J. 2008, 2020; Duxon et al. 2007].

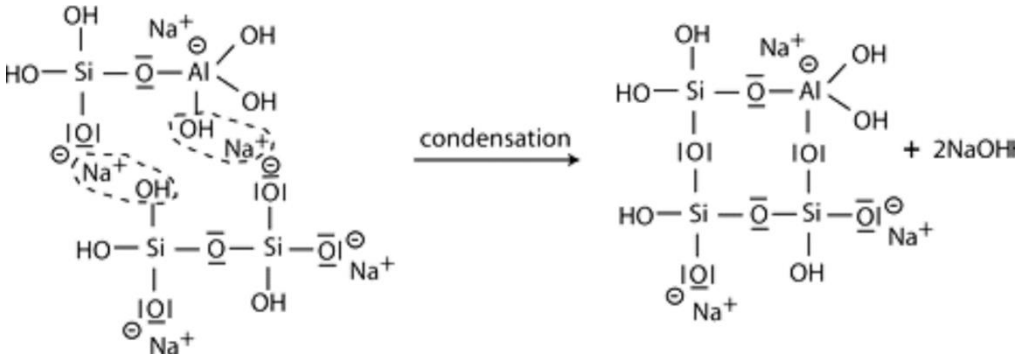

Fig.2-22 Liberation of NaOH.

Extensive research has been carried out, but still there are difficulties in analyzing the heterogeneous nature of most of the aluminosilicate sources such as metakaolin, fly ash and the amorphous nature of the resultant product formed.

It is important to remember that the dissolution rate of metakaolin is slower at lower temperatures (20°C), resulting in slower polymerization of the dissolved species. As the temperature increases to 35°C, the polymerization process accelerates, leading to a decline in the concentration of free Si^{4+} and Al^{3+} species. At 50°C, a significant amount of Si^{4+} and Al^{3+} species is formed, rapidly polymerizing into gels that cover the particle surface, inhibiting further dissolution.

Higher temperatures (90°C-100°C) and lower pH ranges (pH < 10) favor the formation of zeolites but can reduce the final mechanical performance [Khale et al. 2007]. Curing at higher temperatures for extended periods beyond a few hours may impact the development of compressive strength. Strength tends to plateau after a curing period of 48 hours, in contrast to ordinary Portland cement (OPC), where strength decreases with increasing water-to-cement ratio. Fresh geopolymeric material exhibits good workability even at low liquid-to-solid ratios (<0.4). The strength of the material depends significantly on the Si:Al and Na:Al ratios, with higher reactive silica content promoting the formation of a greater amount of alkali aluminosilicate gel and consequently enhancing mechanical strength.

2.5 Geopolymer structure

The chemical composition of a geopolymer material is similar to natural zeolitic materials but its microstructure is amorphous [Davidovits, J. 2008]. The polymerization process involves a substantially fast chemical

reaction under alkaline conditions on Si-Al minerals, resulting in three-dimensional polymeric chains and ring structures consisting of Si-O and Al-O bonds [Davidovits, J. 2008, 2020]. It is proposed that the geopolymer gel can diffuse into larger interstitial spaces between the particles [van Deventer J.S.J. 2002]. A proposed structure of geopolymer is shown in the following Figure 2-23:

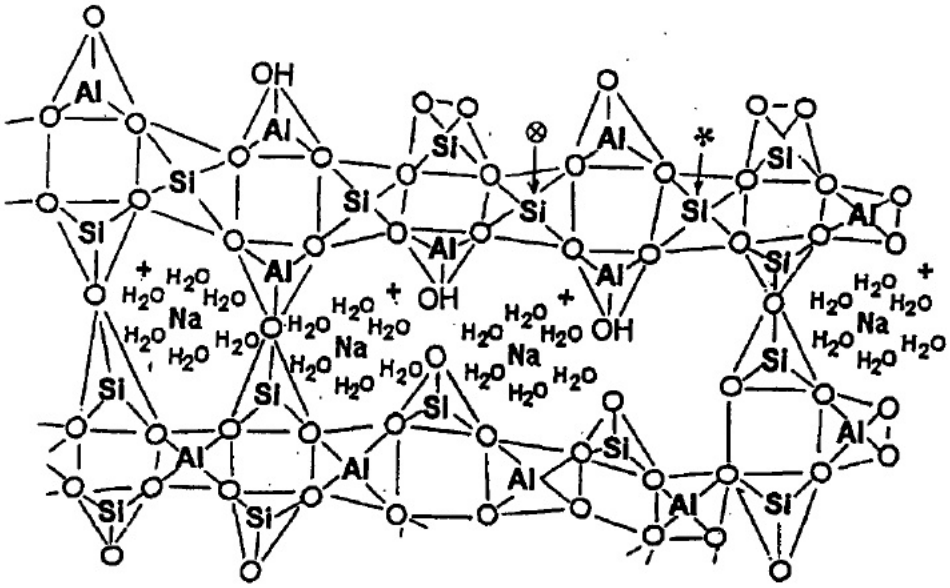

Fig.2-23 Geopolymer structure.

The polysialate network is a framework three-dimensional structure of SiO_4 tetrahedral stacking on top of another in all directions with varying degrees of aluminate substitution.

The ^{27}Al MAS-NMR study has revealed that all of the Al^{3+} in the polysialate network is in the IV-coordination. Consequently, cations such as Na, K and Ca are required for charge neutralisation on the negatively charged AlO_4 tetrahedral units. The term 'sialate' is an abbreviation for silicon-oxo-aluminate and is used here to describe the bonding of silicon by bridging oxygen. The proposed empirical formula of poly(sialates) is:

$$Mp\ \{(SiO_2)zAlO_2\}p\ .w\ H_2O$$

where M = Na, K and/or Ca, p is the degree of polycondensation, z is either 1, 2 or 3 and w describes the water content of the composite. The poly(sialate) oligomers are described as chain and ring polymers with Si^{4+} and Al^{3+} in IV-fold coordination with oxygen and range from amorphous

to semi-crystalline. The oligomeric building units are depicted below in the following Figure 2-24:

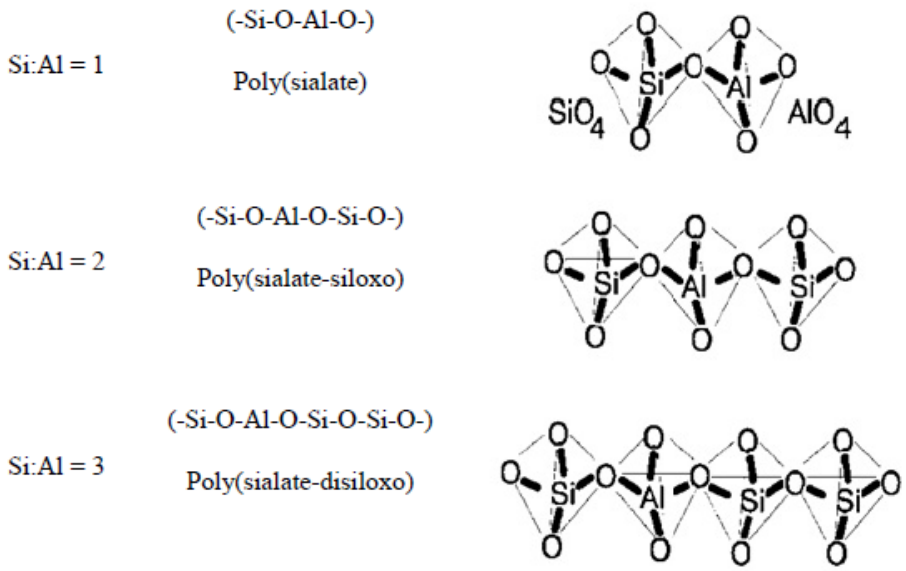

Fig.2-24 Poly(sialate) description [Davidovits, J. 2008].

The different types are abbreviated PS for poly(sialate), PSS for poly(sialate-siloxo), and PSDS for poly(sialate-disiloxo). The subunits alternate between Si and Al units covalently share oxygen atom in order to make the larger macromolecules called geopolymers. The presence of an alkali metal as a positive ion is necessary to the geopolymer structure because it balances the negatively charged aluminate in IV-fold coordination [Davidovits et al. 1998].

Silicon is always 4-coordinated, while aluminum ions can be 4 or 6-coordinated in alumino-silicate structure. The coordination number of aluminum in the starting materials influences on its eventual bonding in the matrix. A highly reactive intermediate gel phase is believed to form by copolymerization of individual aluminoand silicate species. There are quite few studies about the behavior of this gel phase and the extent to which the nature of the starting materials and the actual concentrations in solution are affecting the formation and setting of this gel phase [Xu et al. 2000].

2.5.1 Microstructure and chemical resistance (acid exposure)

The microstructure and chemical resistance of geopolymers have gained significant attention in recent years. Geopolymers, as alternative binder

materials to traditional cement-based systems, offer unique microstructural characteristics and exhibit promising resistance to acid attack. The microstructure of geopolymers is primarily composed of an amorphous three-dimensional network formed through the geopolymerization process. This network consists of interconnected polysialate and polysialate-siloxo species, resulting in a compact and dense structure. The specific composition and arrangement of these species contribute to the overall properties and performance of geopolymers. When subjected to acid attack, the microstructure of geopolymers can undergo various interactions and transformations. The extent and nature of acid attack depend on several factors, including the type and concentration of the acid, exposure time, temperature, and the specific composition of the geopolymer. Geopolymers generally exhibit good resistance to acid attack due to their unique microstructure and chemical composition. The alkaline nature of geopolymers helps neutralize the acid and prevents the dissolution of the binder matrix. The compact and dense structure of geopolymers also hinders the penetration of acid molecules, reducing the likelihood of chemical degradation.

To evaluate the acid resistance of geopolymers, researchers employ various experimental techniques. Immersion tests, where geopolymers are immersed in acid solutions for a specific duration, are commonly used to assess the weight loss and changes in mechanical properties. Surface analysis techniques, such as Scanning electron microscopy (SEM) and X-ray diffraction (XRD), provide insights into the morphological and compositional changes that occur during acid attack. Studies have shown that geopolymers exhibit considerable resistance to a wide range of acids, including mineral acids such as sulfuric acid and hydrochloric acid. The precise level of resistance depends on factors such as the specific geopolymer formulation, curing conditions, and the presence of additional additives or reinforcements.

In 2001 Allahverdi and Skvara [Allahverdi et al. 2001a, 2001b, 2005] postulated that the mechanism of corrosion of hardened paste of geopolymer cement in solution of nitric acid involves two steps:

The first step involves a leaching process in which the alkali cations included in the aluminosilicate framework to charge-balance the tetrahedral aluminium are exchanged by H^+ ions from acidic solution. This occurs along with electrophilic attack by acid protons on framework

Si-O-Al bonds, resulting in the ejection of tetrahedral aluminium from the aluminosilicate framework:

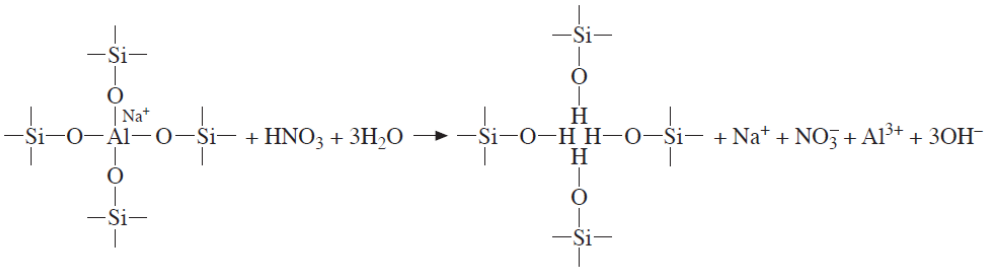

Fig.2-25 Leaching process [Allahverdi et al. 2001].

In the second step the framework vacancies are mostly reoccupied by silicon atoms resulting in the formation of an imperfect highly siliceous framework. The ejected aluminium, converted to octahedral coordination, mostly accumulates in the intra-framework space.

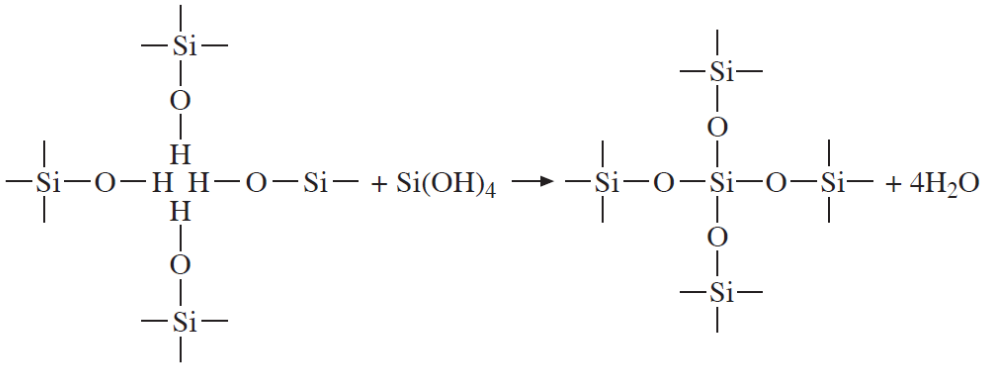

Fig.2-26 Formation of the imperfect siliceous framework and ejection of Al [Allahverdi et al. 2001a, 2001b, 2005].

Additionally, researchers continue to explore methods to further enhance the acid resistance of geopolymers through material modifications and optimization. The acid resistance of geopolymers makes them suitable for various applications, particularly in environments where acid exposure is anticipated. For instance, in chemical storage systems, geopolymers can be utilized as linings or coatings to protect against acid corrosion. In the construction industry, geopolymers can be employed in acid-prone environments, such as wastewater treatment facilities or industrial settings where acidic solutions are present. To enhance chemical resistance, researchers have explored strategies such as incorporating specific additives, tailoring the geopolymer composition, and optimizing curing conditions. Additives

such as silica fume or metakaolin can improve the chemical resistance of geopolymers by densifying the microstructure or altering the pore size distribution. Modifying the geopolymer composition by adjusting the ratio of alkali activators and precursor materials can also enhance chemical resistance. Additionally, optimizing curing conditions, including temperature and duration, can influence the formation of a more chemically stable geopolymeric.

The unique microstructural characteristics, combined with the alkaline nature and dense structure of geopolymers, contribute to their favourable resistance against acids. Geopolymers offer a promising alternative to traditional cement-based materials in acid-prone applications, enabling sustainable and durable solutions in various industries.

2.6 Application of geopolymer materials

Geopolymer have found applications in various fields, ranging from construction and infrastructure to aerospace and environmental sectors.

- Construction and Infrastructure

Geopolymers can be used as a replacement for traditional Portland cement-based concrete. Geopolymer concretes offer improved strength, durability, and chemical resistance compared to conventional concretes. Geopolymer can be also used for the production of precast elements such as beams, columns, and panels. These elements exhibit high early strength and rapid curing, allowing for faster construction processes.

Geopolymer-based repair mortars and grouts are used for the rehabilitation of deteriorated concrete structures. They provide excellent adhesion, low shrinkage, and high chemical resistance, extending the lifespan of existing infrastructure.

- Fire and heat resistance

Geopolymers have excellent fire resistance properties and can be used as fireproofing materials for structural elements, such as steel columns and beams. Geopolymer coatings can provide insulation and protection against high temperatures.

Geopolymer materials can withstand extreme temperatures, making them suitable for lining furnaces, kilns, and incinerators. They offer

superior thermal stability, corrosion resistance, and insulation properties.

- Aerospace

Geopolymers are used in the development of thermal protection systems for spacecraft and re-entry vehicles. They exhibit low thermal conductivity and excellent ablation resistance, protecting the underlying structures from high temperatures during atmospheric re-entry.
Lightweight Composites: Geopolymer-based composites are being explored as lightweight and high-strength materials for aerospace applications. They can be used in the manufacturing of structural components, including aircraft interiors and engine parts.

- Environmental applications

Geopolymerization provides an effective method for stabilizing and immobilizing various industrial byproducts and hazardous wastes, such as fly ash, slag, and mining residues. Geopolymer matrices encapsulate and bind the waste materials, preventing leaching and reducing environmental impact.
Geopolymer materials can be used for water and wastewater treatment applications. They can remove heavy metals and contaminants from water through adsorption or ion exchange processes.
Geopolymers are employed in soil stabilization to improve the engineering properties of weak or problematic soils. They can enhance soil strength, reduce swelling or shrinkage, and provide erosion control in geotechnical projects.
These are just a few examples of the wide range of applications for geopolymer materials. The versatility, durability, and eco-friendly nature of geopolymer matrices make them a promising alternative to traditional materials in numerous industries, contributing to sustainable development and resource conservation.

2.7 Geopolymer with waste material

Researchers have dedicated their efforts to exploring the feasibility of incorporating diverse waste materials into geopolymer formulations [Podolsky et al. 2021; Mohajerani et al. 2019; Mucsi et al. 2014; Ren et al. 2021], leading to innovative solutions for waste management and promoting sustainable construction practices.

The integration of waste materials into geopolymer formulations has garnered considerable attention from researchers and scientists. These waste materials encompass a wide range of industrial byproducts and discarded materials that would otherwise be sent to landfills or require separate disposal processes. Examples of such waste materials include fly ash, slag, silica fume, and various other residues generated by different industries. By incorporating these waste materials into geopolymer formulations, researchers aim to address both environmental concerns associated with waste disposal and the need for sustainable construction materials. Firstly, it tackles the pressing issue of waste management by diverting waste materials from conventional disposal methods. Secondly, the integration of waste materials in geopolymer formulations presents an opportunity to enhance the overall performance and cost-effectiveness of geopolymer composites. The specific properties of waste materials, such as their chemical composition and physical characteristics, can be leveraged to tailor the properties of geopolymer products.

Furthermore, geopolymer composites incorporating waste materials have demonstrated the potential to rival or even surpass the performance of conventional cement-based materials. The utilization of waste materials in geopolymer technology represents a significant advancement in the field of sustainable construction practices. By incorporating various waste materials into geopolymer formulations, researchers strive to address waste management challenges, reduce carbon emissions, and optimize the performance and cost-effectiveness of geopolymer composites. With further research and implementation, geopolymer composites with waste materials have the capacity to revolutionize the construction sector by providing sustainable and cost-effective alternatives to traditional cement-based materials.

2.7.1 Corundum and its use

Corundum is a naturally occurring mineral and a crystalline form of aluminium oxide (Al_2O_3). It is highly valued for its exceptional hardness, heat resistance, and various other properties. Corundum finds widespread applications in industries ranging from abrasives and refractories to electrical insulation and gemstones. Understanding the structure of corundum is essential to comprehend its properties and applications fully. Corundum is an oxide mineral

that crystallizes in the hexagonal crystal system (fig. 2-27 and 2-28). It is commonly found in a variety of colours, including colourless, white, gray, brown, blue, yellow, and red. The red variety of corundum is known as ruby, while all other colours are classified as sapphires. Corundum exhibits a high degree of transparency in gem-quality specimens, making it a sought-after gemstone. The crystal structure of corundum is composed of close-packed oxygen ions (O^{2-}) arranged in a hexagonal close-packed (hcp) lattice.

Crystal Data: Hexagonal. *Point Group:* $\bar{3}\,2/m$. Crystals hexagonal, prismatic or steeply dipyramidal, tabular, rhombohedral, rarely acicular, typically rough, to 1 m; sectorially striated on $\{0001\} \parallel \{10\bar{1}1\}$. Also granular, massive. *Twinning:* Common lamellar $\parallel \{10\bar{1}1\}$, may be an exsolution phenomenon. Contact or penetration twins on $\{0001\}$ or $\{10\bar{1}1\}$, rare.

Physical Properties: *Cleavage:* Partings on $\{0001\}$ and $\{10\bar{1}1\}$, from exsolved böhmite. *Fracture:* Uneven to conchoidal. *Tenacity:* Brittle, tough when compact. Hardness = 9 D(meas.) = 3.98–4.10 D(calc.) = 3.997 May fluoresce or phosphoresce under UV.

Optical Properties: Transparent to translucent. *Color:* Colorless, gray, brown; pink to pigeon-blood-red, orange, yellow, green, blue to cornflower blue, violet; may be color zoned, asteriated; colorless, pale bluish or reddish in transmitted light. *Streak:* White. *Luster:* Adamantine to vitreous; pearly on partings.
Optical Class: Uniaxial (–); commonly anomalously biaxial. *Pleochroism:* Weak; stronger when colored, O = pale to deep blue, E = blue-green to yellow-green, or O = deep purple, E = pale yellow. *Absorption:* $O > E$. $\omega = 1.767$–1.772 $\epsilon = 1.759$–1.763 $2V(meas.) = \leq 58°$

Cell Data: *Space Group:* $R\bar{3}c$ (synthetic). $a = 4.7540(5)$ $c = 12.9820(6)$ $Z = 6$

X-ray Powder Pattern: Synthetic. (ICDD 42-1468).
2.085 (100), 2.551 (97), 1.6014 (82), 3.48 (70), 1.3738 (45), 2.379 (42), 1.7398 (42)

Chemistry: Nearly pure Al_2O_3, with traces of Fe, Ti, and Cr.

Fig.2-27 Structural Properties and Surface Characteristics on Aluminum Oxide Powders [Shirai et al. 2009].

The aluminium ions (Al^{3+}) occupy the octahedral sites within this lattice (Fig.2-28). Each aluminium ion is surrounded by six oxygen ions, forming an octahedral coordination environment. The crystallographic unit cell of corundum consists of three layers stacked on top of each other. The stacking sequence is ABAB, where 'A' represents the aluminium layer and 'B' represents the oxygen layer. The oxygen layers are densely packed, with oxygen ions forming a hexagonal lattice. The aluminium ions are situated in the octahedral sites between the oxygen layers.

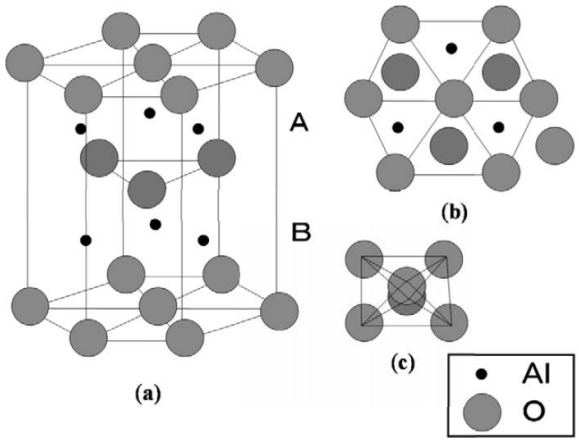

Fig.2-28 Corundum structure in α-Al_2O_3, (b) top view of the corundum structure, and (c) octahedral structure of α- Al_2O_3 [Shirai et al. 2009].

The coordination geometry around each aluminium ion in corundum is octahedral. The oxygen ions form six equidistant bonds with the central aluminium ion, resulting in a stable crystal structure. This coordination arrangement contributes to the hardness and strength of corundum, as the closely packed structure resists deformation and dislocation. The crystal lattice of corundum is responsible for its exceptional hardness, which is second only to diamond on the Mohs scale. The strong ionic bonds between the aluminium and oxygen ions contribute to its resistance to scratching and wear. Additionally, the crystal structure of corundum imparts its anisotropic optical properties.

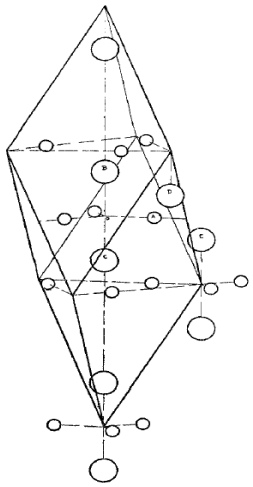

Fig.2-29 The crystal structure of corundum [Pauling L. 1925].

Depending on the crystallographic orientation, corundum exhibits pleochroism, meaning it can display different colours when viewed from different angles. Corundum is a hexagonal crystal system

mineral composed of aluminium oxide (Al_2O_3). Its crystal structure consists of closely packed oxygen ions with aluminium ions occupying octahedral sites. This arrangement contributes to the hardness, heat resistance, and optical properties exhibited by corundum. Understanding the structure of corundum helps elucidate its unique properties and its suitability for a wide range of applications, from abrasives and refractories to gemstones and electrical insulation.

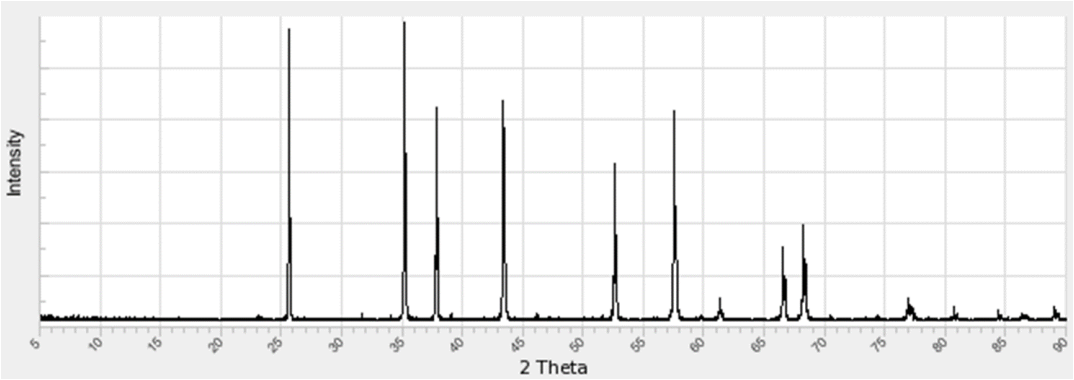

Fig.2-30 XRD spectra of pure corundum (RRUFF database).

Recycled corundum, a residual powder generated from industrial processes such as abrasive manufacturing and refractory production, has gained attention as a potential waste material for geopolymer production. Corundum is primarily composed of Aluminium oxide (Al_2O_3) and possesses high chemical stability, making it an attractive candidate for geopolymer applications. Utilizing recycled corundum as a source of alumina in geopolymer formulations can contribute to the development of geopolymer materials with enhanced mechanical properties. Studies have focused on optimizing the incorporation of recycled corundum into geopolymer matrices, evaluating its impact on the final properties of the geopolymer composites. The addition of recycled corundum has shown potential in improving the strength [Pławecka et al. 2021; Zhao et al. 2007], durability, and thermal properties of geopolymer materials, thus promoting their wider adoption in various construction and infrastructure projects.

2.7.2 Cork and its use

Cork is a versatile and sustainable material that has been utilized by humans for thousands of years. It is derived from the bark of the cork oak tree (Quercus suber) (Fig.2-31) and has a wide range of applications due to its unique properties. Cork is known for its

lightweight nature, resilience, thermal insulation, and excellent sealing capabilities. Let's explore a description of cork and its structure.

Cork is a cellular material that is composed of suberose cells, which are produced by the cork cambium layer of the cork oak tree. These cells are filled with air and a waxy substance called suberin, which gives cork its characteristic properties. The cellular structure of cork consists of numerous small air-filled spaces, called cells or vesicles, that are interconnected by thin walls. These vesicles give cork its distinctive texture and compressibility.

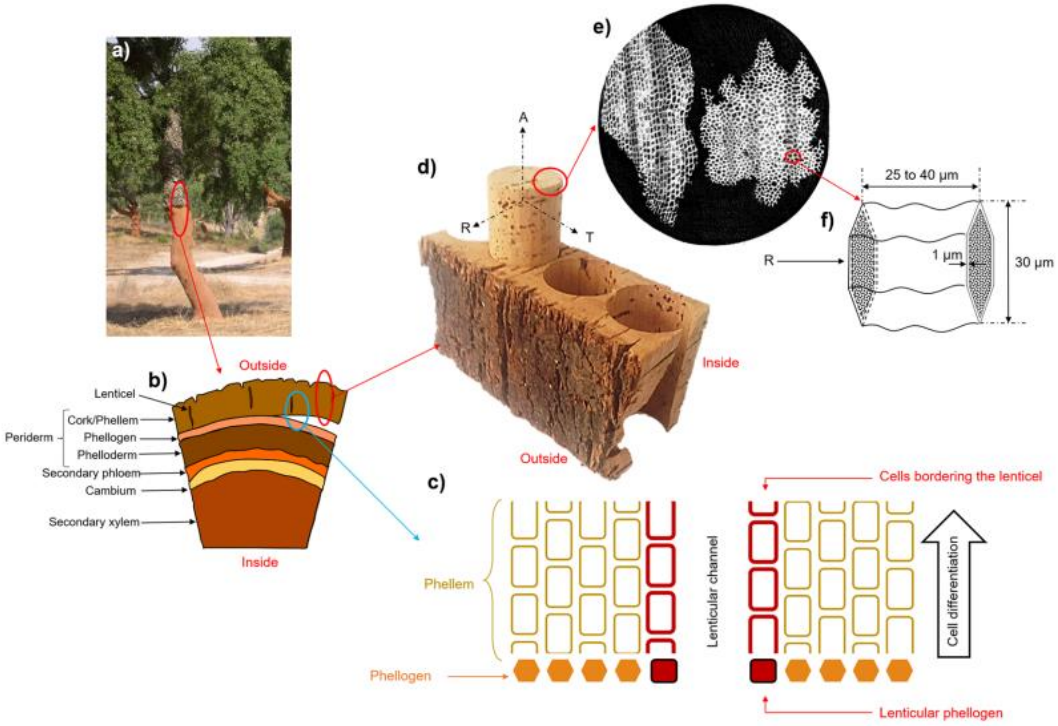

Fig.2-31 Cork composition and origin.

The natural composition of cork gives it several unique qualities. It is lightweight, buoyant, and highly elastic, allowing it to recover its shape even after compression. Cork is also impermeable to liquids and gases, making it an excellent material for sealing and insulation applications. It possesses good thermal and acoustic insulation properties, as the air-filled cells hinder the transfer of heat and sound.

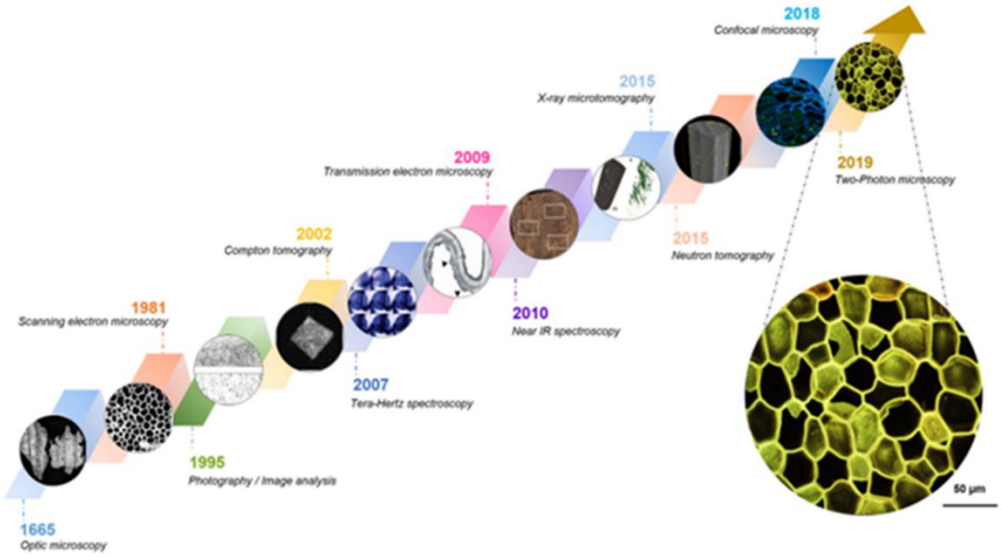

Fig.2-32 Study of cork over the years with the advancement of techniques.

Cork is resistant to rot, mildew, and pests, making it durable and long-lasting. It is also fire-resistant and emits minimal smoke and toxic gases when burned, enhancing its safety characteristics.

The cellular structure of cork is responsible for its exceptional properties. Each cell is shaped like a hexagonal prism, with rounded edges and an irregular surface. The cells are packed closely together, forming a three-dimensional network of interconnected compartments.

The walls of the cork cells are primarily composed of suberin, a waterproof and waxy substance that provides impermeability to liquids and gases. The suberin also contributes to the elasticity and resilience of cork. The air-filled cells, along with the suberin-rich cell walls, create a low-density material with excellent insulation capabilities.

The structure of cork allows it to be easily compressed and deformed, while also enabling it to spring back to its original shape when the pressure is released. This property makes cork ideal for applications such as bottle stoppers, gaskets, flooring, and insulation materials.

Cork is a versatile and sustainable material with a unique cellular structure. Its lightweight nature, resilience, thermal insulation properties, and sealing capabilities have made it a popular choice for various applications. The interconnected air-filled cells and suberin-rich walls contribute to its distinctive properties, providing benefits such as flexibility, impermeability, and durability.

Cork can be utilized in geopolymer applications as a lightweight aggregate or filler material [Novais et al. 2019; Sudagar et al. 2018; Sudagar et al. 2023; Rosper et al. 2017]. Geopolymer is a cementitious material that uses an aluminosilicate precursor and an alkaline activator to form a binder.

Incorporating cork into geopolymer formulations offers several advantages:

Lightweight Geopolymer: Cork is a lightweight material with low density, making it an excellent choice for reducing the overall weight of geopolymer-based products. This is particularly beneficial in applications where weight reduction is desirable, such as in lightweight concrete panels, precast elements, or thermal insulation boards.

Improved Thermal Insulation: Cork possesses natural thermal insulation properties due to its cellular structure and trapped air pockets. When incorporated into geopolymer, it enhances the thermal insulation characteristics of the material. This is advantageous in geopolymer-based insulation products, such as insulation boards or coatings used to reduce heat transfer in buildings or industrial equipment.

Reduced Shrinkage and Cracking: The use of cork in geopolymer formulations can help mitigate shrinkage and cracking issues. Cork's elasticity and resilience provide flexibility to the geopolymer matrix, minimizing the risk of cracking due to shrinkage during the drying and curing process.

Enhanced Impact Resistance: The cushioning effect of cork can improve the impact resistance of geopolymer-based materials. This can be beneficial in applications such as flooring systems or structural elements that require resistance to impact or dynamic loading.

Environmental Sustainability: Cork is a renewable and eco-friendly material. Its utilization in geopolymer helps to promote sustainable construction practices by reducing the reliance on non-renewable materials. Additionally, cork harvesting from cork oak trees contributes to the preservation of forest ecosystems.

It is important to note that the incorporation of cork in geopolymer formulations requires appropriate testing and optimization to ensure compatibility, adhesion, and mechanical properties of the resulting composite. The specific proportions and methods of incorporating

cork into geopolymer can vary depending on the desired application and the geopolymer formulation being used.

Overall, incorporating cork into geopolymer offers the potential to enhance the properties and sustainability of the resulting material, making it suitable for various construction, insulation, and structural applications.

Waste cork, generated from the cork industry and other related activities, has also emerged as a promising waste material for geopolymer production. Cork is predominantly composed of cellulose and lignin, which can act as potential precursors for the synthesis of geopolymer matrices. The incorporation of waste cork into geopolymer formulations offers several advantages, including improved thermal insulation properties and reduced environmental impact. Studies have investigated the influence of waste cork content on the properties of geopolymer composites, such as density, porosity, and compressive strength. The results have demonstrated the potential of waste cork as a valuable additive in geopolymer production, providing opportunities for sustainable waste management and the development of lightweight and energy-efficient construction materials.

3. Experimental

As outlined in the introduction, this chapter delves into the planning, preparation, and characterization of the initial materials, as depicted in Figure 3-1. Following the project planning phase, the focus shifted to the characterization of the raw powder materials metakaolin, post-abrasion corundum, post-erosion corundum, and waste cork. Once these powders were thoroughly characterized and their non-hazardous nature confirmed, the attention turned to the preparation and characterization of activating solutions, namely NaOH and sodium silicate. Subsequently, acidic solutions were prepared.

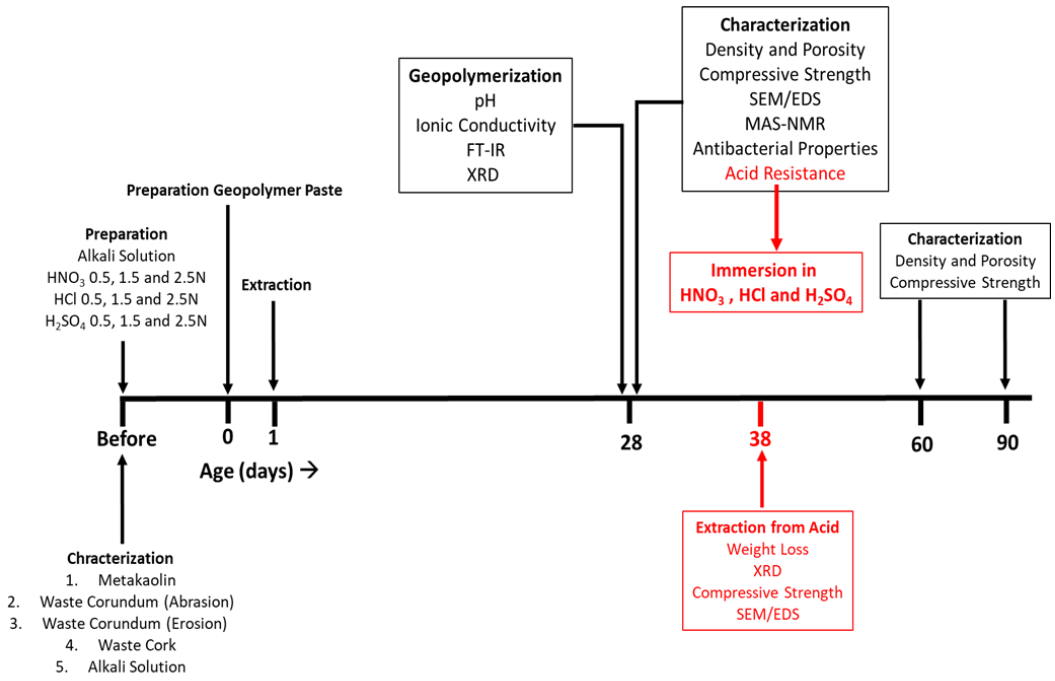

Fig.3-1 Research plan.

In this chapter, an in-depth exploration of techniques employed in the thesis project is reported.

3.1 Powders characterization methods

3.1.1 Particle size analysis

The instrument used is the dynamic light scattering-DLS grain sizer Mastersizer 2000 (Malvern Instruments Ltd., Malvern, UK).

3.1.2 Ionic conductivity and pH

In order to evaluate the overall chemical stability of raw powders, the immersion in water was tested accordingly to ref. [Dal Poggetto et al. 2021] MilliQ water (1:10 = solid: water weight ratio) was added to the grounded geopolymer samples. After stirring the solution, a short time was waited to sediment the solids before analyses. Ionic Conductivity measurements were performed on the eluates with Crison GLP31 and GLP 21 (Hach Lange Spain, S.L.U, Barcelona, Spain), respectively, at t1=0 h, t2=5 min, t3=10 min, t4=30 min, t5=2 h, t6=4 h, t7=6 h, t8=24 h and t9=48 h.

3.1.3 X-ray diffraction patterns

Crystalline phases of the raw material powders were identified via X-ray diffraction (XRD) attained with a X'Pert PRO, PANAlytical, (Malvern Panalyical Ltd., Malvern, UK) diffractometer operated at 40 kV and 40 mA using Cu-Kα radiation (Ni filtered). Diffraction patterns were collected by the X'Celerator detector from 5 to 70° 2θ with a step size of 0.02° 2θ and a counting time of 3 s. It should be noted that the as-received recycled corundum powders were not finely ground to avoid contamination from milling media as the corundum is an extremely hard abrasive (value of 9 on the Mohs hardness scale). The cork powder was not milled too. Mineral phases were identified by comparing the experimental peaks with reference patterns (DIFFRAC plus EVA software, 2005 PDF2, Bruker, Billerica, MA, USA). The powders were analyzed without any kind of pre-treatment.

3.1.4 Fourier transform infra-red spectroscopy

FTIR analysis was performed on raw materials powders with Prestige21 Shimadzu machine equipped with a DTGS KBr (deuterated triglycine sulfate with potassium bromide windows) detector. The analysis was performed in the range of 400-4000 cm^{-1} and with a resolution of 2 cm^{-1} (60 scans). The KBr disks used for the analysis were realised with 2 mg of sample and 198 mg of KBr. FTIR spectra were elaborated by IRsolution and Origin 9 softwares. The powders were analyzed without any kind of pre-treatment and without having been milled.

3.1.5 Scanning electron microscopy

Microstructure observations were conducted by ESEM (ESEM-Quanta200-FEI) equipped with EDS to evaluate the structure of all raw material powders. Before SEM analysis the freshly fractured surface of each specimen was coated with an Au sputtered layer. The raw powders were analysed without any kind of pre-treatment and without having been milled.

3.1.6 ICP-OES and ICP-MS

The ability to leach heavy metals from all powders was checked according to the EN 12457-2:2004 ("Characteri-sation of waste - Leaching - Compliance test for leaching of granular waste materials and sludges - Part 2: One stage batch test at a liquid to solid ratio of 10 l/kg for materials with particle size below 4 mm (without or with size reduction)").

Powders were placed in bi-distilled water with 1:10=solid:water weight ratio, and maintained for 24 h. After the recovery of the filtrated ($d<0.45$ μm) leachates solutions, they were acidified with HNO_3 (69%) solution to pH=2. Then, according to EN ISO 11885:2009 ("Water quality - Determination of selected elements by inductively coupled plasma optical emission spectrometry (ICP-OES"), ionic heavy metal concentrations were determined by ICP-OES and ICP-MS (Inductively coupled plasma-mass spectrometry) (Agilent, Santa Clara, USA). All the ionic metal concentrations are expressed as ppm. The Limit Of Quantitation (LOQ) (the concentration at which imprecision (coefficient of variation) of the method is 5%) for Al, B, Ba, Fe, Mn, Sb and Zn was 5 ppb, the Limit Of Detection (LOD) (the lowest concentration of the measurand that can be detected at a specified level of confidence) of Be, Cd, Co, Cr, Cu, Mo, Ni, Pb, Se, Sn and V was 2 ppb, while the LOQ of Si and Ca was 500 ppb.

3.1.7 Optical microscopy

Optical microscopy (Leica EZ4D, Leica Microsystems, Germany) with 8×, 20× and 35× magnifications was used for the morphological description of waste corkpowder and waste cork composites. The light used is in the visible spectrum. The resolving power of the optical microscope is 0.2 μm. The test was carried out on raw powders and samples aged for over 28 days. Image elaboration to extract the

surface area was IMAGEJ, 1.52v, (Open Source, copyright by the author W. Rasband, National Institute of Mental Health, Bethesda, Maryland, USA.). The powders were analyzed without any kind of pre-treatment and without having been milled.

3.1.8 NMR spectroscopy

For liquid state NMR, all samples (7mL) were transferred in 5 mm tubes together with a capillary filled with deuterium oxide (D_2O) in order to lock the field frequency. The spectra were recorded at 300 K by means of a Bruker Avance II 400 spectrometer operating at 400.15 and 79.49 MHz for the 1H and ^{29}Si nuclides respectively and equipped with an inverse broadband (BBI) probe. ^{29}Si spectra were acquired using a 7.5 µs pulse, a delay time of 10 s, and 8000 scans.

Solid state NMR experiments were performed by the spectrometer described above using a 2.5 mm F/H-X CPMAS probe at 79.49 and 104.26 MHz for the ^{29}Si and ^{27}Al nuclides respectively. ^{29}Si MAS spectra were acquired with a MAS spinning speed of 15 kHz, 2048 scans, a delay time of 60 s and a pulse of 4.5 µs. ^{27}Al MAS spectra were acquired with a MAS spinning speed of 15 kHz, 128 scans, a delay time of 2 s and a pulse of 1 µs.
All spectra were processed using MestReNova.

3.2 Geopolymer characterization

3.2.1 Ionic conductivity and pH

In order to evaluate the overall chemical stability of the 3D aluminosilicate network reticulated within the geopolymer final products, the solid samples were placed in water and the conductivity read as indicated in section 3.1.2.

3.2.2 X-ray diffraction patterns

The procedure is the same as in Section 3.1.3. In this case the all the samples were broken and ground before being analyzed.

3.2.3 Fourier transform infra-red spectroscopy

The procedure is the same as in Section 3.1.4. In this case the all the samples were broken and ground before being analysed.

3.2.4 Scanning electron microscopy

Microstructure observations were conducted by ESEM (ESEM-Quanta200-FEI) equipped with EDS to evaluate the structure of the formation of geopolymeric amorphous phase and the presence of unreacted particles of raw waste powders and aluminosilicate in the hardened samples after 28 days of curing. Before SEM analysis the freshly fractured surface of each specimen was coated with an Au sputtered layer.

3.2.5 ICP-OES and ICP-MS

The procedure is the same as in Section 3.1.6, but in this case the samples, crushed and sieved to particle sizes less than 4 mm, were placed in bi-distilled water with 1:10 = solid:water weight ratio, and maintained for 24 h.

3.2.6 MAS-NMR spectroscopy

The procedure is the same as in Section 3.1.8 for the solid state, furthermore all the samples were broken and ground before being analyzed.

3.2.7 TGA and TDA measurements

Differential thermal analysis-thermo-gravimetry (TGA/DTA) was performed using a LabsysEvo 1600–Setaram apparatus (Setaram, Calurie, France) with a double thermocouple Platinum/Platinum-Rhodium 10%, the thermocouples were calibrated by using, as calibration materials, high-purity elements such as Ag, Au. About 30 mg of powdered sample were placed in an open alumina crucible and heated from 30 °C to 1250 °C at 10 °C/min under argon flux (60 mL min−1); due to the origin of the sample (waste), which could be affected by impurities, the measurements were carried out under inert atmosphere, to avoid side reactions. In the temperature range considered, the error on mass loss determination was 0.2 % and in temperature determination 0.5 %.

3.2.8 Thermal conductivity

The thermal conductivity of GP0 and GP-10CW was measured through a heat flow meter (HFM Lambda, Netzsch-Gerätebau GmbH, Selb, Germany) after 28 days of curing. The equipment was calibrated

with certified reference materials (NIST SRM 1450d) and it is designed according standards ASTM C518, ISO 8301, DIN EN 12664 (not HFM Large), DIN EN 12667, JIS A1412. The mean thermal conductivity was de-rived as the average over three measurements.

Fig.3-12 "HFM Lambda" della NETZSCH.

3.2.9 Compressive strength measurement

To test the mechanical properties of the MK-based geopolymers with 0, 10% and 20%wt of recycled corundum, compression tests were performed with an Instron 5567 Universal Testing Machine (Norwood, MA, USA) after 28 days of curing. For the tests, cylindrical samples with a diameter of 20 mm and a height of 40 mm were used. The load (30 kN load limit) was applied and increased by displacement rate of 1 mm/min. The tests were executed in displacement control mode at a constant loading velocity and no preload. They were stopped after obtaining three valid tests for each different geo-polymer composition. Compressive strength values are assumed to be the mean value of three tests attended with the 2% variance.

3.2.10 Antibacterial characterization

To test potential antibacterial activity, samples were incubated with four bacterial strains. Escherichia coli (American Type Culture Collection-ATCC® 25922™, Manassas, Virginia, USA) and Pseudomonas aeruginosa (ATCC® 27853™) as gram-negative bacteria

and Staphylococcus aureus (ATCC® 25923™) and Enterococcus faecalis (ATTC® 29212™) as gram-positive bacteria.

After the samples were finely ground with a mortar and a pestle, they were sterilized under UV light for 1 h before the incubation with the bacterial strains. The bacterial suspensions of 109 CFU/mL were obtained by diluting the pelletized strains in auto-claved bi-distilled saline water (0.9 % of NaCl). After the bacterial dissolution, E. coli was plated on TBX Medium, (Tryptone Bile X-Gluc, Liofilchem, Italy), S. aureus on Baird-Parker agar (Liofilchem, Italy), P. aeruginosa on Pseudomonas CN Agar (Liofilchem, Italy) and, finally, E. faecalis on Slanetz Bartley agar base (Liofilchem, Italy). All media were sterilized up to 120 °C for 15 minutes. Before the incubation times, 100 mg of sample powders were placed in the middle of Petri dishes. E. coli and S. aureus plates were incubated, respectively, at 44 °C and 36°C for 24 hours, while E. faecalis and P. ae-ruginosa at 36 °C for 48 hours. The diameter of inhibition halos (IDs) was calculated. Three replicates for each sample were carried out to determine the average absolute deviation (AAD). All the entire procedure follows the one reported in [Dal Poggetto et al. 2021].

3.2.11 Density and porosity

Apparent density, ρa, was geometrically evaluated as the ratio between the measured mass and the known volume of the cubic samples [Lee et al. 2018]. The mean apparent density of each hardened composite was computed as the average over three measurements. Real density, ρr, was measured through a helium pycnometer (Micrometrics Accupyc 1330, Micrometrics Instruments, Norcross, GA 30093, USA) using a weighted amount of a pulverized sample.

Using the real and apparent density values, the following formula was used to obtain the total porosity P% value:

$$P\% = (1 - \rho a/\rho r) \times 100$$

3.2.12 Acid exposure

The performance of Geopolymer in different acids was investigated in terms of change in appearance, mass and compressive strength after 10 days based on the procedures of modified ASTM C267. Geopolymer cubes were tested in different concentrations of HCl,

HNO_3 and H_2SO_4 (0.5, 1.5 and 2.5N). Geopolymer concrete cubes were exposed to acid solutions. The ratio of the acid volume (ml) and the samples surface area (cm^2) was fixed at a ratio of 8 [Chang et al. 2005].

The weight loss was obtained by weighing the cubes after having been immersed in acid for 10 days. The samples are washed with tap water and left to dry, finally weighed and the % weight loss calculated. To assess the depth of acid penetration (Fig.3-13) in the geopolymers, the samples were subjected to a post-break examination. A solution of Phenolphthalein 1% was delicately sprayed onto the specimens. The regions that retained their original white colour indicated acid infiltration, whereas the purple areas represented the segments that remained alkaline, signifying the absence of acid reaction.

Fig.3-13 Picture of GP0 sprayed with phenol. 1% after immersion in HNO_3 2.5N.

4. Characterization of raw materials

4.1 Metakaolin

The metakaolin (MK) used in this study was ARGICALTM M1000 (Imerys S.A.-43 Quai de Grenelle, 75015 Paris, France) with chemical composition reported by the producer is indicated in Tab.4-1. The high reactivity of this aluminosilicate precursor is due to its fine particle size (D50 = 8.2 µm; D90 = 33 µm particle size distribution (Figure 4-2), high surface area (B.E.T. = 17 m2/g [Moutinho et al. 2020] and appropriate Si/Al. Its use in literature as reference material for the geopolymer binders is very diffused.

Tab.4-1 Chemical composition of metakaolin.

Oxide wt%	SiO_2	Al_2O_3	Na_2O	K_2O	Fe_2O_3	TiO_2	CaO	MgO	LOI
Metakaolin	55	40	0.4	0.4	1.4	1.5	0.2	0.1	1

4.2 Corundum after abrasion

The recycled corundum powder (RC) used in the lab scale abrasimeter (AP/87 Ce-ramic Instruments, Sassuolo, Italy) is a commercial product: White Corundum FEPA F80 (0.212 – 0.150 mm) (Ceramics Instruments, Sassuolo, Italy, Al_2O_3 99%, while the remaining 1% are traces of MgO, Fe_2O_3, SiO_2 and TiO_2 used for abrasion test of different types of materials (ceramic, glass) and was used as obtained. As it is well-known corundum is inert and does not have toxic and carcinogenic properties, it appears as a white and odourless powder, even after use on the abrasimeter. The RC's particle size of 232 µm ((D50= 232 µm; D90= 300 µm) was checked by dynamic light scattering-DLS grain sizer and reported in Figure 4-2. The chemical composition (Table 4-2) was determined by means of Energy Dispersive X-Ray Fluorescence (EDXRF) spectroscopy using a Shimadzu Spectrometer EDX-720 (GmbH, Duisburg, Germany) equipped with 50 W Rh target x-ray tube, a high-energy resolution Si (Li) detector, and five primary x-ray filters.

Tab.4-2 Chemical composition (XRF) of the as-received corundum abrasive powder.

Al_2O_3	SiO_2	CaO	SO_3	Fe_2SO_3	TiO_2
91.73-92.00 %	2.49-3.58%	2.41-2.81%	1.00-1.30%	0.59-1.06%	0.42-0.61%

The figure 4-1 shows a SEM picture of the microstructure of RC grains. Noticeably, the corundum grains are large and highly visible at very low magnification.

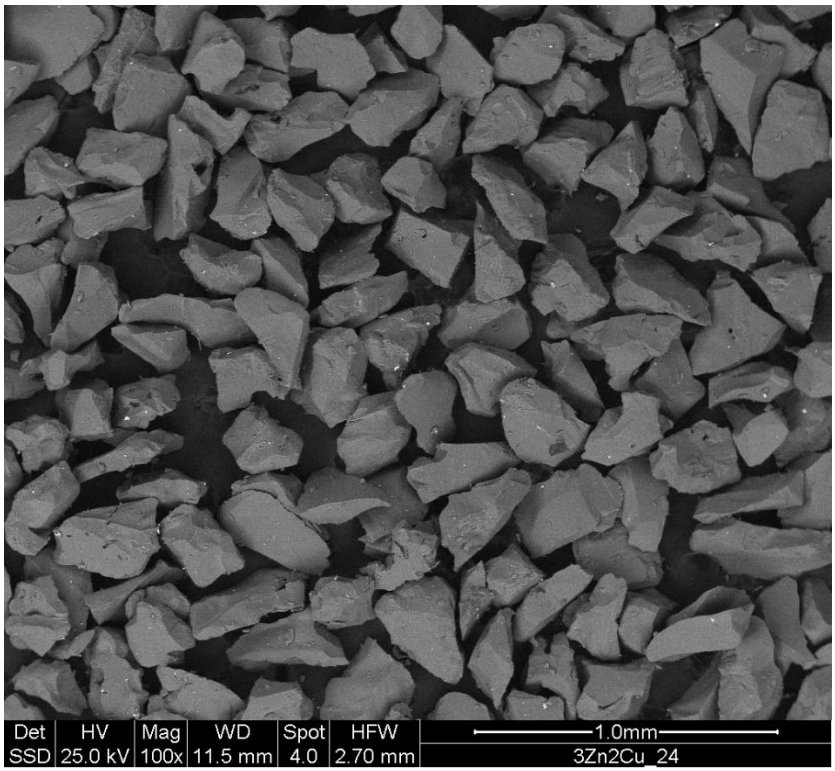

Fig.4-1 Recycled corundum powder after abrasion.

4.3 Corundum after erosion

The waste abrasive powder, also indicated as spent abrasive or recycled corundum, and indicated with the acronym RC, was obtained from pure corundum (Al_2O_3) grains used for erosion tests on different types of materials (ceramic, glass); it was used in the as-received state. This type of waste is typically classified as EWC 12.01.17/non-hazardous waste blasting material, but there are spent abrasive powders that are also classified as EWC 12.01.16*/waste blasting material containing hazardous substances (EWC-European Waste Code, [Commission Notice 2018].

The RC's particle size of about 50 µm, as well as the particle size distribution (D90: 81.43 µm; D50: 52 µm; D10: 34 µm) are reported in Figure 4-2, where the powder of the as-received metakaolin and Corundum Abrasive is also presented. The RC can be considered to be very similar to a fine aggregate (95% particles < 75 µm, as classified by ASTM C136 - 06 Standard Test Method for Sieve Analysis of Fine and Coarse Aggregates), presenting 95% of the particles with a diameter of less than 82 µm (D95 = 82) and 100% less than 90 µm (D100 = 86).

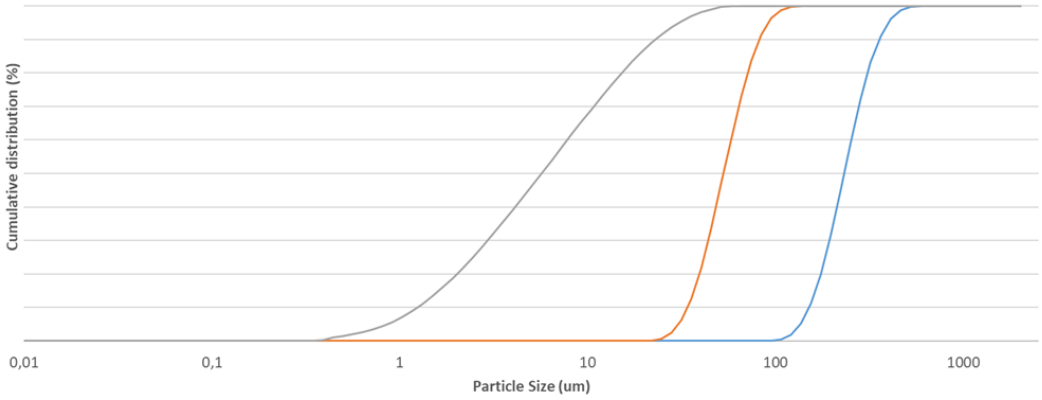

Fig.4-2 Comparison particle size of RC after abrasion (blue) and RC after erosion (orange) with metakaolin.

In Figure 4-3, an SEM image displays the corundum after erosion tests, while Figure 4-4 compares the corundum powders from two different tests. Remarkably, the corundum particles from the abrasion test are significantly larger than the others. The particle size distribution of these powders will substantially impact the physical and mechanical properties of the geopolymers incorporating them, as detailed in Chapters 6 and 7.

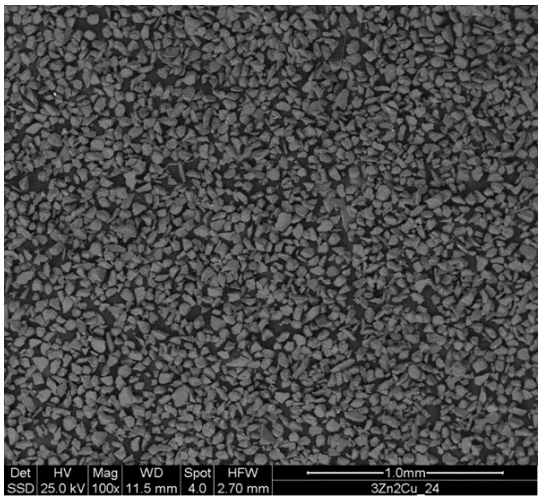

Fig.4-3 Recycled corundum powder after erosion.

4.4 Waste cork

A waste corkfrom the manufacturing process of agglomerated cork bottle caps of a local company (Italsughero, Montecchio Emilia (RE), Italy) was considered. Precisely, this powder waste is generated during the smoothing phase of agglomerated cork caps and is directly collected through a cyclonic air-filtering system. The involved waste corkhas a particle size distribution (Fig.4-4) of 0.063 mm < d < 1 mm and contains polyurethane glue and paraffin which are industrially used as binders and additives for cork particles, respectively.

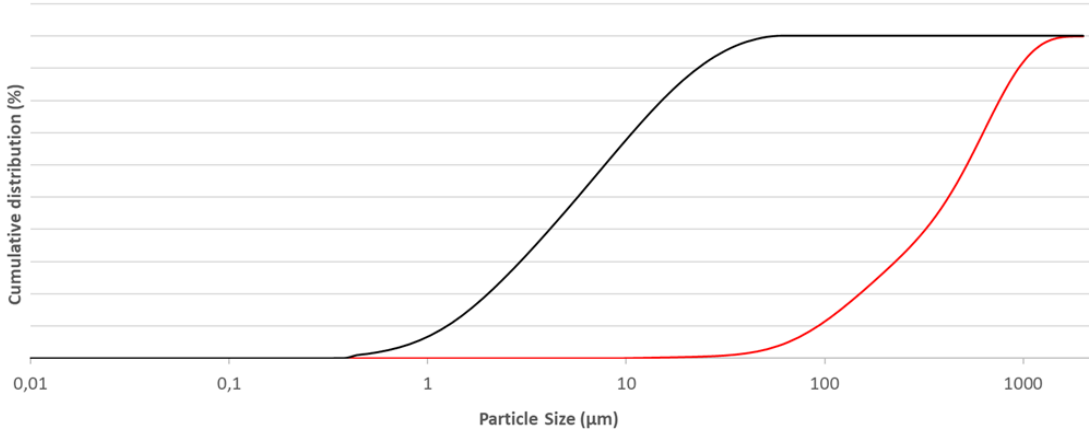

Fig.4-4 Particle size of metakaolin (black) and waste cork (red).

In Figure 4-5, an SEM image displays the waste cork powder.

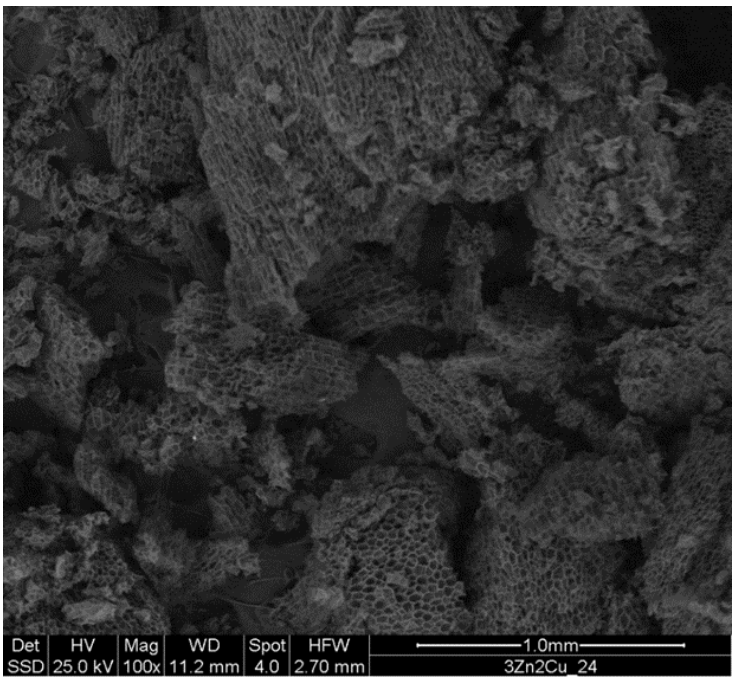

Fig.4-5 SEM picture of waste cork powder.

4.5 Alkali activators

The NaOH solutions were prepared by dissolving laboratory-grade granules (96 wt%, Sigma-Aldrich, Italy) into distilled water to have 6, 8, 10, and 12 M concentrations.

The sodium silicate solution (SiO_2/Na_2O = 3.00 molar ratio; SiO_2 = 26.50 wt%, Na_2O = 8.70 wt%, and pH = 11.7) with bulk density of 1.34 at 20°C was used in the formulation of the geopolymers in combination with NaOH. The solution of sodium silicate was provided by Ingessil, Verona, Italy.

4.6 Acid solutions

The acid solutions used in this thesis investigation are HCl, H_2SO_4 and HNO_3 with different concentrations (0.5 N, 1.5N and 2.5N). To prepare solutions with same moles of H+ we had to calculate our concentrations using Normality due to H_2SO_4 diprotic nature. The starting solution used are the HNO_3 (65%, Sigma Aldrich, Italy) and H_2SO_4 (96%, Carlo Erba, Italy) an HCl (37%, Sigma Aldrich, Italy)

To Normality is the number of H^+, nH^+, to exchange and the relation with the Molarity is:

$$\mathbf{N = nH^+ \cdot M}$$

Tab.4-3 Equivalence between 2.5 molarities, normalities and weight percentages.

Acid solution	Normality (N)	Molarity (M)	w/w (%)
H_2SO_4	2.5	1.25	$\simeq 14$
HNO_3	2.5	2.5	$\simeq 15$
HCl	2.5	2.5	$\simeq 9$

In tab. 4.3 molarities and w/w (%) are also shown for comparison with Normality. All the solutions were prepared as shown in Tab.4-4.

In tab 4.4 the molarities are shown because the calculations usually are based on Molarity.

Tab.4-4 Volume to be taken from starting solutions to prepare 1000mL of the following concentrations.

Starting Acid Solution	***0.5 M***	***1.5 M***	***2.5 M***
HNO_3 65% d= 1.391 (Kg/L)	34.845 mL	104.535 mL	174.224 mL
HCl 37% d= 1.178 (Kg/L)	41.059 mL	123.176 mL	205.293 mL
	0.25 M	***0.75 M***	***1.25 M***
H_2SO_4 96% d= 1.83 (Kg/L)	13.953 mL	41.850 mL	69.767 mL

4.7 Formulations

The reference geopolymer, indicated as GP0, was obtained by adding NaOH, 8M plus Sodium silicate solution to Metakaolin, dry powder, under mechanical stirring, as described in the published article [Dal Poggetto et al. 2022]. All formulations were mixed in a Planetary Mixer (Aucma 1400W, China) then poured into cubic moulds (25 mm x 25 mm x 25 mm). Before closing the samples and letting them rest for 28, 60 and 90 days at room temperature, the bubbles were removed with the shaking table. The molds were opened after 1 day of curing time. Typically, geopolymer binders are compared to Ordinary Portland cement products, hence we chose the 28 days curing/ageing time to have better comparability with literature data.

Waste materials before alkali activation

In this thesis work the MK powder was substituted by different percentage (wt%) of as-received waste powders before the addition of Alkali Activators (Fig.4-6). The formulations maintained constant the MK/NaOH and MK/silicate weight ratio in the different composites.

Waste materials after alkali activation

After the GP0 (MK-based Geopolymer) fresh paste preparation, addition of the as-received waste powders in the amounts of different wt% (percentage of waste powders have been calculated with respect to the total mass of the composite formulation in the wet status) was

performed to produce the geopolymer composites mounts (Fig.4-6). The formulations maintained constant the MK/NaOH and MK/silicate weight ratio in the different composites.

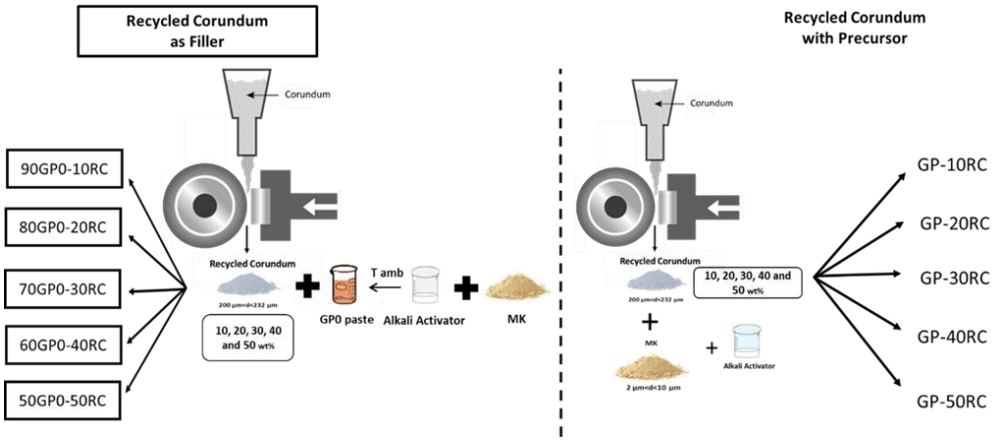

Fig.4-6 Formulation of geopolymer with waste powder added before and after alkali activation.

5. Investigation on best formulation of MK-based geopolymer at room temperature

5.1 The role of alkaline activator

One of the key factors influencing the properties of geopolymers is the SiO_2/Na_2O ratio in the raw materials and the curing time of the alkali-activated solution, typically consisting of sodium hydroxide (NaOH) and sodium silicate (Na-silicate). The SiO_2/Na_2O ratio and curing time play pivotal roles in determining the geopolymer's microstructure, mechanical strength, and chemical resistance. Understanding the intricate relationship between these variables is crucial for tailoring geopolymer formulations to meet specific requirements in diverse applications, such as construction, infrastructure, and environmental remediation.

This chapter delves into the crucial task of comprehending and selecting the optimal geopolymeric formulation based on metakaolin, a pivotal aspect of this thesis project. Building upon the initial material characterization, this step represents a fundamental progression.

The focus was primarily directed towards determining the appropriate mixing time of the NaOH solution with the Na-silicate solution, having already optimized their ratio in previous works. The exploration began by studying individual activator solutions as they are, aiming to discern subtle differences. The study of activators is necessary to ensure their proper use. The SiO_2/Na_2O and Na_2O/H_2O ratios may differ from previously calculated values. The starting silicate might have a non-ideal ratio, for example, or the concentration of prepared sodium hydroxide might need adjustment. Furthermore, preparing geopolymers under incorrect conditions leads to wasted time and materials, as well as skewed results. Subsequently, geopolymers prepared with these activating solutions were examined and compared.

Through systematic analysis, the research aimed to identify a geopolymer formulation that aligned most effectively with the project's objectives and requirements. It is crucial to underscore that, in this thesis project, paramount importance was placed on evaluating the chemical properties of geopolymers rather than solely focusing on their mechanical performance. This approach ensures a comprehensive understanding of the geopolymeric systems and their applicability in real-world scenarios.

5.2 Characterization of alkali solutions

As anticipated in the previous paragraph, the research commenced with the characterization of the three solutions under investigation. The three solutions were prepared as follows:

1. NaOH + Na-silicate solution: The activator solution was prepared by mixing 38g of NaOH 8M with 40g of sodium silicate solution, resulting in a SiO_2: Na_2O ratio of 6.2, corresponding to a weight ratio of 6. The overall molar composition of the well-mixed solutions was $1Na_2O$: $3SiO_2$: $35H_2O$. This solution was used immediately after mixing. In this case the Na-sil solution was tested at the NMR.
2. AS1: The preparation was carried out in the same manner as number 1, but it was allowed to rest for 24 hours.
3. AS2: The preparation was carried out in the same manner as number 1, but it was allowed to rest for 7 days.

The geopolymer prepared with the first solution was labeled as GP0, the geopolymer prepared with the second solution was named GP-AS1, and finally, the sample prepared with the third solution was labeled as GP-AS2. The nuclear magnetic resonance (NMR) analysis was conducted to identify the soluble forms of silica present in the solutions after the aging period. Figure 5-1 illustrates the ^{29}Si NMR spectra of the commercially obtained sodium silicate solution (R3) as well as the two activating solutions (AS1 and AS2).

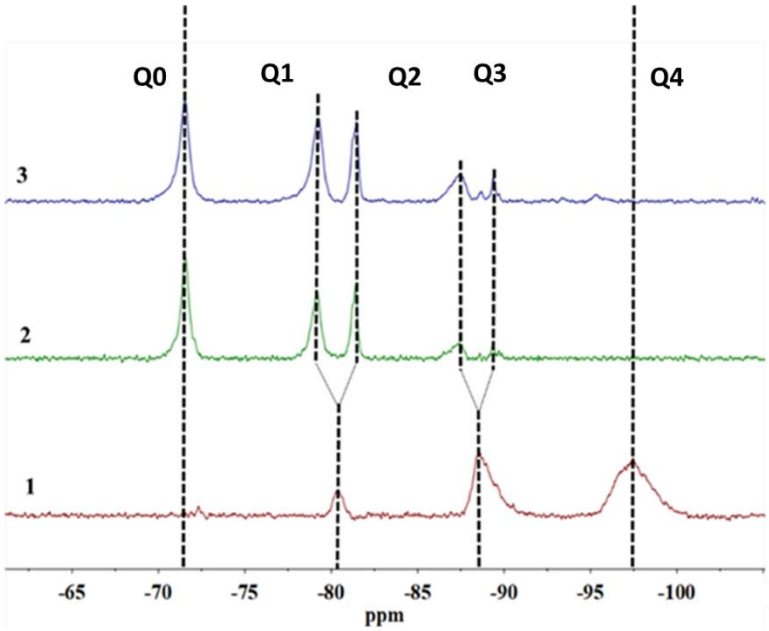

Fig.5-1 ^{29}Si NMR of the alkaline solution. 1) Silicate R3; 2) AS1; 3) AS2.

The spectrum of the initial sodium silicate solution reveals four broad signals. The minor peak at approximately -72 ppm corresponds to the silicate ion (Q0 units). The remaining three peaks, located around -80, -88, and -97 ppm, represent the Q1, Q2, and Q3 silicon units, respectively. The broad nature of these signals indicates the presence of substantial aggregates. However, in the AS1 and AS2 solutions, as outlined in the experimental section, the modulus R (i.e., the SiO_2/Na_2O ratio) decreases due to the addition of NaOH. This reduction in the R modulus results in the splitting of the broad signals into sharper ones, indicating the formation of smaller aggregates resulting from the depolymerization process. Notably, both AS1 and AS2 spectra exhibit a prominent signal at -71 ppm, corresponding to silicate ions $Si(OH)_4$ Q0. Additionally, it is important to observe that all signals shift toward lower field values due to the deprotonation of the Si-OH groups. Furthermore, the Q2 and Q3 signals are fragmented into resonance groups (-80, -82 and -87, -89 ppm, respectively) owing to the presence of diverse species, including monomers, dimers, trimers, and cyclic structures containing up to eight silicon atoms.

5.3 Preparation of geopolymer with different activators

The geopolymer paste GP0, used as the reference, was prepared by combining 38g of freshly mixed sodium hydroxide 8 M and 40g of sodium silicate solution with 100g of metakaolin (MK). In parallel, two other geopolymers, labeled GP-AS1 and GP-AS2, were created by incorporating

activating solution 1 (AS1) and activating solution 2 (AS2) with MK, respectively. Maintaining consistency, all sample preparations adhered to a fixed water content with a nominal molar ratio of H_2O/ Na_2O =17.6. Similar considerations were applied to the Al_2O_3/Na_2O ratio, which was approximately 2, while SiO_2/Na_2O was 6.2, and Si/Al ratio stood at 1.4. These calculations took into account the total number of moles of silica present in the metakaolin, encompassing the quartz phase (as detailed in the XRD paragraph). The water content used in the calculations included both the water from the NaOH solution and the sodium silicate solution.

To ensure precision, multiple batches of fresh pastes were blended, combining powders and liquids in Planetary Mixer (Aucma 1400W, China). Following this preparation, the resulting fresh paste was carefully poured into precise cubic molds, each measuring 25mm x 25mm x 25mm. Thorough removal of any trapped air bubbles was accomplished using a vibrating table, a process spanning 5 minutes. After this step, the molds were sealed and left to cure at room temperature, maintaining 100% relative humidity. Upon completion of a day-long curing period, the molds were opened, allowing the samples to acclimate to the laboratory atmosphere's ambient conditions. Each formulation resulted in a set of twelve samples, ensuring consistency and reliability in subsequent analyses.

5.4 Consolidated geopolymer’s stability in milliQ water

- Ionic conductivity of eluate

In the pursuit of gauging the impact of alkaline silicate solutions on the cross-linking of the geopolymeric network, comprehensive characterization of the consolidated samples GP0, GP-AS1, and GP-AS2 was carried out through ionic conductivity (IC) measurements. The ionic conductivity of the eluate from geopolymers submerged in deionized water is intricately influenced by several factors. These factors encompass the composition of the network, the presence of mobile ions originating from unreacted solutions, and the configuration of the aluminosilicate structure. Within geopolymer networks, the primary source of ionic conductivity stems from alkali ions like Na or K. These ions are generated during the interaction between alkali activators and the

aluminosilicate source material, navigating the network due to its porous and interconnected structure.

Furthermore, the ionic conductivity of a geopolymer network is modulated by the concentration of mobile ions and the level of hydration within the structure. Networks with higher concentrations of mobile ions exhibit enhanced conductivity, while increased hydration augments ion mobility, consequently elevating conductivity. Additionally, the arrangement of the network structure plays a pivotal role, networks characterized by openness and interconnectivity demonstrate superior ionic conductivity compared to those with closed and compact structures. This property holds paramount significance, as it delineates the network's ability to conduct electrical charges and is closely intertwined with its mechanical and thermal properties. A profound comprehension of the underlying mechanisms governing ionic conductivity in geopolymer networks is pivotal for the advancement of cutting-edge materials and applications. Figure 5-2 illustrates that after 28 days of curing, the ionic conductivity of the eluates of GP0 and GP-AS1 appears comparable, while GP-AS2 exhibits higher conductivity. This variance can likely be attributed to differences in the activating solutions employed, underscoring the profound influence of solution composition on the resultant ionic conductivity values.

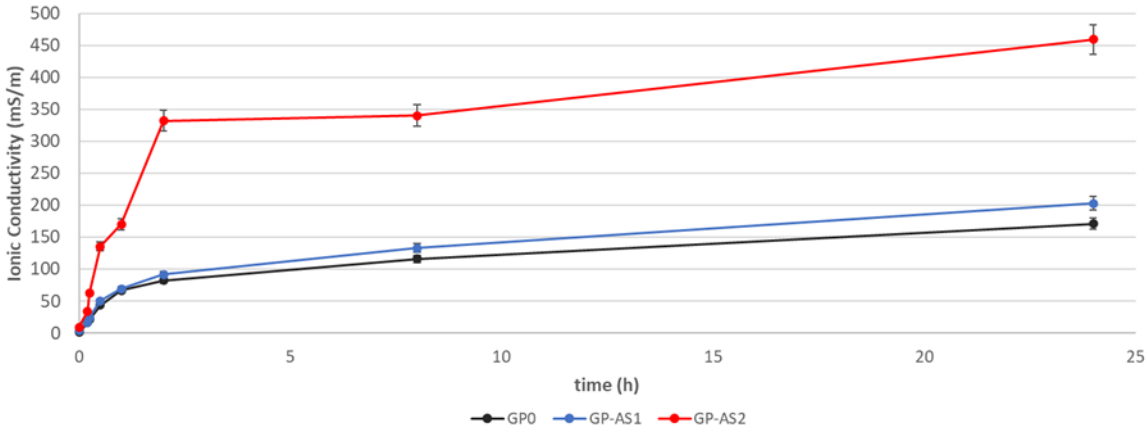

Fig.5-2 Ionic conductivity (mS/m) of the 3 samples after 28 days of curing.

5.5 Geopolymerization

- XRD

As illustrated by the X-ray diffraction patterns collected on the 3 geopolymers at 28 days of curing time in Fig. 5-3, only the crystalline phases of the metakaolin are visible: alpha quartz, anatase together with

some traces of kaolinite planes not affected by dihydroxylation at around 20° in 2θ.

For the pure MK, the characteristic broad hump in the 2θ range of 15 to 30° indicates the presence of the typical lack of long-range order of the amorphous silicates obtained by the dehydroxylation process of kaolinite [Scherb, S. 2020]. Such XRD feature of MK varies with NaOH solution decreasing its intensity towards the high 2θ values. Nevertheless, the XRD traces of the samples GP0, GP-AS1 and GP-AS2 show a slight shift in the amorphous hump towards higher values (from ~23° to ~28° in 2θ) typical of the geopolymers with an X-ray amorphous network richer in Al [Nasab et al. 2014]. The multiple peaks around 20° in 2θ typical of MK disappear in the geopolymer XRD patters leaving a single anatase peak. It has been recently proved that crystalline TiO_2 is not soluble in alkaline media, thus it does not take part to the geopolymerization reaction [Scherb et al. 2020].

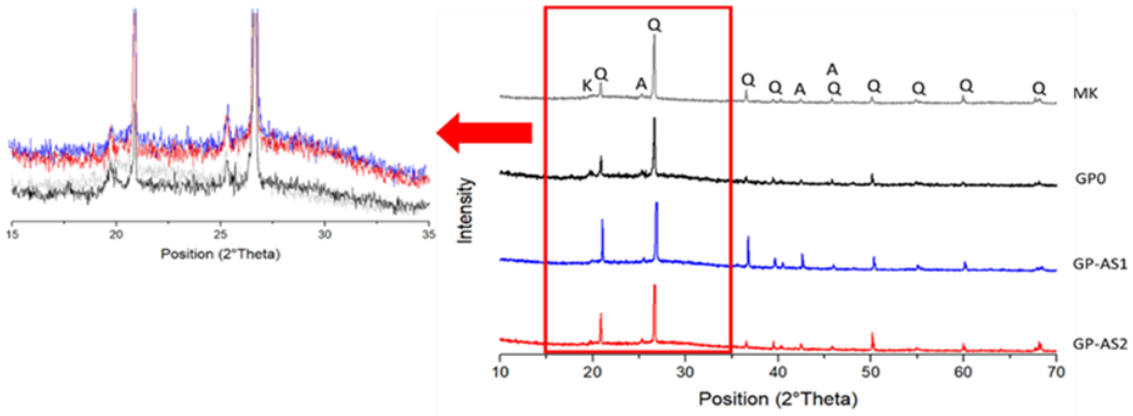

Fig.5-3 XRD patterns of the 3 geopolymers after 28 days of curing compared with the starting MK. Enlarged area shows the area from 15° to 35° 2Θ. Q = Quartz, K = Kaolinite, A = Anatase.

- NMR characterization of hardened geopolymers

The ^{27}Al MAS-NMR spectra of the GP0, GP-AS1 and GP-AS2 materials are reported in Figure 5-4. All spectra show two well defined resonances at 7.5 and 63 ppm which are due to Al species in octahedral and tetrahedral coordination, respectively. No signals coming from five coordinated Al is present in the spectra. From the analysis of signals integrals, the quantity of Al in tetrahedral coordination are 82, 84 and 78% for the GP0, GP-AS1 and GP-AS2 samples respectively. This is in agreement with the

occurrence of polymerization up to a degree which is typical of amorphous geopolymers. It is worth noting that the GP-AS2 sample shows the lowest quantity of tetrahedral coordinated aluminium [BRUS 2016]. This could be evidence of a lower degree of geopolymerization.

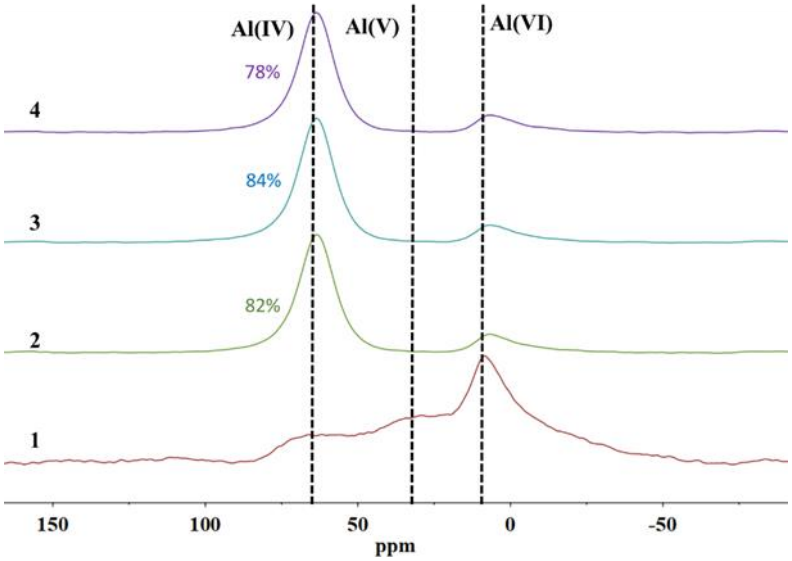

Fig.5-4 ^{27}Al MAS NMR of 1) MK; 2) GP0; 3) GP-AS1; 4) GP-AS2 hardened samples.

The ^{29}Si MAS-NMR spectra of the GP0, GP-AS1 and GP-AS2 materials are reported in Figure 5-5. All spectra show a very broad signal which is due to the convolution of resonances belonging to all the silicon species Q4(nAl) with n ranging from 0 to 4. This notation was first used by Engelhardt et al. [Engelhardt et al.1974; 1984] to indicate the number of O-Al groups bonded to silicon atoms in tetrahedral coordination in many aluminosilicate materials.

This broad signal is centred at around 90 ppm, which is typical of sodium based geopolymers. In order to quantify all the Q4(nAl) species a deconvolution process was performed using five gaussians shaped component bands.

Results of the deconvolution are reported in Table5-1.

Fig.5-5 ^{29}Si MAS-NMR spectra of the 1) MK 2) GP0, 3) GP-AS1 and 4) GP-AS2.

The chemical shifts values of the five gaussians were taken from literature [Duxson et al. 2005; Wan et al. 2019; Engelhardt et al. 1988] together with the variable parameter used for the fitting procedure. The data comparison for the three samples shows that the ones obtained

with the AS1 and AS2 activating solutions have lower quantity of Q4(2Al) species and higher quantity of Q4(1Al) and Q4(4Al). In particular, the GP-AS2 sample shows a dramatic decrease of Q4(2Al) species, thus confirming the ^{27}Al results describing a geopolymer with a lower degree of polymerization.

Tab.5-1 Distribution of Q4 species as derived from the deconvolution of ^{29}Si MAS-NMR spectra.

	Q4(mAl) (% ± 0.5)				
	Q4(4Al)	**Q4(3Al)**	**Q4(2Al)**	**Q4(1Al)**	**Q4(0Al)**
GP0	15.6	30.0	28.2	17.1	8.8
GP-AS1	17.2	29.3	26.5	18.7	8.3
GP-AS2	17.2	29.1	23.6	21.6	8.5

In order to check the reliability of the deconvolution process, equation 1 was used as reported by Duxon et al. [Duxson et al. 2008] to calculate the Si/Al ratios:

$$Si/Al = \sum_{m=0}^{4} I_{Si(mAl)} / \sum_{m=0}^{4} \frac{m}{4} I_{Si(mAl)} \qquad (1)$$

In this equation, Si(mAl) is the intensity of the signals obtained by deconvolution of each species in the ^{29}Si spectra. Si/Al ratio values obtained for the GP0, GP-AS1 and GP-AS2 samples were 1.76, 1.75 and 1.78 respectively. These values which are slightly higher than the nominal ones (1.4) can be explained taking into account of the Al-O-Al species that may be present and not involved in the geopolymer structure. Thus, the presence of these units leads to an overestimation of the Si/Al ratio as obtained through the deconvolution procedure.
Over time, the environment around the Si atoms remains almost unchanged, as visible in Figure 5-6, with a slight increment of Q4(3Al) species for the GP0-AS1 and Q4(1Al) species for the GP0-AS2 after 3 months of ageing. The Q4(2Al) of GP0 seems unstable and transform toward higher interconnected species, Q4(1Al) and Q4(0Al), where more SiO_2 pure areas are present.

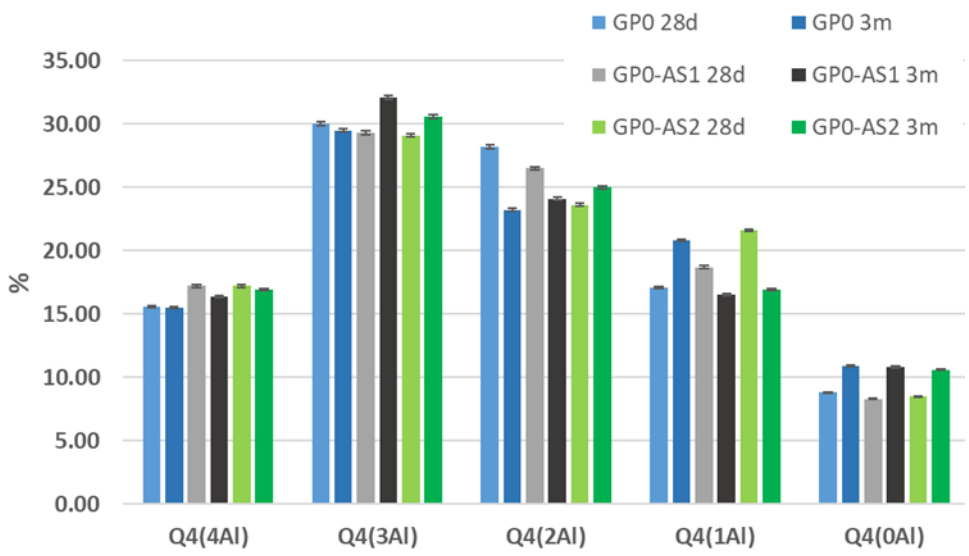

Fig.5-6 Environment around the Si atoms.

5.6 Microstructure

- Compressive strength

Figure 5-7 compares the compressive strength values of the three geopolymers cured at 28 days of curing. It can be seen that the GP-AS1 sample has better compressive strength. The difference with the GP0 reference sample is due to the difference of Si/Al ratio, as already verified in other studies [Mostafa et al. 2018; Qu et al. 2021]. The lower value of GP-AS2 compared to the other two samples reflects what measured with the ion conductivity (Fig.5-2). Being the release of ions in the solution greater is an indication of a greater presence of pores and cavities that affect the resistance of the material. In fact, the ionic conductivity of GP-AS2 is much higher than GP0 and GP-AS1 conductivity (Fig.5-2).

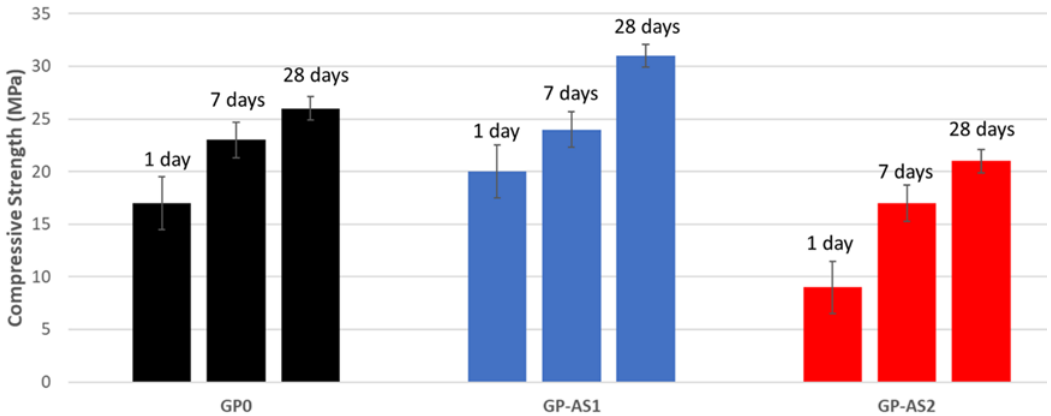

Fig.5-7 Mechanical performance in terms of compressive strength (MPa) for all the three geopolymers vs curing time.

5.7 Resistance to acid attack

The most recent examinations aimed to understand the behavior of the three distinct geopolymers were of a chemical nature, specifically focusing on acid resistance tests. These tests didn't just assess the materials' ability to withstand three different acids (HCl, HNO_3 and H_2SO_4), but also examined how these acids affected the 3D network and microstructure of the samples. Following immersion in the acids, all at identical concentrations as detailed in section 3.2.12, the samples were subjected to a comprehensive characterization process.

- Weight loss

Figure 5-8 shows the weight loss of the three geopolymers cured at 28 days after the acid attack. As can be seen, the reference geopolymer GP0 always has a resistance higher than GP-AS1 and GP-AS2.

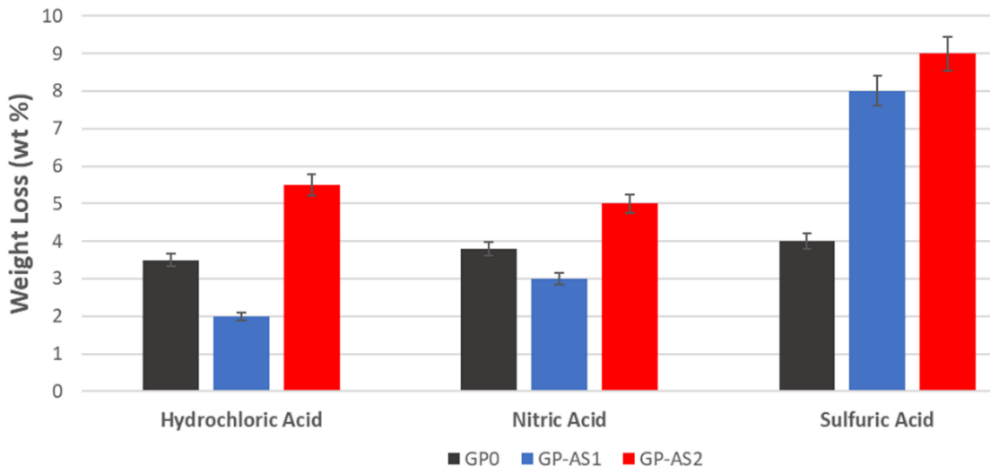

Fig.5-8 Weight Loss of the Three sample cured 28 days after immersion in acid solution.

- XRD

In Figures 5-9 and 5-10, the XRD spectra of the GP-AS1 and GP-AS2 samples before and after immersion in the three different acids are shown. After the immersion in acid, all the geopolymer series shows a decrease of the intensity of the amorphous hump around 20-30 in 2 Theta, indicating the destruction of the newly formed disordered lattice despite the type of acid tested.

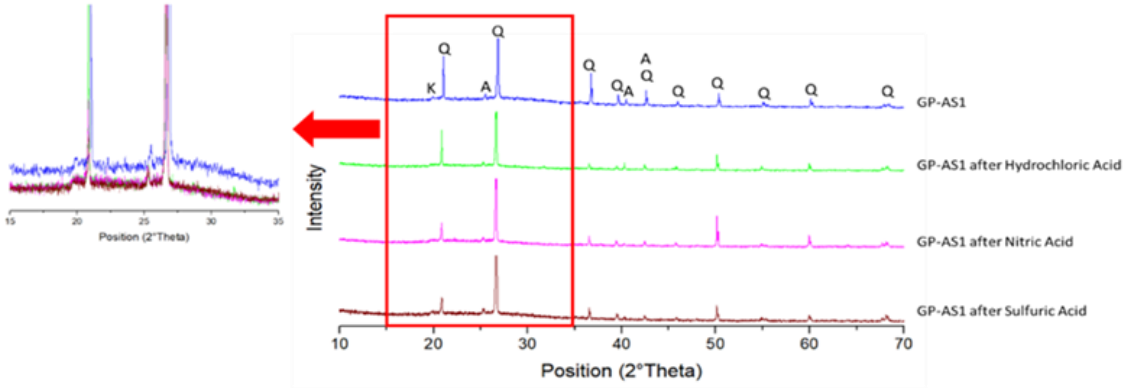

Fig.5-9 XRD patterns of the GP-AS1 sample at 28 days curing time after immersion in the 3 different acidic solutions compared with the reference geopolymer. Enlarged area shows the amorphous halo. Q = Quartz, K = Kaolinite, A = Anatase.

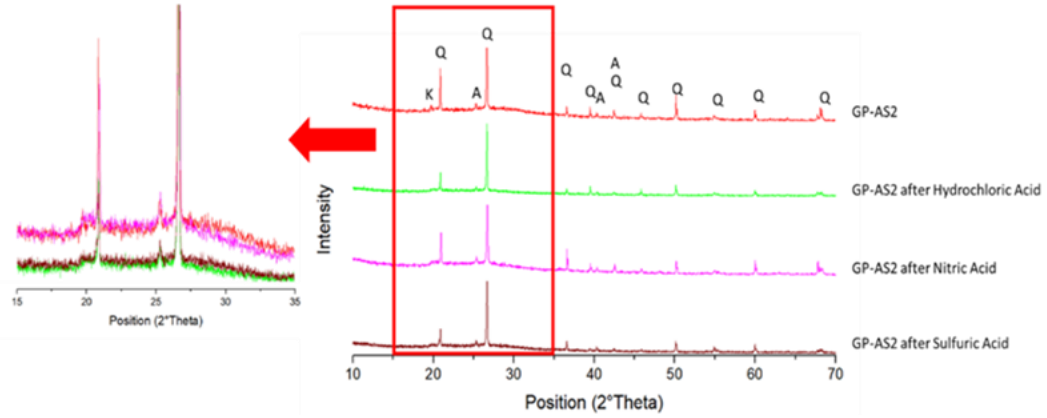

Fig.5-10 XRD patterns of the GP-AS2 sample at 28 days curing time after immersion in the 3 different acidic solutions compared with the reference geopolymer. Enlarged area shows the amorphous halo. Q = Quartz, K = Kaolinite, A = Anatase.

Figure 5-11 displays the spectra of GP0, GP-AS1, and GP-AS2 after being subjected to HNO_3 attack. It is evident that the three spectra are almost identical, although a slight variation in the hump between 20-40° 2θ is noticeable in the GP-AS2 sample.

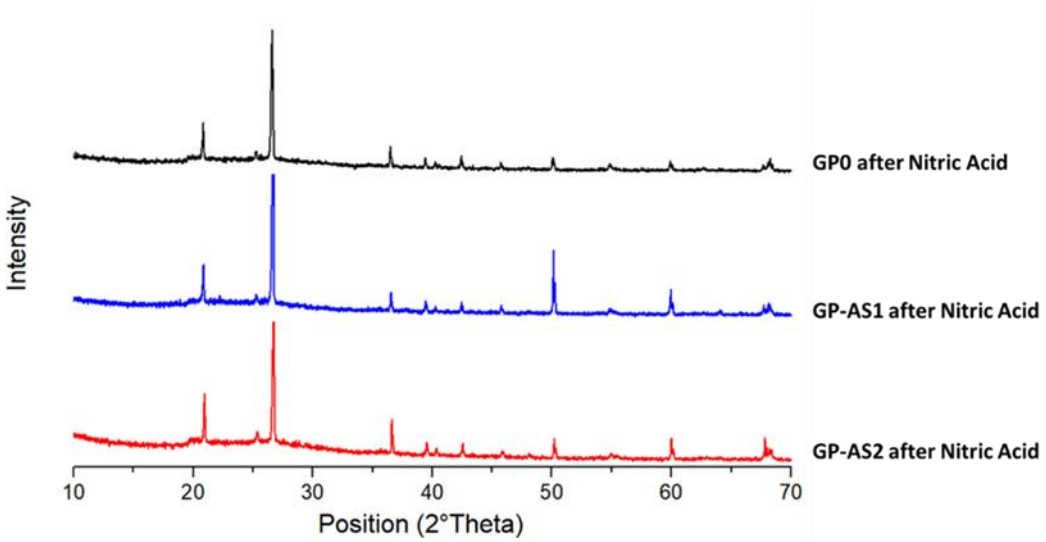

Fig.5-11 XRD spectra of the three geopolymer after immersion in HNO_3.

- Compressive strength

In Figure 5-12, the chart illustrates the compression strength values of the three different samples after immersion in acid. After immersion in acids the GP0 values are better than those of GP-AS1 even if with little difference. The resistance of GP-AS2 after acids drops dramatically compared to before immersion. Compared to GP0 and GP-AS1, GP-AS2 values are very low after every acid attacks.

Despite the higher weight loss observed in GP0 after extraction (Fig.5-8), it still maintains its status as the geopolymer with the most favorable chemical properties. The significant disparity between the values before and after immersion in GP-AS1 (see Fig.5-7) samples indicates excellent mechanical properties, albeit with lower resistance to changes in the surrounding chemical environment. Conversely, GP-AS2 proves to be the least robust among the three, as its resistance becomes almost negligible after exposure to acids. This suggests that GP-AS2 not only exhibits poor mechanical properties but also falls short of expectations in the presence of aggressive chemical surroundings.

Additionally, it is noteworthy that the margin of error (maximum deviation calculated from all the tested samples) is higher in GP-AS1 and GP-AS2 samples, whereas it remains low in GP0. This reaffirms the consistency and stability of GP0 samples in the face of changing conditions, highlighting their uniformity.

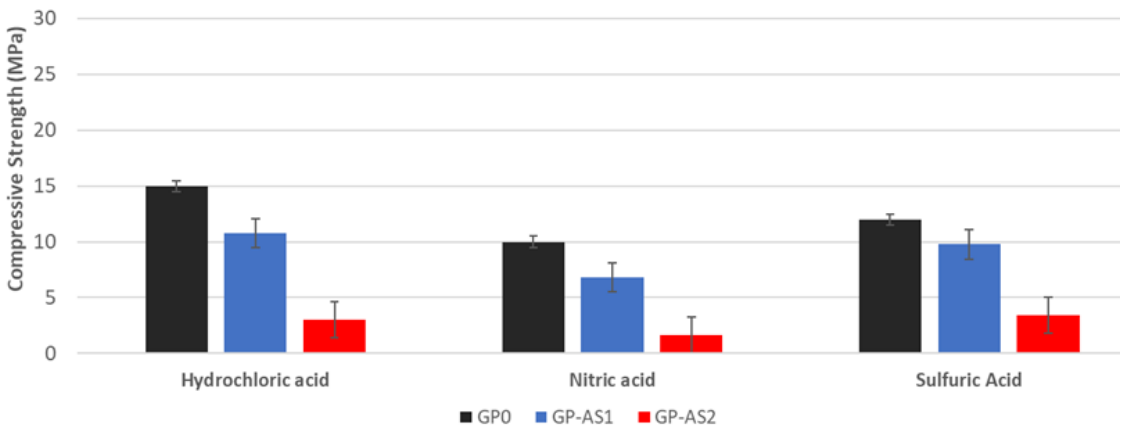

Fig.5-11 Compressive Strength of all sample after acid attacks.

5.8 Discussion and Conclusions

The structure of sodium silicate solutions at pH > 11 (in our case pH is 11.7 for the commercial solution R=3) depends on SiO_2/Na_2O ratio, presenting small colloidal particles in the tens of nm range above the ratio of 2.0–2.5 [Böschel et al. 2003]. For value below 2.0–2.5 it is proposed that the silicate solutions contain mostly low molecular weight species such as mono- and dimeric species [Engelhardt et al. 1975]. Additionally, a relevant variable for silica speciation in sodium silicate solutions is the concentration of the solution. In the case under investigation the concentration of SiO_2 is 26.5wt% with SiO_2: Na_2O ratio of 3.0, similar to those studied by Marsmann [Marsmann et al. 1974]. In particular, for a solution of 27.2 wt% SiO_2 and a SiO_2/Na_2O ratio of 3.3, he proved that 35% of the silica is fully polymerized. These literature data indicate that the addition of the NaOH solution to the Na silicate solution with R=3 and high concentration, as that presented in this study, induce depolymerization. The experimental results presented polymerized Q_2, Q3 and Q4 species in ^{29}Si spectra of the commercial sodium silicate solution that was added together with NaOH solution directly to metakaolin in the GP0 formulation. Solutions AS1 and AS2 are depolymerized and present a high amount of monomeric Q0 species. The AS2 solution already at 7 days of ageing presents an increase in Q3 signal indicating an incipient polymerization. These results indicate that in order to have a solution rich in monomeric, hence more reactive Si species in solution, is suggestable to prepare the activator mixture no more than 24 hours in advance to its use.

Once mixed to the MK, these 3 solutions produce dense and well reticulated geopolymers where the coordination of Al has found to be

prevalently in four-fold geometry, indicating an almost complete dissolution of the six- and the complete dissolution of the five-fold sites typical of the metakaolinite product [Massiot et al. 1995]. The presence of unreacted metakaolin in geopolymers has been recorded elsewhere in literature and it is statistically acceptable [Provis, J.L. 2005]. The XRD investigation did not prove to be sensitive enough to the variation of the amorphous structure of the three hardened geopolymers. The presence of low Q4 species in GP-AS2 can be explained by two concomitant features: the lower number of monomers in AS2 solution with respect to AS1 solution as well as the absence of the high number of OH- groups as in the fresh NaOH solution used in GP0. The absence of the resonance of ^{27}Al at 80 ppm assigned to the signal of aqueous $Al(OH)_4$ [Zibouche et al. 2009] indicates that the species released during dissolution of the metakaolin [Davidovits, J. 2008, 2020] react completely during the geopolymerization and do not stay in the pores of the hardened material. Apart from these details, we can assess from the NMR that the amorphous MK powder characterized by a disordered polymerized silicon and aluminium network has been almost completely reacted to produce a 3D aluminosilicate network via dissolution and condensation in all the three activator solutions used for this study.

Therefore, based on these conclusions, the GP0 sample was chosen as the reference geopolymer. This decision was carefully considered for several reasons. Upon reviewing all the results and as thoroughly discussed, the GP-AS2 sample was ruled out as the reference for the thesis. Both GP0 and GP-AS1 samples displayed impressive mechanical and microstructural qualities. However, GP-AS1 exhibited some instability in acidic environments. GP0, on the other hand, demonstrated excellent mechanical properties both before and after acid immersion. Additionally, the long-term tendency towards the increment of SiO_2 rich areas further solidified the selection of GP0 as the preferred reference sample.

6. Geopolymer with recyeld corundum after abrasion test

In this chapter, we focused on the formulations of geopolymer containing recycled corundum powder recovered from the abrasimeter, referred to as recycled corundum (RC).

Despite being crystalline, RC acts as a semi-reactive filler in the metakaolin-based geopolymer formulation, as reported in existing literature [Riahi et al. 2021], RC could offer a partial yet significant contribution to the alkaline solution by introducing various Al^{3+} species. This addition effectively lowers the Si/Al ratio, as demonstrated in Riahi's study [Riahi et al. 2021].

The examination of morphology demonstrated the successful chemical bonding and microstructural integration of alumina-coated steel onto the steel substrate. The partial dissolution mentioned here plays a crucial role in forming a robust interface between the MK-based binder and the Al_2O_3 particles. This newly formed interface enhances fracture-deviation reinforcement mechanisms. Despite this predicted reactivity, it's important to note that a considerable portion of corundum particles is expected to remain undissolved. Consequently, these inert solid fillers retain their ability to withstand compressive stress [Tchakouté et al. 2018].

Additional goals were:

1) control the 3D network lattice integrity of the geopolymer (FTIR);
2) verify the reactivity of crystalline phases (XRD);
3) assess the release of hazardous cations (ICP-OES and ICP-MS)

In addition to the release of Na^+, Al^{3+}, and Si^{4+} from the geopolymeric network, we anticipate an effective encapsulating response from part of the geopolymeric matrix [Ponzoni et al. 2015], resulting in a dense and safe binder suitable for non-structural building materials. Previous investiagations show that the heavy metals immobilization through geopolymerization process is efficient and encourages the application of this technology also for liquid hazardous waste, containing metals different from chromium.

The chapter 6 is divided in 3 Sections:

Section 6.1: Characterization and Reassessment of recycled corundum and its incorporation into the Geopolymeric Matrix prior to Alkaline

Activation. In this section we focused on geopolymers prepared by mixing Recycled Corundum to the dry metakaolin powder before the addition of the alkali activator solution, to understand the role of this waste in the chemical reactivity of the fresh paste and how it affects the reticulation.

Section 6.2: The effect of recycled corundum added after the Alkali activation of MK-based Geopolymer

In this section the recycled corundum was added after the alkali activation of metakaolin. In these formulations, RC was used as a filler/reinforcement for the geopolymeric matrix.

Section 6.3: Comparison of physical, chemical, and mechanical properties of geopolymers with recycled corundum Incorporation before and after alkaline activation.

To evidence the effect of the mixing procedure investigated in the two previous paragraphs, in this section all the results of sections 6.1 and 6.2 are compared and discussed.

6.1 Characterization of recycled corundum and its incorporation into the geopolymeric matrix prior to alkaline activation

6.1.1 Characterization of RC after abrasion test

The alkaline treatment modifies the surface chemistry of the recycled corundum particles. Corundum, being a relatively inert material, might not readily bond with the geopolymer matrix. By subjecting it to an alkaline solution, just the surface of the corundum particles becomes more reactive. This enhanced reactivity promotes chemical interactions between the corundum and the alkaline-activated geopolymer matrix. The alkaline treatment can lead to the partial dissolution of the corundum particles. This dissolved corundum becomes incorporated into the geopolymer matrix, contributing to the formation of new reaction products or the dissolution of some impurities in the corundum. This can lead to a more effective integration of the RC within the matrix, potentially enhancing the overall mechanical and structural properties of the resulting composite material. The basic treatment can also help in reducing any impurities or surface contaminants present on the corundum

particles. This purification process ensures that the corundum integrated into the geopolymers is of higher quality and better suited for the intended application.
The alkaline treatment of corundum before adding it to geopolymers improves its reactivity, promotes better bonding with the matrix, and enhances the overall performance of the resulting composite material.

- RC solubility in concentrated NaOH solution

Recycled Corundum was checked for its reactivity in alkaline environment after immersion in different NaOH solutions. To choose the most reactive concentration of NaOH for RC to be used for geopolymer formulations, we carried out 4 tests on the recycled corundum powders using increasing NaOH concentrations: 6, 8, 10 and 12 M. The NaOH solutions were prepared by dissolving laboratory-grade granules (96 wt%, Sigma Aldrich, Italy) into distilled water to have 6, 8, 10 and 12 M concentrations.

Tab.6-1 Preparation of NaOH at different concentrations.

NaOH Concentrat. (M)	NaOH pelletes (g)	H_2O (mL)
6	239,9826	1000
8	319,9768	1000
10	399,971	1000
12	479,9652	1000

The mineralogical analysis of the recycled corundum abrasive powder was conducted both before and after subjecting it to NaOH attack at a temperature of 85°C [Temuujin et al. 2009]. X-ray diffraction (XRD) was employed for this characterization, and Figure 6-1 displays the corresponding spectra. The XRD spectrum of the recycled corundum powder before the NaOH attack aligns with the results from XRF analysis, confirming a significant proportion of crystalline corundum. This outcome is consistent with what is typically obtained through the fusion of pure Al_2O_3 in an electric arc furnace. Additionally, minor traces of other compounds were detected, likely arising from the previous use of this powder in the abrasimeter. Upon subjecting the recycled corundum powder to NaOH attack at different

concentrations (6, 8, 10, 12M), it was observed that the powder did not dissolve well. Consequently, only a few phases were formed as a result of the attack. However, when the NaOH concentration was 8M, the situation differed. The recycled corundum powder exhibited better dissolution behavior, leading to the disappearance of certain peaks in the 2θ values (8° and 16°) associated with the impurities of the recycled corundum. Moreover, peaks at 57°, 68°, and 69° in 2θ, typically attributed to corundum, were also eliminated in the spectrum.

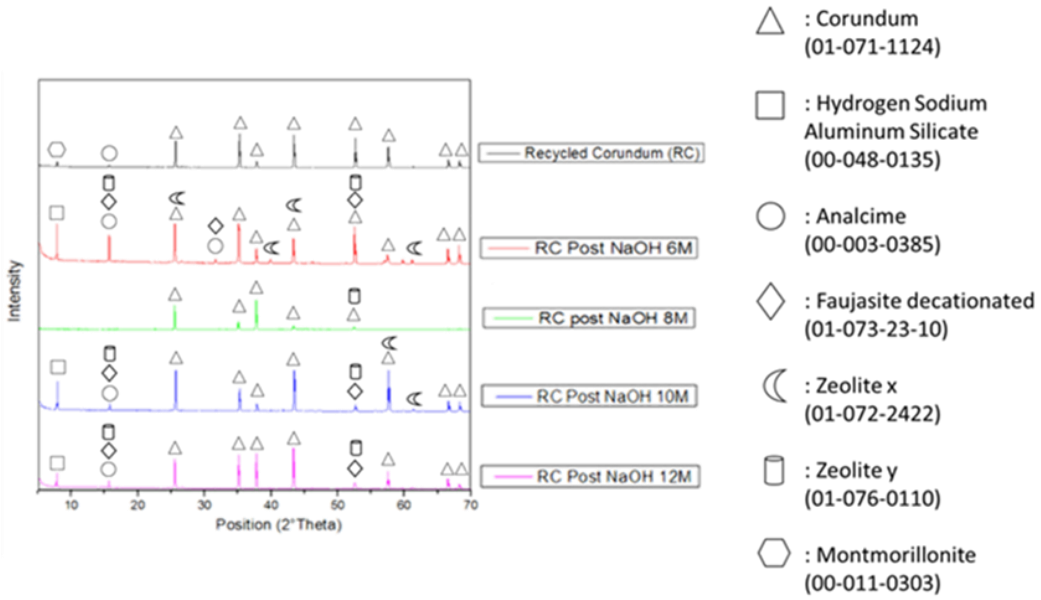

Fig.6-1 XRD patterns for RC raw materials and RC post basic attack of NaOH at different concentrations.

6.1.2 Geopolymer formulation

The initial geopolymer reference, referred to as GP0, was prepared by mixing 30 mL of 8M NaOH and 30 mL of sodium silicate with 100 g of dry MK powder while subjecting the mixture to mechanical stirring. To create the geopolymer composites designated as GP-10RC and GP-20RC, GP-30RC, GP-40RC and GP-50RC 10, 20, 30, 40 and 50 wt% of the original MK powder were respectively replaced with as-received recycled corundum powder (Fig.6-2).

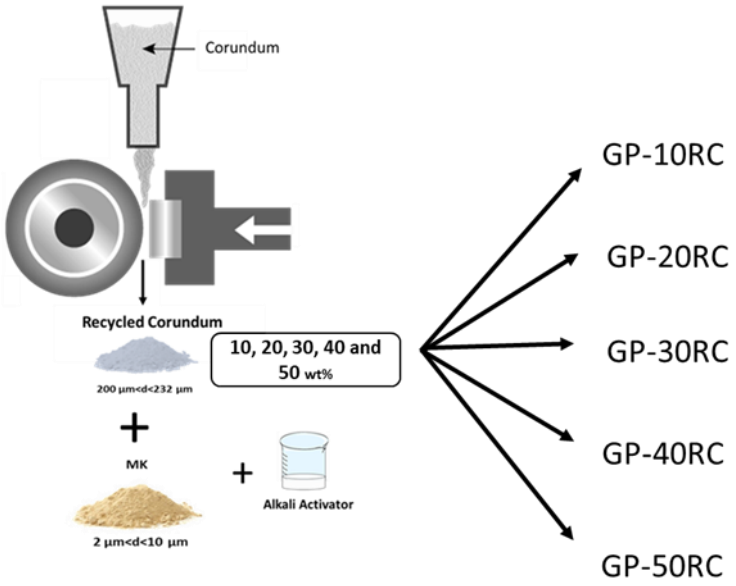

Fig.6-2 Geopolymer formulations with recycled corundum before AA.

Tab.6-2 Geopolymer composition.

	Weight %					
Mix ID	**MK (g)**	**RC (g)**	**NaOH 8M (g)**	**Na-silicate solution (g)**	**L/S**	H_2O
GP0	100	0	38	40	7.8	32
GP-10RC	90	10	34	36	7.0	30
GP-20RC	80	20	30	32	6.2	28
GP-30RC	70	30	28	30	5.8	24
GP-40RC	60	40	24	26	5.0	19
GP-50RC	50	50	17	20	3.7	16

Fig.6-3 Picture of GP0 paste.

All geopolymers were prepared through Planetary Mixer (Aucma 1400W, China) (Fig.6-4). The fresh paste was poured into silicon cube molds (25 mm × 25 mm × 25 mm). After removing all the bubbles with the vibrating table, the molds were closed and geopolymers cured at room temperature at 100% relative humidity. The silicon molds were opened after 28 d of curing time to proceed with the proper characterization. A minimum of 10 samples per each formulation were obtained.

Fig.6-4 Planetary Mixer photo (Aucma 1400W, China) and Mixer Table (right).

6.1.3 Stability in water

- Weight loss

Figure 6-5 depicts the weight loss of all geopolymers with and without recycled corundum (RC) after 24 hours in H_2O. As can be observed, with the addition of 10% RC, the weight loss remains nearly unchanged. However, with 20% RC, a significant increase is evident, which also impacts the mechanical properties (Fig.6-14) of the compound. Following this peak, a consistent trend is established, in which the weight loss decreases as the percentage of added corundum increases.

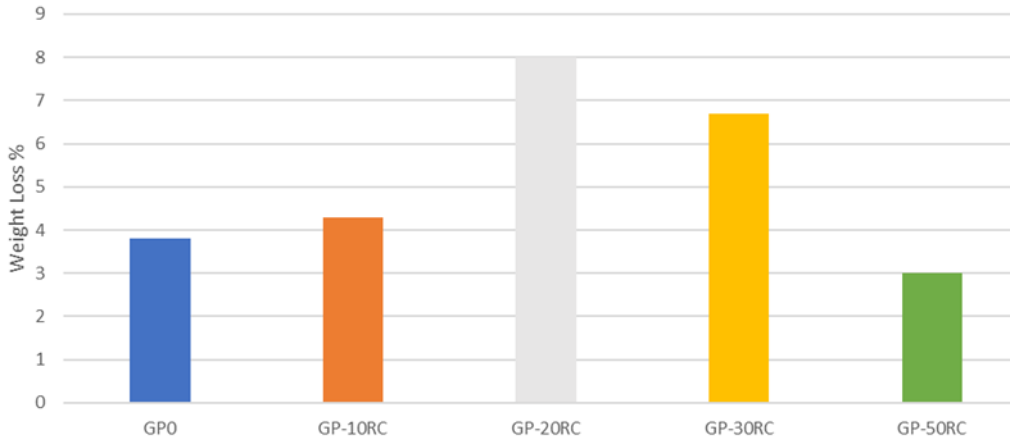

Fig.6-5 Weight loss of geopolymers with RC.

- Ionic conductivity and pH of the eluate

We conducted a study to evaluate the chemical stability and leaching behavior of geopolymer matrices containing recycled corundum (RC) to understand their environmental characteristics and potential risks. Concerning the chemical stability of the aluminosilicate network, it is important to note that the higher reactivity of the alkaline solution with metakaolin (MK) or RC, when present, leads to a lower release of ionic and cationic species. Regarding pH analyses, samples containing 10% and 20% of RC exhibited behavior very similar to the MK-based geopolymer (GP0).

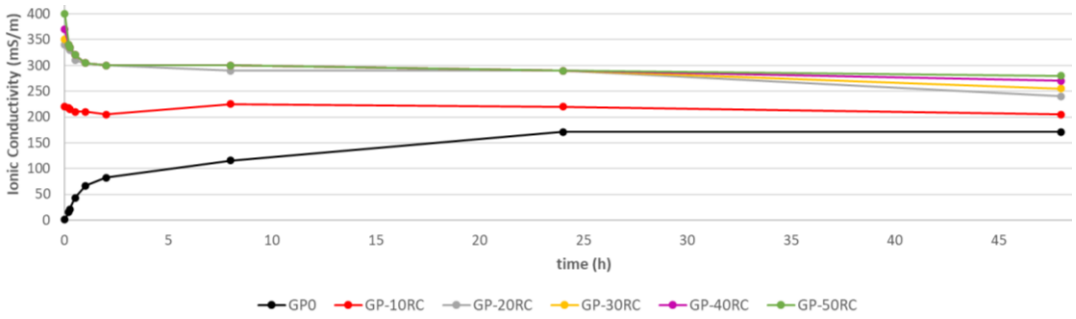

Fig.6-6 Ionic conductivity of the eluate (1:10=solid:water weight ratio) vs immersion time of the three geopolymers cured 28 day. (The reproducibility of the test was calculated to be within an error of 5%).

The pH decreased initially and stabilized around 10 after 48 hours, with values of 9.86, 9.98, and 10.17 (with an error of ±2%) for GP0, GP-10RC, and GP-20RC, respectively. In contrast, the ionic conductivity analyses (Figure 5-6) showed different results. The ionic conductivity stabilized after approximately 10 hours and remained nearly constant or slightly varied for each analyzed sample. Furthermore, the mechanical properties confirmed the reticulation of the 3D geopolymeric network, as indicated in Figure 6-21.

- Leaching of the consolidated geopolymer through ICP-OES and ICP-MS

In accordance with the procedural guidelines outlined in section 3.3.6, a comprehensive evaluation was conducted, encompassing all test specimens. Specifically, these test specimens comprised two distinct proportions, namely, 10% and 20%, of discarded corundum material, juxtaposed against two comparative benchmarks: pure corundum powder and the benchmark geopolymer denoted as GP0. This testing regimen sought to elucidate the performance characteristics and properties of the samples under examination, with particular emphasis on the influence of varying levels of recycled corundum content on their behavior and attributes. By subjecting the specimens to rigorous testing protocols and analyzing their response in relation to both corundum powder and GP0, a comprehensive understanding of their performance relative to established standards and references was achieved.

Figure 6-7 presents the findings on the release of heavy ionic metals. The histogram clearly indicates that the prominent heavy ionic metals

released are Aluminum (Al), Calcium (Ca), Silicon (Si), and Vanadium (V). Other metals are only present in minimal amounts.

Specifically, the release of aluminum ions by the RC is observed to be at very low concentrations. The samples containing 10% and 20% RC exhibit lower aluminum release compared to the GP0 sample. On the other hand, GP0 shows the highest release of silicon, as the Si-bearing impurities in RC are not easily leached. This trend is consistent with decreasing silicon release from GP-10RC to GP-20RC. As for calcium release, it is higher in the presence of RC and decreases from GP-20% RC to GP0. Lastly, the release of vanadium appears to be influenced by the amount of metakaolin in the geopolymer samples. It is suggested that vanadium is not introduced into the geopolymeric matrix through the waste itself, but rather it is a contaminant originating from the natural mineral that forms metakaolin.

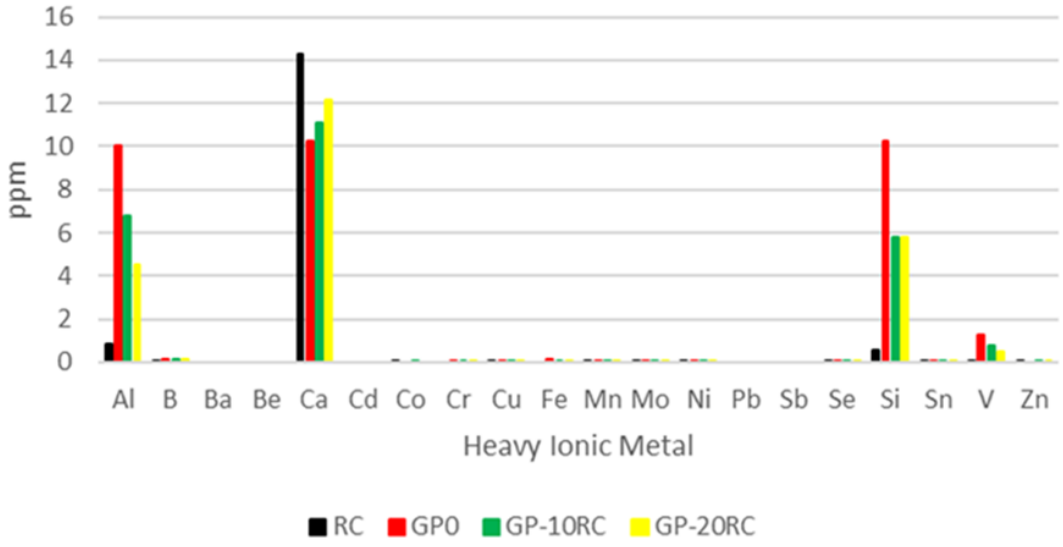

Fig.6-7 Results of the leaching test of the recycled corundum and the geopolymers samples. All the samples were diluted 1:10 and 1:20 to obtain the Al release. All the other heavy metals are detected without any dilution of the leachates.

6.1.4 Geopolymerization

In order to ascertain the presence of geopolymers in both the samples, those containing corundum as well as those without, a comprehensive array of analytical techniques were systematically employed. These investigations served to provide a robust confirmation of the geopolymers' formation and characteristics within the test specimens. The initial analytical tool utilized was IR

spectroscopy (Infrared Spectroscopy), which enabled the detection and characterization of the Al-O-Si bond formation. This technique proved instrumental in elucidating the chemical structure of the geopolymers, offering insights into the specific molecular bonds that are indicative of their presence. Subsequently, X-ray Diffraction (XRD) analysis was conducted to delve further into the crystalline structure of the samples. By observing the amorphous band, a hallmark feature of geopolymers, this method facilitated the identification of the characteristic structural patterns associated with these materials. Moreover, it was instrumental in flagging any potential impurities that might be present within the samples, thereby ensuring the purity and integrity of the geopolymers. Lastly, the investigation turned to Magic Angle Spinning Nuclear Magnetic Resonance (MAS-NMR), an advanced technique that allowed for an in-depth examination of the influence of corundum on the geopolymers. This high-resolution spectroscopic method shed light on the intricate interplay between RC and the Si-O-Al bonds, unraveling the unique effects that RC imparts on the geopolymers' structural composition. Collectively, this multifaceted approach not only confirmed the presence of geopolymers in the test samples but also provided valuable insights into their chemical nature, crystalline structure, and the modifying influence of Reactive Corundum on the Si-O-Al bonds, thus advancing our understanding of these materials and their applications.

- FTIR

Figure 6-8 illustrates the FTIR spectra of MK, RC powders, and the composite geopolymers GP-RC ranging from 0%wt to 20%wt. All spectra display characteristic -OH stretching and bending peaks at 3440 and 1640 cm^{-1}, respectively. The MK spectrum exhibits Si-O-T (T= Si or Al) bands at 1080 cm^{-1}, which are also referred to as DOSPM (Density of Staxte Peak Maximum) and are used to monitor geopolymerization [Perna et al. 2021; Rattanasak et al. 2009; Dal Poggetto et al.2021; Priya et al. 1997]. The shift of this peak to lower wavenumbers (1019-1014 cm^{-1}) indicates an increase in Si-O-Al bonds, suggesting the progress of geopolymerization. Although this shift appears slightly lower for geopolymers with RC compared to the reference GP0, it indicates that the geopolymerization process is not significantly affected by the inclusion of recycled waste. In the MK

spectrum, the band at 800 cm^{-1} is attributed to the presence of quartz, while the band at 560 cm^{-1} corresponds to Al-O vibration in six-fold coordination [Škvára et al. 2012; Ponzoni et al. 2015; Panias et al. 2007; Makreski et al. 2004]. The band at 470 cm^{-1} in both MK and GP (0 to 20%wt of RC) is associated with Si-OH bending mode (also in line with the comments on the peak at 460 cm^{-1} from RC). As for the RC spectrum, it exhibits sharper bands characteristic of crystalline compounds. The main signal is a sharp band at 1089 cm^{-1} corresponding to Al-O vibration. The presence of peaks at 1089 cm^{-1}, 800 cm^{-1}, and 780 cm^{-1} suggests some disorders in the corundum network, possibly due to the presence of additional types of coordination for the aluminum atoms (AlO_4 and AlO_3) [Joo Hyun et al. 2002]. Another band at 459 cm^{-1} is attributed to Al-O bending. This band appears sharply intense in the recycled corundum spectrum and, along with the band at 470 cm^{-1}, becomes rounded but intense in geopolymer samples with higher RC content. In the spectra of GP0, GP-10, and GP-20RC, bands at 1448-1385 cm^{-1} are observed, indicating the formation of carbonates on their surfaces, possibly due to the interaction of sodium and calcium ions with atmospheric CO_2. These bands are more prominent in GP-10RC and GP-20RC, likely due to the presence of CaO in the RC, as confirmed by XRF analysis. This hypothesis is further supported by the presence of the band at 1384 cm^{-1} in the RC spectrum and the significant release of calcium ions observed in the leaching test. In the extended IR range at 500-400 cm^{-1} (Figure 5-8B), the presence of vanadium, titanium, iron, calcium, silicon, and aluminum oxides is confirmed. This band is more pronounced in MK and GP0, while it is less intense in geopolymers with 10% and 20% wt of RC. This finding aligns with the data obtained from the leaching test, where MK and GP0 exhibited higher vanadium release compared to RC and GPs with RC. Additionally, the medium broad band at 474 cm^{-1} (particularly visible for GP0, GP-10RC, GP-20RC, and as a shoulder in RC) is attributed to Al-O vibration, while peaks at 453 and 442 cm^{-1} could be related to Fe-O vibrations [Moutinho et al. 2020; Joo Hyun et al. 2002]. Finally, the Ti-O absorption broad bands are assigned to 436 and 426 cm^{-1} [Moutinho, et al. 2020.; Joo Hyun et al. 2002], and the sharp band at 420 cm^{-1} corresponds to Ca-O vibration [Ruiz-Santaquiteria et al. 2011].

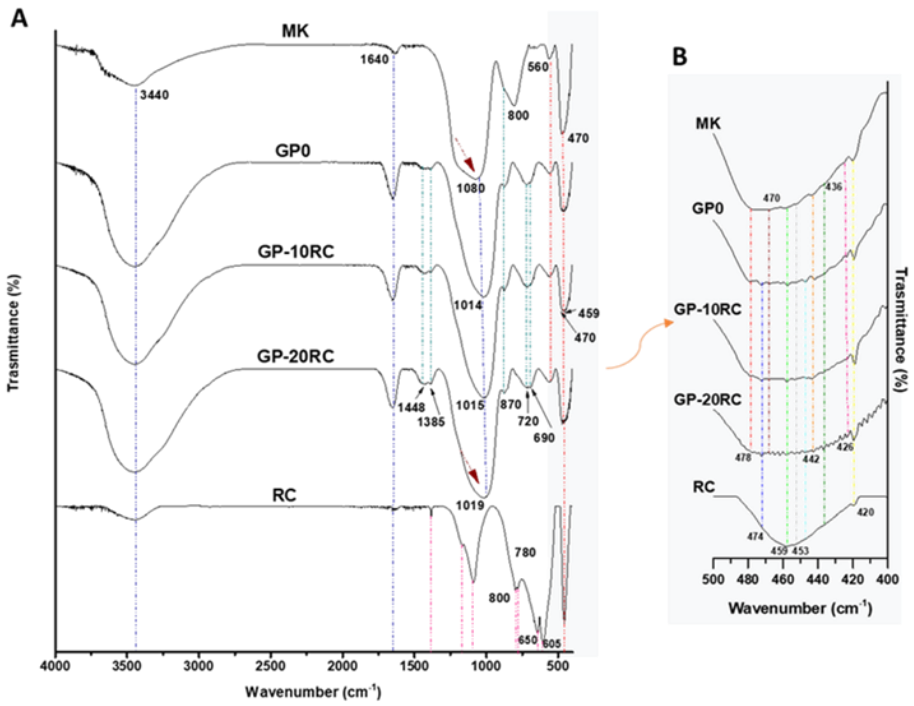

Fig.6-8 A) FTIR spectra of MK powder, GP0, GP-10RC, GP-20RC and RC powder. B) Focus on 500-400 cm^{-1} IR range.

- MAS-NMR

The analyses of the geopolymeric samples were carried out in strict accordance with the procedural guidelines delineated in section 3.1.8 This systematic adherence to the specified protocol ensured the thorough and consistent examination of the samples, guaranteeing the reliability and accuracy of the obtained results. By following the prescribed methodology outlined in section 3.1.8, a rigorous and standardized approach was upheld, facilitating a comprehensive assessment of the geopolymeric specimens and enabling meaningful comparisons and insights to be drawn from the data collected. The analysis of the ^{29}Si NMR GP0 deconvolution reveals (Fig.6-9) a distinct composition within GP0, primarily characterized by the presence of Q4(4Al), Q4(3Al), and Q4(2Al) species. This observation is notably in agreement with the findings obtained from the ^{27}Al GP0 spectrum, which indicates the presence of both Al(IV) and Al(VI) species, along with minimal traces of Al(V) originating from the initial metakaolin precursor. These spectroscopic results provide robust confirmation of the insights gained through X-ray Diffraction (XRD) analysis. They collectively demonstrate that our GP0 material is not solely amorphous but incorporates a crystalline component within its structure. This nuanced characterization underscores the complexity

and heterogeneity of the GP0 material, shedding light on its structural diversity and potential implications for its properties and applications.

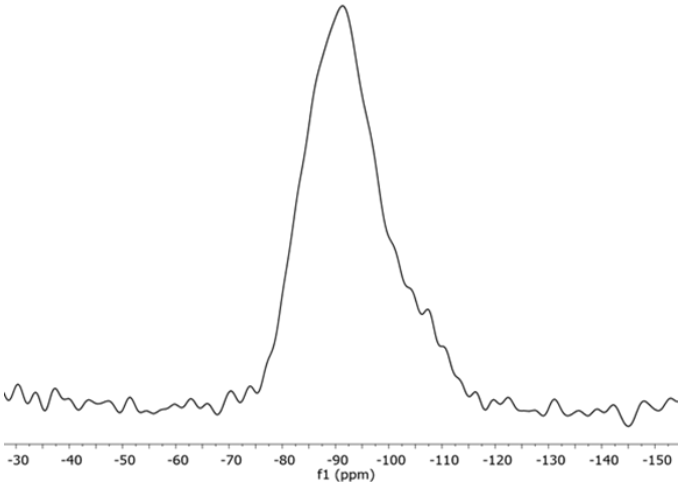

Fig.6-9 ^{29}Si MAS-NMR spectra of GP0.

Within Figure 6-10, one can readily discern the ^{29}Si spectrum of GP0, GP-20RC and GP-50RC. A closer examination of this spectrum, achieved through the process of deconvolution, reveals a notable shift in the composition. Specifically, the introduction of RC (presumably referring to a particular substance or condition) leads to a discernible increase in the presence of Q4(3Al) species, accompanied by a corresponding decrease in the abundance of Q4(2Al) species. This observed shift in the distribution of aluminum coordination environments (from Q4(2Al) to Q4(3Al)) in the ^{29}Si spectrum upon the inclusion of RC signifies a meaningful alteration in the underlying chemistry or structure of the material. Further analysis and interpretation of these findings could provide valuable insights into the impact of RC on the properties and characteristics of GP-20RC, shedding light on its potential applications or modifications.

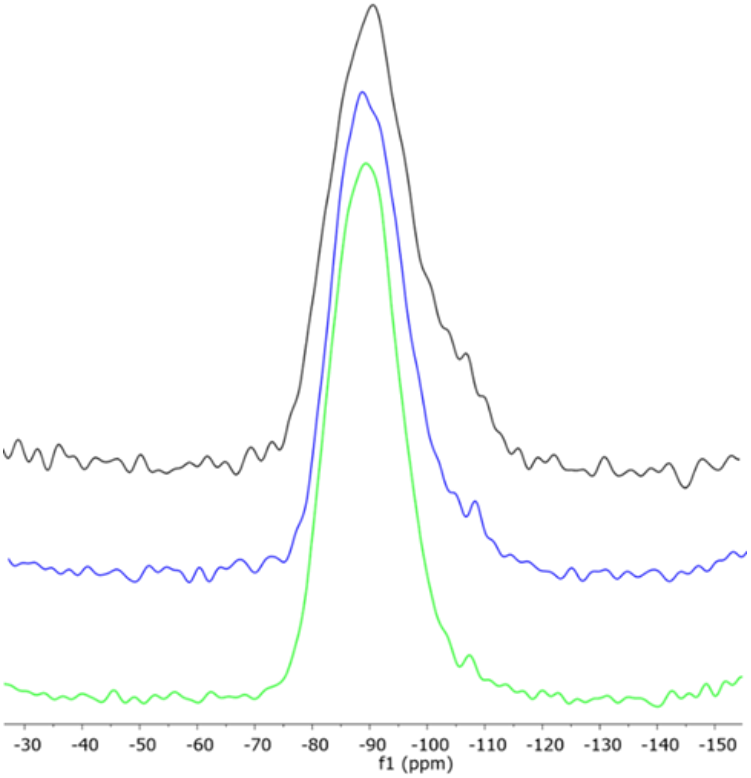

Fig.6-10 Comparison of ^{29}Si MAS-NMR spectra GP0, GP-20 and GP-50RC.

Figure 6-11 presents the ^{27}Al spectrum of GP0, and, as previously mentioned, it offers a glimpse into the composition of aluminum species within the geopolymeric matrix. Within this spectrum, one can discern the presence of both Al(IV) and Al(VI) species, which are integral components of the geopolymeric network, alongside unreacted Al(V) originating from the metakaolin (MK) precursor. This initial characterization lays the foundation for understanding the aluminum chemistry in GP0. The plot takes an intriguing turn with the introduction of RC. This is readily apparent in Figure 6-12, where the aluminum spectrum undergoes a discernible transformation. Notably, the emergence of Al(VI) species from corundum becomes evident, marked by distinctive peaks that are notably concentrated at approximately 10 ppm. This observation signifies a significant shift in the aluminum environment, introducing a new component derived from the presence of RC. As the concentration of RC is increased, the intensity of these Al(VI) peaks originating from corundum becomes even more pronounced. This heightened intensity affords a clearer demarcation between the Al(VI) species within the geopolymeric network and those attributed to the corundum additive. Furthermore, a noteworthy revelation is that Al(V) is conspicuously

absent in the geopolymer samples containing RC, implying a transformative impact on the aluminum species' composition. These findings illuminate the profound influence of RC on both the structural and chemical aspects of the material. In particular, they underscore the pivotal role played by RC in reshaping the aluminum coordination environment within the geopolymer matrix. Such insights have the potential to unlock novel avenues for tailoring the properties and applications of geopolymeric materials, making this study a valuable contribution to the field of materials science.

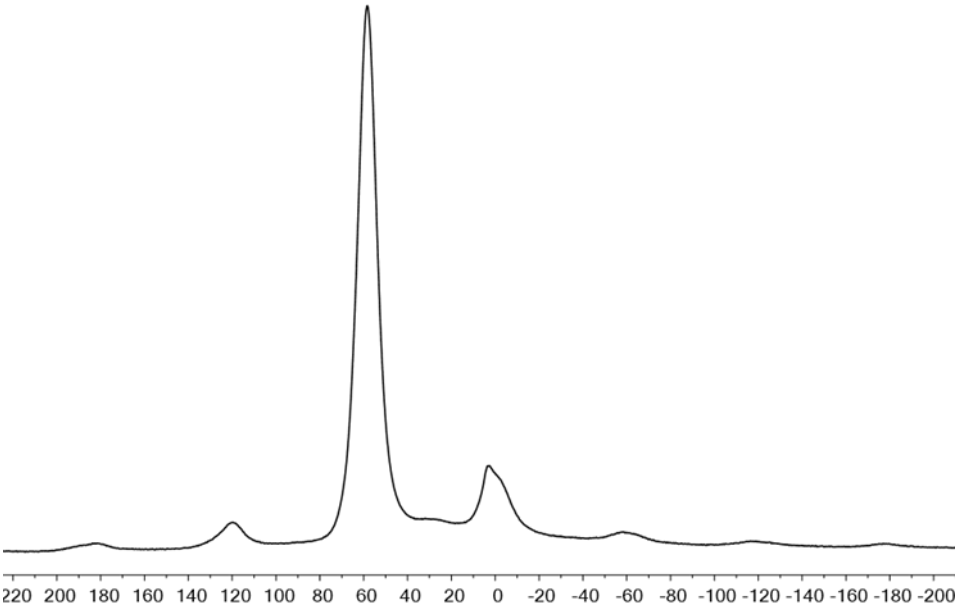

Fig.6-11 ^{27}Al MAS-NMR spectra of GP0.

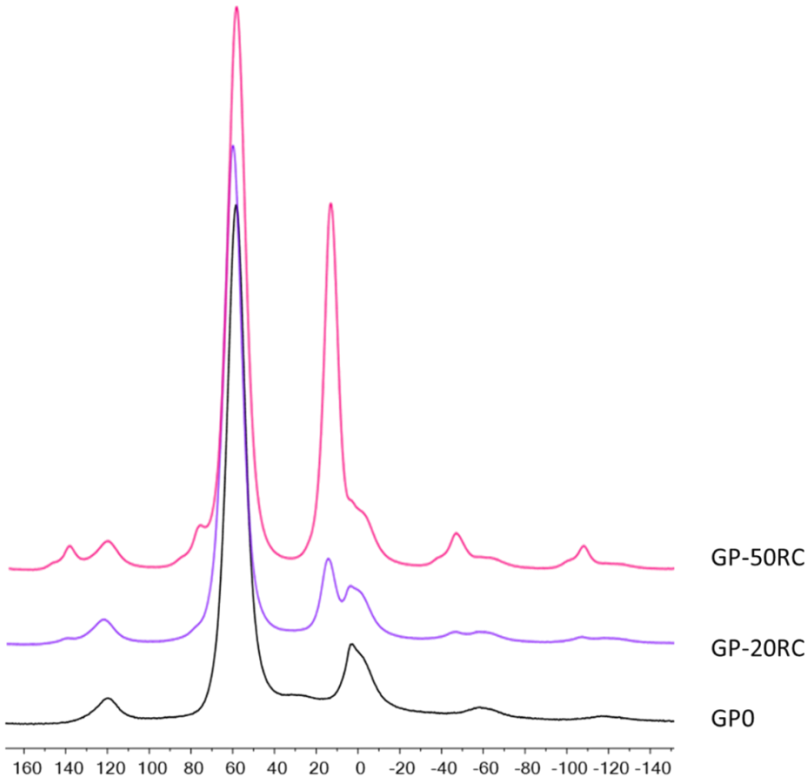

Fig.6-12 Comparison of all ^{27}Al MAS-NMR spectra.

- XRD

In the diffraction pattern from metakaolin (Figure 6-13) it is evident a diffuse reflection identified as the typical large band of the amorphous aluminosilicate structure plus shaper peaks identified as anatase, and α-quartz. The diffraction patterns from GP0 and GP-RC series were similar (Figure 6-14), and all these three geopolymers had a diffuse reflections characteristic of amorphous aluminosilicate network at about 26–28° in 2θ [Nakajo et al. 2006]. By increasing the percentage of recycled corundum, a peak around 8° (present in the RC spectra) can be seen in the all the sample, which confirms the presence of recycled co-rundum that has not reacted perfectly, which is not noticeable in the GP-10RC spectrum due to the lower amount of RC.

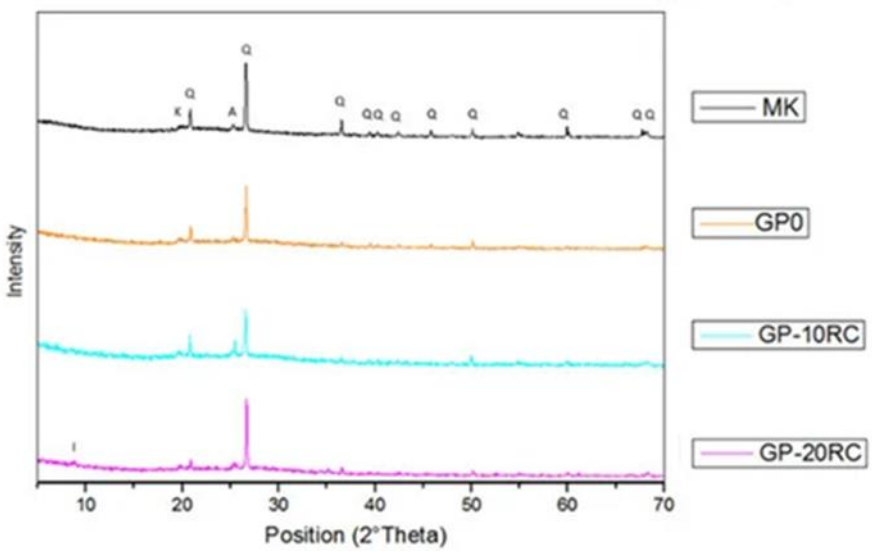

Fig.6-13 Diffraction patter of geopolymer with 10 and 20wt% of RC compared with GP0 and MK powder. Crystalline phases identification label: Q = Quartz, K = Kaolinite, A = Anatase.

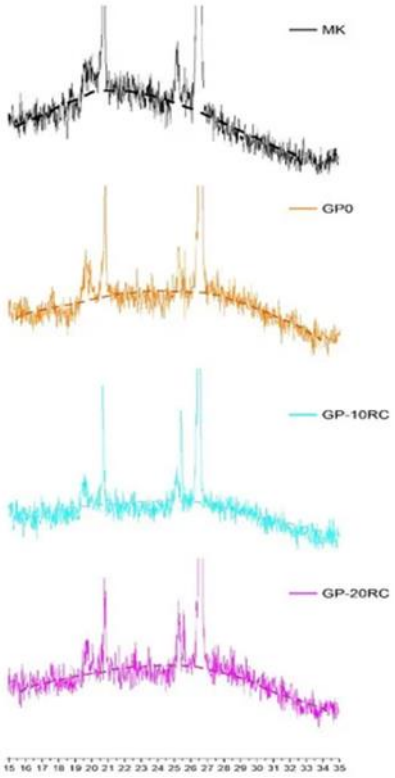

Fig.6-14 Enlargement of spectra 5-14 in the range 20–35° (2 theta).

6.1.5 Microstructure

- Characterization via SEM

Scanning electron microscopy (SEM) observations have unveiled a fascinating microstructural landscape, as depicted by the conspicuous yellow region in Figure 6-15. This intricate microcosm reveals that the recycled corundum irregular grains have become intricately enmeshed within the geopolymeric network, forming a densely interwoven structure. Interestingly, when we examined the elemental distribution maps for aluminum (Al), silicon (Si), sodium (Na), and oxygen (O), we observed a uniform dispersion within the geopolymer matrix, making it challenging to discern specific microstructural features. Further scrutiny at high magnifications, as shown in Figure 6-15B, did not yield substantial insights, as it primarily showcased the densely packed geopolymeric gel. In stark contrast, we did notice some unreacted metakaolin (MK) lamellar particles, highlighted in a magnified black area within Figure 6-15B. These particles, in contrast to their unreacted counterparts, exhibited a fully transformed, spongy-like geopolymeric structure, a hallmark of successful reaction, as demonstrated in Figure 6-15A.

Perhaps most intriguingly, when RC was introduced into the mix, its distribution was found to be impressively uniform throughout the geopolymeric matrix, contributing to the overall homogeneity of this intricate microstructure.

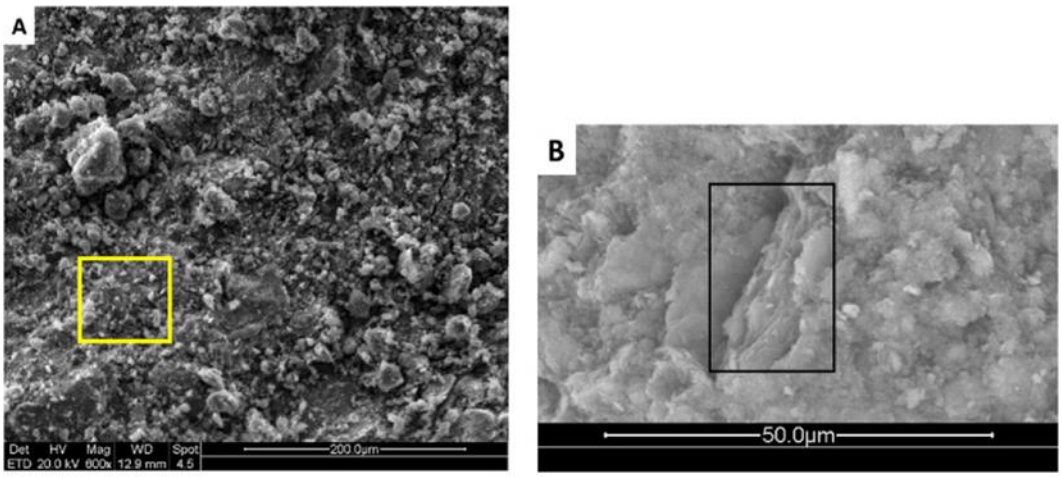

Fig.6-15 Scanning electron microscopy images taken at low magnification (600×) to evidence the different toughening mechanics of GP0.

Upon the incorporation of RC, we made a noteworthy discovery: its dispersion throughout the geopolymeric matrix exhibited an impressive level of homogeneity. This uniform distribution is a testament to the efficacy of the mixing process. When we examined this phenomenon at lower magnifications, as illustrated in Figure 6-16 (B and C), a fascinating interplay of mechanisms came into view. We could clearly discern the crack deflection mechanism, characterized by the conspicuous red area in the figure, operating in tandem with the pull-out mechanism, represented by the striking green region. These two mechanisms serve as vital toughening agents, and their presence suggests a crucial insight into the nature of the interface between the RC grain and the matrix. The relatively weak interface between the RC grain and the matrix can be attributed to the low reactivity of the crystalline corundum surface. These finding sheds light on the intricate interactions occurring within this composite material. In the pull-out region, a notable occurrence was the observable densification of the matrix at the surface of the corundum particle. This visual confirmation reinforces the idea that, in each composition tested, the metakaolin (MK) particles have undergone complete reaction with the activator solution. This successful reaction is facilitated by the impervious nature of the corundum grain's surface, which prevents the absorption of the activator solution, ensuring the full reactivity of the MK particles. This interplay of factors contributes to the overall mechanical robustness of the material, with the crack deflection and pull-out mechanisms playing a pivotal role in enhancing its structural integrity.

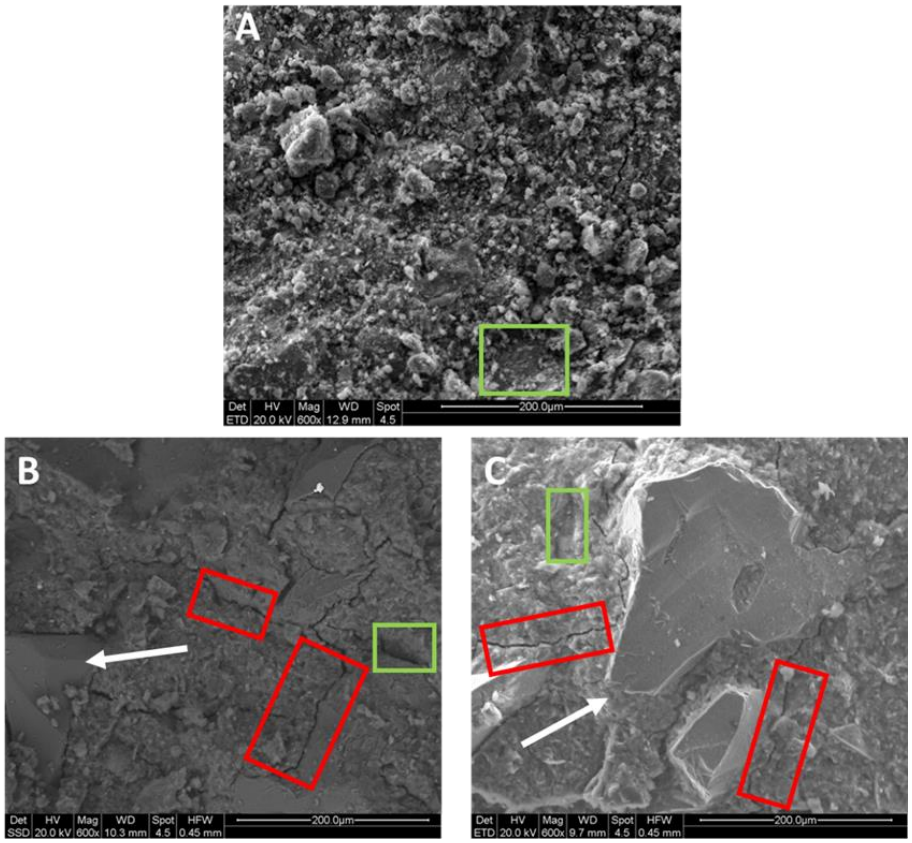

Fig.6-16 Scanning electron microscopy images taken at low magnification (600×) of A) GP0; B) GP-20RC and C) GP-50RC.

- Compressive strength

The compressive strength tests were performed after 28 days of curing on all the consolidated geopolymer samples. Figure 6-17 illustrates the mechanical properties of all geopolymers with varying percentages of corundum compared to GP0. It can be observed that there isn't a clear trend, but up to the addition of 40%, the compressive strength tends to decrease and then remain constant. When testing the strength of geopolymers with 50% RC, it increased again. To ensure that higher additions of corundum wouldn't lead to excessively high values, the GP-70RC formulation was prepared and tested, observing a significant decrease in values once more. The GP-50RC formulation returns to higher values, likely due to a more uniform dispersion of RC within the geopolymeric matrix.

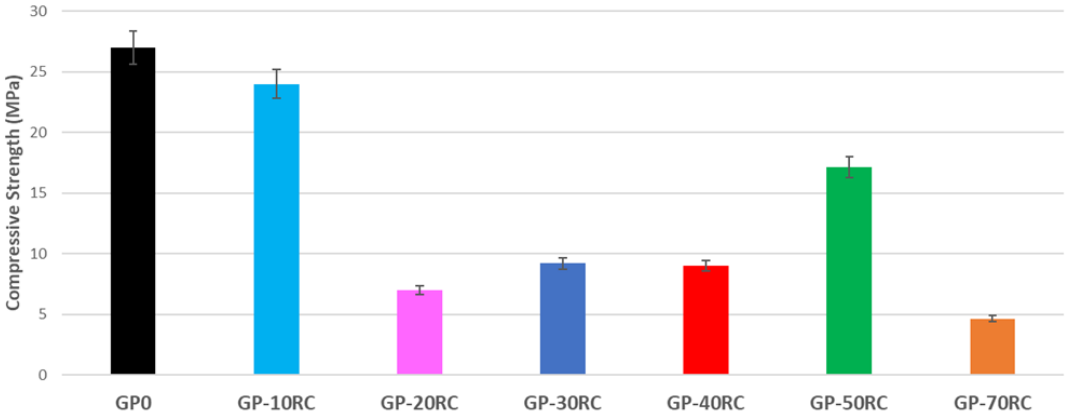

Fig.6-17 Compressive strength of all geopolymer with recycled corudum.

6.1.6 Antibacterial activity

In order to investigate the potential antibacterial properties for non-structural building applications, such as glazes on ceramic tiles, we conducted experiments where both gram-positive and gram-negative bacterial strains were cultivated in the presence of the synthesized geopolymers. The results, depicted in Figure 6-18, show images of the bacterial growth on plates with the presence of the geopolymers. From the pictures, it is evident that there are not distinct inhibition halos. This observation can be attributed to the fact that none of the geopolymer samples released heavy metals in the culture broth at concentrations that negatively affected bacterial growth, as confirmed by the release test. However, a more detailed examination of the back of the Petri plates revealed that P. aeruginosa and E. faecalis managed to grow on the geopolymer samples. In contrast, S. aureus and E. coli were unable to grow on the same samples, as depicted in Figure 6-19. This discrepancy can be explained by the resistance of the former bacterial strains to both potential metal release and pH environment changes [Nakajo et al. 2006].

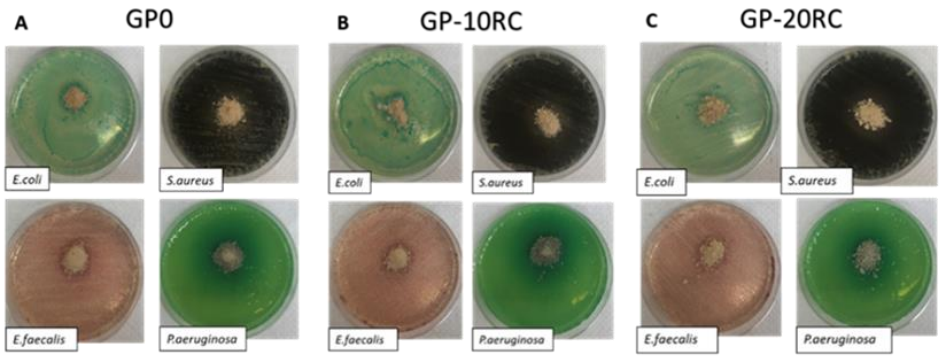

Fig.6-18 Inhibition halo of *E.coli*, *S.aureus*, *E.faecalis*, and *P.aeruginosa* for samples: (A) GP0; (B) GP-10RC; and (C) GP-20RC.

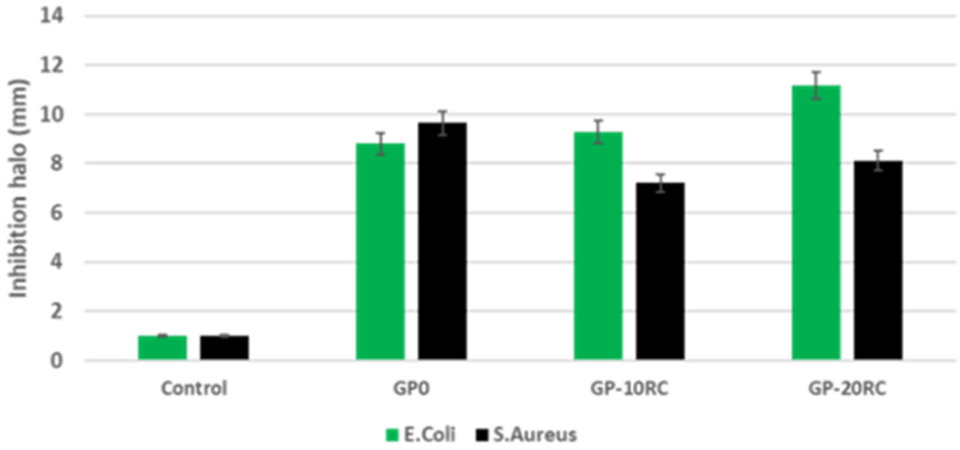

Fig.6-19 Comparison of the inhibition halo of *E.coli* and *S.aureus* for the three geopolymers.

6.2 The effect of reclcyed corundum added after the alkali activation of MK-based geopolymer

6.2.1 Geopolymer formulation

After the GP0 fresh paste (see Section 6.1) preparation, addition of the as-received recycled corundum powder in the amounts of 10, 20, 30, 40 and 50 wt% (percentage of RC have been calculated with respect to the total mass of the composite formulation in the wet status) was performed to produce the geopolymer composites labelled 90GP-10RC, 80GP-20RC, 70GP0-30RC, 60GP0-40RC and 50GP0-50RC, respectively, as indicated in Table 6-3.

Amounts of RC higher than 50 wt% compromised the workability of the mix. The formulations maintained constant the MK/NaOH and MK/silicate weight ratio in the different composites. All formulations were mixed as already discussed in section 6.1.

Tab.6-3 Mix proportion of Geopolymers with RC added after the Alkali activation. L is liquid (NaOH+Nasilicate), S is solid (MK + RC).

Weight %

Mix ID	MK (g)	RC (g)	NaOH 8M (g)	Na-silicate solution (g)	L/S	H_2O
GP0	100	0	38	40	7.8	32
90GP0-10RC	51	10	19	20	6.4	28
80GP0-20RC	45	20	17	18	5.4	25
70GP0-30RC	39	30	15	16	4.5	22
60GP0-40RC	34	40	12	14	3.5	19
50GP0-50RC	28	50	11	11	2.8	16

Tab.6-4 Percentages of oxides in raw materials and solutions.

Weight %										
Material	**SiO_2**	**Al_2O_3**	**Na_2O**	**CaO**	**K_2O**	**TiO_2**	**Fe_2O_3**	**MgO**	**H_2O**	**LOI**
Metakaolin	55	40	0.5	0.2	0.3	1.5	1.4	0.1	-	1
Recycled Corundum	2.49-3.58	91.72-92	-	2.41-2.81	-	0.42-0.61	0.59-1.06	-	-	-
NaOH 8M	-	-	19.47	-	-	-	-	-	80.53	-
Na-silicate sol.	27.09	-	8.85	-	-	-	-	-	64.06	-

Tab.6-5 Percentages of oxides in geopolymer samples.

Mix ID	SiO_2	Al_2O_3	Na_2O	$CaO+K_2O$	H_2O	LOI and other OXides
GP0	37	22	6	2	32	1
90GP0-10RC	34	30	5.5	1.5	28	1
80GP0-20RC	30	36	5	4	24	1
70GP0-30RC	26	41	4.5	4	23	1.5
60GP0-40RC	22	47	4	5	20	2
50GP0-50RC	19	53	3.5	5.5	18	1

6.2.2 Stability in water

In Figure 6-20, the specimens underwent the treatment detailed in the earlier section, Section 3.3.2. It is discernible that the contrast between GP0 and the remaining samples is marginal. This phenomenon can be attributed to the occurrence of geopolymerization and the influence of Corundum, which has a tendency to desiccate the material and deter water retention. Indeed, as the proportion of RC escalates, there is a noticeable reduction in weight loss. The implications of these observations are noteworthy. The minimal difference in Figure 6-20 suggests that the geopolymerization process was effective across all samples, with Corundum playing a significant role in drying out the material and minimizing water absorption. This is particularly intriguing because it signifies the potential for increased efficiency and durability in materials incorporating Corundum and geopolymerization. Additionally, the inverse relationship between the percentage of RC and weight loss indicates a promising avenue for fine-tuning the properties of the material, offering opportunities for enhanced structural performance and reduced susceptibility to moisture-related degradation.

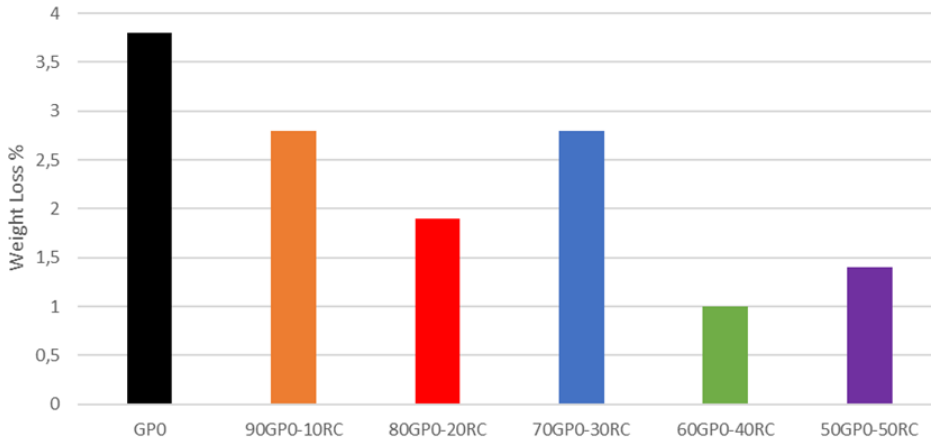

Fig.6-20 Weight loss (%) of all sample.

- Ionic conductivity of the eluate

Following immersion of geopolymer specimens in water, the solutions' ionic conductivity increases due to the leaching out of unreacted alkaline solution. A direct correlation emerges: the greater the unreacted alkaline activator fraction, the higher the resulting

ionic conductivity of the solution. Observing Figure 6-21 it becomes evident that the disparity between GP0 and the geopolymer holds significance within the formulations ranging from 90GP0-10RC to 60GP-40RC. Meanwhile, the formulation involving 50 wt% of RC more closely resembles GP0. Over a 24-hour immersion period, all formulations stabilize at a consistent value. Notably, the addition of 10 wt% and 20 wt% RC yield remarkably similar outcomes, whereas 30 wt% and 40 wt% show only marginal increases (Figure 6-21). Strikingly, the formulations 90GP0-10RC and 80GP0-20RC, exhibiting the lowest ionic conductivity, align with the most intricately interconnected MK-geopolymeric matrix and concurrently demonstrate the highest mechanical strength (see Figure 6-38).

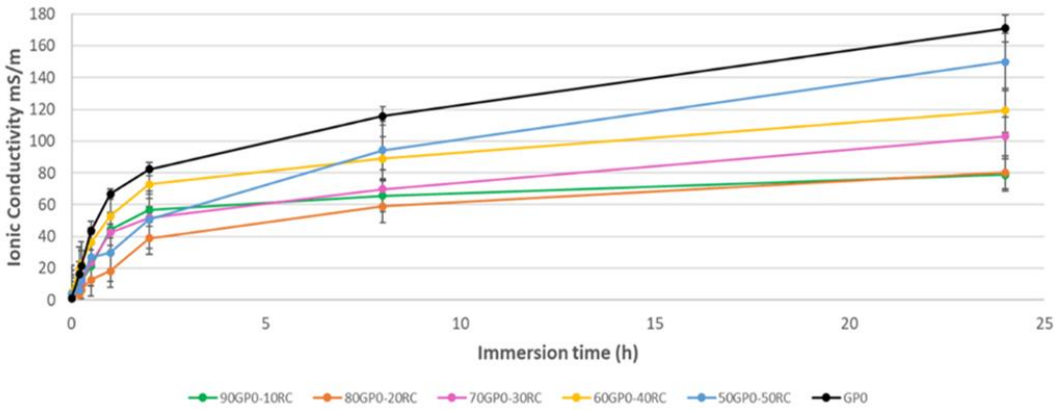

Fig.6-21 Evolution of the ionic conductivity of the solution where the geopolymers were immersed for at least 24h. The error is ±5%, due to sample variability, rather than to the sensitivity of the conductivity cell.

6.2.3 Geopolymerization

- FTIR

The FTIR spectra of metakaolin and geopolymer blends containing recycled corundum (RC) after 28 days of curing are depicted in Figure 6-22. These spectra affirm that the inclusion of RC at various proportions does not disrupt the metakaolin's reticulation following alkali activation. Within the MK spectrum, the peaks at 3440 cm−1 and 1640 cm^{-1} correspond to the stretching and bending vibrations of water's hydration [Tchakouté et al. 2017]. The band at 1077 cm^{-1} signifies asymmetric stretching vibrations of Si–O–Si or Si–O–Al bonds [Catauro et al. 2020]. Notably, this band shifts to lower wavenumbers

(1018–1011 cm^{-1}) for all geopolymers, both with and without RC. This shift implies an augmented count of Si-O-Al bonds, indicating the orderly occurrence of geopolymerization, as is the norm for MK-based geopolymers. Upon the introduction of recycled corundum, the proportion of aluminum capable of bonding with silicon rises. However, a pronounced shift of this band towards lower wavenumbers cannot be definitively determined. The observed Si-O bands at 800 and 460 cm−1 confirm the presence of quartz [Tchakouté et al. 2017], aligning with the XRD patterns displayed in Figure 6-34. The absorption band at 560 cm^{-1} is potentially associated with the existence of Al-O vibrations in a six-fold coordination arrangement [Tchakouté et al. 2017], potentially attributed to traces of illite within the MK [Tchakouté et al. 2016].

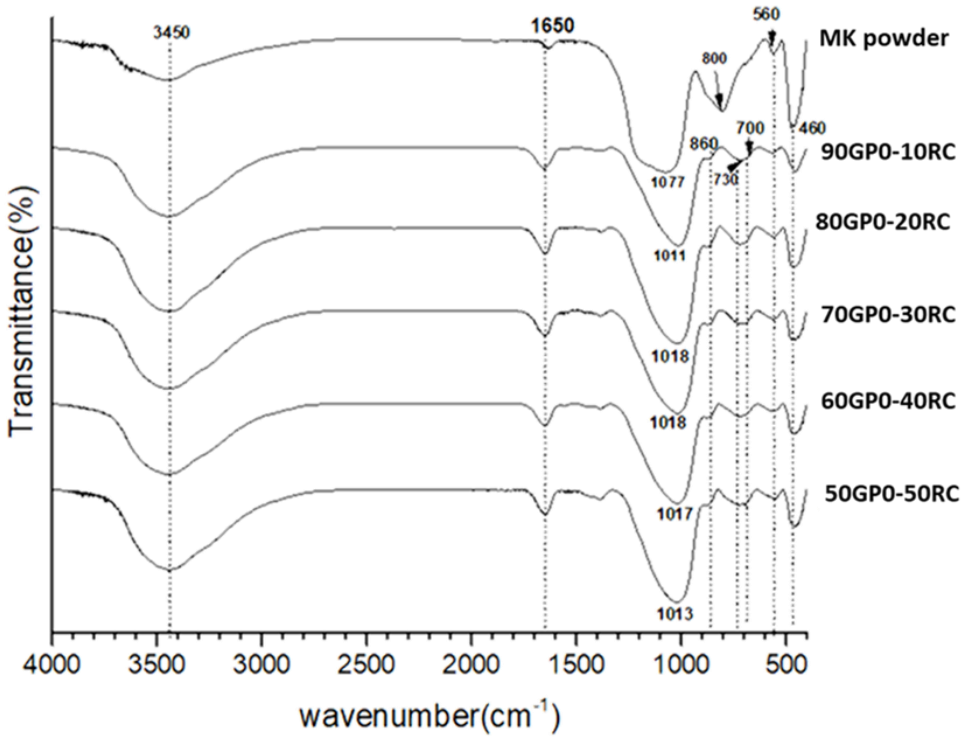

Fig.6-22 FTIR spectra of MK powder and all geopolymers with RC.

- MAS-NMR

By adhering to the specified methodology detailed in section 3.1.8, a rigorous and standardized approach was maintained, enabling a thorough evaluation of the geopolymeric specimens. This approach facilitated meaningful comparisons and insights to be derived from the collected data.

In Figure 6-23, the spectra of 80GP0-20RC and 50GP0-50RC are compared with GP0. A slight shift towards -90 ppm can be observed, which could be attributed to the presence of RC. Upon closer examination of spectra of 80GP0-20RC and 50GP0-50RC using deconvolution, a noticeable change in composition becomes apparent. Specifically, the introduction of different percentage of RC after the alkali activation results in a distinct increase in the presence of Q4(3Al) species, accompanied by a corresponding decrease in the abundance of Q4(2Al) species. This observed shift in the distribution of aluminum coordination environments (from Q4(2Al) to Q4(3Al)) in the ^{29}Si spectrum, upon the incorporation of RC, indicates a significant alteration in the material's underlying chemistry or structure.

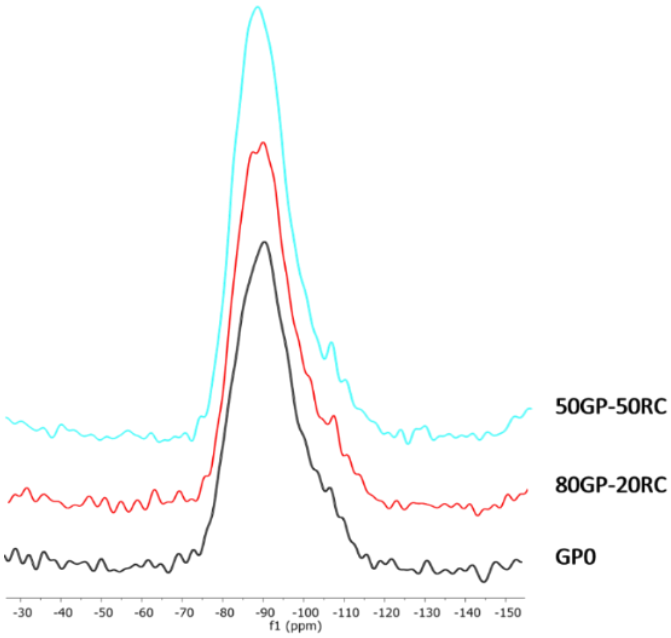

Fig.6-23 Comparison of all ^{29}Si spectra.

The figure 6-25 shows the ^{27}Al spectra of GP0, 80GP0-20RC and 50GP0-50RC, the presence of Al(VI) species from corundum is evident, marked by distinct peaks concentrated around 10 ppm. This observation indicates a significant alteration in the aluminum environment, introducing a new component resulting from the presence of RC. With an increase in RC concentration, the intensity of these Al(VI) peaks from corundum becomes more pronounced. This heightened intensity provides a clearer distinction between the Al(VI) species within the geopolymeric network and those associated with the corundum additive.

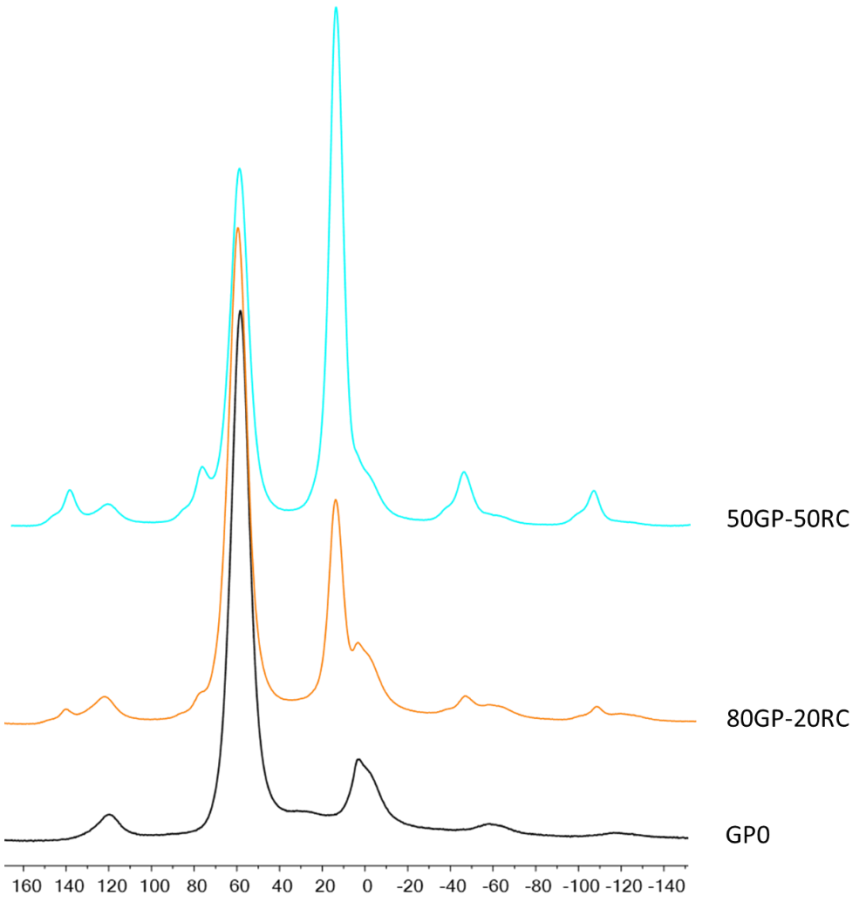

Fig.6-25 Comparison of all ^{27}Al spectra.

- XRD

The diffraction pattern acquired from the finely ground GP0 sample (Fig. 6-26) showcases the characteristic diffuse reflection signature of the amorphous aluminosilicate structure. Alongside this, more defined peaks emerge, identified as anatase (TiO_2) and alpha-quartz (α-SiO2), both inherent to the metakaolin. The initial crystalline structure of kaolinite ($Al_2Si_2O_5(OH)_4$), located around 20° in 2 θ, is evident in the as-received MK, observable in all patterns except for 50GP-50RC, which contains a lower MK proportion. In the formulation starting from 80GP0-20RC, the anatase impurity experiences a peak diminishment (this pattern has been magnified along the y-axis) due to decreasing MK content. The diffraction patterns are discernible from 90GP0-10RC to 60GP0-40RC, characterized by diffuse reflections indicative of amorphous geopolymer around 26–28° in 2θ [Temuujin et al. 2009; Catauro et al. 2020]. Upon introducing RC, the telltale corundum, α- Al_2O_3 peaks

gradually emerge, intensifying with rising RC percentages. It's notable that spectra from 90GP0 to 60GP0 lack peaks at 8° and 16° in 2θ, attributed to impurities like montmorillonite $(Na,Ca)_{0.3}(Al,Mg)2Si_4O_{10}(OH)2{\cdot}n(H_2O)$ and analcime, $NaAlSi_2O_6{\cdot}(H_2O)$, present in the recycled corundum. This suggests the environment is sufficiently basic for these RC impurities to react as well. Shifting amorphous humps in XRD patterns affirm the transition from Si-O-Si to Si-O-Al networks within the amorphous geopolymeric fraction. Additionally, in Fig. 6-26, the 50GP0-50RC sample's diffraction reveals the crystalline impurity peaks of the recycled corundum (both patterns magnified along the y-axis). This means that these crystalline phases remain undissolved in the alkaline media utilized as an activator for metakaolin.

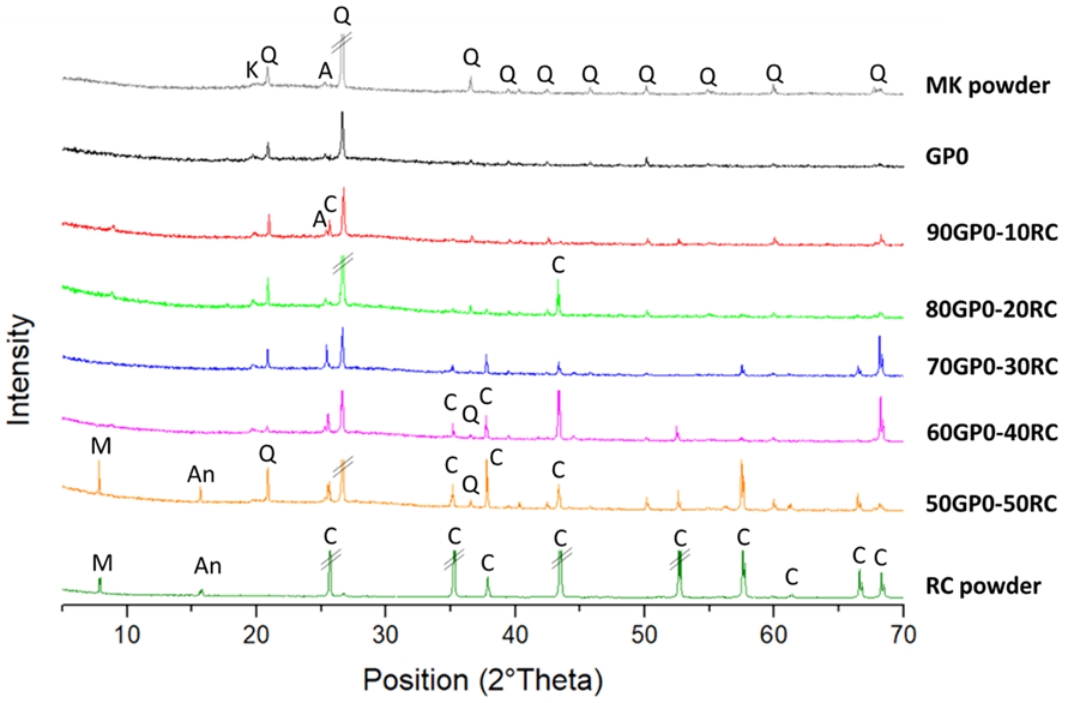

Fig.6-26 XRD patterns for MK powder, GP0, 90GP0-10RC, 80GP0-20RC*, 70GP0-30RC, 60GP0-40RC, 50GP0-50RC* and Recycled Corundum* powder. Crystalline phases identification label: Q = Quartz, K = Kaolinite, A = Anatase, M = Montmorillonite, An = Analcime and C = Corundum. *Larger Y-axis scale.

6.2.4 Microstructure

- Characterization via SEM

Scanning electron microscope (SEM) analysis revealed the presence of a remarkably compact microstructure (highlighted in yellow in Figures 6-27; 6-28 and 6-29), where in the irregular grains of recycled corundum are embedded within the geopolymeric network. However, attempts to characterize specific microstructures using individual element maps (Al, Si, Na, O) yielded uniform distributions across the geopolymer matrix. These maps did succeed in pinpointing the locations of RC grains (Figure 6-27).

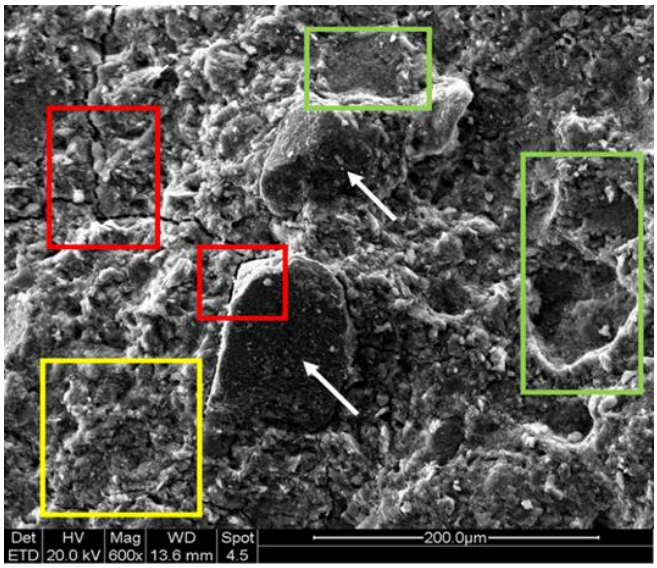

Fig.6-27 Scanning electron microscopy images taken at low magnification (600x) of 90GP0-10RC.

Conversely, SEM images at higher magnifications did not yield significant insights, as they predominantly displayed the dense geopolymeric gel (refer to Figure 6-15). In contrast to certain unreacted MK lamellar particles (enlarged black region in Figure 6-15), the remaining aluminosilicate powder exhibited complete reaction, showcasing the typical sponge-like geopolymeric structure (Figure 6-19). Upon incorporating RC, its distribution was uniform within the geopolymeric matrix. Upon closer examination, lower magnification observations revealed the occurrence of crack deflection mechanisms (red area in Figure 6-27) alongside pull-out phenomena (green area in Figure 6-27).

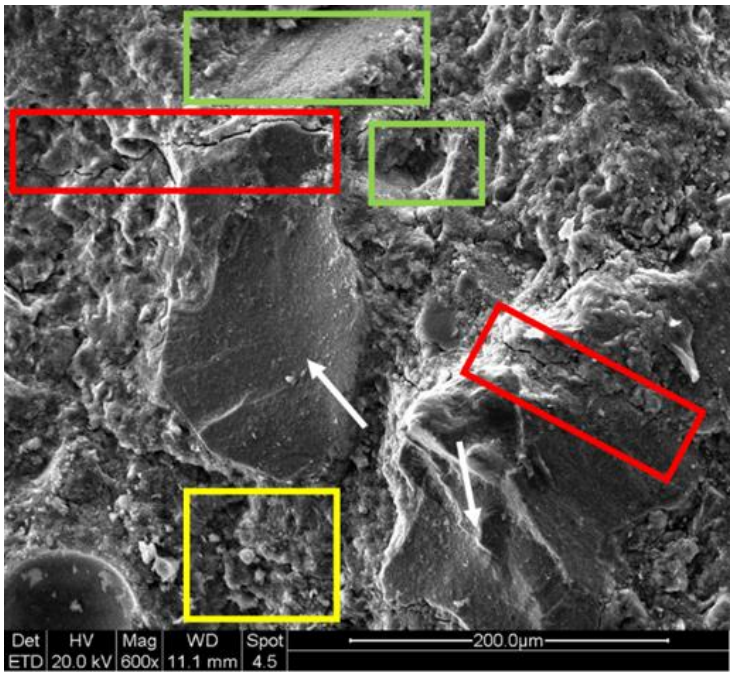

Fig.6-28 Scanning electron microscopy images taken at low magnification (600x) of 80GP0-20RC

These two toughening mechanisms suggest a weak interface between the RC grain and the matrix due to the limited reactivity of the crystalline corundum surface. In areas demonstrating pull-out, it became evident that the matrix densified at the corundum particle's surface. This observation is further supported by Figs. 6-28 to 6-29 for other composite compositions. This observation reaffirms that, within each composition, MK particles have undergone complete reaction with the activator solution, attributed to the impervious nature of the corundum grains.

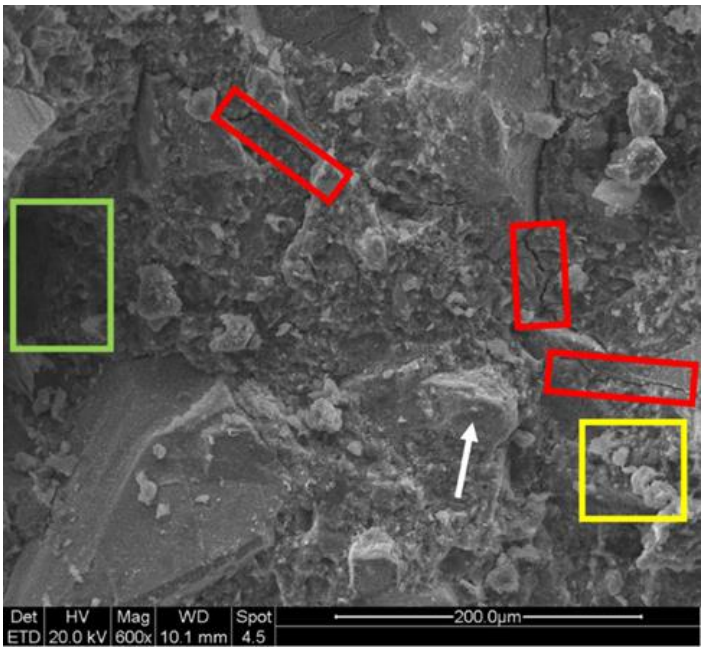

Fig.6-29 Scanning electron microscopy images taken at low magnification (600x) of 50GP0-50RC.

- Mechanical properties

After a curing period of 28 days, compressive strength tests were conducted on all the geopolymer samples. According to ACI 318 M-05 [ACI M318-05 2005, 2005], concrete's 28-day compressive strength should reach a minimum of 28 MPa for fundamental engineering applications (Table 6-6).

Tab.6-6 Requirements for special exposure conditions for concrete [ACI M318-05 2005].

Exposure Condition	Minimum MPa
Low permeability when exposed to water	28
Exposure to freezing and thawing in humid conditions or deicing chemicals	31
Sulfate Exposure	28-31
Exposure to chlorides from deicing chemicals, salt, salt water, brackish water, seawater	35

In this section, the presence of corundum powder can be likened to that of fine aggregates, akin to sand in a mortar. Therefore, we can approximate our mixes to those of binders based on Ordinary Portland cement combined with fine aggregates. It's worth noting

that our RC percentage remains below 50 wt%. It's important to mention that the values in Table 6-6 for comparison are rooted in concretes, which encompass both fine and coarse aggregates. Our work, however, doesn't involve concrete formulation, meaning we aren't introducing coarse aggregates that significantly enhance compressive resistance. Despite this, the strength achieved by our materials stands comparably high in relation to concrete's. As depicted in Figure 6-30, the addition of 10% by weight of recycled corundum doesn't significantly alter the value compared to the GP0 formulation. The scenario shifts when 20 wt% of recycled corundum is added, leading to a notable increase in compressive strength. For additions of 30 and 40 wt%, the values remain favorable but begin to decline. Notably, the 50GP0-50RC formulation exhibits the lowest compressive strength.

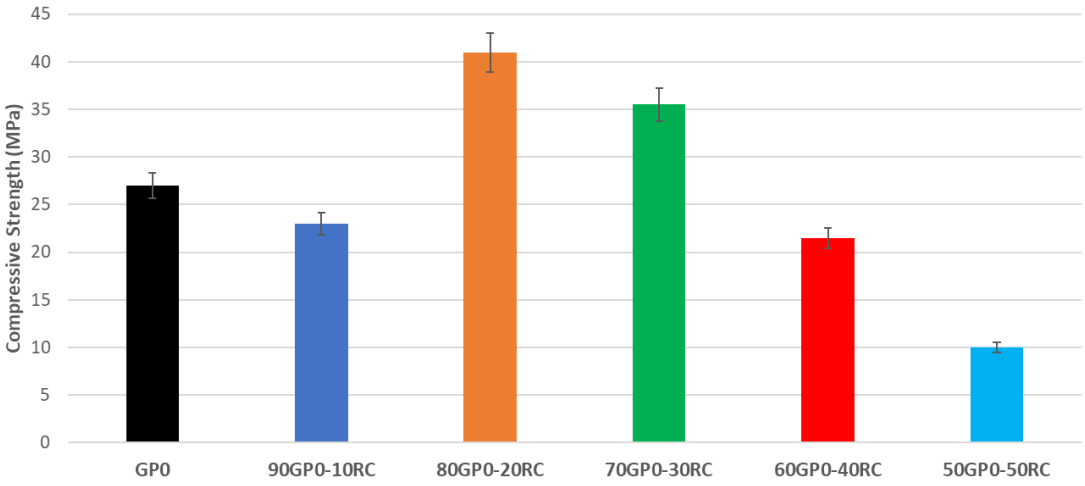

Fig.6-30 Compressive strength of all sample.

Both the 60GP0-40RC and 50GP0-50RC samples exhibit diminished bulk material compactness in Figure 6-30, rendering the matrix more exposed to higher levels of water and increased ion leaching. Research has shown that the connection between strength and porosity in concrete composition exhibits limited dependence. With increased RC content, the geopolymeric paste in the GP0 formulation reduces up to a point (roughly 20–25% of RC calculated against the sum of RC and MK powders) where porosity begins to undermine mechanical strength due to its unfavorable influence. The interaction between paste and inert filler improves through enhanced suspension compactness around aggregate particles and an increase in the total interface area. These mechanisms indicate that using finer

RC fillers will likely have a more pronounced strengthening effect than the grain size studied in this investigation.

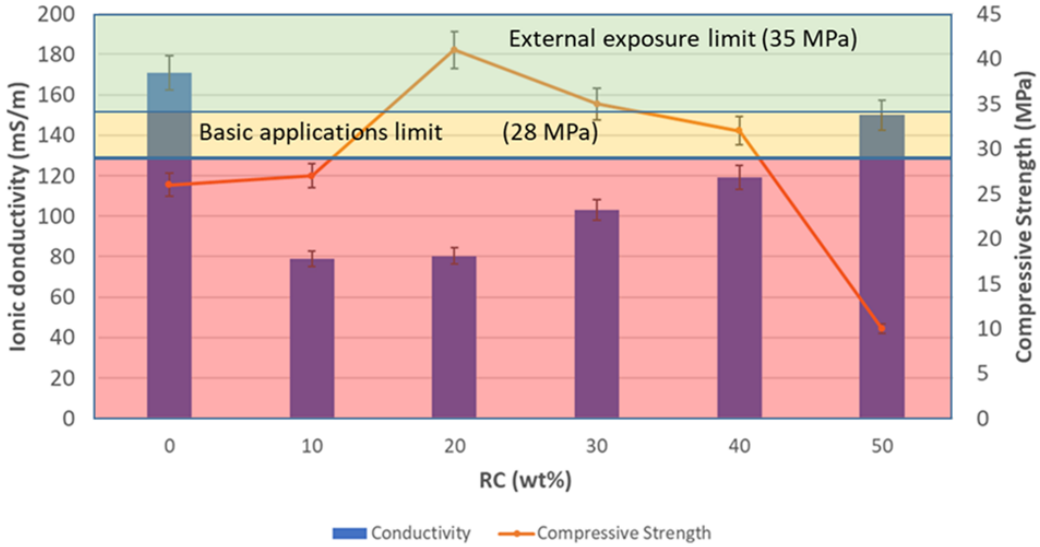

Fig.6-31 Compressive strength correlated with the ionic conductivity of the leachate solution after 24 h of immersion time, i.e. when the measurements recorded a constant number. All the samples after 28 days are correlated with values of Table 6-6.

- Thermal behavioiur

All examined samples exhibit a consistent pattern during the TGA/DTA analysis, displaying a single-stage mass reduction attributed to the release of combined free water along with water generated from the dehydroxylation step. This aligns with findings presented in literature by [Duxson et al. 2008] describing a similar composition. Fig. 6-32a provides a comparison of TGA curves across the various samples, revealing that the initiation of mass loss appears unaffected by the varying quantities of added RC. Fig. 6-32b illustrates the relationship between mass reduction under heating and the sample's composition. Notably, Fig. 6-32a demonstrates an absence of correlation between the initial mass loss and the RC content. Conversely, Fig. 6-32b distinctly demonstrates an inversely linear correlation between mass loss and the percentage of corundum present in the sample.

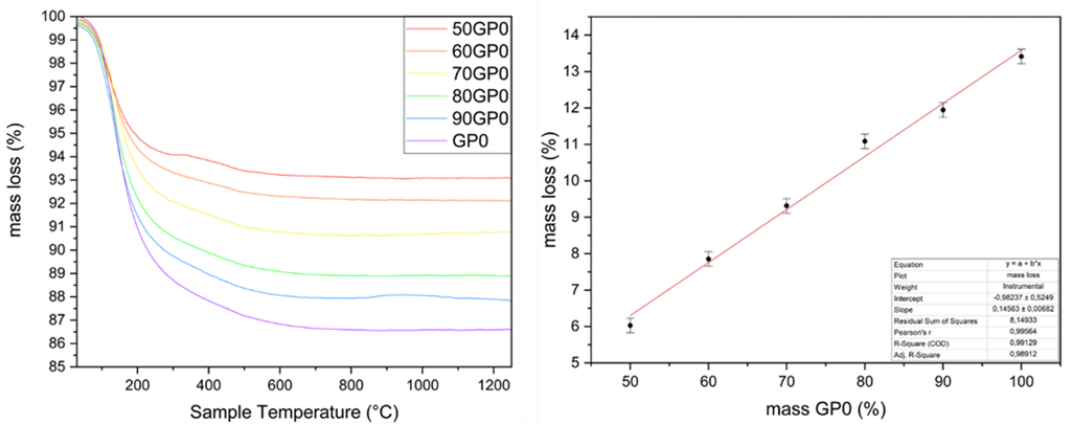

Fig.6-32 a) TGA curves for the different samples, b) mass loss (mass%) vs sample composition.

Furthermore, Fig. 6-33a showcases the heat flow associated with the dehydration process across diverse samples, displaying a consistent incremental pattern with increasing GP0 proportions within the mixture. This relationship is graphically depicted in Fig. 6-33b, revealing a linear decrease in heat flow with the addition of RC. A substantial distinction of about 50% in mass losses is observed between the GP0 and 50GP0 samples. Notably, both the mass loss and heat flow processes follow linear trends, implying the absence of chemical interaction between the geopolymer and recycled corundum.

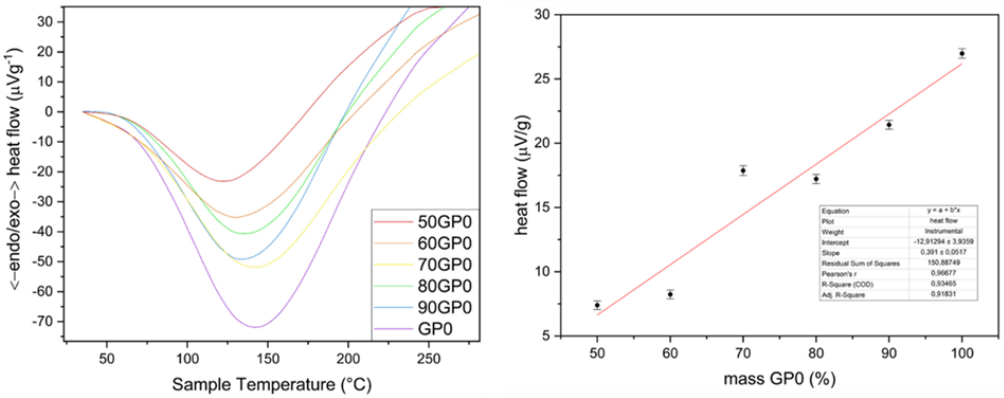

Fig.6-33 a) heat flow involved during heating in the mass loss temperature range; b) heat involved (heat flow) vs sample composition.

6.2.5 Antibacterial activity

The investigation of antibacterial properties extended to geopolymers incorporating RC filler, representing a critical aspect of the study. The detailed methodology for this assessment has been previously elucidated in Section 6.1, ensuring a comprehensive

understanding of the experimental procedures. Figures 6-34 to 6-36 serve as a visual representation of the outcomes derived from the analysis of geopolymers containing varying concentrations of RC filler, ranging from 10 to 40 wt%. These figures provide a comprehensive view of the results obtained, shedding light on the intriguing interactions between the RC filler and bacterial strains. In the case of E. coli, a notable observation emerges regardless of the RC concentration, the inhibition zone for all samples consistently falls within the range of 6 to 8 centimeters.

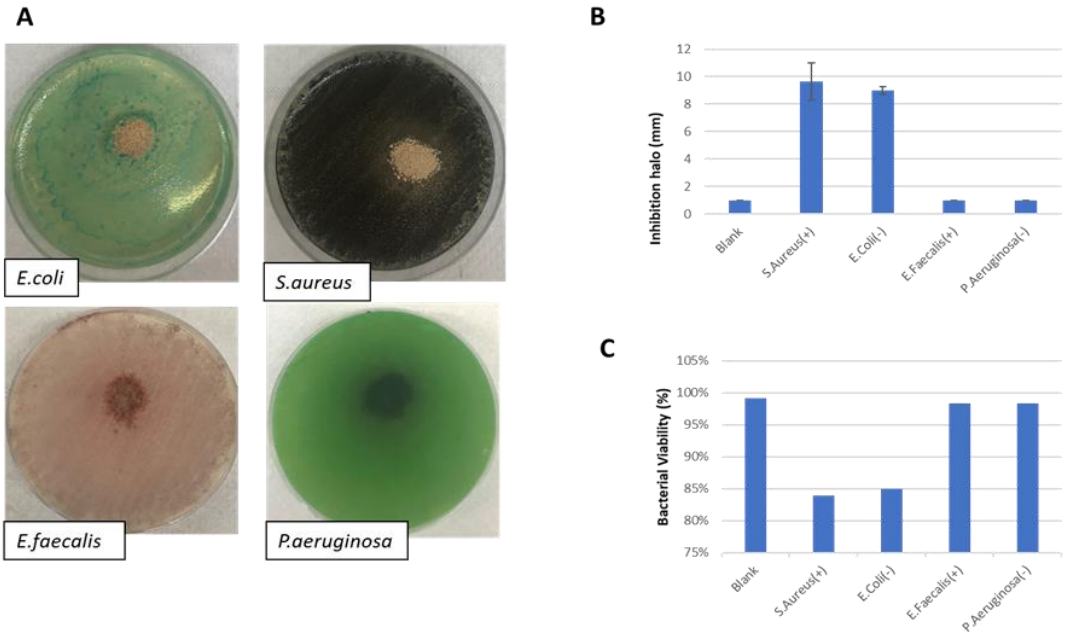

Fig.6-34 Antibacterial properties of 90GP0-10RC.

This implies a robust and relatively uniform antibacterial effect against E. coli across the different compositions of geopolymers. Furthermore, the assessment of bacterial viability reveals a similar trend, with values remaining relatively stable at approximately 80-85%, suggesting that the presence of RC filler does not significantly affect the viability of E. coli. However, a more intriguing narrative unfolds when dealing with S. aureus, a gram-positive bacterium. Here, we observe a more pronounced variation among the samples. The inhibition zone, for instance, exhibits notable fluctuations, spanning from 10 centimeters (in the case of 90GP0-10RC) to 5 centimeters (in the case of 70GP0-30RC).

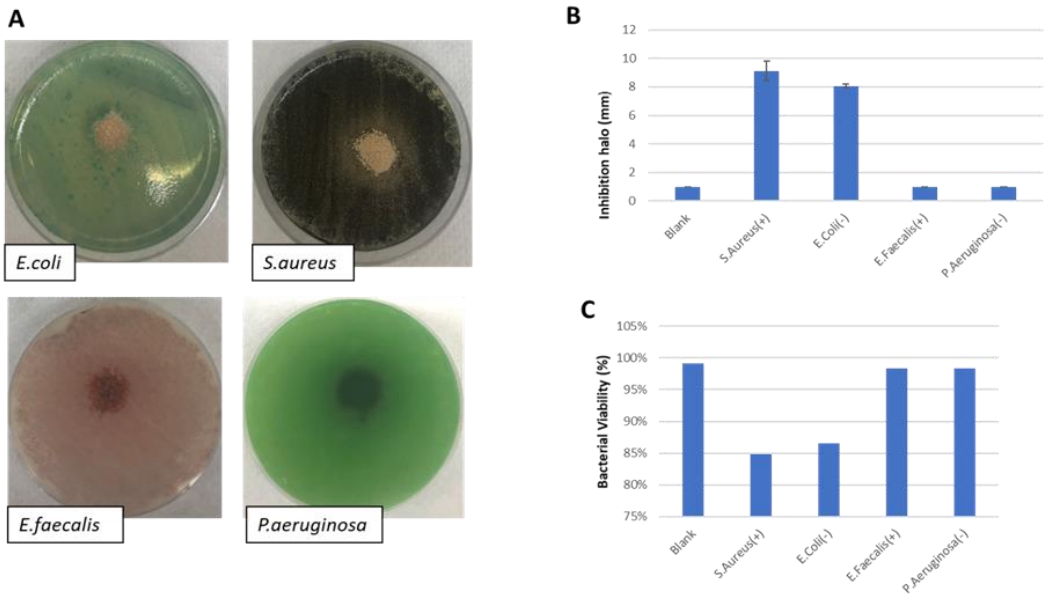

Fig.6-35 Antibacterial properties of 80GP0-20RC.

This variance indicates that the effectiveness of the geopolymers against *S.aureus* is contingent upon the specific composition, with higher concentrations of RC potentially leading to a more pronounced inhibition effect. Parallelly, the assessment of bacterial viability in the presence of *S.aureus* corroborates this observation, revealing a discernible difference in the viability rates among the various samples. This intriguing variability underscores the influence of the RC filler on the antibacterial performance of geopolymers when exposed to *S.aureus*, thereby adding depth and complexity to the study's findings.

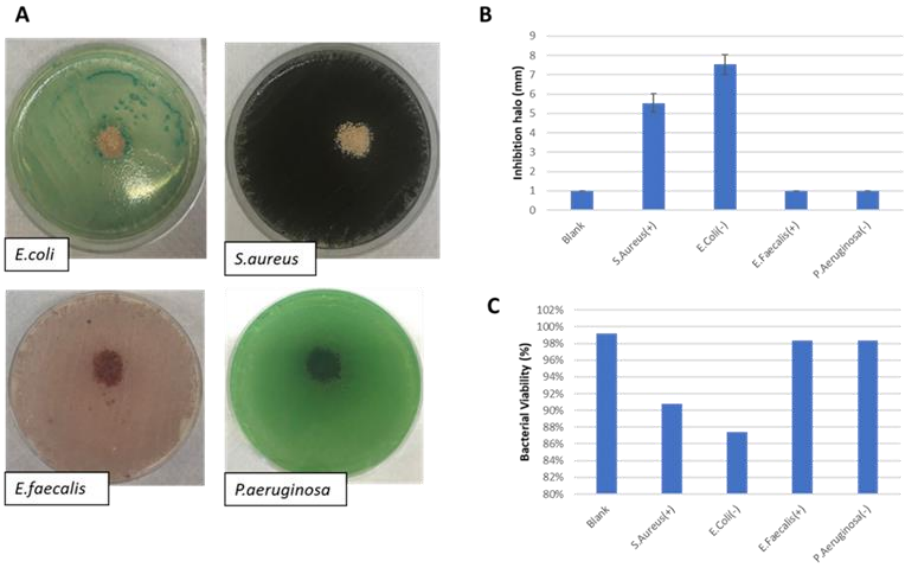

Fig.6-36 Antibacterial properties of 60GP0-40RC.

6.3 Comparison of physical, chemical and mechanical properties of geopolymer with recycled corundum incorporation before and after alkali activation

In this section, we will analyze the data presented in sections 6.1 and 6.2, focusing on comparing some of the most intriguing and unique findings. We will start by investigating the differences in reaction chemistry and then explore the impact of the two mixing methods on the microstructure of the geopolymers.

6.3.1 Geopolymer formulation

The two formulations used in sections 6.1 and 6.2 are depicted and compared in the figure 6-37.

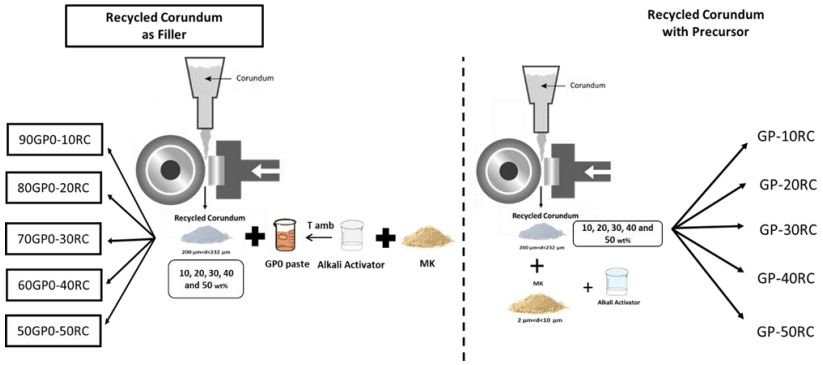

Fig.6-37 Comparison between two formulations.

6.3.2 Stability in water

- Ionic conductivity

Figure 6-38 provides a comprehensive representation of the ionic conductivity data for all the samples that were examined in both sections 6.1 and 6.2. This graphical representation effectively showcases the notable impact of incorporating RC (Reactive Component) on the electrical conductivity of geopolymers. More specifically, when RC is introduced into the formulation before the AA (Alkali activation), there is a discernible and substantial increase in the measured conductivity values. This increase in conductivity due to the introduction of RC before AA is readily evident when comparing the data presented in Figures 6-39 and 6-40. These subsequent figures offer a more detailed perspective, highlighting the contrasts between the baseline GP0 and the geopolymers with the addition of RC at both

20% and 50% loading levels, both before and after the AA. These visual representations help to elucidate the significant influence of the sequence of RC on the resulting ionic conductivity properties of the geopolymers, underscoring the importance of this factor in the formulation and performance of these materials.

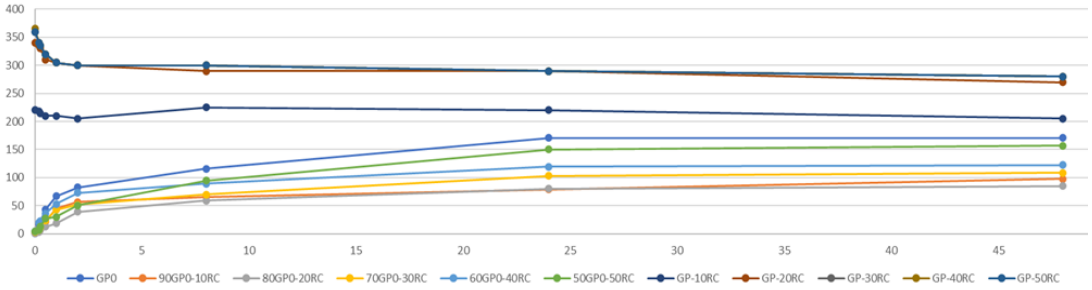

Fig.6-38 Ionic conductivity of all samples.

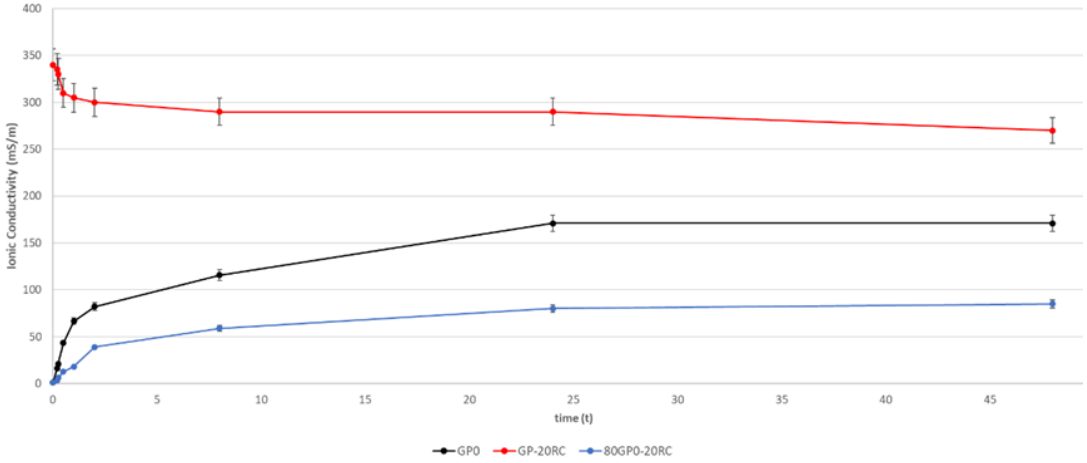

Fig.6-39 Ionic conductivity of GP0, GP-20RC vs 80GP0.

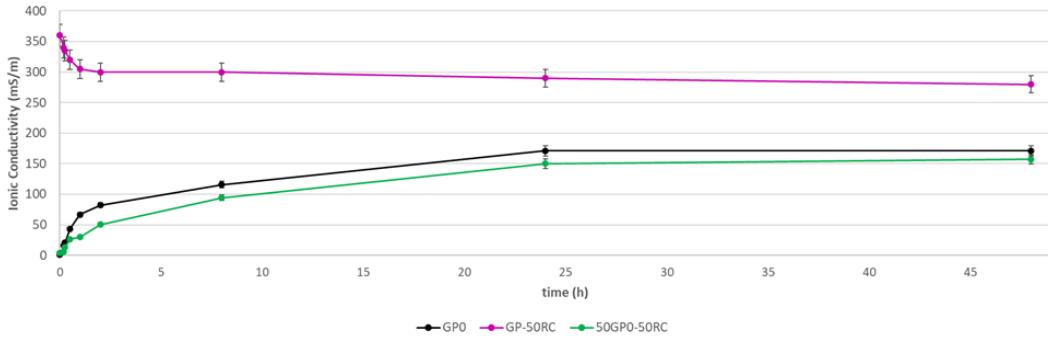

Fig.6-40 Ionic conductivity of GP0, GP-50RC vs 50GP0-50RC.

6.3.3 Geopolymerization

- FTIR

As mentioned earlier, one of the key peaks to observe in the infrared spectrum (IR) for a geopolymer falls between 1100-1010 cm^{-1}. This specific peak signifies the successful formation of the Si-O-Al bond, thereby confirming the occurrence of the geopolymerization reaction. The figure 6-41 illustrates the shifts in this peak for geopolymers with Corundum added both before and after alkaline activation, in comparison to the reference geopolymer (GP0) containing only MK. A noticeable trend emerges when corundum is introduced to MK before the mixing process, while there is no clear pattern when added afterward. Although the differences in these shifts are relatively minor, they could be attributed to various factors aside from the presence of RC. However, the consistency observed in geopolymers with RC added beforehand indicates a more effective blending of corundum with MK powder and the geopolymeric paste.

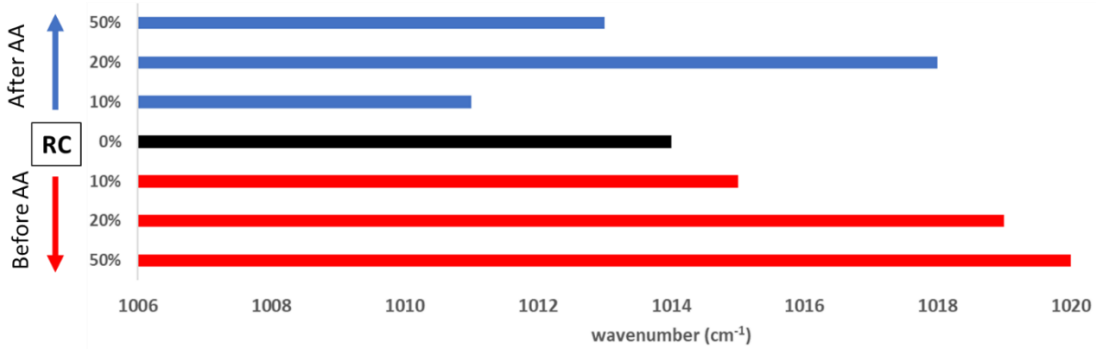

Fig.6-41 Formation of Si-O-Al.

- MAS-NMR

In this section, we compared the ^{27}Al NMR spectra of the samples analyzed in sections 6.1 and 6.2. We did not compare the ^{29}Si spectra as the differences were not very prominent. Figure 6-42 illustrates the spectra of geopolymeric samples with 20% and 50% RC added before and after the activation step, juxtaposed with the reference sample GP0. As discussed earlier, the presence of RC is distinctly visible with a peak at 10 ppm. In samples containing 20% RC, such as GP-20RC and 80GP0-20RC, the peak corresponding to Al(VI) from MK is more pronounced. However, with a higher RC quantity, the peak around 0 ppm seems to diminish. Notably, in all RC-containing samples, the

Al(V) peak vanishes. From a chemical standpoint, the key distinction among these samples lies in the variation of the added RC, which, as confirmed, does not alter or shift the formation of the geopolymeric network. It is intriguing to observe that a minimum 20% RC addition is necessary to detect the presence of corundum. Moreover, as the intensity of the corundum peak increases, the intensity of the geopolymer's Al(IV) peak diminishes, revealing a nuanced interplay between these components.

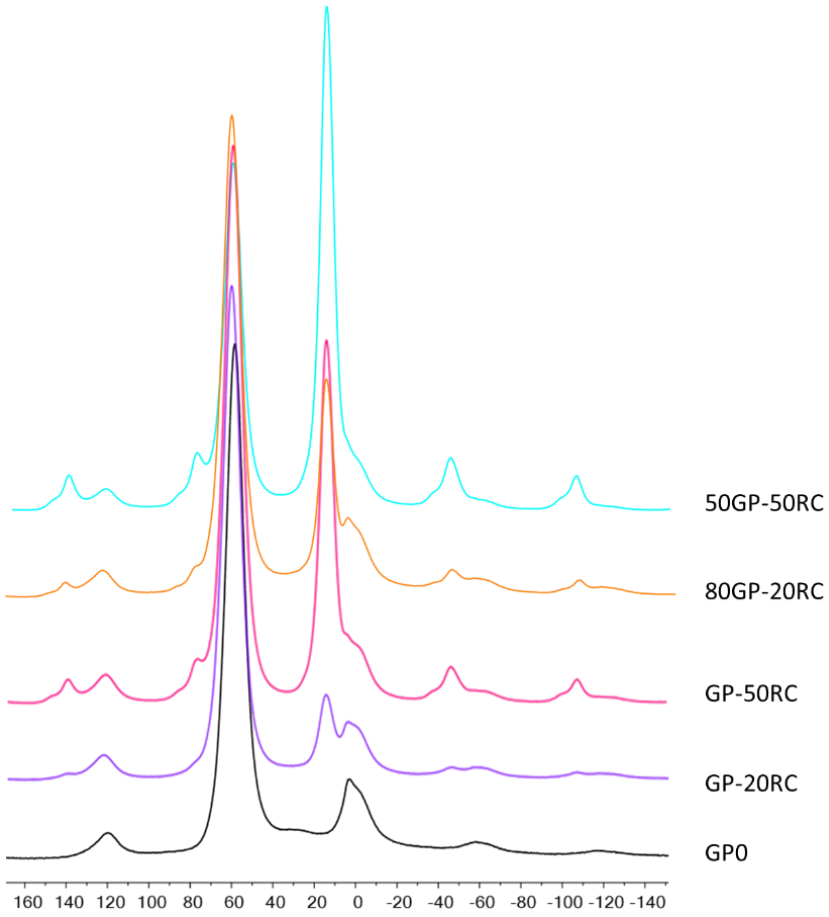

Fig.6-42 ^{27}Al MAS-NMR spectra of sample with RC before and after alkali activation compared with GP0.

- XRD

In the following figures, we are presented with a detailed examination of the distinctions among various Geopolymers incorporating RC. Figure 6-43 offers a compelling comparison between GP-20RC and 80GP0-20RC, both of which incorporate a common element, the addition of 20wt% of RC, albeit in different manners. Notably, the presence of an amorphous hump in the X-ray diffraction patterns,

spanning roughly from 20 to 40 degrees, is readily discernible in both formulations. However, it is noteworthy that this amorphous feature appears slightly more pronounced in the 80GP0-20RC sample, hinting at nuanced differences in the microstructural characteristics of these two geopolymers. The disparities become increasingly conspicuous with the introduction of a higher concentration of RC, specifically, 20wt%. In the case of 80GP0-20RC, the influence of RC on the XRD pattern becomes notably more pronounced. Moreover, the amorphous hump in this sample more closely approximates that of MK, presenting a significant departure from the spectrum observed in GP-20RC. These detailed spectral comparisons underscore the intricate interplay between the presence and concentration of RC in the geopolymers, shedding light on the evolving crystalline and amorphous phases within the materials. Such insights into the microstructural variations are pivotal in understanding and optimizing the performance and properties of these geopolymers in various applications.

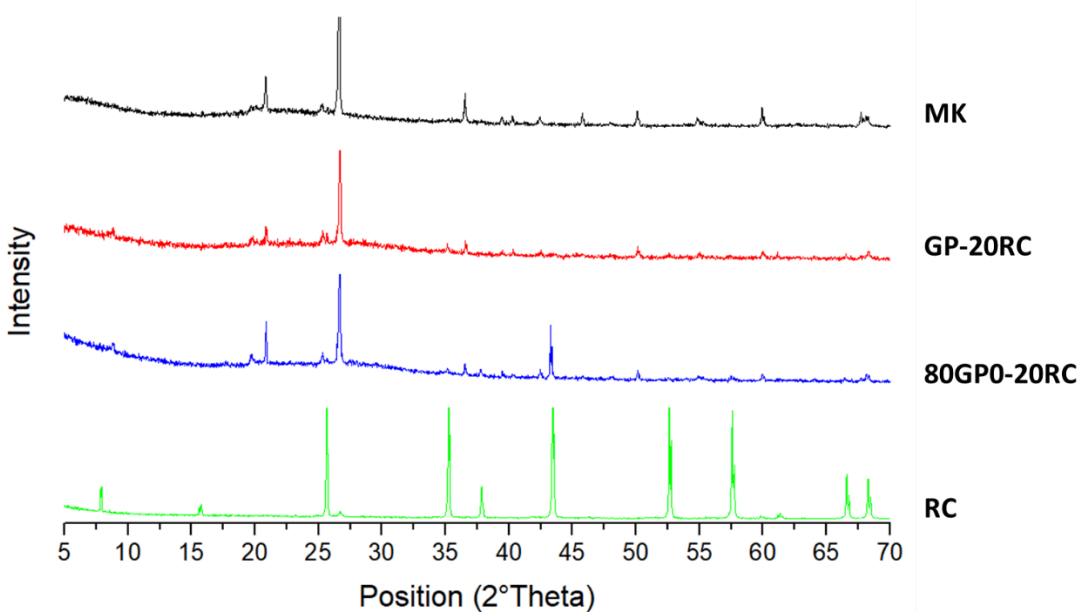

Fig.6-43 XRD spectra of 80GP0-20RC compared with GP-20RC, MK and RC.

6.3.4 Microstructure

- SEM

In this section, we compared two formulations with the highest percentage of recycled corundum. Figure 6-44 displays GP-50RC (refer to Figure 6-44C) and 50GP0-50RC (refer to Figure 6-44D).

Initially, the microstructural differences between these two geopolymers might not be obvious. However, upon closer inspection, it becomes apparent that geopolymerization of MK with activators is more pronounced in 50GP0-50RC. Interestingly, the introduction of RC after activation results in a progressively disorderly arrangement within the network. Consequently, the strength of samples with RC added post-activation decreases with higher RC percentages. On the other hand, GP-50RC exhibits more prominent cracks but fewer instances of pull-out, leading to a noticeable improvement in mechanical strength.

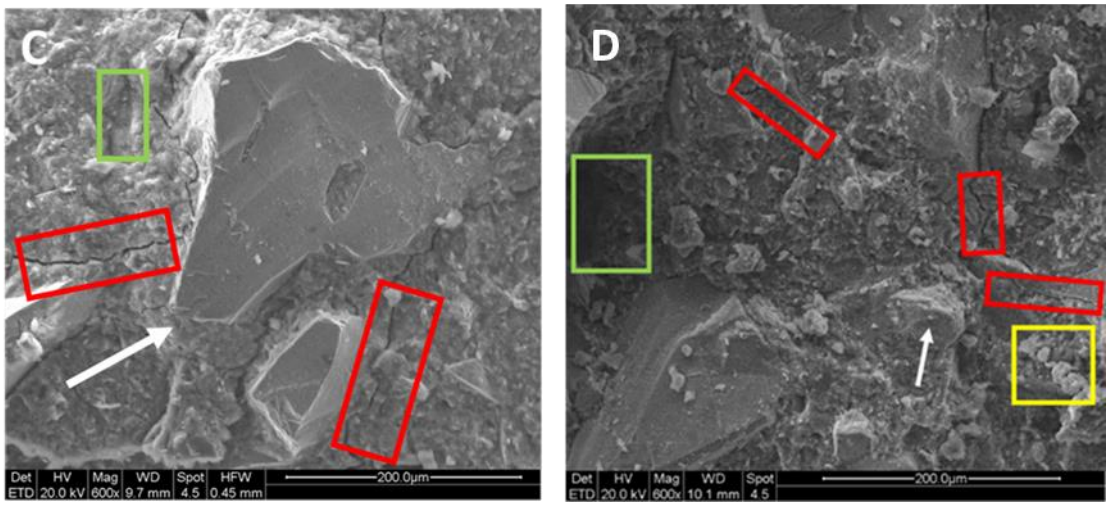

Fig.6-44 Comparison between GP-50RC (left) and 50GP0-50RC (right).

- Mechanical properties

Figure 6-45 provides a comprehensive comparison of the compression stress values for samples containing corundum, with the corundum being introduced both before and after alkali activation. These samples were previously examined in Sections 6.1 and 6.2. The intriguing observation is the substantial performance enhancement of geopolymers when recycled corundum is added as a filler after alkali activation. Interestingly, a distinct pattern emerges when scrutinizing the stress values. Samples on the left exhibit a tendency towards a gradual decrease, whereas those on the right experience an ascent leading to a peak, followed by a subsequent decline. Importantly, even after this descent, the stress values on the right side of the graph remain notably higher compared to those of the MK-

based Geopolymer (GP0). Furthermore, the addition of 10% RC in both formulations doesn't result in a significant shift in the compression stress values, indicating a stable performance in this context. However, it's crucial to highlight a noteworthy exception within this comparative analysis the introduction of 50% RC. Remarkably, the GP-50RC exhibits greater strength than the blend 50GP0-50RC, representing a remarkable outlier in the dataset.

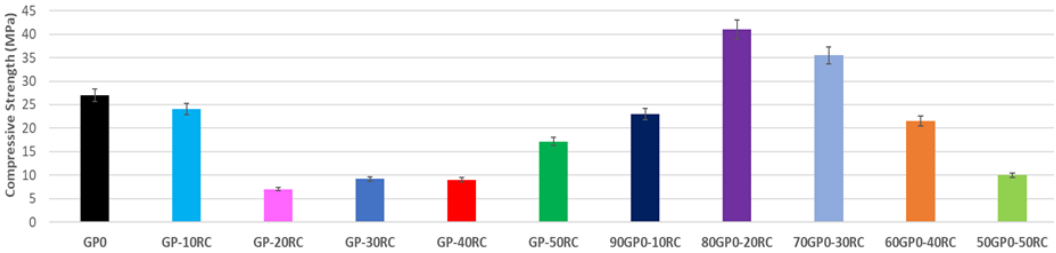

Fig.6-45 Comparison of geopolymer with RC added before and after AA.

7. Geopolymer with recycled corundum after erosion test

Unlike the previous chapter, this chapter discusses geopolymers with corundum after erosion tests. As seen in Chapter 4, this corundum exhibits different phases and has a different particle size distribution.

7.1 Characterization of RC after erosion test

- Basic attack

As previously explored in Chapter 6, the properties of recycled corundum were tested under alkaline conditions before its incorporation into the geopolymeric matrix. Fig.7-1 displays the XRD spectra of pure alumina and fine corundum powder following exposure to 8 M NaOH. The inclusion of pure alumina spectra after the basic attack serves to highlights the distinctions between the two powders after the reaction with NaOH. Notably, alumina powder remains unaffected in the presence of sodium hydroxide, while the spent corundum powder shows changes, as evident by comparing the spectra in Fig. 7-1 with those of RC before alkali attack, as shown in Fig.7-3. Before the alkali attack, RC exhibited traces of contaminants from eroded materials, specifically montmorillonite $(Na,Ca)_{0.3}(Al,Mg)_2Si_4O_{10}(OH)_2 \cdot nH_2O$ and valleriite $2[(Fe,Cu)S] \cdot 1.53[(Mg,Al)(OH)_2]$. However, these contaminants were no longer present after the basic attack, which led to the decision of using NaOH at this specific concentration for the experiment.

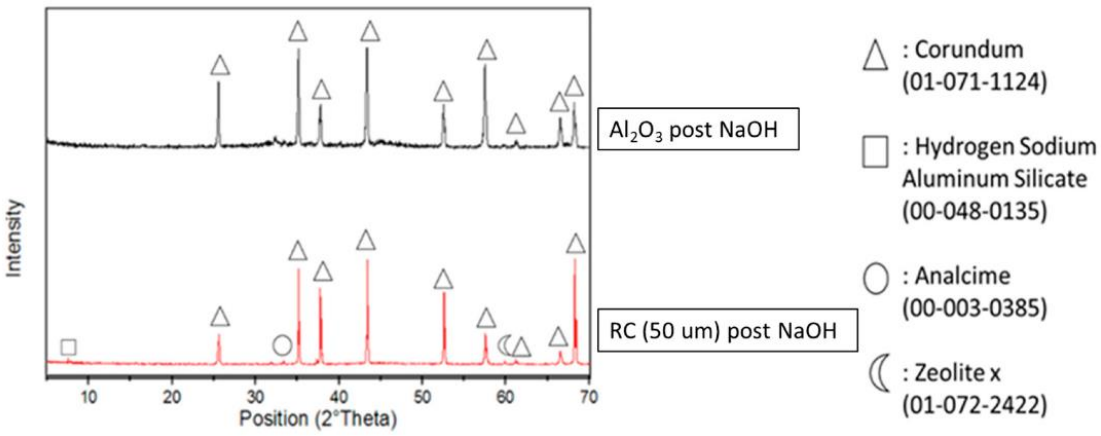

Fig.7-1 XRD patterns for alumina and RC after immersion in NaOH 8M.

7.2 Geopolymer formulation

Geopolymers were produced through the addition of NaOH + Na-silicate solution to MK under mechanical stirring to create the reference geopolymer, GP0 (see Table 7-1). To explore the possibility of substituting MK with as-received waste (RC), two geopolymer mortars were formulated, denoted as GP-10RC and GP-20RC, where RC replaced 10% and 20% by weight (measured on the dry powders), respectively (see Table 7-1). The percentages of RC in the total amount of fresh paste were 5.88% and 12.84%, respectively. Additional formulations were prepared by adding 10% and 20% by weight of corundum to the geopolymer fresh paste (similar to GP0), labelled as 90GP0-10RC and 80GP0-20RC, respectively. In these two mixes, the percentages of RC in the total amount of fresh paste were 10% and 20%, respectively. Throughout all compositions, a consistent alkali activator solution (NaOH + NaSilicate = L) to MK weight ratio of 0.765–0.780 was maintained. The pastes were all mixed using an Aucma 1400W Planetary Mixer (China). The resulting fresh binder paste was poured into silicone cube molds (25 mm × 25 mm × 25 mm). The geopolymer pastes obtained were quite viscous, and no additional water was added to any formulation. As shown in Table 7-1, the liquid (8 M NaOH plus sodium silicate solution) to solid (MK and RC) mass ratio ranged from 0.54 to 0.78, with higher MK content leading to greater workability of all pastes. The inclusion of impervious RC grains enhanced paste flowability, as is typical with fine fillers, and required only minimal water addition. After removing any bubbles, the molds were carefully sealed, and the geopolymers were cured at room temperature. After 28 days of hardening, the silicone molds were opened to proceed with the subsequent characterization. A minimum of 15 samples were obtained for each formulation.

Tab.7-1 Mix design of mortar formulations containing various amounts of RC.

Mix ID	MK (g)	RC powder (wt%)	NaOH (g)	Na2SiO3 (g)	L/S (wt/wt)	SiO_2 (wt%)	Na_2O (wt%)	Al_2O_3 (wt%)	H_2O (wt%)	Other Oxides (wt%)
GP0	100	0	38	40	0.78	37	22	6	32	3
GP-10RC	90	5.88	34	36	0.7	35	27	6	30	2
GP-20RC	80	12.34	30	32	0.62	33	31	5	28	3
90GP0-10RC	51	10	19	20	0.64	34	30	5	28	3
80GP0-20RC	45	20	17	18	0.54	30	36	5	25	4

7.3 Stability in water

- Ionic conductivity and pH of the eluate

The investigation of ionic conductivity (IC) served as a valuable tool to glean structural insights into the chemical stability of geopolymers, especially when waste materials were introduced both in the precursor and as a filler. Unlike vibrational spectroscopy techniques such as FTIR and Raman spectroscopy, this type of analysis provides an indirect measure of the degree of reticulation within the aluminosilicate matrix. Essentially, it offers a quantitative assessment of how well the components within the geopolymer are interconnected. One significant aspect influencing IC is the presence of Al^{3+} in tetrahedral coordination within the geopolymer structure. A higher concentration of Al^{3+} in this coordination indicates that fewer Na^{+} ions are leached from the matrix. Additionally, the reaction between OH^{-} ions from the alkali activator and aluminosilicate precursors plays a pivotal role in reducing leaching. In essence, the ionic conductivity of the eluate solution obtained after geopolymer immersion provides a quantifiable measure of its reticulation degree. In the formulations we examined, there was a noticeable increase in IC with the addition of corundum powder to the metakaolin (MK) powder. This outcome was in line with expectations when incorporating a non-reactive or partially reactive component into the mix (Figure 7-2A). Notably, the difference between the reference geopolymer (GP0) and the formulations was most pronounced for those containing RC filler, ranging from GP-10RC to 80GP0-20RC. However, the formulation with 10% of RC as filler exhibited ionic conductivity values closer to GP0. As the RC content increased, the IC continued to rise when introduced as a filler, although samples like 90GP0-10RC and 80GP0-20RC, introduced as fillers after about 24 hours, began to exhibit similar IC values. This indicated that the reticulation of the geopolymeric paste was minimally affected by the addition of RC when introduced in this manner. In cases where RC was added to the MK powder, the IC values were lower, primarily due to the presence of Al_2O_3 before alkali activation. The overall trend of ionic conductivity could be correlated with the total content of alkali activator (NaOH 8M plus Na silicate), showing a strong inverse proportionality (Figure 7-2B). In other words, the higher the alkaline solution content, the lower the release of ions in the water during the immersion test. This excellent proportionality, as

indicated by a high R-squared value (R^2 = 0.9794), suggested that the reactivity of the solid components, both MK and RC, increased in response to higher liquid activator content, coinciding with an increase in MK content. Further analysis was performed by separately correlating the IC values with the two solid components, RC and MK (Figure 7-2C, D). Intriguingly, similar correlations were observed for RC (R^2 = 0.9571) and MK (R^2 = 0.9547), indicating that the mix design was effectively executed. This allowed for the maximum reactivity and OH^- uptake from the reactive fraction of the formulation, specifically MK. In essence, these results emphasized the careful balance of components and activator content, crucial for optimizing the reactivity and reticulation of the geopolymeric matrix.

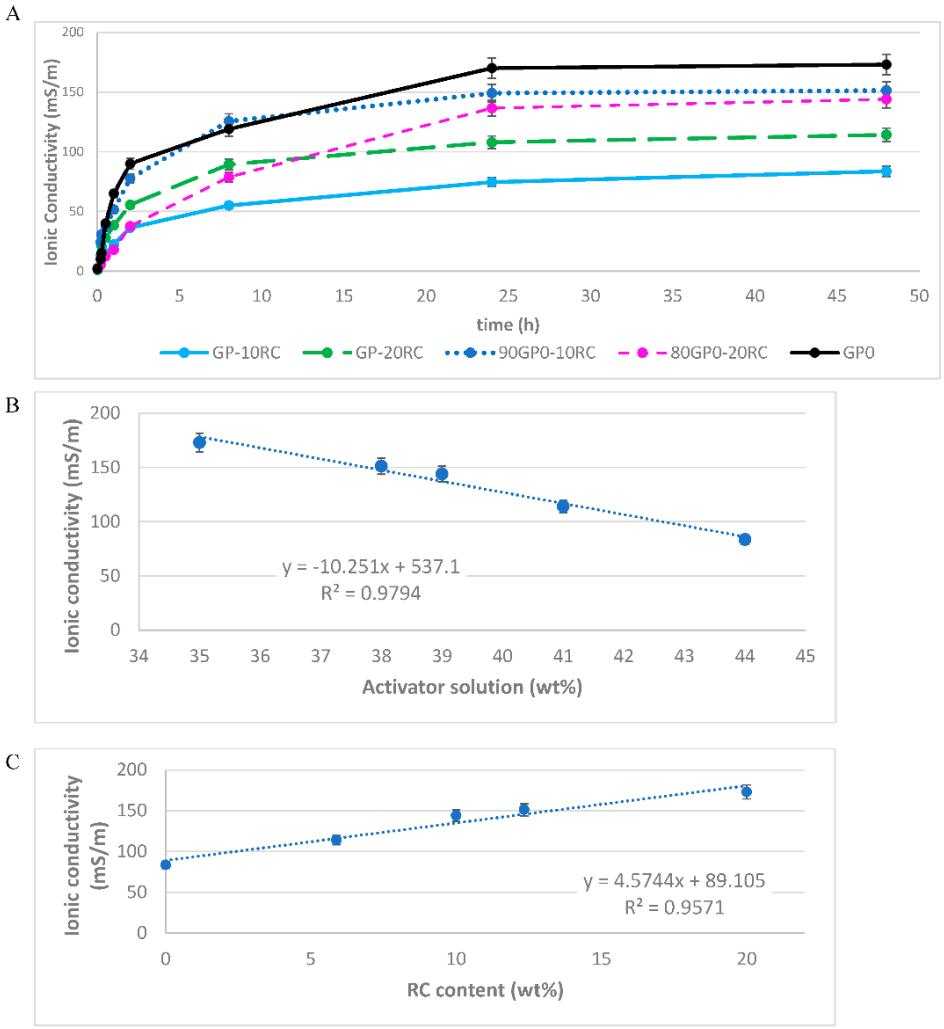

Fig.7-2 Ionic conductivity (IC) at 48 h of immersion vs. (A) immersion time of all geopolymers cured 28 days; (B) IC vs. the alkaline solution content; (C) IC vs. RC content. (Reproducibility of the test was calculated to be within an error of ±5%).

7.4 Geopolymerization

- FTIR

Figure 7-3 provides a comprehensive overview of the FTIR spectra, encompassing Metakaolin (MK), Recycled Corundum (RC) powders, and the composite Geopolymers denoted as GP-RC, covering a weight percentage range from 0% to 20%. Within all these spectra, notable features emerge at approximately 3440 cm^{-1} and 1660 cm^{-1}, corresponding to -OH stretching and bending vibrations. In the MK spectrum, a distinctive band at 1080 cm^{-1} signifies the presence of Si-O-T bonds (where T represents either Si or Al). Notably, this band undergoes a noticeable shift towards lower wavenumbers (specifically 1019–1014 cm^{-1}), indicative of an augmented prevalence of Si-O-Al bonds. Within the MK spectrum, the appearance of a band at 800 cm^{-1} is attributed to the presence of quartz, while another at 560 cm^{-1} is associated with Al-O vibrations in a six-fold coordination arrangement. Additionally, both the MK and GP spectra (spanning from 0 to 20 wt% of RC) manifest a distinctive band at 470 cm^{-1}, ascribed to the Si-OH bending mode. Further details regarding this specific peak can be found in Table 7-2, along with pertinent commentary concerning the 460 cm^{-1} peak observed in the RC spectrum.

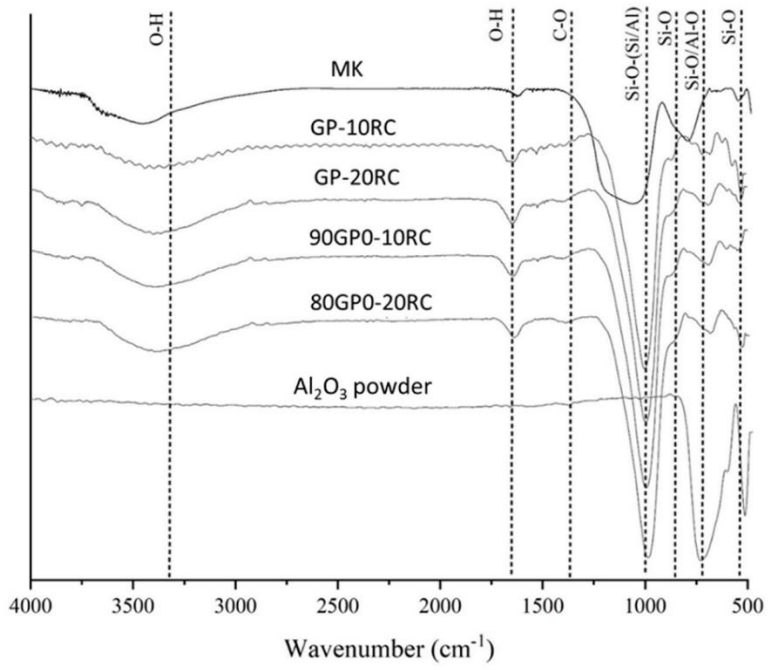

Fig.7-3 FTIR spectra of MK powder, all geopolymers with Al_2O_3, and Al_2O_3 powder.

Tab.7-2 List of vibrations of aluminosilicates and corundum in the FTIR range.

Wavenumbers (cm^{-1})	Interpretation	References
3695-3660 cm^{-1}	Hydroxyl groups in the kaolinite	[Pantongsuk et al. 2021]
3450 and 1650 cm^{-1}	Hydration water	[Dal Poggetto et al. 2021]
1454 cm^{-1}	Na_2CO_3	[Dal Poggetto et al. 2021]
1080-1050 cm^{-1}	Asymmetrical Si-O-Si Stretching vibration	[Dal Poggetto et al. 2022]
1010-980 cm^{-1}	Si-O-Al stretching vibration	[Dal Poggetto et al. 2022]
912 cm^{-1}	Al (VI)-OH stretching	[Dal Poggetto, G.; 2020, 2022]
800-500 cm^{-1}	Al-O-Si bending vibrations	[Dal Poggetto, G.; 2022]
450-470 cm^{-1}	Si-O-Si bending vibrations	[Dal Poggetto et al. 2021, 2022]
1089 cm^{-1}	Al-O vibration	[Dal Poggetto et al. 2022]
1089, 800 and 780 cm^{-1}	Disorders in Corundum network	[Dal Poggetto et al. 2022]
459 cm^{-1}	Al-O bending	[Dal Poggetto et al. 2020, 2021, 2022]
474 cm^{-1}	Al-O vibration (Al_2O_3)	[Dal Poggetto et al. 2022]

- XRD

Figure 7-4A provides a detailed comparative analysis of the spectra of recycled corundum and metakaolin powders in conjunction with two distinct geopolymers, GP-10RC and GP-20RC. Within the diffraction pattern of the metakaolin, we observed a conspicuous diffuse reflection, characteristic of the typical broad band exhibited by amorphous aluminosilicate structures. This was complemented by sharper peaks, unequivocally identified as anatase (TiO_2) and alpha-quartz (α-SiO_2). It is noteworthy that the diffraction patterns for GP-10RC and GP-20RC closely resembled each other (as depicted in Figure 6-3A). These two geopolymers displayed a discernible shift in their diffuse halos, positioned at higher angles, approximately between 26 to 28° in 2θ. This particular shift aligns with previous observations in MK-based

geopolymers, indicating the presence of a 3D network of Si- and Al-tetrahedra. As the proportion of RC was incrementally increased, a distinctive peak emerged at approximately 8° in 2θ, distinctly discernible in the GP-20RC sample. This peak unequivocally affirmed the presence of recycled corundum, which exhibited incomplete reactivity within the system. Intriguingly, such a feature remained largely imperceptible in the spectrum of the GP-10RC sample, primarily due to the lower concentration of RC therein. Figure 7-4B offers a comprehensive comparison involving MK and RC powders, with the added element of geopolymers featuring RC as a filler. In the diffraction patterns of both 90GP0-10RC and 80GP0-20RC, the presence of diffuse halos characteristic of amorphous geopolymers was notably evident, corroborating earlier findings [Catauro et al. 2020, M.; Dal Poggetto et al. 2021, 2022]. With the inclusion of RC, a conspicuous absence of peaks was observed at around 8° and approximately 14° in 2θ, signifying the successful dissolution of impurities inherent to the recycled corundum within the alkaline environment. Remarkably, the peaks corresponding to corundum (α- Al_2O_3) remained conspicuously intact and discernible, further affirming the unique reactivity patterns and compositional changes induced by RC in the geopolymers.

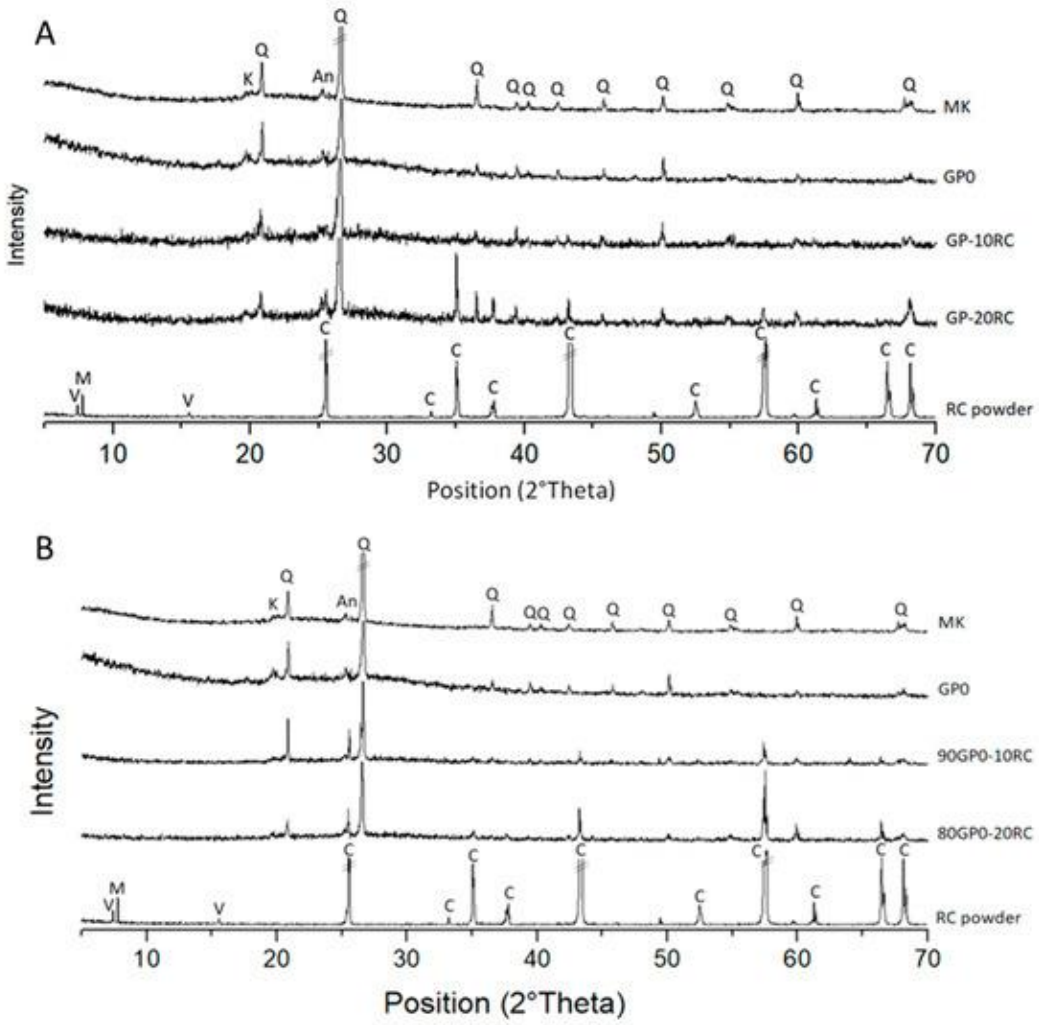

Fig.7-4 (A) XRD patterns for RC raw materials MK, GP-10RC, and GP-20RC recycled corundum-based geopolymers. (B) XRD patterns for RC raw materials MK, 90GP0-10RC, and 80GP0-20RC. Crystalline phases identification labels: Q = alpha-quartz (01-083-0539), K = kaolinite (01-075-0938), C = corundum (01-071-1124) An = anatase (01-071-1167), M: montmorillonite (00-012-0232), V: valleriite (01-073-0516).

7.5 Microstructure

- SEM

The SEM analyses, though conducted subsequent to the compressive strength test, revealed the presence of surface cracks on the specimens. Figure 7-5 offers a glimpse into the morphological characteristics of the geopolymers, shedding light on the unreacted recycled corundum grains nestled within the matrix. Within this microcosm, two discernible phases emerge: firstly, the unreacted recycled corundum or partially reacted particles, and secondly, the sponge-like geopolymer gels, identified as "A" and "B," respectively. Intriguingly, a more pronounced presence of

geopolymer gels is discernible in specimens featuring higher recycled corundum contents, indicative of a more extensive degree of geopolymerization [Ren et al. 2014]. Taking a closer look at Figure 6, it becomes evident that the specimen labeled 90GP0-10RC boasts a denser and more compact structure in comparison to the other formulations. Consequently, it exhibits the highest compressive strength among the various geopolymer specimens. Conversely, 80GP0-20RC contains a larger proportion of recycled corundum, resulting in a higher aluminum content within its chemical composition. This is accompanied by a heightened quantity of geopolymer gel. To delve deeper into the chemical compositions, elemental analysis via Energy Dispersive X-ray Spectroscopy (EDS) was carried out for the geopolymers, yielding the results shown in Tab.7-3. It's noteworthy to mention that these compositional figures carry a margin of error ranging from 5% to 15%.

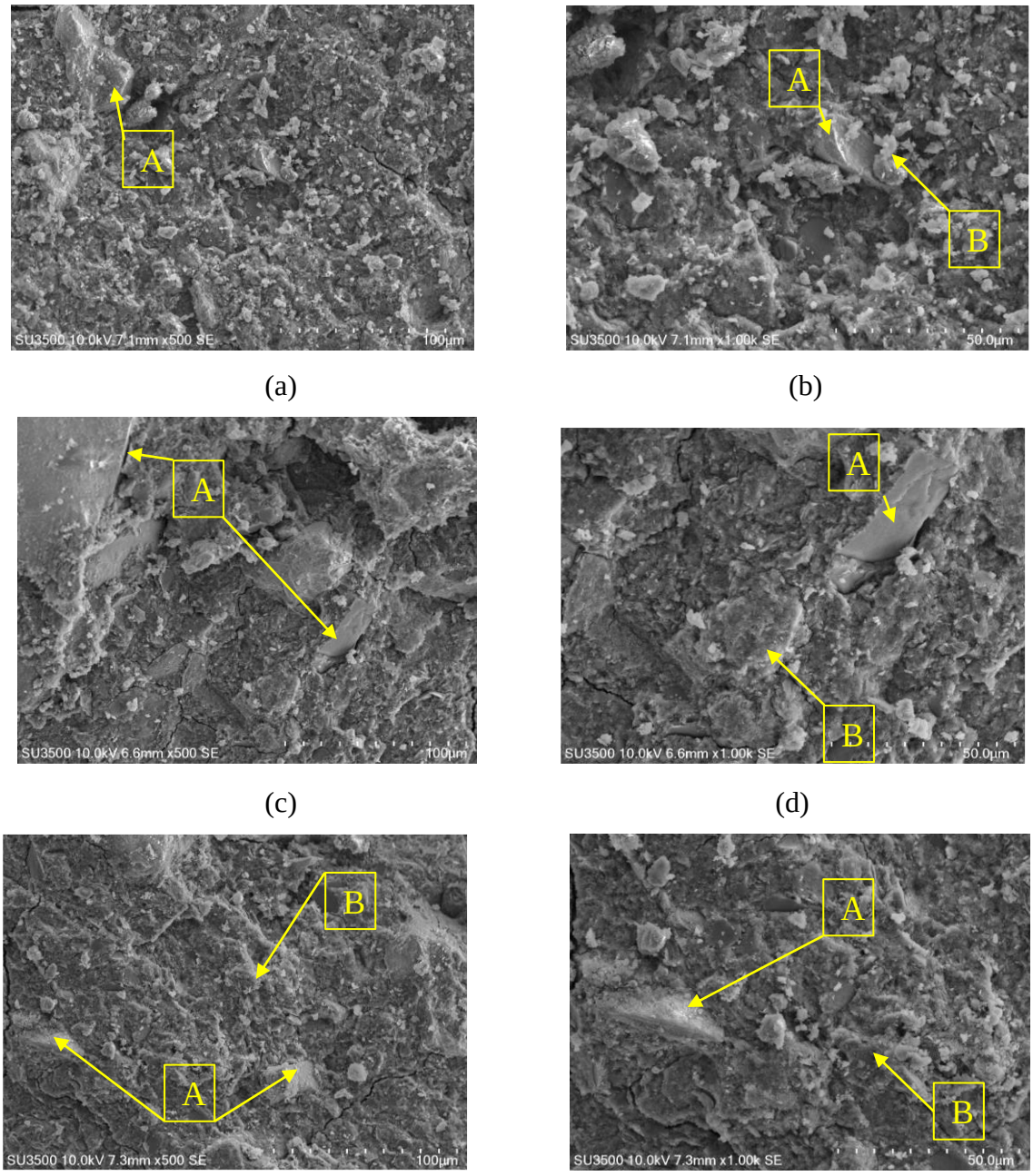

Fig.7-5 Microstructures of fresh surfaces of the different mortars: (a) GP-10RC, 500X; (b) GP-10RC, 1000X; (c) GP-20RC, 500X; (d) GP-20RC, 1000X; (e) 90GP0-10RC, 500X; (f) 90GP0-10RC, 1000X; (g) 80GP0-20RC, 500X; and (h) 80GP0-20RC, 1000X. Unreacted recycled corundum or partially reacted particles and sponge-like geopolymer gels are denoted by “A” and “B”, respectively.

Tab.7-3 Chemical composition of the matrix analysed by EDS.

Sample label	Chemical composition (wt%)						
	C	Na	Al	Si	K	Ca	Fe
GP-10RC	9.82	12.04	29.49	45.57	0.55	0.13	2.40
GP-20RC	9.36	12.46	29.32	45.27	0.83	0.23	2.53
80GP0-20RC	10.29	12.42	30.17	44.29	0.70	0.23	1.90
90GP0-10RC	11.48	13.64	28.90	43.34	0.67	0.16	1.81

- Compressive strength

When examining the compressive strength data (Figure 7-6), it becomes apparent that the introduction of RC into the MK matrix led to a slight improvement in mechanical properties. However, it is crucial to note that, in all cases, the compressive strength values exhibited a significant decrease compared to the reference geopolymer GP0, as previously discussed in the section on ionic conductivity. This reduction in strength is attributed to the altered composition and structure resulting from the inclusion of RC. Interestingly, when 10% by weight of RC was added as a filler after the alkali activation had already occurred, there was an increase in compressive resistance. In contrast, when the addition was increased to 20%, a considerable decrease in resistance was observed, as also mentioned in the context of ionic conductivity. This decrease can be attributed to the excessive presence of RC relative to the reacted geopolymeric paste. It's worth noting that the GP-20RC sample had an actual RC fraction of 12.34 wt% of the total paste weight (as detailed in Table 7-1), which deviated from the expected 20% fraction for 80GP-20RC. The distinction between adding RC to MK or incorporating RC into the paste as a filler becomes more evident when analyzing mechanical properties (Figure 7-6) compared to ionic conductivity (Figure 7-8). In the GP-10RC and GP-20RC formulations, a positive correlation between ionic conductivity and compressive strength is observed. In other words, higher conductivity corresponds to increased compressive strength. However, for the 90GP0-10RC and 80GP0-20RC samples, although their ionic conductivity values were similar after 48 hours, their compressive strength exhibited significant variations. This discrepancy underscores the intricate relationship between the composition, curing process, and

resulting mechanical properties in geopolymers containing RC. Furthermore, geopolymers with higher RC content (30, 40, 50 wt%) were tested as fillers to observe if there was a trend. It can be observed that the values tend to decrease progressively until reaching a plateau after the addition of 40%.

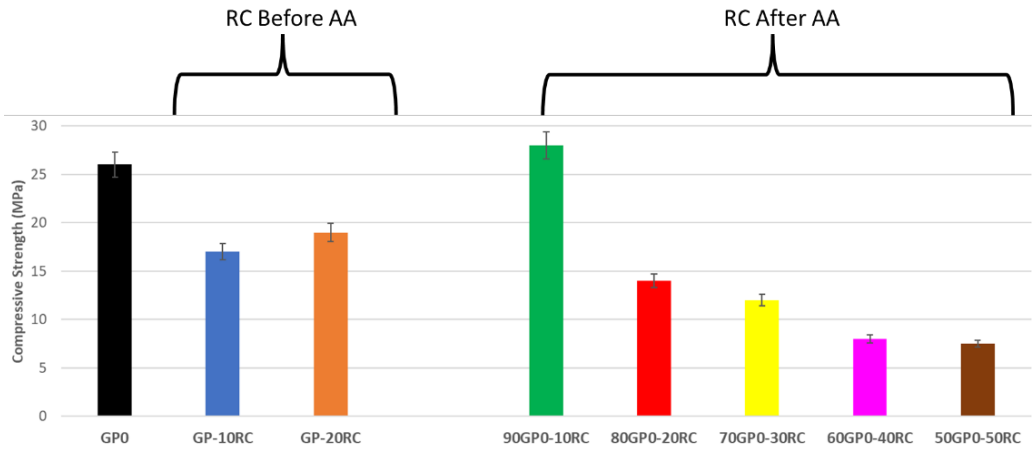

Fig.7-6 Compressive strength of all samples.

- Density

Density calculations, in accordance with Equation showed in section 3.2.11 revealed interesting findings within our study. For the reference geopolymer (GP0), the density remained consistently within the range of 1.8–2.2 g/cm^3. These values align with those reported in the existing literature for metakaolin-based geopolymers [Ghanbari et al. 2017; Duxson et al. 2007; Li et al. 2019]. However, it's important to note that the density values of the geopolymers slightly exceeded that of GP0. This difference in density can be attributed to the inclusion of a denser filler, namely RC (Recycled Corundum). The experimental density value for the spent corundum was determined to be 3.83±0.27 g/cm^3, which, interestingly, was marginally lower than the density of pure corundum, typically falling within the range of 2.94–4.1 g/cm^3 [Xin et al. 2018; Yin et al. 2018]. This observation suggests that the recycled corundum had undergone some degree of alteration during its previous use. Notably, the introduction of RC into the geopolymer formulations, ranging from 10 to 20 wt%, prior to the addition of the alkali activator in GP0-10RC and GP0-20RC, resulted in a slight increase in density. A similar trend was observed for 90GP0-10RC and 80GP0-20RC when the recycled corundumwas mixed with the fresh geopolymeric paste. These density trends correspond well with the anticipated data, specifically the

theoretical densities, which were calculated using the mixture rule applied to the geopolymer formulations, taking into account the actual RC content as outlined in Table 7-1. It's important to acknowledge that the small disparities between the experimental and theoretical density values fall within the range of sample variability, introducing an error of approximately 7% to the density measurements. Interestingly, it's evident that the densification of the geopolymer is more pronounced when RC is introduced as a filler. In these cases, the experimental density values surpass the theoretical values compared to formulations where RC was substituted for MK, irrespective of the overall RC fraction. This trend aligns with SEM observations, which also indicate a higher degree of densification within the geopolymeric matrix when RC is introduced as a filler.

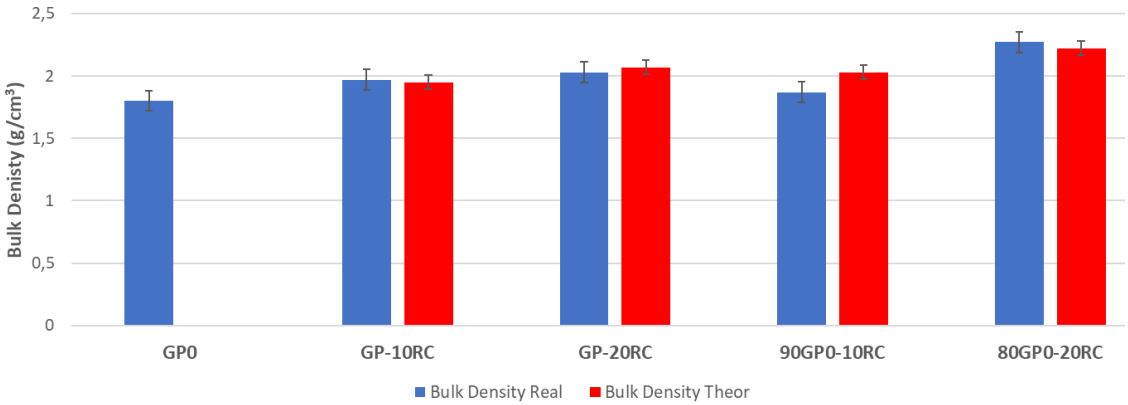

Fig.7-7 Theoretical and calculated density values for all the geopolymers with RC after 28 days of curing time.

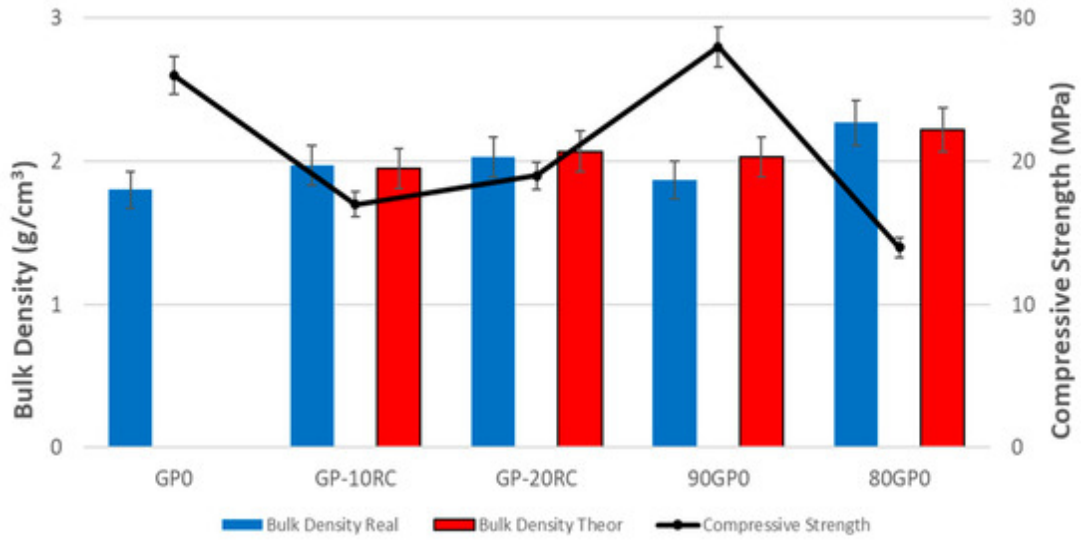

Fig.7-8 Compressive strength compared with Density for all of the geopolymers.

7.6 Discussion and Conclusions

Corundum-based abrasives are available in various grain size fractions, each characterized by distinct mineralogical and chemical purities [Perec et al. 2017; Valasek et al. 2015]. Corundum, known for its chemical and thermal inertness, holds promising recycling potential, provided that the contamination from abraded or eroded materials doesn't introduce hazardous elements. The assessment of such contaminants was a primary concern in our study. In this investigation, we employed X-ray diffraction (XRD) analysis (Figure 7-1 and 7-4) and energy-dispersive X-ray spectroscopy (EDS) to confirm that the waste abrasive powder collected post-erosion testing exclusively contained α-Al_2O_3 corundum. Minor phases consistent with ceramic materials, montmorillonite, and trace metals like valleriite were also identified. Unlike pure corundum (Figure 7-1), the spent abrasive powder exhibited some reactivity in the hot sodium hydroxide (NaOH) reactivity test. This reactivity was primarily attributed to the presence of contaminant aluminosilicate phases, which led to the formation of a zeolite-like phase a characteristic response to alkaline aluminosilicate solutions at temperatures exceeding room temperature [Chen et al. 2019]. These findings suggested that the fine RC powder, consisting of grains smaller than 80 µm (with an average value or D50 of 52 µm confirmed via laser scattering grain sizer and SEM), was insufficient to fully dissolve the corundum phase, as evidenced by Fourier-transform infrared spectroscopy (FTIR) (Figure 7-3) and XRD investigations (Figure 7-4). However, it did facilitate the dissolution of contaminants, thereby promoting the formation of a sponge-like geopolymer gel derived from the dissolution and reticulation of metakaolin (MK), as depicted in SEM images (Figure 7-5). Remarkably, the presence of RC powder, up to the maximum test addition of 20% (as indicated in Table 7-1), did not hinder the reticulation of the three-dimensional aluminosilicate geopolymer network. This was confirmed by analyzing peak positions in the FTIR spectra (Figure 7-3). Density measurements corroborated that MK reticulation occurred consistently in all our formulations, as the alkaline solution to MK weight ratio remained constant at approximately 0.77 (falling within the range of 0.765–0.780; see Table 7-1). The experimentally determined density values aligned with theoretical values (Figure 7-7), calculated as if the reticulation in all samples were the same as in the GP0 formulation. To gauge the degree of geopolymer reticulation, we adopted an indirect yet

sensitive analytical approach measuring the ionic conductivity of the eluate after immersing a piece of consolidated geopolymer in distilled water [Ruiz-Santaquiteria et al. 2011]. As outlined before an increase in ionic conductivity correlated with the overall amount of the liquid activator, entirely independent of the RC content (Figure 7-2). Consistently employing the same curing process across all formulations, and thus yielding an identical geopolymeric matrix primarily formed by MK rather than RC, emphasized the role of corundum grains as inert fillers. A noticeable enhancement in compressive strength was observed in formulations containing around 10 wt% of RC, particularly when RC addition followed proper mixing of MK with the alkaline solutions. In this scenario, the intimate contact between MK lamellas and the activator led to better reticulation and improved bonding with RC grains [Ribeiro, R.A.S. 2019].

8. Geopolymer with waste cork

This chapter delves into the exploration of geopolymers incorporating waste cork. Beginning with the characterization of the waste material to ensure its no toxic nature, the chapter progresses to the formulation and subsequent preparation of the geopolymers. Similar to previous sections, the impact of cork on the chemical reaction and microstructure was thoroughly investigated using a variety of techniques.

8.1 Characterization of waste cork

Prior to its utilization in this project, comprehensive characterizations were performed on cork powders, specifically to the [B. Malchiodi, R. 2022]. This study extensively examined the cork powder using FTIR and STA techniques, as detailed in this publication (Fig.8-1). In the FTIR spectrum of Figure 8-1a, the characteristic peaks of cork can be identified at 3400 cm^{-1} (-OH bond), 2920, 2850 cm^{-1} (stretching) and 1737 cm^{-1} (bending). Paraffin can be detected at 1459 cm^{-1} (bending), and polyurethane glues at 1235, 1156, 1094 (bending) and 721 cm^{-1} (bending-rocking).

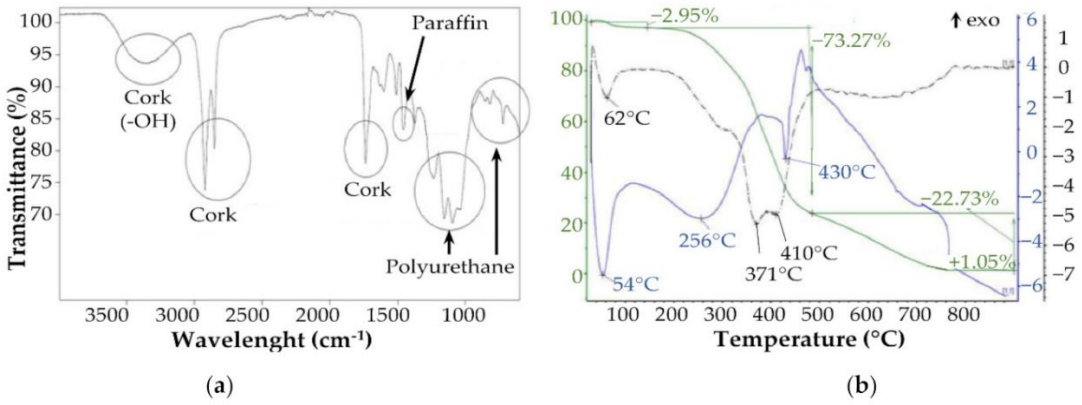

Fig.8-1 Composition of waste corkthrough ATR FTIR analysis (a) and STA analysis (b). In Figure 8-1b are displayed the following curves: TGA (green line), first derivative of TGA (DTGA, black dashed line) and DSC (blue line).

Considering DTGA (Figure 1b, black dashed line), the complete degradation of cork can be observed at around 371°C and 410°C. The other exothermic peaks (between 600°C and 800°C) can be attributed to the degradation of paraffin and polyurethane glue. Moreover, the TGA curve (continuous green line) showed a mass loss of around 76.22% related to cork degradation and a mass loss of 22.73% attributable to the

degradation of paraffin and polyurethane glue [Malchiodi B. 2022]. Contrary to expectations, a greater content of glue and paraffin (>21 wt%) was observed. This is attributable to the fact that, during the production of agglomerated cork caps, the glue and paraffin tend to concentrate on the cap surface, which is the part subject to smoothing and from which the waste corkis generated. So, the waste corkunder investigation displayed a slight difference in composition compared to the original agglomerated cork cap [Malchiodi et al. 2022].

8.2 Geopolymer formulation

To formulate the reference geopolymer, denoted here as GP0, a specific amount of MK dry powder was mixed with an 8 M NaOH solution and a sodium silicate solution. The paste homogenization amalgamation was achieved through mechanical stirring. Subsequently, we introduced various percentages of waste corkpowder, specifically 2, 5, 7 and 10% (also after AA) by weight based on the dry MK component, to create geopolymer composites designated as GP-2CW, GP-5CW, and GP-10CW, 90GP0-10CW respectively (as outlined in Table 8-1). The selection of these waste cork (CW) incorporation levels stemmed from preliminary experiments [Malchiodi et al. 2022; Dal Poggetto et al. 2023] that how adding approximately 10 wt% by weight caused issues with workability and necessitated excessive water. Additional information regarding the geopolymer compositions is provided in Table 8-1. It's worth noting that in two of the formulations, we had to introduce water to maintain the desired workability of the fresh pastes. Consequently, the liquid-to-solid ratio (L/S), considering both NaOH and sodium silicate solutions plus water as the liquid phase and MK and cork powder as the solid phase, was maintained within the range of 0.65 to 0.68 (as indicated in Table 8-1). The preparation of all the fresh pastes involved the thorough mixing of powders and liquids using a planetary mixer (Aucma 1400W, Acuma CO., LTD., Shandong, China). The resulting fresh paste was poured into silicone cubic molds (measuring 25 × 25 × 25 mm3) and plastic molds (245.54 × 233.82 × 26.37 mm3) for subsequent thermal conductivity testing. After eliminating any entrapped air bubbles using a vibrating table, the molds were sealed, and the geopolymers were allowed to cure at room temperature under 100% relative humidity conditions. The silicone molds were opened after a curing period of 1 day. A minimum of

15 samples were prepared for each formulation. Characterization of all samples was conducted following aging periods of different days.

Tab.8-1 Compostion of geopolymers with waste cork.

Weight %						
Sample	**MK (g)**	**NaOH (g)**	**Na-SIlicate sol. (g)**	**Waste cork(g)**	**H_2O (g)**	**L/S (wt/wt)**
GP0	100	38	40	0	32	7.8
GP-2CW	98	38	40	2	32	7.8
GP-5CW	95	36.5	38	5	30.7	7.45
GP-7CW	93	35.7	37.2	7	30.4	7.3
GP-10CW	90	34	36	10	29.7	7.0
95GP0-5CW	53	20	21	5	29	7.1
90GP0-10CW	51	19	20	10	28	6.4

8.3 Stability in water

- Weight loss

After allowing the geopolymers to age for 28 days, all samples were submerged in deionized water for 24 hours to assess their stability in water. It is evident that the weight loss shows a linear increase with the percentage of waste corkwhen added before alkaline activation along with MK (as shown in Figure 8-2). The addition of waste corkseems to disrupt the reticulation of the geopolymeric matrix, possibly due to the partial absorption of the activator solution by some cork dust particles, depleting MK of its necessary reactant fraction. This linear trend persists even when CW is added after alkali activation (as observed in 95GP0-5CW and 90GP0-10CW). However, the values for the same percentages deviate differently from GP0. Interestingly, adding CW to the fresh geopolymer waste, rather than to the dry MK, appears to have a lesser impact on weight loss in water, resulting in a more stable composite at least within the first 24 hours of immersion. This aligns with the hypothesis made in the previous series of composites, where cork dust was added to the already mixed geopolymeric paste, minimizing the sequestration of alkaline activator by some cork dust particles.

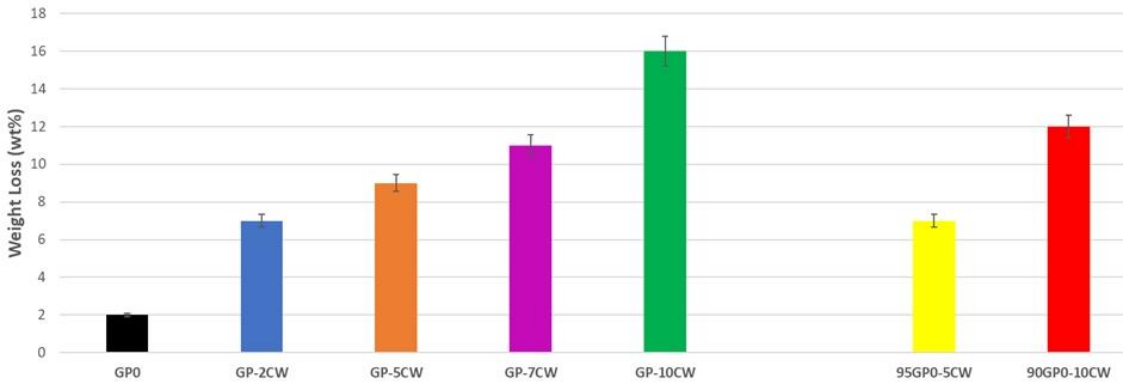

Fig.8-2 Weight loss of all geopolymers after 24 h immersion in water (samples were aged for 28 days before test).

- Ionic conductivity and pH of the eluate

Figure 8-3 offers a comprehensive overview of the ionic conductivity values of the eluate after immersion in water for the composite samples, providing a comparative analysis against GP0. This visual representation enables us to gain valuable insights into the influence of cork presence within the geopolymeric matrix on the overall geopolymer conductivity. The experimental data reveals a significant trend. When waste cork (CW) is introduced into metakaolin (MK) before the addition of the activator, the ionic conductivity values follow a distinct pattern. Specifically, as the proportion of cork in the mixture increases, there is a corresponding rise in ionic leaching, leading to an increment in measured ionic conductivity. This observation suggests that incorporating cork into the dry powders hampers the reticulation of the geopolymeric matrix, resulting in a higher release of ions in the solution [Lancellotti et al. 2013]. Conversely, when CW is incorporated into the sample as a filler with the primary purpose of reducing density or enhancing lightweight characteristics, the ionic conductivity values remain relatively low and similar to that of the matrix (GP0). This consistency implies that the presence of cork does not significantly disrupt or alter the cross-linking and structure of the geopolymeric matrix, corroborating the results from Figure 8-2. Therefore, it can be inferred that the preparation process used for samples 95GP0-5CW and 90GP0-10CW, where CW is added as a filler, has a minor impact on the composite's chemical stability in water over a short period (24 h) compared to the procedure involving the addition of cork dust to MK. This outcome underscores the potential utility of this method in creating lightweight geopolymer composites without compromising their chemical properties.

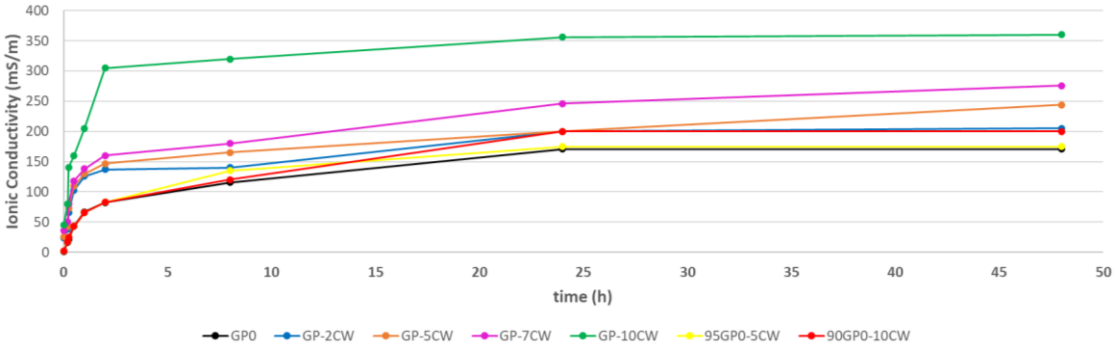

Fig.8-3 Ionic conductivity of the water after immersion of all samples compared with GP0 (The reproducibility of the test was calculated to be within an error of 5%).

- Leaching of the consolidated geopolymer through ICP-OES and ICP-MS

Figure 8-4 provides a detailed insight into the release values (in parts per million - ppm) observed in two sample sets: GP-10CW and 90GP0-10CW, in comparison to Waste cork. These findings shed light on the composition and potential implications of these materials, particularly with regard to their environmental impact. The notable presence of potassium (K) in the release is predominantly attributed to the inclusion of cork in the samples, a fact readily apparent from the data. Similarly, elevated levels of calcium (Ca) can also be correlated with the cork content. These elements, K and Ca, are inherently linked to the chemical makeup of cork, contributing to their detectable presence in the released materials. Intriguingly, the values of aluminum (Al), silicon (Si), and sodium (Na) in the releases closely resemble those typically encountered in geopolymers incorporating recycled corundum. This suggests that, despite the addition of cork, the presence of these elements remains relatively consistent with the established composition of geopolymeric matrices containing other waste materials. Lastly, the identification of vanadium (V) serves as a significant revelation. It confirms that V is an impurity exclusive to the metakaolin (MK) component, as it is conspicuously absent in cork. However, it is reassuring to note that the V concentration remains quite low. This low level of vanadium poses no significant risk or concern, particularly when considering the potential utilization of these samples in applications such as cladding or insulation panels. In summary, figure 8-4 underscores the complex interplay of elemental compositions within the examined materials, highlighting the

unique contributions of cork and MK. The presence of certain elements can be directly linked to the chosen components, and the overall environmental impact and safety profile of these materials appear to be favorable for their intended applications in construction and insulation.

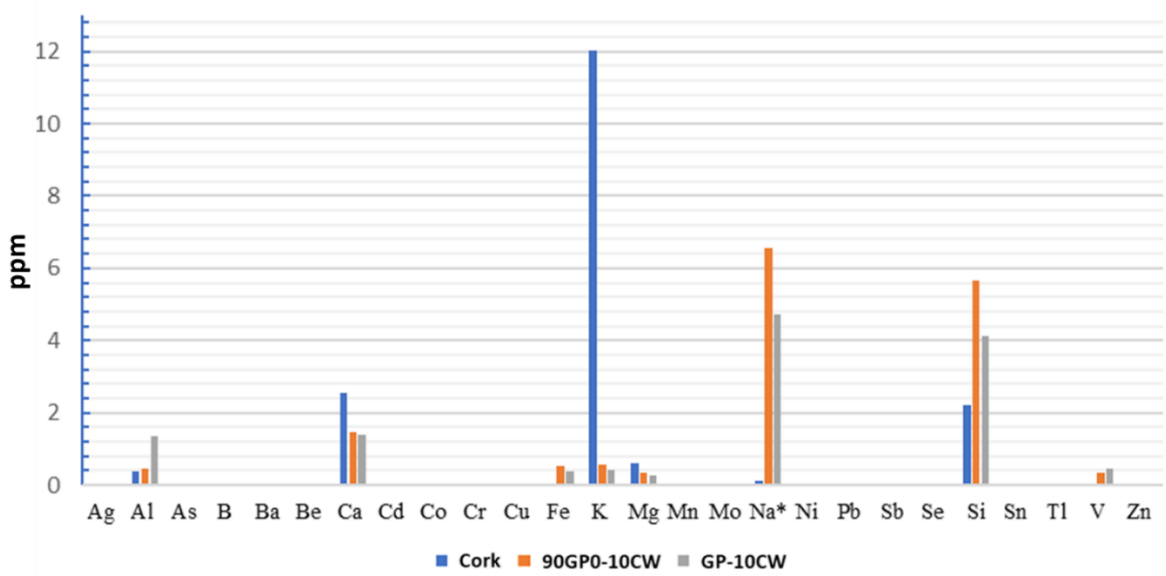

Fig.8-4 Results of the leaching test of the waste corkand the geopolymer samples. All the samples were diluted 1:10 to obtain the Al release. All the other heavy metals are detected without any dilution of the leachates.

8.4 Geopolymerization

- FTIR

In Figure 8-5, the spectra of the samples with 10 wt% of waste cork inserted before and after the AA are shown. As can be seen, the spectra are almost identical, allowing us to assert that the CW does not affect geopolymerization, confirmed by the main peak around 1030 cm^{-1}.
The distinctive features of cork manifest as peaks at 3400 cm^{-1} (indicative of the -OH bond), 2920 cm^{-1}, and 2850 cm^{-1} (representing stretching), along with a peak at 1737 cm^{-1} (indicative of bending) [Malchiodi et al. 2022]. Paraffin content is discernible at 1459 cm^{-1} (reflecting bending) [Kalidasan B. 2021], while polyurethane glues are identifiable through peaks at 1235, 1156, and 1094 cm−1 (associated with bending), as well as at 721 cm^{-1} (indicative of bending-rocking) [Malchiodi et al. 2022; Van Oosten et al. 2011].

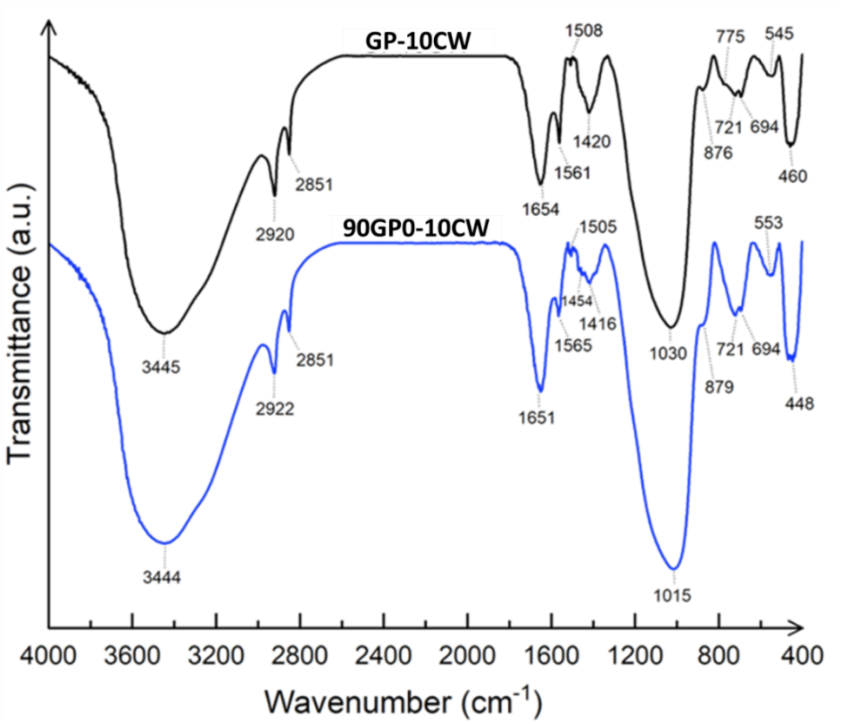

Fig.8-5 FTIR spectra of GP-10CW and 90GP0-10CW.

- XRD

A mineralogical analysis was carried out on all samples (see Figure 8-6). Interestingly, the spectra of the remaining samples (GP-2CW, GP-5CW, GP-7CW, and 95GP0-5CW) closely resembled those of the two spectra presented in Figure 8-6A. The focus was exclusively on these two spectra due to their notably high cork content, suggesting the likelihood of significant changes in these specific samples. In the diffraction pattern of GP0 (Figure 8-6A), a diffuse reflection is clearly visible, indicating the typical broad band of the amorphous aluminosilicate structure. Additionally, there are distinct sharper peaks identified as anatase and alpha-quartz. The diffraction patterns of all samples are similar, displaying these characteristic features. All three geopolymers exhibit diffuse reflections typical of an amorphous aluminosilicate network at approximately 26–28° in 2θ [Temuujin et al. 2009; Dal Poggetto et al. 2022]. It is apparent that the three spectra are identical, indicating that XRD analysis does not provide sufficient information to determine whether cork disrupts the geopolymeric network. Furthermore, Figure 8-6B makes it even clearer that cork, whether added before or after alkali activation, does not significantly alter the chemistry of the geopolymer.

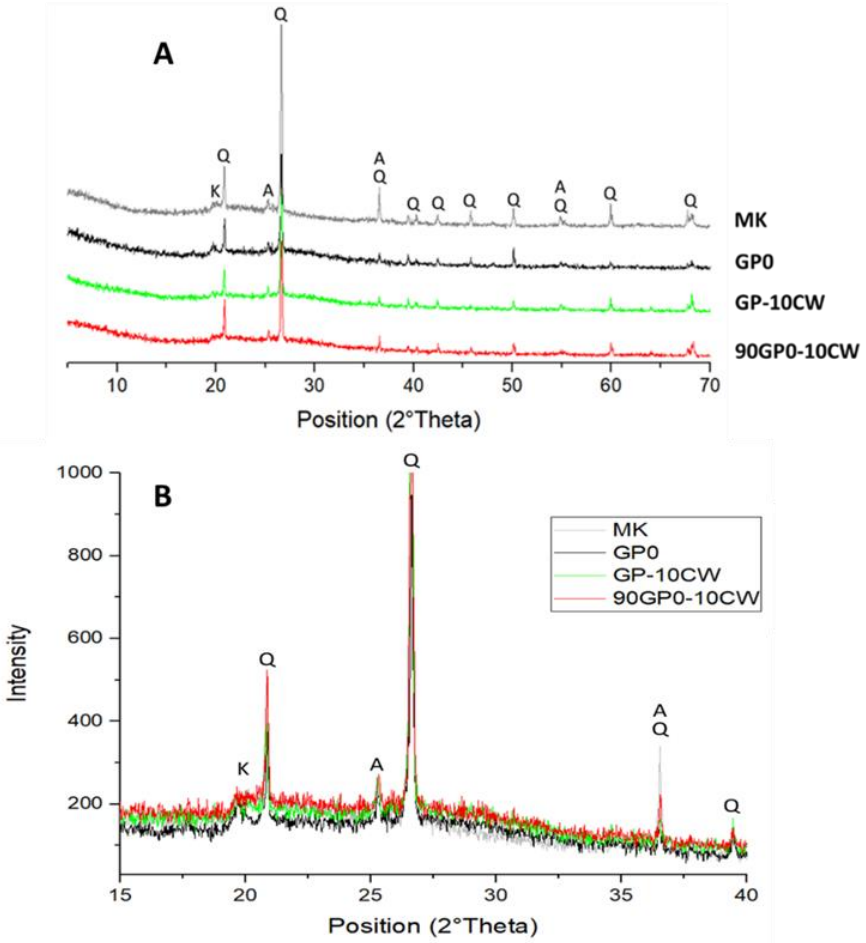

Fig.8-6 XRD spectra of: A) GP-10CW and 90GP0-10CW compared with MK powder and MK-based geopolymer GP0; B) Enlargement of spectra A at the same intensity in the range 15-40° in 2 theta.

8.5 Microstructure

- Characterization via SEM

In Figure 8-7, the SEM image of waste corkis presented, showcasing its characteristic irregular surface structure. This surface is marked by a network of small cavities, pores, and grooves. The unique porous composition of cork, crucial for its insulating properties, is clearly depicted, with numerous visible pores and voids within its structure.

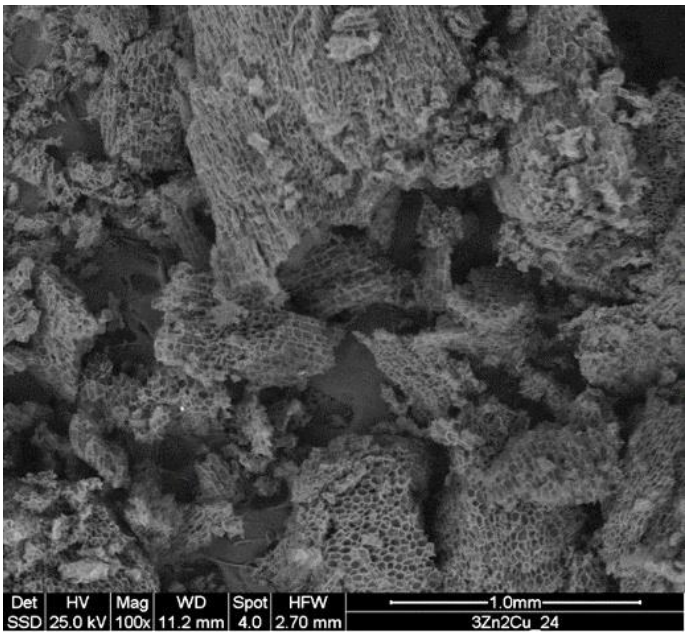

Fig.8-7 Scanning electron microscopy image of the as-received waste cork.

In Figure 8-8, SEM images of geopolymers incorporating waste cork are presented. Remarkably, the waste corkis clearly visible within the geopolymeric matrix (indicated by the purple rectangle) without compromising the geopolymerization process, as confirmed by XRD and FTIR analyses. The characteristic microstructure of the geopolymer is evident within the yellow rectangle. Additionally, the presence of crack deflections (highlighted by the red rectangle) is attributed to exposure to air and excessive water penetration due to the presence of waste cork. Moreover, pores, as indicated by the white arrow, are distinctly visible.

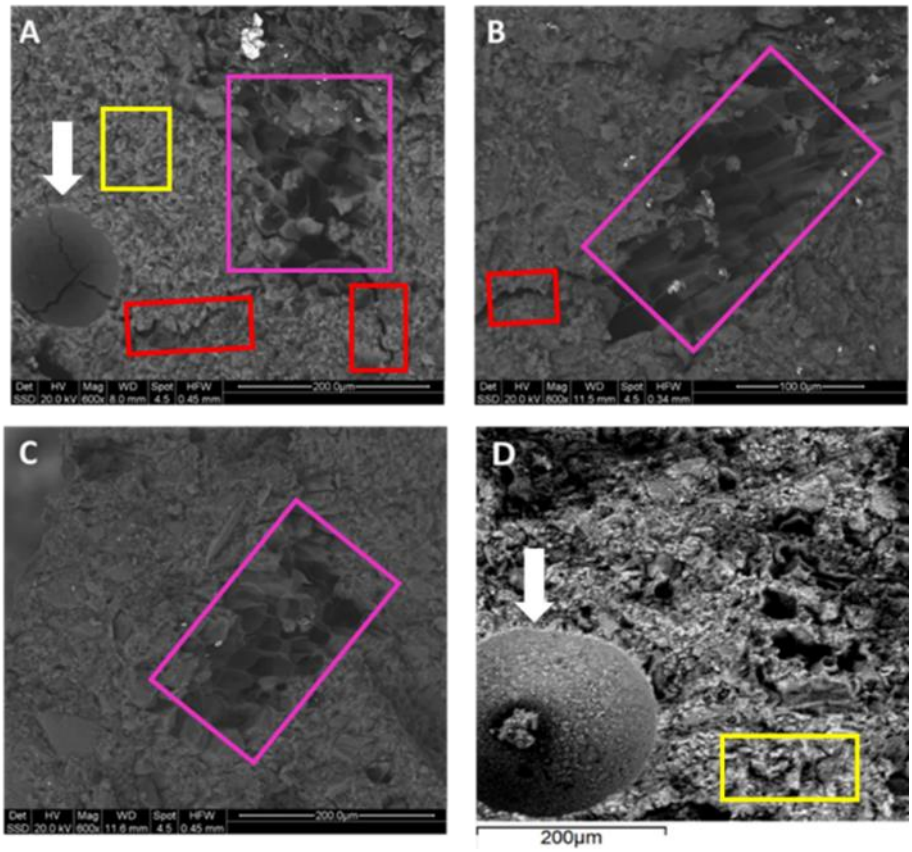

Fig.8-8 Scanning electron microscopy images taken at low magnification of A) GP-2CW; B) GP-5CW C) GP-10CW; D) 90GP-10CW.

Moving to Figure 8-9, the focus shifts to samples containing 10wt% cork, added both before and after alkaline activation. In the GP-10CW sample, unreacted cork is noticeable (indicated by the purple rectangle), along with crack deflections (red rectangle) and pull-outs (green rectangle). Meanwhile, the 90GP0-10CW sample exhibits a considerable presence of unreacted cork sites (purple rectangle) and visible pores (white arrow).

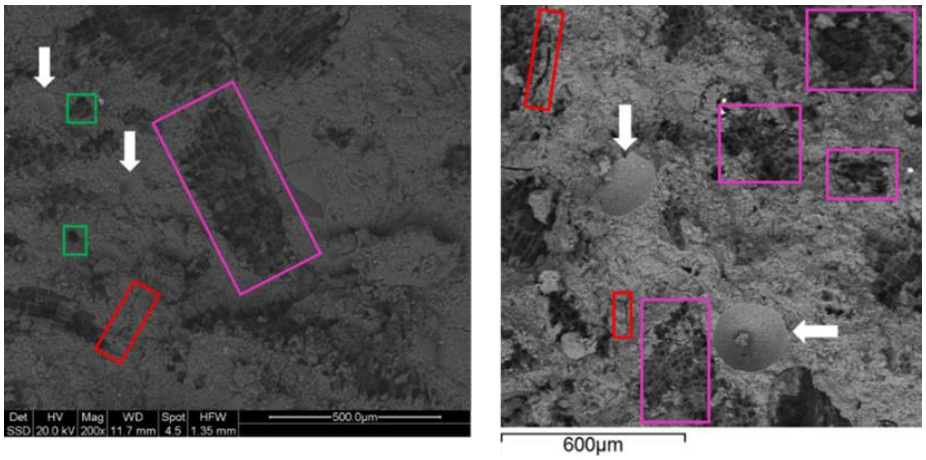

Fig.8-9 Focus on sample GP-10CW (left) and 90GP-10CW (right).

- Thermal conductivity

The evaluation of thermal conductivity for both GP0 and GP-10CW was conducted using a heat flow meter (HFM Lambda, Netzsch-Gerätebau GmbH, Selb, Germany) after 28 days curing period. This assessment holds particular significance because if the geopolymer with 10% CW (waste cork) demonstrates inadequate insulation properties, it implies that lower additions of CW would likely yield similar results. To ensure the accuracy of our measurements, the equipment underwent a calibration process involving certified reference materials (NIST SRM 1450d) and was designed in accordance with ASTM C518 standards [ASTM C518 2021]. The mean thermal conductivity values were determined as the average of three measurements. In Figure 8-10, you can observe the flat surfaces of both the front and rear sides of the test plate, possessing dimensions of 245.54 mm in length, 233.82 mm in width, and 26.37 mm in thickness. Prior to the thermal conductivity assessments, these plates were dried at room temperature while exposed to the laboratory atmosphere, guaranteeing that their weight remained constant throughout the experimentation process. This approach was taken to ensure the reliability and consistency of our thermal conductivity measurements.

Fig.8-10 Sample GP-10CW for thermal analysis.

The thermal conductivity assessment was conducted on two distinct samples: one was the formulation devoid of waste cork, while the other was GP-10CW, comprising 10% waste cork, aged for a duration of 28 days. The thermal conductivity value (K) obtained was 0.1146 ± 0.0001

W/mK. Remarkably, this value bears a striking resemblance to the thermal conductivity of 0.122 ± 0.03 W/mK observed in a metakaolin (MK) geopolymeric sample containing approximately 87 ± 2.5 vol% porosity, achieved through the incorporation of aluminum (Al) powder [Kamseu et al. 2014]. Considering GP-10CW overall porosity, which hovers around 56%, coupled with a cork content of 24 vol%, the current formulation predominantly comprises about 80 vol% of the insulating phase, encompassing both pores and cork. This composition closely mirrors the material profile documented in the literature. In a related study [Kamseu et al. 2022], Kamseu et al. reported thermal conductivity values in the range of 0.5–0.6 W/mK for various geopolymer formulations possessing different Si/Al ratios in their dense state. This range is in close proximity to the thermal conductivity value of approximately 0.45 W/mK attained for GP0.

Figure 8-11 presents a comparative analysis of GP-10CW alongside other geopolymer formulations documented in the literature [Jaya et al. 2018. Ghosh et al. 2018; Gómez-Casero et al. 2022.]. Notably, when juxtaposed with formulations consisting solely of metakaolin, GP-10CW exhibits significantly lower thermal conductivity. Moreover, when compared to conventional construction materials like concrete (where K ≈ 0.28 W/mK for insulating mortars and K ≈ 1.6 W/mK for base mortars [Jaya et al. 2018]), the thermal conductivity of GP-10CW is notably lower. It is approximately one-third lower for insulating mortars and nearly fifteen times lower than that of base mortars. However, it's important to note that GP-10CW cannot be categorized as a fully-fledged thermal insulator, as per the standards outlined in UNI EN 998-1 [Malchiodi et al. 2022], which stipulate the need for thermal conductivity values to fall within the range of 0.06–0.09 W/mK for proper thermal insulation. Nevertheless, the thermal conductivity value achieved for the GP-10CW composite is commendable. It positions the geopolymer as a material with low sensitivity to heat, not an absolute insulator, but one that outperforms traditional construction materials in terms of thermal efficiency.

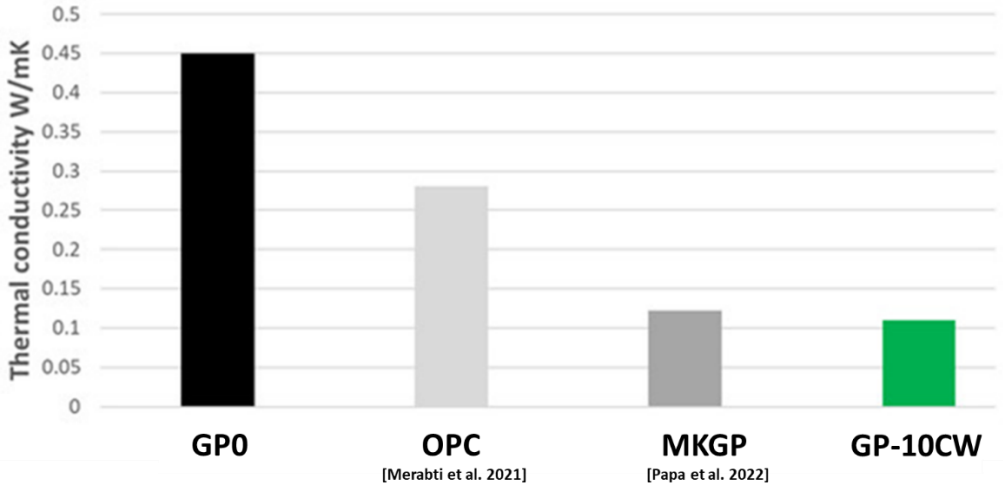

Fig.8-11 Thermal conductivity values for samples GP0 and GP-10CW after 28 days compared to the literature data of aerated Portland cement (OPC) and porous MK-based geopolymers.

- Compressive strength

Compressive strength tests were conducted on all geopolymer samples after 28, 60, and 90 days of curing (Fig.8-12). The properties of GP0 align with findings from previous studies [Davidovits, J. 1988; Davidovits, J. 2008, 2020; Duxson et al. 2007].

In contrast, the behavior of samples containing cork is intriguing. After 28 days, these cork-containing samples exhibit significantly lower properties than GP0, and this trend persists with a higher percentage of cork, regardless of whether it was added before or after alkaline activation. At the 60-day and 90-day marks, it's worth noting that 90GP0-10CW did not yield measurable results. This was not due to compromised geopolymer integrity but rather the impossibility of testing. The excessive presence of unreacted cork caused 90GP0-10CW to absorb a substantial amount of water, making the sample malleable yet resistant to breaking. For the other samples, there is a noticeable peak in their properties at 60 days, followed by a decline after 90 days. Adding cork after alkaline activation indeed imparts lightweight and ductile properties to the material. However, if intended for reinforcement, it must be incorporated with MK before alkaline activation.

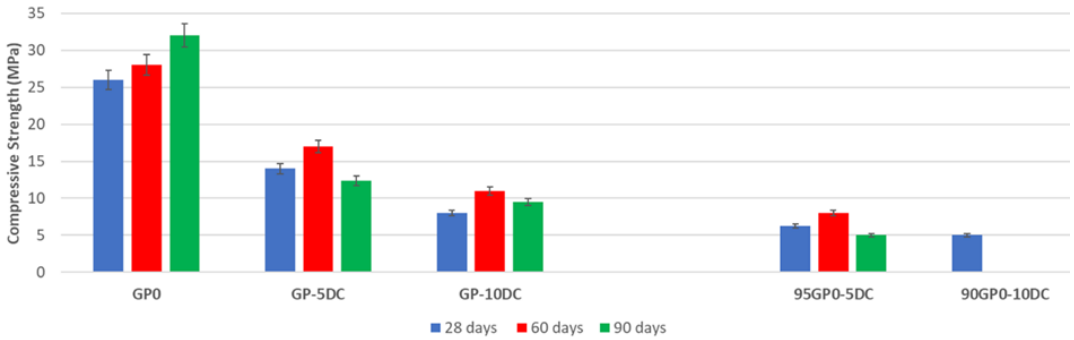

Fig.8-12 Compressive strength of all samples after 28, 60 and 90 days of ageing.

- Density

In Figure 8-13, it can be observed how the apparent density decreases as the percentage of cork increases for both series of cork-containing composites aged 28 days, as a light and porous materials inserted into the geopolymer matrix that lightens the compound [Provis J.L. 2009.].
Moreover, cork, being highly sensitive to humidity and inherently porous, further complicates the scenario. A single wine cork stopper boasts around 700 million cells, a result of the intricate cellular composition of the cork oak tree's inner bark, comprising independent tetradecahedron cells. Even after processing, this cellular arrangement persists in cork stoppers. [Malanho et al. 2021]. Figure 8-13 illustrates a conspicuous decline in real density as the proportion of cork escalates over 28 days. The introduction of this lightweight, porous material into the geopolymer matrix serves to lighten the overall compound. The trend in total porosity mirrors the observations in Figure 2, reflecting the corresponding water loss values. The data depicted in Figure 7 delineate also the progression of porosity over 28 days of ageing.
Notably, the sample with the highest addition of waste corkbefore alkali activation exhibits an exceptionally high porosity value, approximately 35%. When cork is added after alkaline activation, the porosity reaches up to 42% for both compositions. It is crucial to note that geopolymers based on metakaolin inherently possess nanoporosity in the range of 35–40%, characterised by nanopores within the mesoporous scale (2–50 nm). The challenge arises from the intricate evaporation of condensation water through these ultrafine pores. This complexity is further compounded by the introduction of cork powder, accompanied by the formation of voids around it due to the challenging workability of the material in its fresh geopolymer paste state.

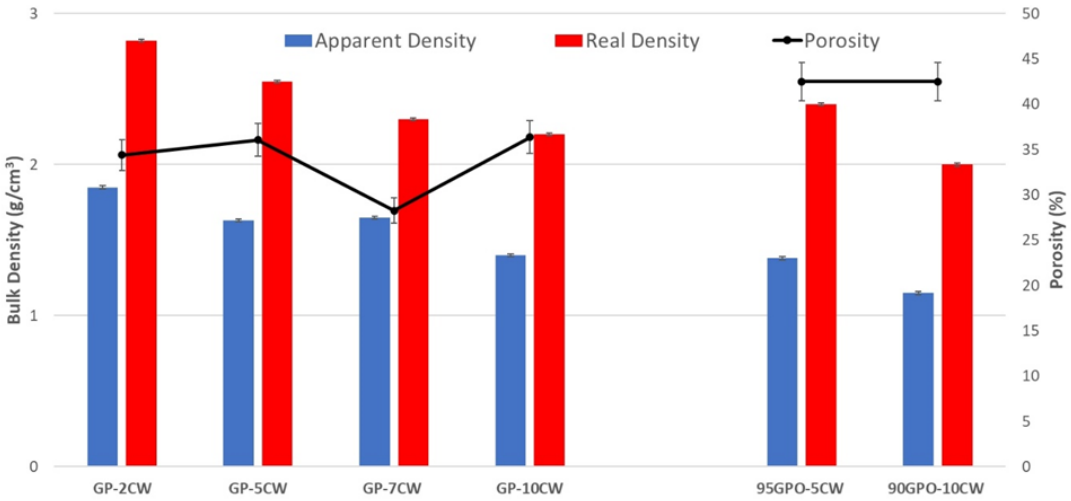

Fig.8-13 Real density, apparent density and porosity of all geopolymers aged 28 days.

Figure 8-14 illustrates the apparent and true densities associated with the porosity of geopolymers containing 5% and 10% waste corkafter 28, 60, and 90 days. It is evident from the trend that the real density decreases over time. Consequently, the porosity of the samples also decreases correspondingly.

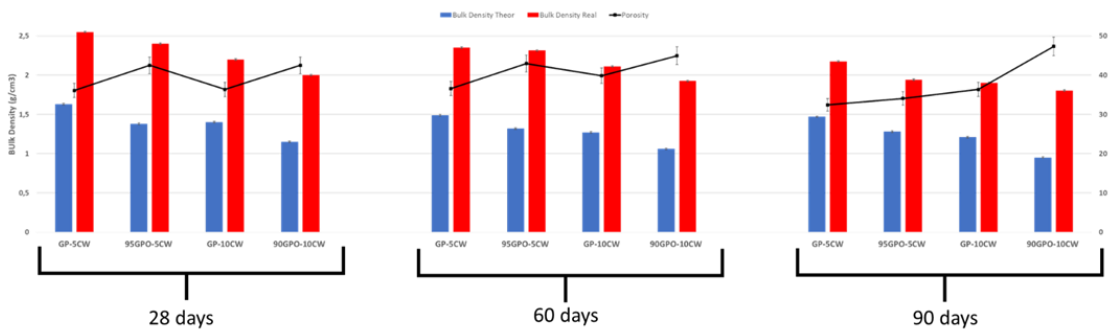

Fig.8-14 Real density, apparent density and porosity of all geopolymers aged 28, 60 and 90 days.

For a better comprehension of all the data reported in the figure before in figure 8-15 the compressove strength is compared with the porosity after 28 days.

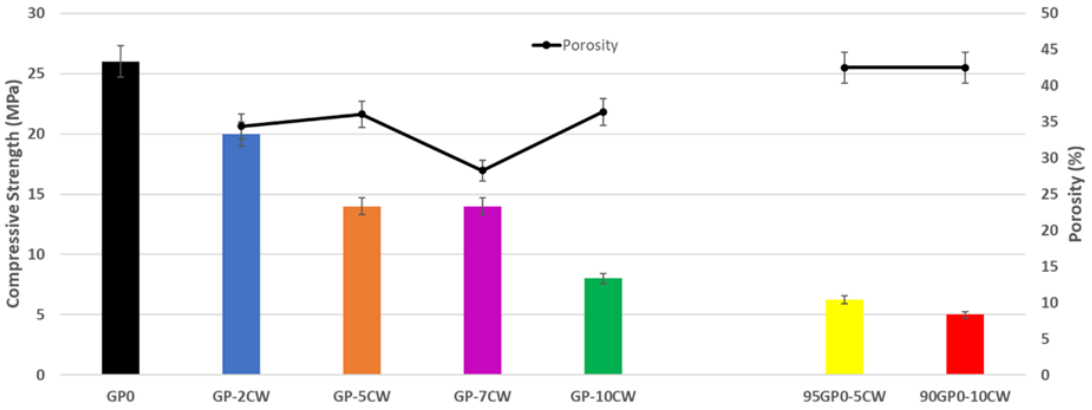

Fig.8-15 Compressive strength compared with porosity after 28 days.

8.6 Antibacterial activity

The cork alone, as also reported in the literature [Sudagar et al. 2018], had antibacterial properties against both *E.coli* and S. *aureus*. However, unlike what is reported in the literature, where cork would seem to have a greater antibacterial power against S.*aureus* than *E.coli* (Fig.8-16), from our results the inhibition against the two bacteria was the same, with an inhibition halo of the size of the disk of about 1.3 cm. The antibacterial activity occurred also in the other samples, and, as for the cork, the inhibition halos were greater against *E.coli* compared to S.aureus. In particular, the inhibition halos against S.*aureus* was always about 1.3, while against *E.coli* was different according to the specimens. In particular, GP-10CW showed the greatest inhibition halo of about 1.97 cm. Following GP-7CW and GP-5CW had an inhibition halo of about 1.7 and 1.57 respectively. Finally, GP-2CW and 90GP0-10CW showed lower inhibition halo measurements of about 1.51 and 1.3 respectively. Looking at Figure 8-16, it is possible to point out that, apart from the inhibition halos, there is a further halo where the growth of bacteria, even if present, is limited. This behaviour, known as bacteriostatic activity, is possessed by GP-2CW, GP-5CW, GP-7CW, GP-10CW and 90GP0-10CW samples against *E.coli* bacteria.

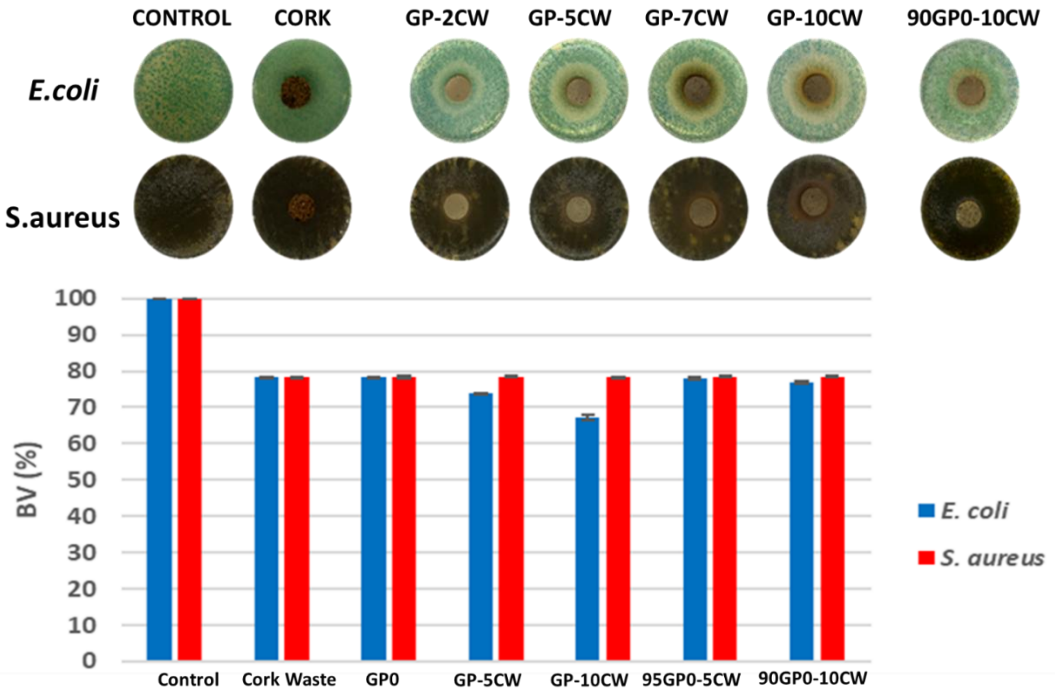

Fig.8-17 Inhibition Halo of all sample compared with the control.

8.7 Discussion and Conclusions

The utilization of lightweight waste materials in the context of geopolymers has been an area of insufficient exploration, as highlighted in existing research [Zaid et al. 2022; Samuel et al. 2022]. It is noteworthy that such waste materials possess the potential to significantly impact the cost-effective disposal of waste while concurrently enhancing the prospective applications of geopolymers as insulating materials. Moreover, literature on the valorization of waste cork as a lightweight filler or aggregate is relatively scarce [Novais et al. 2019]. In the initial phase of our research, which focuses on the direct utilization of as-received waste cork, our primary objective centered on formulating geopolymers that are not only viable but also adaptable, as detailed in the current manuscript. Once we confirmed the successful establishment of the geopolymeric network, we proceeded to undertake a comprehensive evaluation encompassing physical, mechanical, chemical, and microstructural aspects of the geopolymers. Comparing our findings to prior studies on geopolymer composites incorporating lightweight materials, particularly waste cork, and taking into account the analyses presented in the preceding sections, several significant observations come to light:

- In direct comparison to cement composite materials, our use of MK-based geopolymers in conjunction with waste cork yielded materials with superior strength characteristics. Specifically, the compressive strength achieved with the incorporation of approximately 2% cork in our study reached approximately 10 MPa, in stark contrast to the values reported in [Malchiodi et al. 2022], where they did not surpass 2 MPa. A similar trend was observed when incorporating about 5% CW.
- Within the framework of the MK-based geopolymer matrix, the lightweight compositions discussed in the study [Samuel et al. 2022.] did not exceed 5 MPa. To elaborate further, these authors documented the addition of pyrolyzed cork ranging from approximately 2.5% to 3.75% by weight, achieving compressive strengths of 3.5–5.0 MPa.
- The significance of thermal insulation materials in construction cannot be overstated, given their pivotal role in reducing the energy consumption of buildings. Among the critical structural elements of buildings, external walls are of paramount importance.

Examining Ashby's chart (Figure 8-17), illustrating common applications of lightweight building materials/ceramics, as provided in ANSYS GRANTA EduPack R2021, our geopolymer lightweight composites fall well within the range of insulating and building materials conventionally employed [Ashby, M.F. 2011]. Moreover, in reference to the thermal conductivity values cited in the study [Samuel et al. 2022], our recorded value of approximately 0.11 W/mK is notably lower than the corresponding figures reported for 18 vol% pyrolyzed cork, which stood at 0.56 W/mK.

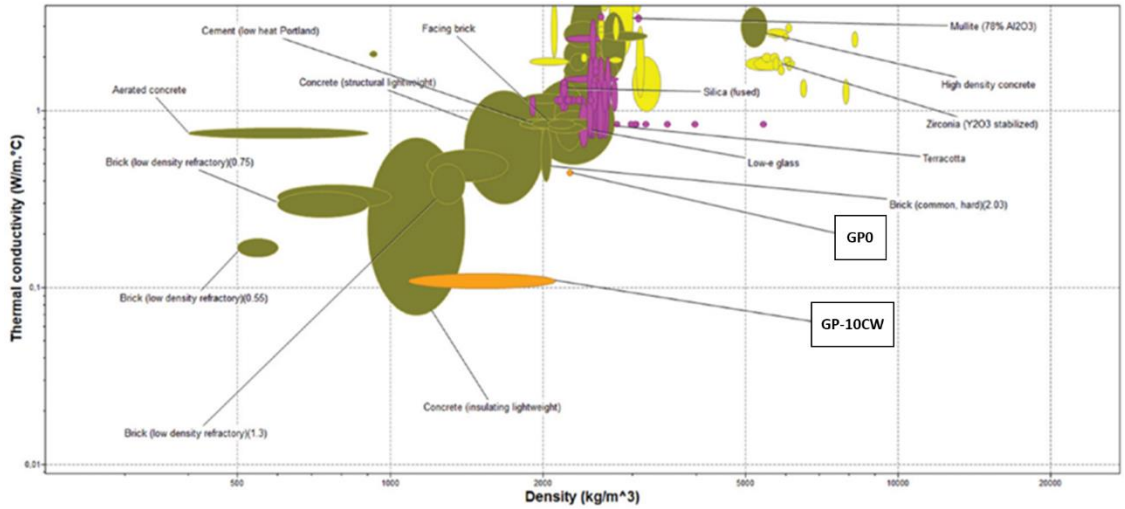

Fig.8-17 Ashby chart: thermal conductivity vs density for GP0 and GP0-10CW in comparison to other insulating inorganic materials.

The absence of waste corkpre-treatments and thermal curing of the final composites allowed us to indicate the mixes optimized in this work as sustainable fire-resistant insulation materials with a reduced environmental footprint, when compared to expanded polystyrene systems [Malanho et al. 2021].

9. Acid exposure

9.1 Introduction

In this concluding chapter of experimental results, the investigation on the impact of acid attacks on specific formulations selected in the proceeding chapters is detailed. The study centered around samples incorporating two waste materials: abrasive corundum (RC) and waste cork. Following a 28-day ageing period, the selected samples were immersed in three acid solutions at varying concentrations for 10 days; subsequently, characterization analyses were carried out.

9.2 Weight loss

After the immersion process outlined in section 3.2.12, the weight loss of the various studied samples was calculated as weight difference before and after immersion in the acid solutions.

- Geopolymer with recycled corundum

In Figure 9-1, the samples with recycled corundum after alkaline activation (AA) are depicted. It is evident that as the concentration of acidic solutions increases, the weight loss also escalates. Following immersion in 0.5N acid solutions, the weight loss remained low, staying below 10%. As the percentage of RC increased, the loss also rose, albeit remaining relatively modest. Importantly, this increase did not significantly impact the mechanical strength of the samples (Fig. 9-24). When the solutions' concentration was elevated to 1.5N, more pronounced differences emerged between the samples, particularly for those with at least 30% RC. Nevertheless, the overall trend persisted. The most compelling results were observed with the higher acid concentrations, 2.5N. GP0 continued to exhibit commendable performance even with escalating concentrations, a trait shared with 80GP0-20RC. However, the remaining samples gradually began to display the effects, noticeable in both penetration (Fig. 9-9.10) and mechanical properties (Fig. 9-24, 9-25).

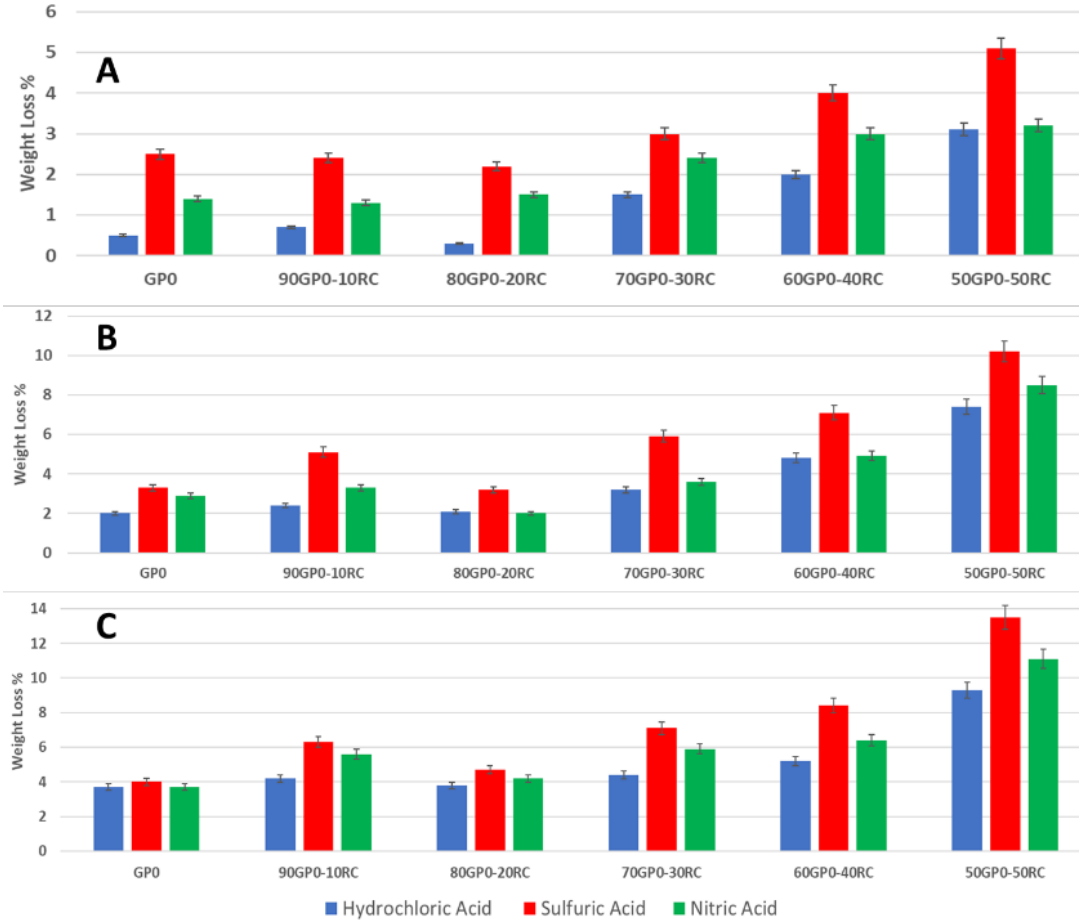

Fig.9-1 Weight loss of geopolymer with RC (after AA) after immersion in A) 0.5N acids; B)1.5N acids; C) 2.5N acids.

In Figure 9-2, the weight losses of samples with RC added before alkaline activation are reported after immersion in acid. At low concentrations, the weight loss remains minimal. A unique trend emerges after immersion in 1.5N acids; the weight loss increases up to 40% and then decreases to 50%. Finally, after immersion in more concentrated acids, the trend becomes even more pronounced, consistent with the observations in the mechanical tests (Fig. 9-24).

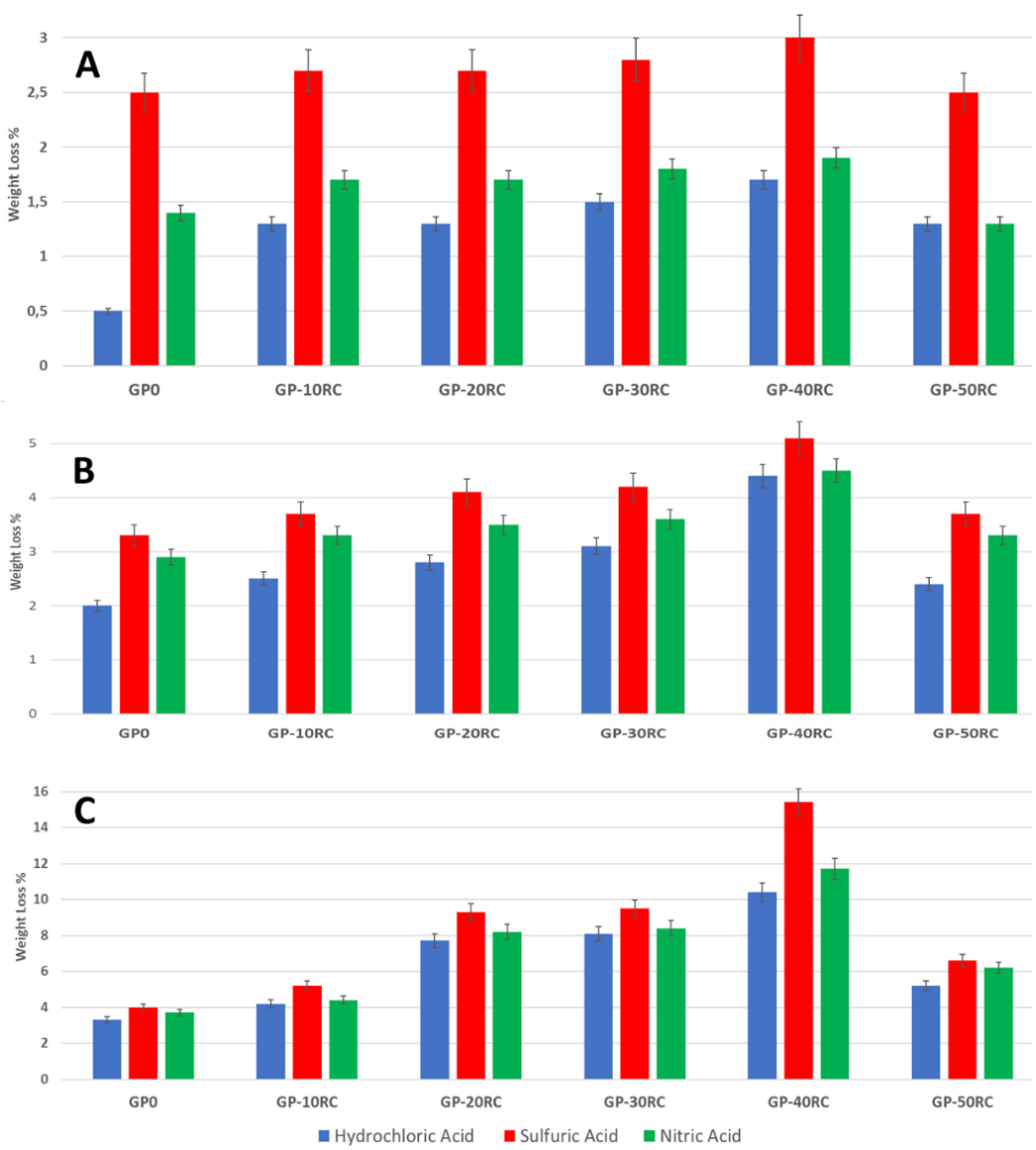

Fig.9-2 Weight loss of geopolymers with RC (before AA) after immersion in A) 0.5N acids; B)1.5N acids; C) 2.5N acids.

After discussing the results of the two formulations, the focus shifted to comparing formulations with 20% and 50% RC added both before and after the acid attack. The results showed significant disparities, highlighting the profound impact of adding RC at different percentages before and after the AA into geopolymers. Specifically, when 20% RC was added before the AA, the weight loss and subsequent mechanical tests (Fig. 9-25) indicated lower values than those of the GP0 sample. However, adding 20% RC after the Alkali activation enhanced the chemical performance of the geopolymeric sample. These improvements were also observed prior to the acid attack, as detailed in Chapter 5. The addition of 50% RC before and after the AA had contrasting effects. Before alkaline activation, RC likely integrated more

effectively into the geopolymeric network, thereby enhancing its performance. However, incorporating this percentage of RC in the paste, especially after the AA, substantially reduced the geopolymer's performance. This trend was previously noted in Chapter 5 as well.

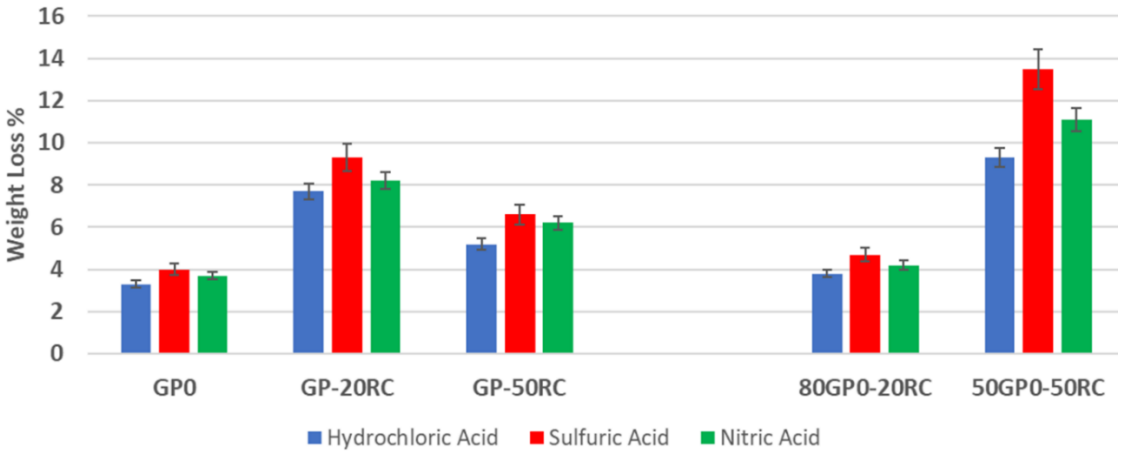

Fig.9-3 Comparison weight loss of geopolymers with different percentage of RC after immersion in 2.5N acids.

Regarding samples containing waste cork (CW), significant differences in weight loss after immersion were observed between CW added before and after the alkali activation. It is crucial to emphasize that geopolymers immersed in 0.5N acid solutions show minimal damage. However, when the samples are exposed to 2.5N acid solutions, noticeable weight losses occur, corresponding to the subsequent poor mechanical performance (Fig. 9-27). After 10 days, geopolymeric samples with CW added before the AA display considerably high weight losses. It is likely that if they had been immersed for a longer period, the weight loss would have increased exponentially.

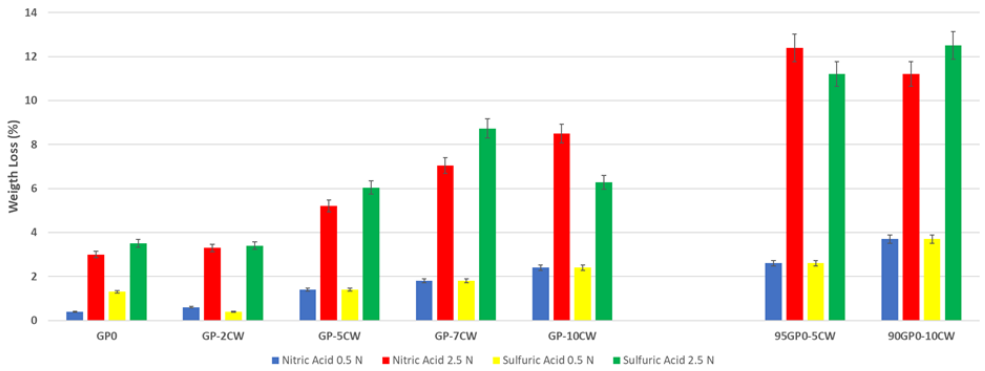

Fig.9-4 Weight loss of geopolymer with waste cork after immersion in 0.5 and 2.5N acids.

- Comparison between geopolymer with RC and CW

The comparison depicted in Figure 9-5 between Geopolymers containing corundum and cork clearly demonstrates how corundum significantly improves the geopolymer's performance in contrast to cork. These results are consistent across observations of acid penetration (Fig. 9-10), the impact on microstructure (Fig. 9-20), and ultimately, mechanical performance.

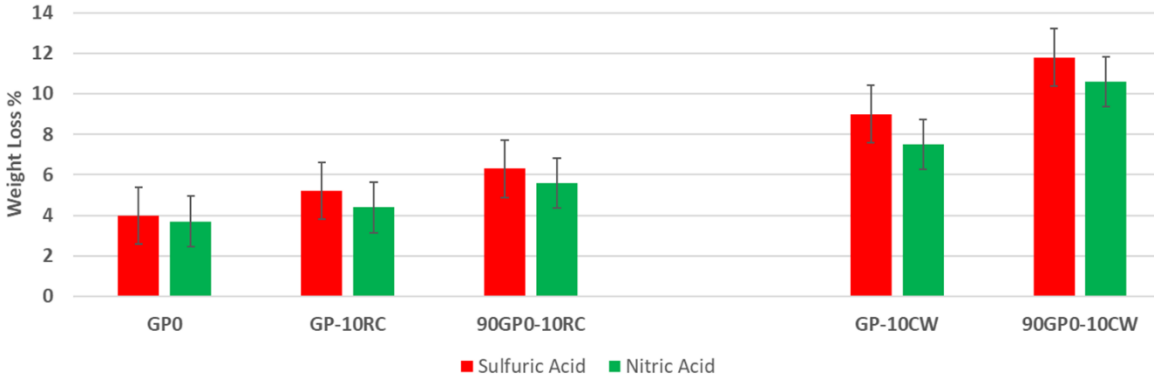

Fig.9-5 Comparison weight loss of geopolymer with RC and CW.

9.3 Penetration test

In order to enhance the visualization of the geopolymer sections immersed in acid solutions, a 1% phenolphthalein solution was employed. Spraying this solution onto the samples section provided visual cues (coloration or lack thereof, indicating pH levels) to assess the depth of acid penetration. After identifying the areas primarily affected by acids, they were examined using a different technique (XRD, MAS-NMR, SEM/EDS). This methodology proved instrumental as it allowed for a comprehensive study of the disparities between damaged and undamaged segments of the geopolymer, as evidenced in the NMR analysis (Figure 9-15).

- Geopolymer with recycled corundum

In Figure 9-1, a photo of the GP0 sample extracted after 10 days of immersion in 2.5N H_2SO_4 and sprayed with 1% phenolphthalein is shown. The sample is clearly divided into two distinct zones: a white (colorless) area with a pH below 8.2, indicating cationic exchange, and a purple area with pH > 8.2, representing the intact and undamaged geopolymer core not reached by the acid solution. The damaged outer portions, located within the white zone, were extracted and characterized, providing valuable insights into the geopolymer's acid induced changes.

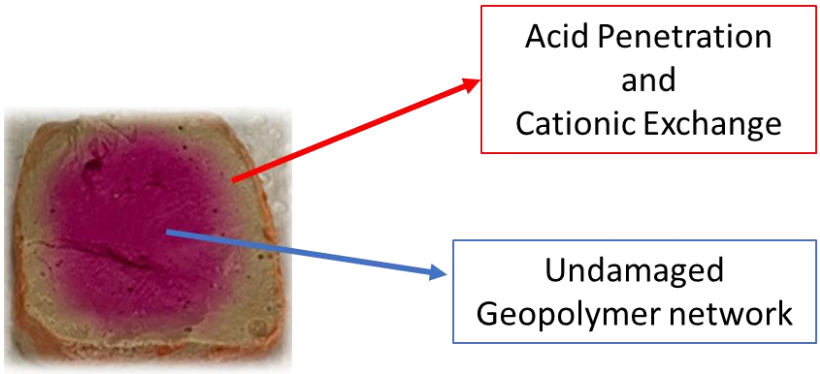

Fig.9-6 GP0 after H_2SO_4.

Figure 9-7 compares the samples 80GP0-20RC and GP-20RC. The penetration in the geopolymer sample with 20% RC before the acid attack (GP-20RC) is greater than in the other geopolymer. This observation is consistent with the diverse results obtained in various characterizations.

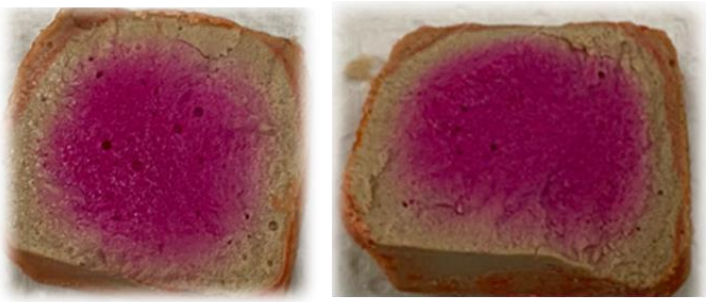

Fig.9-7 GP-20RC (left) and 80GP0-20RC (right) after H_2SO_4.

The samples containing 50% RC were also analyzed. Figure 9-8 provides a comparison, highlighting how GP-50RC exhibits superior resistance to acids and is less permeable to their infiltration. In contrast, 50GP0-50RC emerges as the least effective among all tested samples, showing not only high permeability to acids but also greater irregularity in protecting the geopolymeric network. Notably, this figure underscores another aspect of the discussion regarding the optimal dispersion of corundum. GP-50RC remains largely intact and undamaged, emphasizing the crucial role of well-dispersed corundum in enhancing the geopolymer's structural integrity.

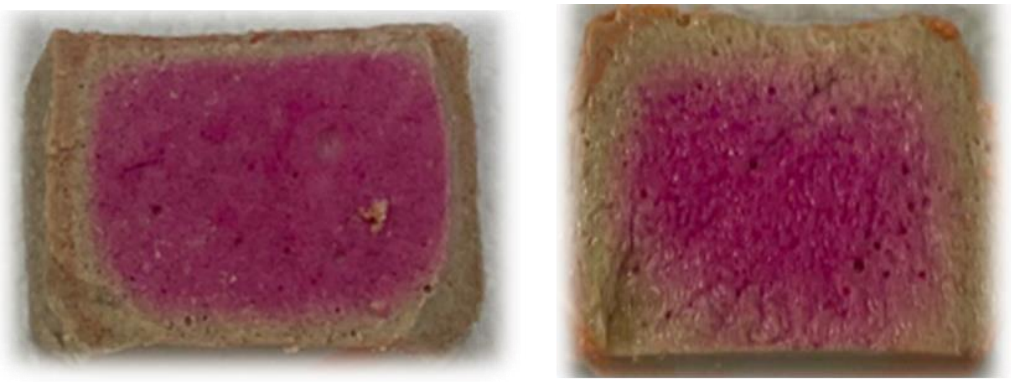

Fig.9-8 GP-50RC (left) and 50GP0-50RC (right) after H_2SO_4.

- Geopolymer with waste cork

In the samples containing waste cork, a significant difference becomes evident as the percentage of cork increases, underscoring the pivotal role played by CW, whether added before or after the acid attack, in shaping the geopolymer's properties. Figure 9-9 vividly demonstrates that with the rise in the percentage of CW, the sample's permeability to solutions, not limited to acidic ones, escalates. Concurrently, porosity, elaborated upon in Chapter 8, experiences a consistent increase, allowing acids to deeply permeate the geopolymer's microstructure. The samples depicted in Figure 9-9 underwent extraction for 10 days in 2.5N H_2SO_4 and were subsequently sprayed with 1% phenolphthalein solution. Strikingly, no violet zones are visible; only colorless regions are apparent, indicating varying degrees of sulfuric acid-induced damage to the structure. Notably, in the cases of GP-2CW and GP-5CW, acid penetration extended throughout the geopolymer. Nevertheless, these samples effectively prevented the acid from causing internal structural damage, enabling penetration without internal harm. In contrast, sample 90GP0-10CW effectively highlights the distinction between penetration and damage. Acid permeated the entire sample; yet, unlike the others, 90GP0-10CW experienced more extensive destruction, underscoring the delicate balance between acid penetration and maintaining structural integrity.

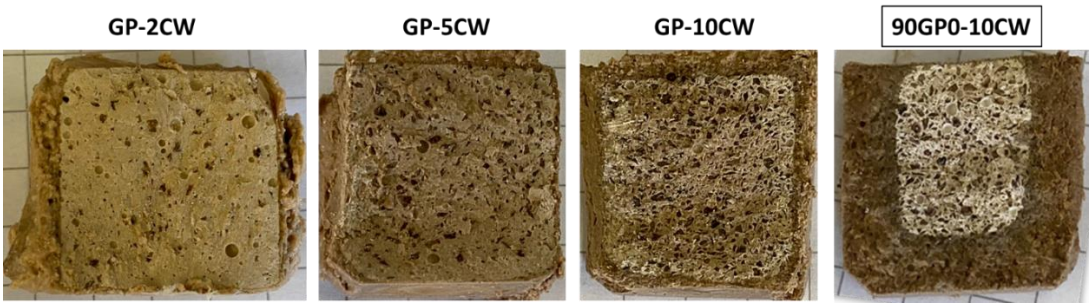

Fig.9-9 Geopolymer with CW after H_2SO_4.

- Comparison between geopolymer with RC and CW

Figure 9-10 compares 80GP0-20RC and 90GP0-10CW, presenting a compelling contrast between the effects of two waste materials, one inorganic and one organic, on the geopolymer structure. This comparison sheds light on the nuanced differences between mere penetration and penetration coupled with structural damage. In 80GP0-20RC, penetration is intricately linked with the damage inflicted by H_2SO_4. Meanwhile, in the case of 90GP0-10CW, as noted earlier, it becomes crucial to differentiate between these aspects. Although penetration extended to the core of the sample, the structural "damage" was limited to a depth of 5mm. This distinction underscores the intricate interplay between material composition and the resultant geopolymer behavior, providing valuable insights into the complex interactions within these systems.

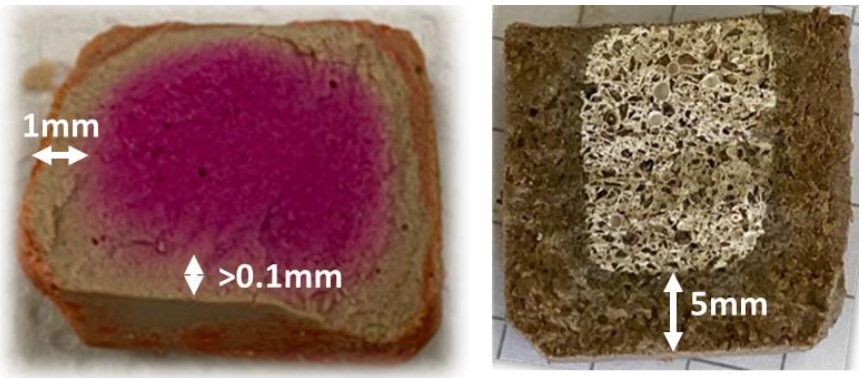

Fig.9-10 Comparison of 80GP0-20RC with 90GP0-10CW after H_2SO_4.

9.4 Geopolymerization

- XRD

In Figures 9-11, 12, and 13, the XRD spectra of GP0, GP-20RC, and 80GP0-20RC are displayed after being subjected to extraction in 2.5N sulfuric acid for 10 days. The areas analyzed using X-rays correspond to the portions damaged by the acid, as previously explained. The sole noticeable difference observed before and after exposure is the presence of gypsum, attributed to the trace amounts of calcium found in both RC and MK. All other crystalline phases have remained unaltered.

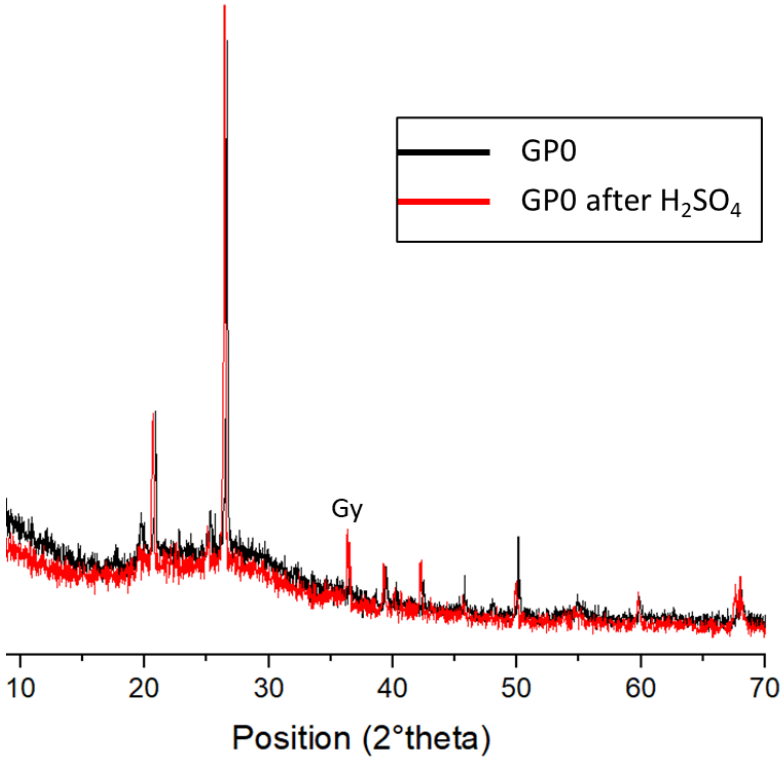

Fig.9-11 XRD spectra of GP0 before and after exposure to H_2SO_4 (Gy=gypsum, $CaSO_4 \cdot 2(H_2O)$).

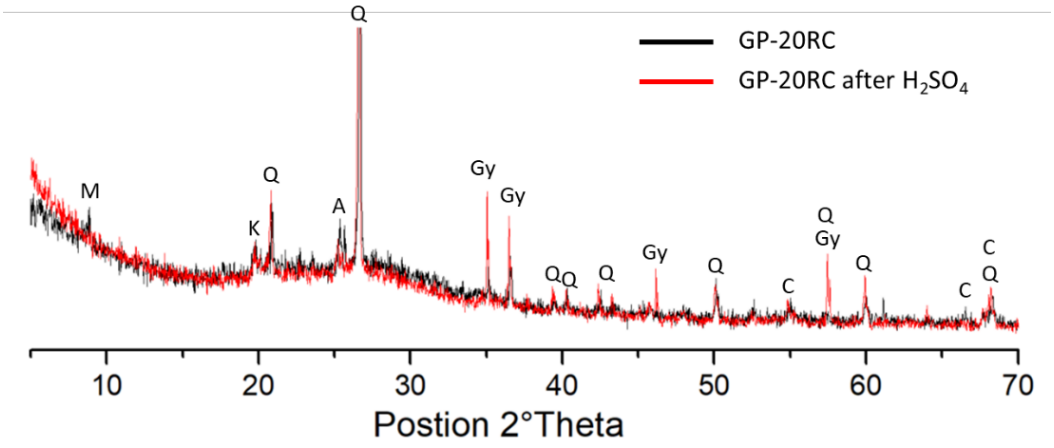

Fig.9-12 XRD spectra of GP-20RC before and after exposure to H_2SO_4.

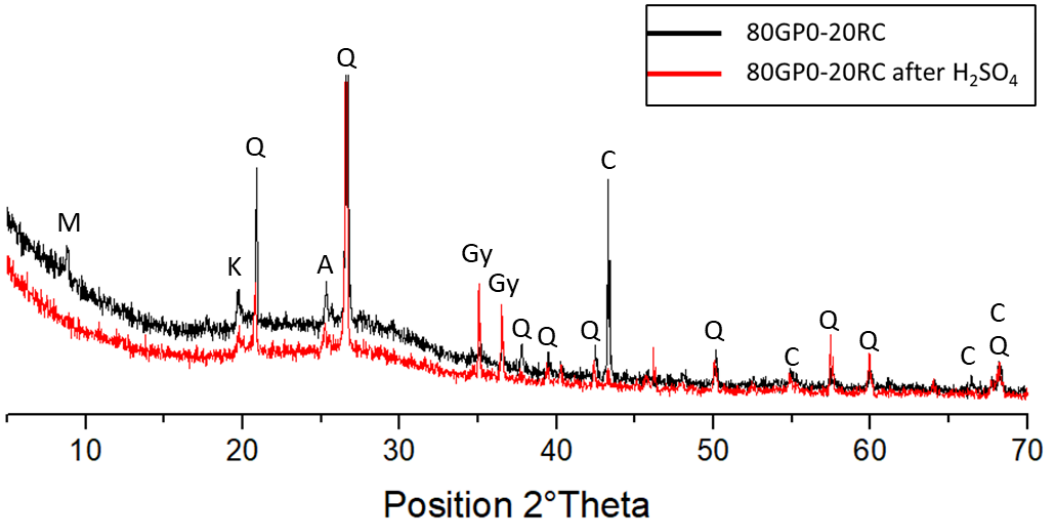

Fig.9-13 XRD spectra of 80GP0-20RC before and after exposure to H_2SO_4.

- MAS-NMR

Studying the acid attack of geopolymers through ^{27}Al MAS-NMR spectroscopy provides valuable insights into the composition and structure of these inorganic materials during the acid-induced reactions. Geopolymers, being silicate or aluminosilicate-based materials, possess complex structures where aluminum atoms (Al) can exist in various chemical environments. When subjected to acid attack, which involves reactions with acids, the aluminum atoms within the geopolymer structure can undergo different chemical transformations.

In Figure 9-14, the ^{27}Al MAS-NMR spectra of the reference sample GP0 are presented before and after exposure to 2.5N sulfuric and nitric acid. As explained in both Chapter 4 and Chapter 5, the key peaks in

geopolymers' spectra are around 60 ppm (representing Al(IV)), at 0 ppm (representing Al(VI)), and around 25 ppm (indicating possible Al(V) presence). After exposure to sulfuric acid (red spectrum), these three peaks persist, yet notable differences emerge. Al(IV) remains relatively stable under these exposure conditions, as does Al(V). However, the Al(VI) peak around 0 ppm exhibits a doublet, likely due to the presence of both Al(VI) within the network and octahedral Al(VI) that has exited the structure during the exchange and arranged around it [A. Allahverdi 2001a; A. Allahverdi 2001b.] A similar pattern is observed in the GP0 spectrum after nitric acid treatment (green spectrum). Once again, the doublet in the Al(VI) peak can be explained as described earlier. Although the exact chemical impact of HSO4-, SO4 2-, and NO3- ions remains unclear, their evident influence on microstructural properties is discussed in section 9.5.

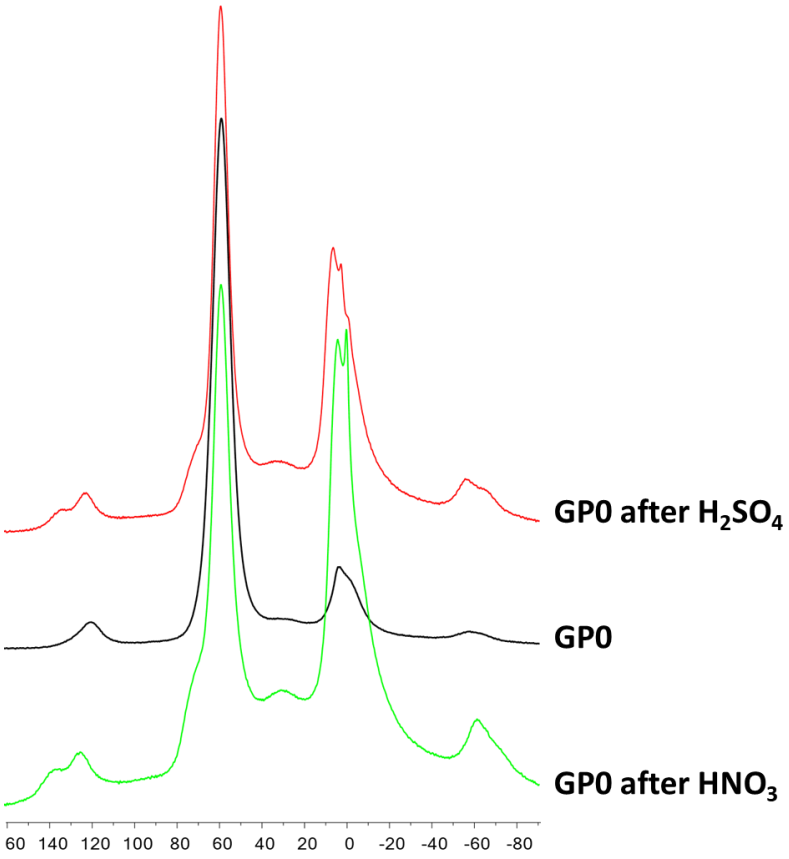

Fig.9-14 ^{27}Al MAS-NMR of GP0 before after HNO_3 and H_2SO_4.

As previously elucidated (section 9.3), the utilization of phenolphthalein colouration proved to be indispensable in determining which portions of

the section to analyze. Figure 9-15 serves as striking evidence: the spectrum within the geopolymer after acid exposure remains unchanged compared to the spectrum before exposure. This reaffirms the absence of acid penetration and, by extension, the absence of any cationic exchange.

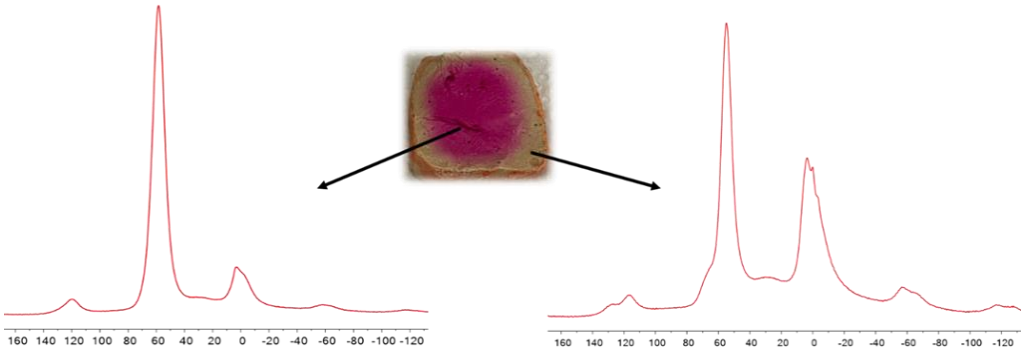

Fig.9-15 ^{27}Al MAS-NMR of different part of GP0 after H_2SO_4.

Figures 9-16, 17, 18, and 19 showcase the NMR spectra of the samples containing RC as studied in Chapter 6. These spectra illustrate, as previously discussed, the presence of the Al(VI) peak in Corundum before the acid exposure. Across all spectra, the absence of Al(V) is evident both before and after exposure to the two acids. Following the sulfuric acid exposure of GP-20RC (depicted in Figure 9-16, red spectrum) and GP-50RC (shown in Figure 9-17, red spectrum), a distinct variation in the Al(VI) peak is observable. In GP-20RC, the double peak representing Al(VI) rearranged around the geopolymeric network is notably pronounced. Conversely, in GP-50RC, it appears as a distinctive hump, likely due to the high corundum content in the sample. A similar pattern emerges in the spectra following HNO_3 exposure (green spectra), where the intensity of Al(IV) diminishes, and the double peak of Al(VI) becomes more prominent. This difference is markedly more noticeable in GP-20RC than in GP-50RC. Moreover, this distinction is also observable between 80GP0-20RC (Figure 9-18) and 50GP0-50RC (Figure 9-19).

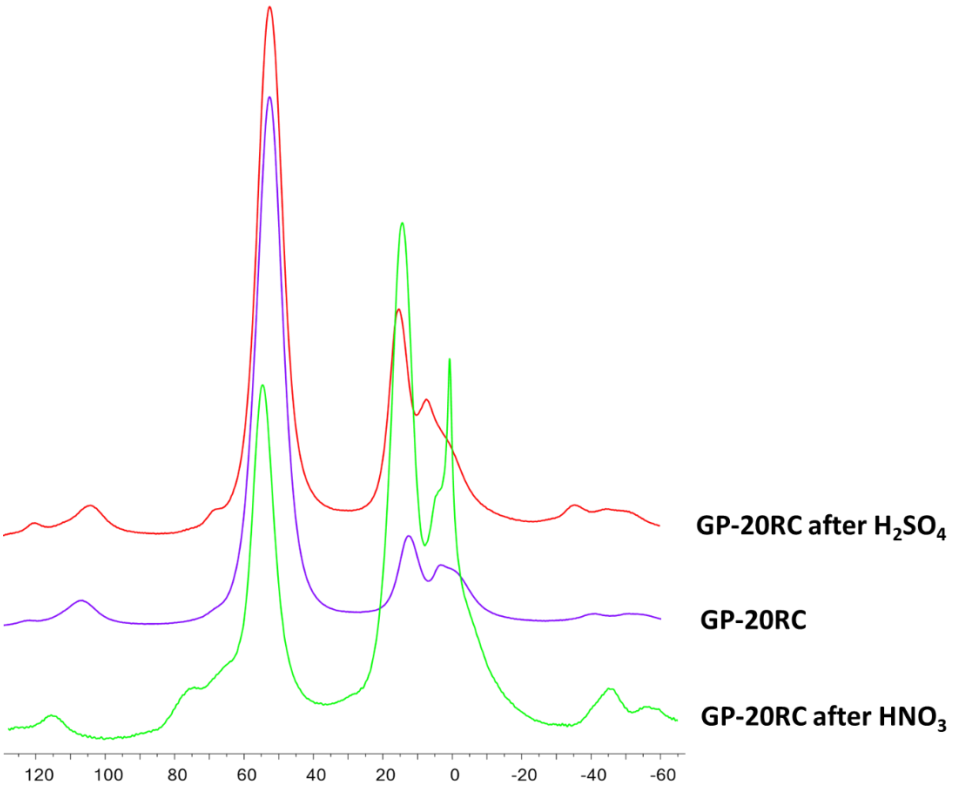

Fig.9-16 ^{27}Al MAS-NMR of GP-20RC before after HNO_3 and H_2SO_4.

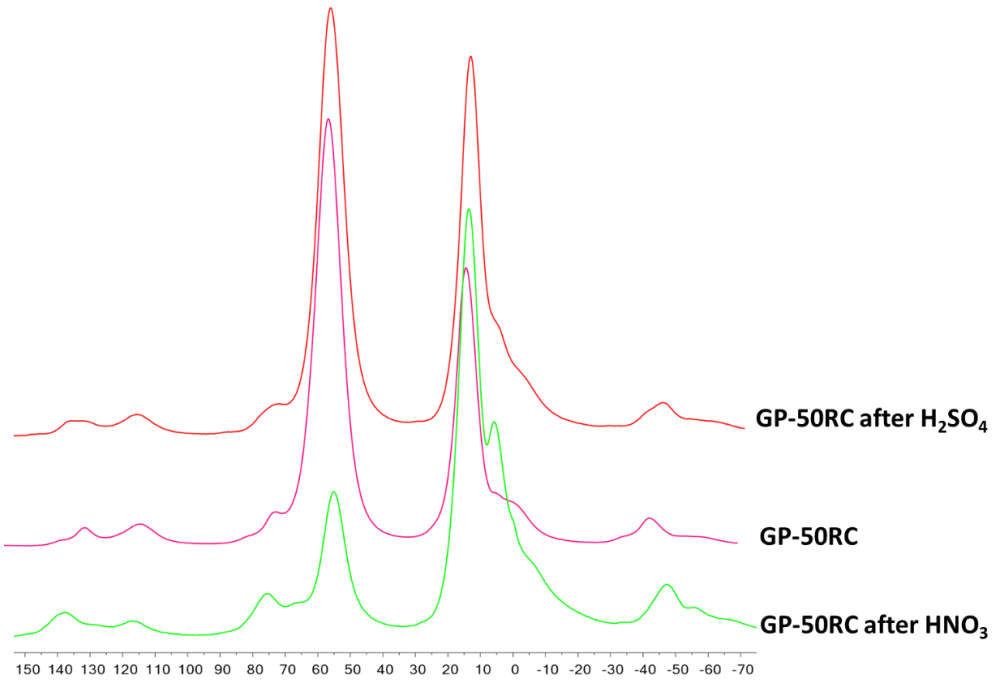

Fig.9-17 ^{27}Al MAS-NMR of GP-50RC before after HNO_3 and H_2SO_4.

Figure 9-18 displays the spectra of 80GP0-20RC before and after exposure. A clear distinction is visible between the spectra obtained with sulfuric acid and nitric acid. In this instance, apart from indicating the presence of Al(VI) from corundum and the octahedral structure located outside the network, there is also an observable effect caused by the NO3- ion. This effect additionally contributes to a shift, a phenomenon not observed in the other samples.

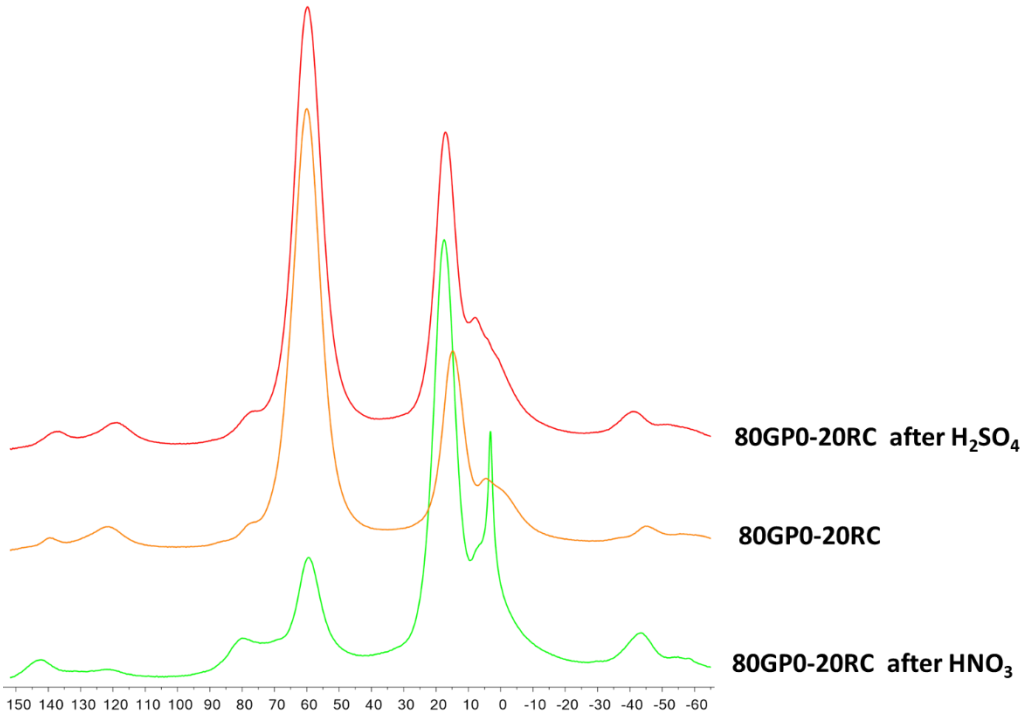

Fig.9-18 ^{27}Al MAS-NMR of 80GP0-20RC before after HNO_3 and H_2SO_4.

The sample 50GP0-50RC displays three notably distinct spectra. The pre-acid attack sample has been previously discussed. Regarding the spectra after exposure, both exhibit the same trend, in contrast to the observations made for the 80GP0-20RC sample. In both cases, there is a significant change in Al(IV) due to the acid's deeper penetration. Similar to the observation in GP-50RC, it is evident here that there are not clearly defined double peaks around 0 ppm; instead, there is a noticeable hump. The high presence of RC remains unscathed by the acid, enabling the acid to more readily attack various parts of the geopolymeric network. As discussed in Chapter 6, this network demonstrates greater crack deflection compared to other samples.

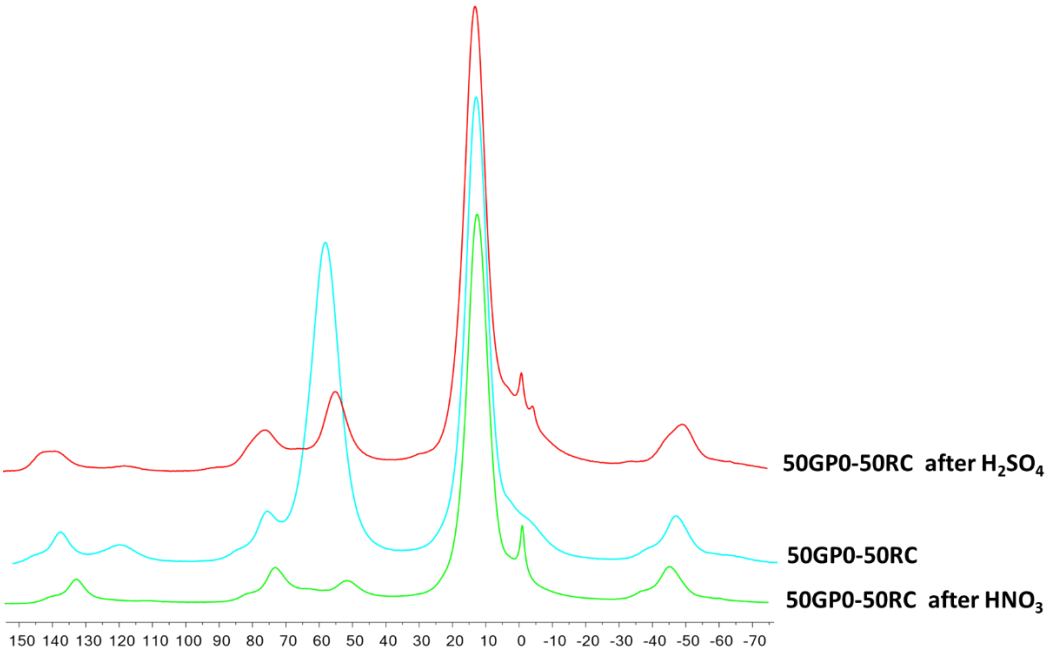

Fig.9-19 ^{27}Al MAS-NMR of 50GP0-50RC before after HNO_3 and H_2SO_4.

9.5 Microstructure

9.5.1 SEM / EDS

In this section, we delved into the microstructural characteristics of geopolymers containing waste materials after immersion in sulfuric acid, the acid that had the most pronounced effect on the samples. The initial step involved analyzing the reference sample GP0, which was then compared to the various other samples for detailed examination.

- Geopolymer with recycled corundum

No comparison was made with geopolymers containing corundum, as they did not exhibit significant structural damage due to the corundum presence. In fact, the changes observed in the RC-containing samples closely mirrored those studied in GP0. This similarity arises from the fact that the acid attacks targeted the geopolymeric network and not the RC component. These results align with existing literature [Allahverdi et al. 2001a; Allahverdi et al. 2001b.] and the findings from Chapter 5, which unequivocally demonstrated that corundum neither influenced the geopolymerization process nor was a part of it. Examining the GP0 sample (Fig.9-20) post-immersion in H_2SO_4 2.5N solution, notable differences emerge when compared to the SEM image of GP0 before the

acid exposure (Fig.6-19). The pores (white rectangle) are now penetrated by deep cracks (black arrows) induced by sulfuric acid. It's essential to distinguish these cracks from the pre-existing crack deflections (red rectangles) present in the geopolymer prior to acid exposure. The acid-induced cracks are significantly deeper, sharply dividing the sample's areas.

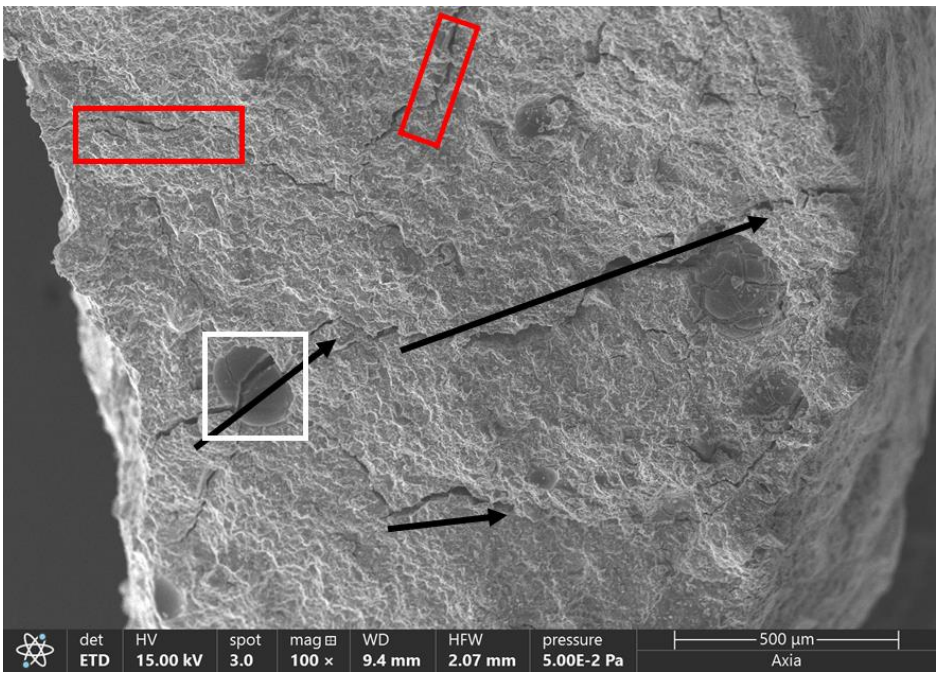

Fig.9-20 Scanning electron microscopy images taken at low magnification after acid attack of GP0.

- Geopolymer with waste cork

After treating the samples with acids, we conducted SEM analysis to examine the impact on their microstructure. To pinpoint specific areas for investigation, we employed phenolphthalein 1% to determine the extent and locations of acid penetration. In Figure 9-21, it is evident that the pores (white rectangle) suffered damage upon exposure to the H_2SO_4 [Gluth et al. 2022]. Moreover, the H_2SO_4 caused structural degradation, forming distinct grooves (black arrow). These grooves, resulting from sulfuric acid exposure, should not be mistaken for crack deflections (red rectangle). This distinction is clearly visible in Figure 9-22C. Importantly, the cork material (purple rectangle) remained remarkably inert to this type of chemical attack.

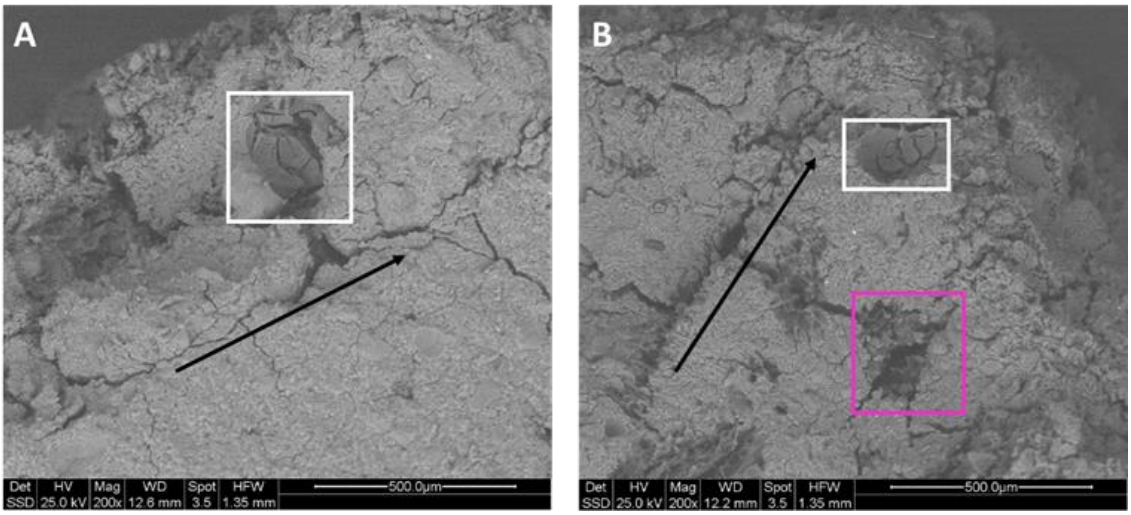

Fig.9-21 Scanning electron microscopy images taken at low magnification after acid attack of A) GP-2CW; B) GP-5CW.

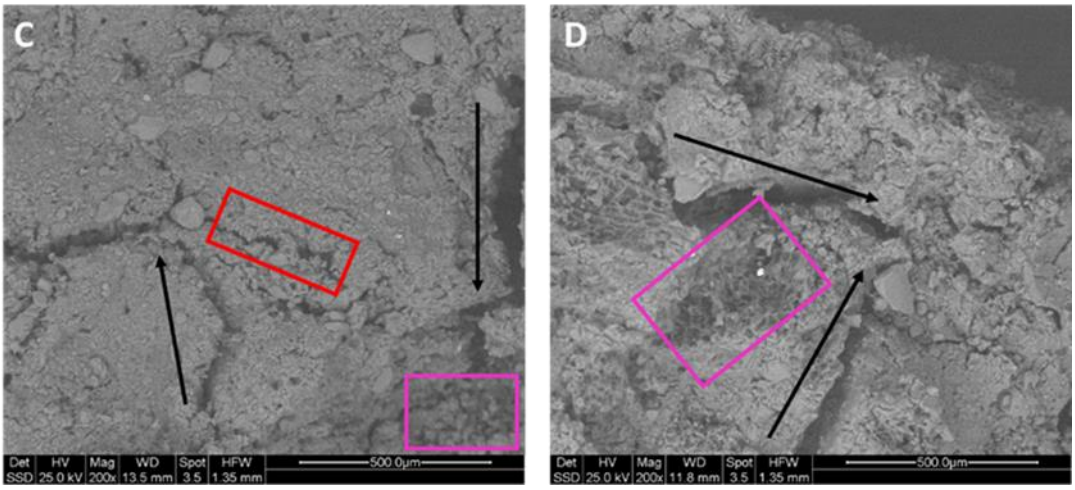

Fig.9-22 Scanning electron microscopy images taken at low magnification after acid attack of C) 90GP-10CW inner part; D) 90GP-10CW surface.

The infiltration of S into the geopolymers' microstructure was investigated through EDS. Figure 9-23 presents the SEM image of the 90GP0-10CW sample, supplemented by EDS data from four distinct areas, spanning from the innermost to the outermost regions. Remarkably, the analysis reveals a diminishing S penetration as it nears the geopolymer's core. This observation suggests that the interior of the geopolymer experienced a comparatively milder chemical attack. The Na profile is the opposite of the S one, proving the ionic exchange with H^+ as expected from previous studies and modelling [Wan et al. 2020].

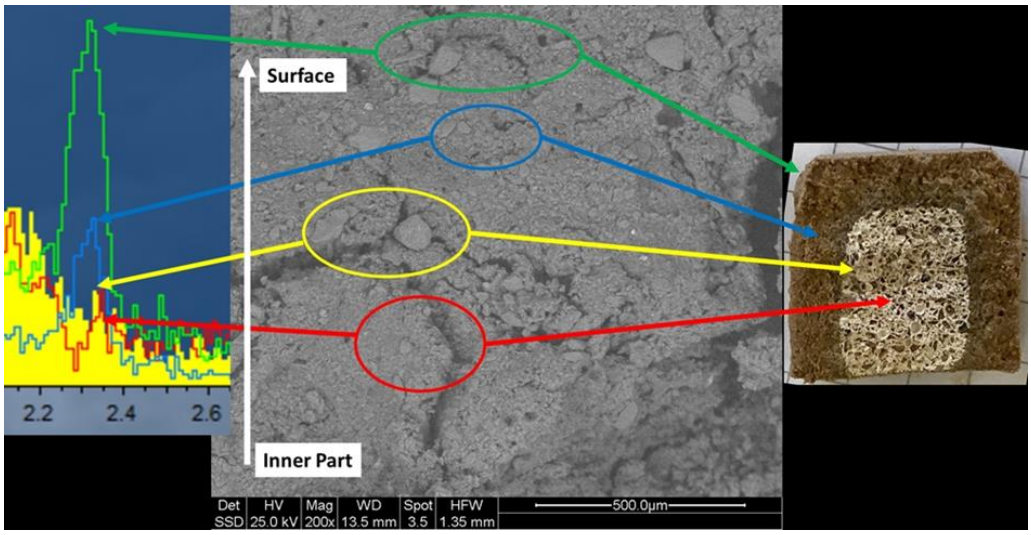

Figure 9-23 SEM and EDS analyses of sample 90GP0-10CW with an enlargement around the peak of sulphur 2.3 keV to evidence the penetration of sulphate ions, as visualised via the phenolphthalein test.

9.5.2 Compressive strength

- Geopolymer with recycled corundum

As mentioned previously, the mechanical properties of the samples containing RC exhibited varying responses depending on the acid concentration. Following immersion in 0.5N acid, all values remained largely unchanged, as depicted in Figure 9-24. However, as the acid concentration increased, noticeable alterations became apparent. Even the acids with a concentration of 1.5N had a slight disruptive effect on the geopolymeric system with RC. This trend was further corroborated by the weight loss data (Fig. 9-1), indicating that the geopolymers were significantly impacted by exposure to more concentrated acids. The most prominent case was observed in the 50GP0-50RC sample, which, although structurally intact, couldn't be subjected to testing due to extensive cracks induced by sulfuric acid. Despite these challenges, the formulation showing the most promising results remained 80GP0-20RC. However, there still exists a noticeable disparity between its properties before and after acid exposure. Notably, GP0, as demonstrated in Chapter 4, continues to exhibit exceptional resistance even under the harsh conditions of acid exposure.

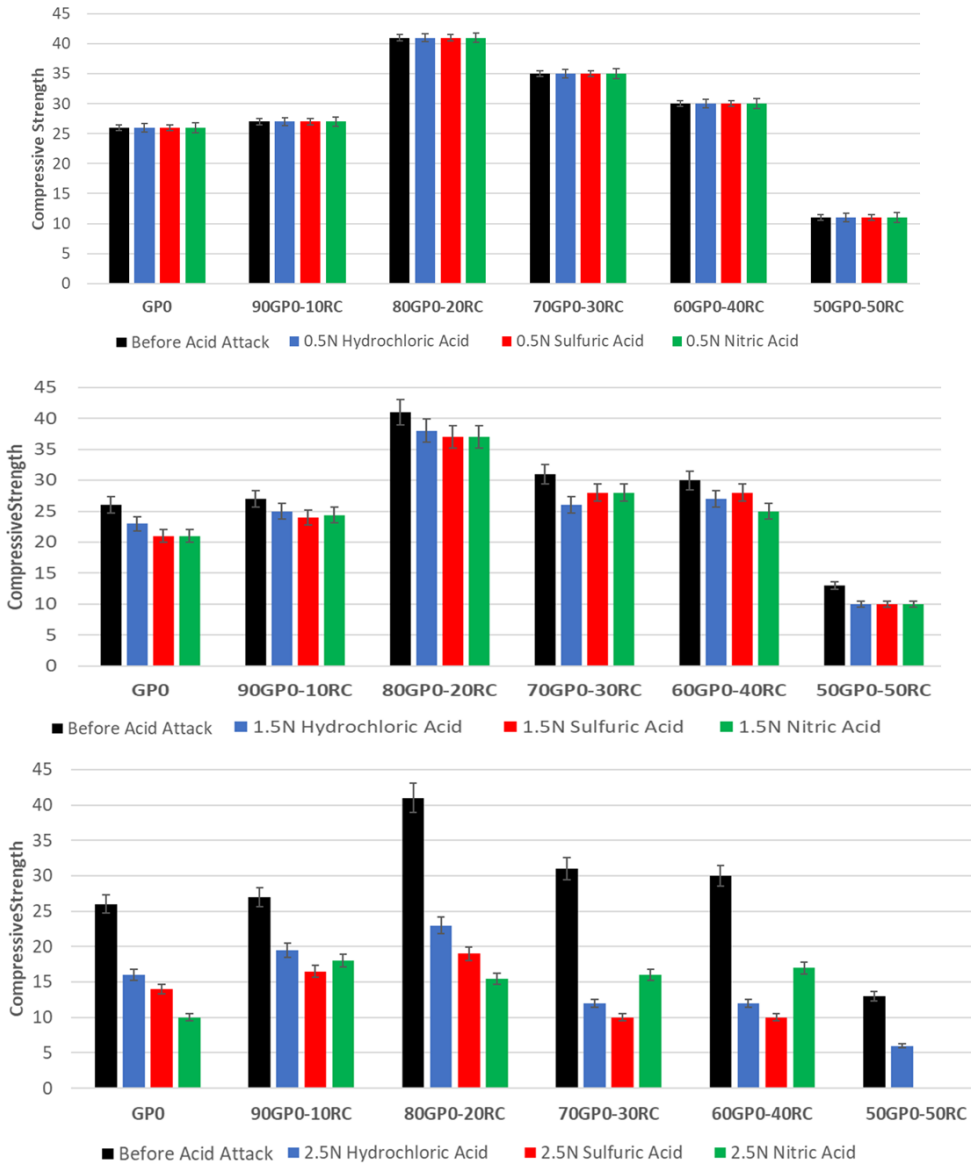

Fig.9-24 Comparison of compressive strength of geopolymers with RC before and after acid exposure.

In Figure 9-25, the mechanical tests of the samples incorporated with RC before alkaline activation are depicted. At lower acid concentrations, the geopolymers exhibited remarkable resistance during exposure. In solutions with a concentration of 1.5N, minor changes were observed in the geopolymers. However, notable alterations became apparent after exposure to higher acid concentrations. Following exposure to sulfuric acid at 2.5N, the samples GP-20RC, GP-30RC, and GP-40RC were no longer suitable for mechanical testing, indicating significant deterioration. Moreover, their resistance to nitric and hydrochloric acid remained exceedingly low. Once again, these results reinforce the initial hypotheses, particularly evident in the case of GP-50RC. This sample exhibited mechanical properties after the acid attack that were

remarkably close to those of GP0. These findings underscore the crucial influence of acid concentration on the mechanical behavior of geopolymers and provide further validation for the study's initial assumptions.

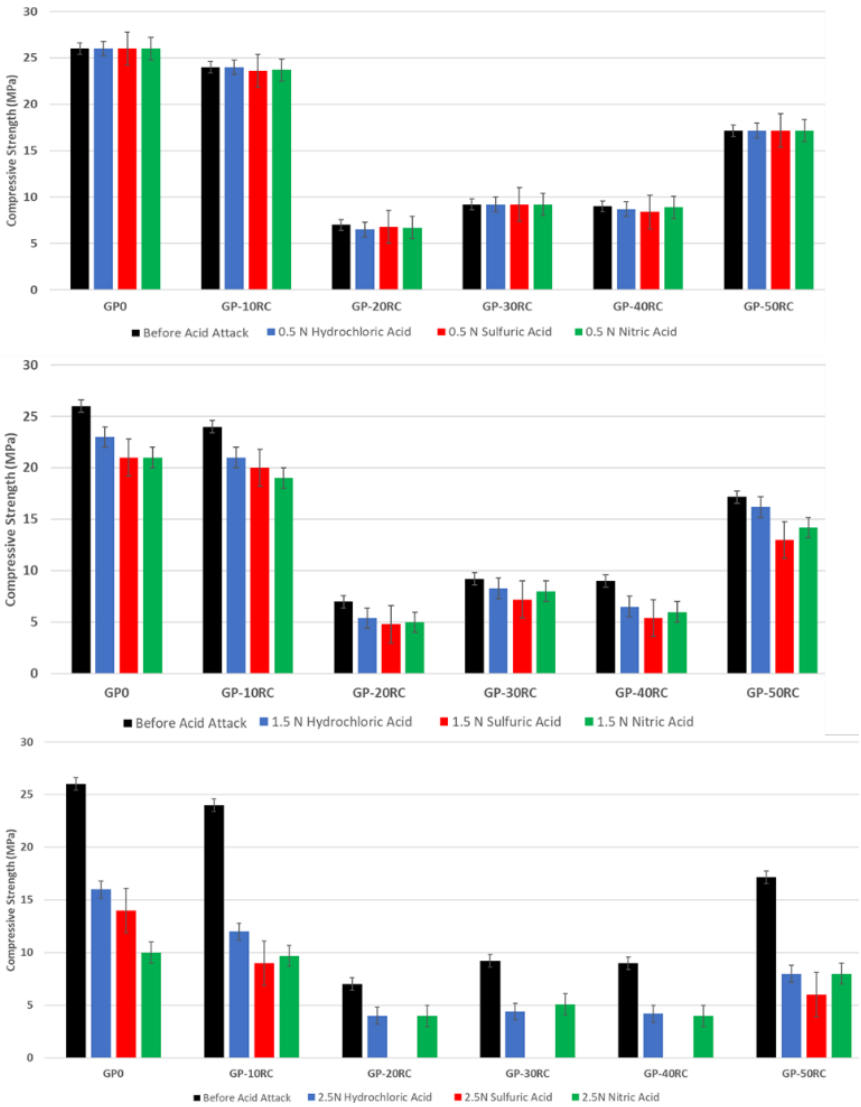

Fig.9-25 Comparison of compressive strength of geopolymers with RC before and after acid exposure.

Figure 9-26 presents a comparison between the samples with RC added before and after the alkali activation. It is worth noting that the formulation 80GP0-RC stands out as the most superior among all configurations. However, what adds to the intrigue is the compelling behavior exhibited by the geopolymer when 50% RC is incorporated with MK before the alkaline activation process. This observation suggests a unique interaction between the components, potentially leading to enhanced properties or novel material characteristics.

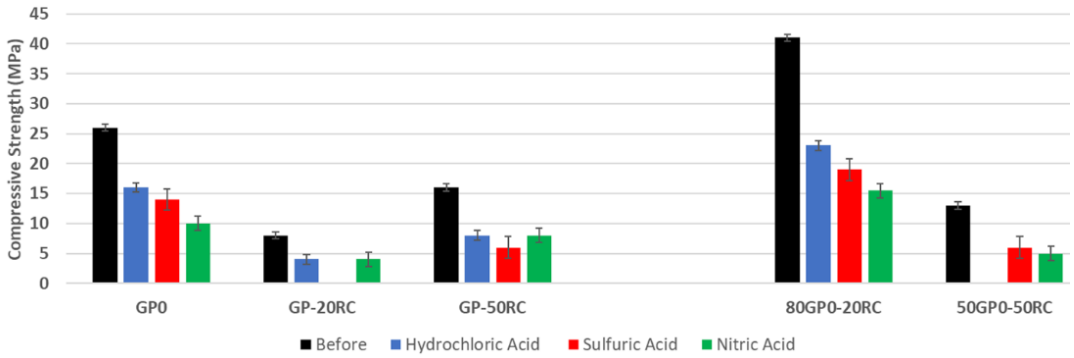

Fig.9-26 Comparison of compressive strength after acid attack of geopolymers with RC added beofore and after AA.

- Geopolymer with waste cork

After testing the geopolymers before and after immersion in acids, the results were compared (Figure 9-27). The mechanical properties remained fairly consistent when extracted from low-concentration acidic solutions. However, divergent outcomes emerged at higher concentrations. Notably, in Figure 9-27, it is apparent that the two of the composites incorporating cork after alkali activation, specifically 95GP0-5CW and 90GP0-10CW, were omitted from testing. This omission did not result from their inability to withstand the acid attack, as the weight loss was not excessive. Rather, the cork absorbed so much solution that it disintegrated under minimal pressure. In contrast, the other samples GP-2CW, GP-5CW, GP-7CW, and GP-10CW underwent testing, yielding lower values. The contrast in performance between these formulations primarily stems from cork's capacity to absorb a significant amount of acid solution due to its high porosity and enhanced diffusivity within the bulk sample.

As a conclusive remark on the results of the mechanical resistance after the acid immersion of the samples, we can assess that the ionic exchange of H^+ or H_3O^+ for Na^+ is indeed the most aggressive process [Vogt et al. 2020]. The two acids have the same normality, that is to say that they have the same concentration of H^+ and produce the same depletion of mechanical performance, notwithstanding the type of anion, either sulphate or nitrate. The permeation of the acid with the composite volume is proportional also to the porosity as well as diffusivity, indicating that the microstructure plays a relevant role [Rozière et al. 2011]. The presence of cork dust as filler favours the entrance of acid solution and accelerates the composite decomposition.

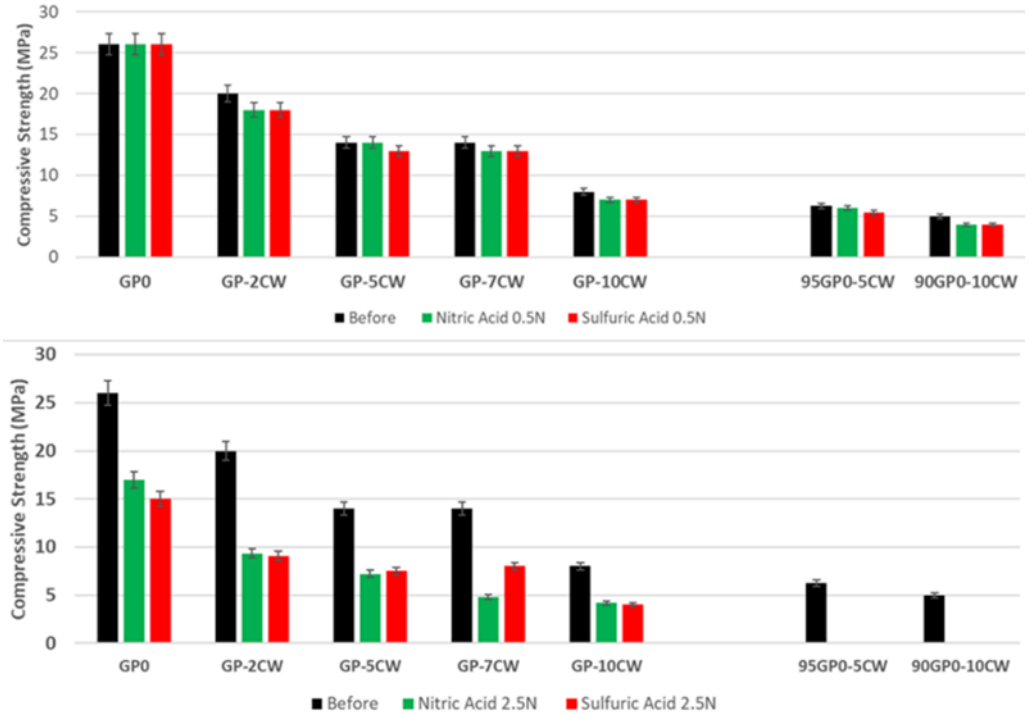

Fig.9-27 Comparison of compressive strength of geopolymers with CW before and after acid exposure.

- Comparison between geopolymer with RC and CW

When examining the mechanical properties after exposure to acids with a concentration of 2.5N, a striking contrast emerges between the samples containing RC and waste cork (Fig.9-28). While the addition of cork endows the geopolymers with lightweight characteristics and insulating capability, these samples lack the resilience needed to withstand acidic or aggressive environments. This disparity underscores the critical role of material selection in tailoring geopolymeric formulations for specific applications. Furthermore, it is crucial to note that even after the alkali activation, the introduction of waste cork failed to contribute to any noticeable improvement in the microstructural properties of the geopolymer. This finding underlines the limitations of waste corkin enhancing the structural integrity of geopolymers under acidic conditions. These observations not only emphasize the challenges associated with incorporating certain waste materials into geopolymeric compositions but also highlight the necessity for careful evaluation of material interactions to develop geopolymers with robust and tailored properties, especially in the face of corrosive environments.

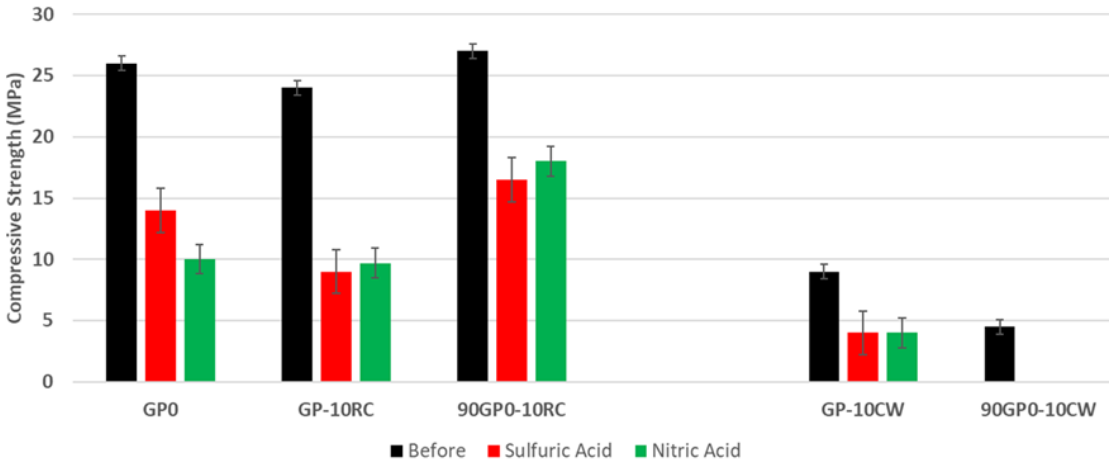

Fig.9-28 Comparison of compressive strength of geopolymers with RC and CW.

In conclusion, materials containing RC are suitable also for outdoors applications, where the encounter with acid rains is more probable, oppositely, the CW containing materials are more appropriate for indoor applications.

10. Conclusions and Future aspects

In this chapter, all the concepts analysed in the thesis have been summarised and an attempt has been made to provide a future outlook on the basis of the results obtained.

Best MK-based geopolymer

The project began with the selection of the best formulation of geopolymers containing only metakaolin. Various tests were carried out on three formulations, varying the resting time of the alkaline solution containing NaOH and Na-silicate. After several tests, the GP0 formulation was selected, in which NaOH and Na-silicate were mixed just prior to preparation. Although formulation GP-AS1 (NaOH + Na-silicate 24h) showed better mechanical performance, it had a worse chemical stability.

Several important results emerged from these tests:

- The importance of the Na_2O/H_2O ratio, which significantly affects the mechanical properties.
- A lower percentage of Al(IV) in the geopolymer leads to incomplete geopolymerization and therefore imperfections in the network, making it more mechanically and chemically fragile.
- The addition of NaOH and Na-silicate directly to the MK powder results in the formation of fewer voids for acid infiltration.
- To ensure a solution rich in reactive Si species, it is advisable to prepare the activator mixture no more than 24 hours in advance.

The innovative aspect of this first part of the thesis lies in the correlation of the NMR characterization of the alkali activator with the chemical and mechanical performance of the hardened geopolymer.

Waste material in geopolymer matrix

In the second part of the thesis, three types of waste materials were added to the GP0 formulation: recycled corundumfrom abrasion tests, recycled corundumfrom erosion tests, and industrial waste cork. After characterizing the wastes, they were incorporated into GP0 in two different ways: before and after the alkaline activation of the MK

geopolymeric paste. The geopolymerization, as well as microscopic and macroscopic properties of the different samples were then studied, yielding different results. For example, corundum after abrasion tests gave better mechanical resistance without changing the chemistry of the process. Waste cork made the material lighter with better thermal insulation properties.

The key points observed during these tests for future considerations are:

- Optimization of geopolymers with a content of spent corundum powders from erosion and abrasion tests is possible up to 50 wt% on the total paste. This up-cycling avoid the disposal of corundum, as it is classified as special (hazardous) waste. This type of disposal is very expensive.
- It is recommended to reuse recycled corundum that still contains a high percentage of Al_2O_3.
- The use non-dried cork prevents the absorption of all the water present in the alkaline solution.
- The incorporation of waste materials into geopolymers is efficient if it does not alter the chemistry of the network.
- The method of adding of the waste material to the aluminosilicate powders or to the fresh geopolymer paste can affect the structure of the final materials in different ways. Corundum added after alkaline activation shows completely different results to that added before.

In this part of the thesis, the geopolymerization process in presence of the non-reactive or partially reactive filler was investigated and properly assessed.

Acid resistance

The final part of the thesis focused on the acid resistance of the samples studied in parts 1 and 2. Using ^{27}Al and ^{29}Si MAS-NMR, an attempt was made to understand how the samples chemically interacted with different acids at different concentrations. As expected, the samples containing waste cork were not very resistant to acid attack, whereas those containing corundum were.

The main results were:

- The presence of corundum, Al(VI) in ^{27}Al MAS-NMR, did not undergo the effect of acid attack.
- During the attack, it is necessary to monitor the presence of Na^+ inside and outside the geopolymer to better understand the exchange with H^+.
- The anions of the acids (Cl^-; NO_3^-; HSO_4^-; SO_4^{2-}) behave differently in terms of diffusion from the solution to the first layer of the hardened geopolymer.
- The release of octahedral Al from the geopolymer network was observed.

Future Aspect

The results gathered in this thesis project can serve as a basis for various future research and applications. Corundum has proven to be an excellent filler for geopolymers. By further improving the interaction between the geopolymer paste and corundum, not only could waste material be reused, but corundum could also be incorporated in building materials. As for waste cork, with further study, it could be used in insulating panels for various applications.

11. References

ACI M318-05 2005.

Allahverdi, A. and Skvara, F. Nitric acid attack on hardened paste of Geopolymericcements Part I, Ceramics – Silikaty 2001a, 45(3), 81-88.

Allahverdi, A. and Skvara, F. Nitric acid attack on hardened paste of Geopolymericcements Part II, Ceramics – Silikaty 2001b, 45(4), 143-149.

Allahverdi, A. and Skvara, F. Sulphuric acid attack on hardened paste of Geopolymer cements Part I: mechanism of corrosion at relatively high concentrations, Ceramics –Silikaty 2005, 49(4), 225-229.

Ashby, M.F. Materials Selection in Mechanical Design, 4th ed.; Elsevier: New York, NY, USA, 2011.

ASTM C518; Standard Test Method for Steady-State Thermal Transmission Properties by Means of the Heat Flow Meter Apparatus. ASTM: West Conshohocken, PA, USA, 2021.

Bakharev, T. Durability of Geopolymer materials in sodium and magnesium sulphate solutions, Cement and Concrete Research 2005a, 35(6), 1233-1246.

Bakharev, T. Geopolymeric materials prepared using class F fly ash and elevated temperature curing, Cement and Concrete Research 2005b, 35(6), 1224-1232.

Bakharev, T. Resistance of Geopolymer materials to acid attack, Cement and ConcreteResearch 2005c, 35(4), 658-670.

Bakharev, T., Sanjayan, J. G. and Cheng, Y.-B. Sulphate attack on alkali-activated slagconcrete, Cement and Concrete Research 2002, 32(2), 211-216.

Bakharev, T., Sanjayan, J. G. and Cheng, Y.-B. Resistance of alkali-activated slag concrete to acid attack, Cement and Concrete Research 2003, 33(10), 1607-1611.

Biljana R, Alexandra A. and Ljiljana R. (2010), "Thermal Treatment of Kaoilin Clay to obtain MK", Institute for Testing of Materials, Belgrade, Serbia, Scientific Paper, Hem. ind. 2010, 64 (4), 351356.

Blaszcynski TZ, Krol MR. Alkaline Activator Impact on the Geopolymer Binders. IOP Conference Series: Materials Science and Engineering 2017, 245, 2.

Böschel D, Janich M, H. Roggendorf, J. Colloid Interface Sci. 267 (2003) 360–368.

BRUS, Annual Reports on NMR Spectroscopy, 2016, 88, 79-147.

Catauro, M.; Dal Poggetto, G.; Sgarlata, C.; Vecchio Ciprioti, S.; Pacifico, S.; Leonelli, C. Thermal and microbiological performance of metakaolin-based geopolymers cement with waste glass. Appl. Clay Sci. 2020, 197, 105763.

Chandra, S. Hydrochloric acid attack on cement mortar - an analytical study, Cementand Concrete Research 1988, 18(2), 193-203.

Chang, Z.-T., Song, X.-J., Munn, R. and Marosszeky, M. Using limestone aggregates and different cements for enhancing resistance of concrete to sulphuric acid attack, Cement and Concrete Research 2005, 35(8), 1486-1494.

Chen, S.; Zhang, W.; Sorge, L.P.; Seo, D.-K. Exploratory Synthesis of Low-Silica Nanozeolites through Geopolymer Chemistry. Cryst. Growth Des. 2019, 19, 1167–1171.

Commission Notice on Technical Guidance on the Classification of Waste, Report ID: C/2018/1447. Available online: https://eur-lex.europa.eu/legal-content/EN/TXT/?uri=uriserv:OJ.C_.2018.124.01.0001.01.ENG&toc=OJ:C:2018:124:TOC.

Criado M., Fernandez-Jimenez A., Palomo A. Alkali activation of fly ash: Effect of the SiO2/Na2O ratio: Part I: FTIR study Microporous and Mesoporous Materials, 106, 1–3, 2007, 180-191

Dabbebi R., S. Baklouti, J.L. Barroso de Aguiar, F. Pacheco-Torgal, B. Samet Investigations of geopolymeric mixtures based on phosphate washing waste. Science and Technology of Materials 2018, 30, 1-5.

Dal Poggetto, G.; D'Angelo A.; Blanco, I.; Piccolella, S.; Leonelli, C.; Catauro, M. FTIR Study, Thermal Analysis, and Evaluation of the Amtibacterial Activity of MK-Geopolymer mortar using glass waste as fine aggregate. Polymers 2021, 13, 2970.

Dal Poggetto, G.; D'Angelo, A.; Catauro, M.; Barbieri, L.; Leonelli, C. Recycling of Recycled corundum Abrasive Powder in MK-based geopolymers. Polymers 2022, 14, 2173.

Dal Poggetto, R. Marchetti, I. Lancellotti, C. Leonelli, L. Barbieri, Applied Sciences (Swi) 2023, 13(3), 1804.

Davidovits, J. Synthesis of new high-temperature Geopolymers for reinforced plastics and composites, SPE PACTEC'79, Costa Mesa, California, Society of Plastics Engineers 1079, 151-154.

Davidovits, J. Mineral polymers and methods of making them, US patent 1982, 4, 349-386.

Davidovits, J. Ancient and modern concretes: what is the real difference? Concrete International 1987, 9(12), 23-28.

Davidovits, J. Geopolymers: inorganic polymeric new materials, Journal of ThermalAnalysis 1991, 37, 1633-1656.

Davidovits, J. Global warming impact on the cement and aggregates industries, WorldResource Review 1994a, 6(2), 263-278.

Davidovits, J. Properties of Geopolymer cements, Proceedings of the 1st International Conference on Alkaline Cements and Concretes, Kiev State Technical University 1994b, 131-149.

Davidovits, J., Comrie, D. C., Paterson, J. H. and Ritcey, D. J. Geopolymeric concretesfor environmental protection, Concrete International 1990, 12(7), 30-40.

Davidovits, J. and Davidovics, M. Geopolymer: room temperature ceramic matrix forcomposites, Ceramic Engineering and Science Proceedings 1988, 9(7-8), 835-842.

Davidovits, J. and Davidovics, M. Alkaline aluminosilicate Geopolymeric matrix for composite materials with fibre reinforcement and method for obtaining same, US patent5, 1998, 798, 307.

Davidovits, J. Geopolymer. Chemistry and Applications. Institute Geopolymere, Saint-Quentin, France 2008.

Davidovits J. Geopolymer. Chemistry and Applications 5th. Institute Geopolymere, Saint-Quentin, France 2020

Duxson, P., Fernández-Jiménez, A., Provis, J. L., Lukey, G. C., Palomo, A., & van Deventer, J. S. J. Geopolymer technology: the current state of the art. Journal of Materials Science 2007, 42(9), 2917-2933.

Duxson P. The structure and thermal evolution of metakaolin geopolymers. PhD Thesis, University of Melbourne, Australia 2006.

Duxson P, Provis JL, Lukey GC, Mallicoat SW, Kriven WM, Van Deventer JSJ Colloid Surf A 2005, 269, 47.

Duxson, P., Mallicoat, S. W., Lukey, G. C., Kriven, W. M. and Van Deventer, J. S. J. The effect of alkali and Si/Al ratio on the development of mechanical properties of metakaolin-based geopolymers. Colloids and Surfaces A – Physicochemical and Engineering Aspects 2007, 292, 8–20.

Duxson, P., & Provis, J. Designing precursors for geopolymer cements. Journal of the American Ceramic Society 2008, 91(12), 3864-3869.

Engelhardt, G. and Michel, D. High-resolution solid-state NMR of silicates and zeolites,Chichester (West Sussex), New York, Wiley 1987.

Fernandez-Jimenez, A. and Palomo, A. Alkali activated fly ash concrete: alternative material for the precast industry, Geopolymer 2002, Melbourne, Australia.

Fernandez-Jimenez, A. and Palomo, A. Characterisation of fly ashes, potential reactivityas alkaline cements, Fuel 2003, 82, 2259-2265.

Fernandez-Jimenez, A. and Palomo, A. Composition and microstructure of alkali activated fly ash binder: Effect of the activator, Cement and Concrete Research 2005, 35(10),1984-1992.

Fernandez-Jimenez, A., Palomo, A. and Criado, M. Microstructure development of alkali-activated fly ash cement: a descriptive model, Cement and Concrete Research 2005, 35(6), 1204-1209.

Fernandez-Jimenez, A. M., Lachowski, E. E., Palomo, A. and Macphee, D.E. Microstructural characterisation of alkali-activated PFA matrices for waste immobilisation, Cement and Concrete Composites 2004, 26(8), 1001-1006.

Ghosh, A.; Ghosh, A.; Neogi, S. Reuse of fly ash and bottom ash in mortars with improved thermal conductivity performance for buildings. Heliyon 2018, 4, 934.

Glukhovsky V.D., Soil silicates, their properties, technology and manufacturing and fields of application, Doct Tech Sc. Degree Thesis. Civil Engeneering Institute, Kiev, 1965.

Gluth G.J.G., C. Grengg, N. Ukrainczyk, F. Mittermayr, M. Dietzel, RILEM Technical Letters 2022, 7, 58-67.

Gómez-Casero, M.A.; de Dios-Arana, C.; Bueno-Rodríguez, J.S.; Pérez-Villarejo, L.; Eliche-Quesada, D. Physical, mechanical and thermal properties of metakaolin-fly ash geopolymers. Sustain. Chem. Pharm. 2022, 26, 100620.

Grube, H. and Rechenberg, W. Durability of concrete structures in acidic water, Cementand Concrete Research 1989, 19(5), 783-792.

Halstead, P. E. An investigation of the erosive effect on concrete of soft water of lowpH value, Magazine of Concrete Research 1954, 6(17), 93-97.

Hanna, R. and Su, G.-J. Infrared absorption spectra of sodium silicate glasses from 4 to40 microns, Journal of the American Ceramic Society 1064, 47(12), 597-601.

Hardjito, D., Wallah, S. E. and Rangan, B.V. Study of engineering properties of fly ash based Geopolymer concrete, Journal of the Australian Ceramic Society 2002, 38(1), 44-47.

Hardjito, D., Wallah, S. E., Sumajouw, D. M. J. and Rangan, B. V. Properties of Geopolymer concrete with fly ash as source material: effect of mixture composition, the 7th CANMET/ACI International Conference on Recent Advances in Concrete Technology 2004a, Las Vegas, USA.

Hardjito, D., Wallah, S. E., Sumajouw, D. M. J. and Rangan, V. B. On the development of fly ash based Geopolymer concrete, ACI materials journal 2004b, 101(6),467-471.

Heidrich, C. (2002). Ash Utilization an Australian Perspective, Geopolymer 2002 – Turn Potential into Profit, ISBN: 0975024205, Melbourne, Australia.

Hewlett, P. C. Lea's chemistry of cement and concrete, London, New York, Arnold; Copublished in North, Central, and South America by J. Wiley, ISBN 0340565896, 1998, 324-327, 458, 759.

Higginson, E. C. Effect of steaming curing on the important properties of concrete, Journal of American concrete institute 1961, 58(2), 281-298.

Horlyck, L. and Salome, F. Corrosion rates of concrete and steel in sewers, Australian Corrosion Association Proceedings C&P-99, Sydney, Australia 1999, 39-016.

Hos, J. P., McCormick, P. G. and Byrne, L. T. Investigation of a synthetic aluminosilicate inorganic polymer, Journal of Materials Science 2002, 37, 2311-2316.

Hou, X., Kirkpatrik, R. J., Struble, L. J., and Monteiro, P. J. M. Structural investigationof alkali silicate gels, Journal of American Ceramic Society 2005, 88(4), 943-949.

Hughes, B. P. and Guest, J. E. Limestone and siliceous aggregate concrete subjected to sulphuric acid attack, Magazine of Concrete Research 1978, 30(102), 11-18.

Husung, R. D. and Doremus, R. H. The infrared transmission spectra of four silicateglasses before and after exposure to water, Journal of Materials Research 1990, 5(10), 2209-2217.

Ikeda, K. Preparation of fly ash monoliths consolidated with a sodium silicate binder atambient temperature, Cement and Concrete Research 1997, 27(5), 657-663.

Imre, B. Concrete Corrosion and Concrete Protection, in: (Ed). Chemical Pub. Co., NewYork, 1967, 247-248.

Jahanian, S. and Rostami, H. Alkali ash material, a novel material for infrastructureenhancement, Engineering Structures 2001, 23(6), 736-742.

Jaya, N.A.; Yun-Ming, L.; Al Bakri Abdullah, M.M.; Cheng-Yong, H.; Hussin, K. Effect of Sodium Hydroxide Molarity on Physical, Mechanical and Thermal Conductiv-ity of Metakaolin Geopolymers. IOP Conf. Ser. Mater. Sci. Eng. 2018, 343, 012015.

Jiang, W. M. Alkali activated cementitious materials: mechanism, microstructure and properties, the Pennsylvania State University, USA, PhD thesis, 1997, 209.

Jiang, W. M. and Roy, D. M. Hydrothermal processing of new fly ash cement, Ceramic Bulletin 1992, 71(4), 642-647.

Kaempfer, W. and Berndt, M. Estimation of service life of concrete pipes in sewer networks, Durability of Building Materials and Components 8, 1999, 37-45.

Kalidasan B., A. Pandey, S. Shahabuddin, M. George, K. Sharma, M. Samykano, V. Tyagi, R. Saidur, Renew. Energy 2021, 173, 1057-1069.

Kamseu, E.; Ngouloure, Z.N.M.; Nait-Ali, B.; Valentini, L.; Zekeng, S.; Rossignol, S.; Leonelli, C. Pore network and microstructure in the prediction of heat flux transport in sponge-like geopolymers for thermal insulation. J. Therm. Anal. Calorim. 2022, 147, 12329–12344.

Katz, A. Microscopic study of alkali-activated fly ash, Cement and Concrete Research 1998, 28(2),197-208.

Kolesova, V. A. A study of the structure of alkali aluminosilicate glasses based on their infrared absorption spectra, The Structure of Glass (Volume 2), in: Mendeleev, D. I. and Vavilov, S. I. (Ed). Consultants Bureau, 1960, 177-179.

Kossler, D. J. and Sheppard, W. L. Acid resistant floor construction, Metal Finishing 2000, 98(1), 657-664.

Krivenko, P. Alkaline cements: terminology, classification, aspects of durability, Proceedings of the 10th International Congress on the Chemistry of Cement, Gothenburg, Sweden 1997.

Krivenko, P. Alkaline cement: from research to application, Geopolymer 2002 -- TurnPotential into Profit, ISBN: 0975024205, Melbourne, Australia 2002.

Kurashige, I. and Uomoto, T. (2000). Deterioration of concrete due to sulphuric acid, Transaction of the Japan Concrete Institute, 22, 167-174.

Lancellotti, I.; Catauro, M.; Ponzoni, C.; Bollino, F.; Leonelli, C. Inorganic polymers from alkali activation of metakaolin: Effect of setting and curing on structure. J. Solid-State Chem. 2013, 200, 341–348.

Lee, W. K. W. Solid-gel interaction in Geopolymers, the University of Melbourne,Australia, PhD thesis, 2002, 320.

Lee, W. K. W. and van Deventer, J. S. J. Use of Infrared spectroscopy to study Geopolymerisation of heterogeneous amorphous aluminosilicates, Langmuir 2003, 19(21),8726-8734.

Lee, J.R.; Hasolli, N.; Jeon, S.M.; Lee, K.S.; Kim, K.D.; Kim, Y.H.; Lee, K.Y.; Park, Y.O. Optimization fluidization characteristics conditions of nickel oxide for hydrogen reduction by fluidized bed reactor. Korean J. Chem. Eng. 2018, 35, 2321.

Leong HY, Leong Ong DE, Sanjayan JG, Nazari A. The effect of different Na_2O and K_2O ratios of alkali activator on compressive strength of fly ash based-geopolymer. Construction and Building Materials 2016, 106, 500-511.

Lippmaa, E., Maegi, M., Samoson, A., Tarmak, M. and Engelhardt, G. Investigation ofthe structure of zeolites by solid-state high-resolution silicon-29 NMR spectroscopy, Journal of the American Chemical Society 1981, 103(17), 4992-4996.

Malanho, S.; Veiga, R.; Farinha, C.B. Global Performance of Sustainable Thermal Insulating Systems with Cork for Building Facades. Buildings 2021, 11, 83.

Malchiodi, B.; Marchetti, R.; Barbieri, L.; Pozzi, P. Recovery of cork manufacturing waste within mortar and polyurethane: Feasibility of use and physical, mechanical, thermal insulating properties of the final green composite construction materials. Appl. Sci. 2022, 12, 3844.

Malek, R. I. A. and Roy, D. M. Synthesis and Characterization of New Alkali-activatedCements, Proceedings of the 10th International Congress on the Chemistry of Cement, 1997, Gothenburg, Sweden.

Malhotra, V. M. Sulphur concrete and sulphur-infiltrated concrete, New Concrete Material -- (Concrete Technology and Design volume 1), in: Swamy, R. N. (Ed). SurreyUniversity Press, London 1988, 13-21.

Merabti, S.; Kenai, S.; Belarbi, R.; Khatib, J. Thermo-mechanical and physical properties of waste granular cork composite with slag cement. Constr. Build. Mater. 2021, 272, 121923.

Mohajerani A., David Suter, Tristan Jeffrey-Bailey, Tianyang Song, Arul Arulrajah, Suksun Horpibulsuk and David Law. Recycling waste materials in geopolymer concrete. Clean Technologies and Environmental Policy 2019, 21, 493–515.

Mucsi G, Lakatos J, Molnar Z, Szabo R. Development of geopolymer using industrial waste materials. The 9th International Conference “ENVIRONMENTAL ENGINEERING” 22–23 May 2014, Vilnius, Lithuania.

Novais, R.M.; Saeli, M.; Caetano, A.P.F.; Seabra, M.P.; Labrincha, J.A.; Surendran, K.P.; Pullar, R.C. Pyrolysed cork-geopolymer composites: A novel and sustainable EMI shielding building material. Constr. Build. Mater. 2019, 229, 116930.

Nodehi M, Taghvaee VM. Alkali-Activated Materials and Geopolymer: a Review of Common Precursors and Activators Addressing Circular Economy. Circular Economy and Sustainability 2022, 2,165–196.

Odler, I. Special inorganic cements, London, E & FN Spon, ISBN: 0419227903. 2000, 125-130, 266-268.

Palomo, A., Alonso, S., Fernandez Jimenez, A., Sobrados, I. and Sanz, J. Alkaline activation of fly ashes. NMR study of the reaction products, Journal of the AmericanCeramic Society 2004, 87(6), 1141-1145.

Palomo, A., Blanco, M. T., Granizo, M. L., Puertas, F., Vazquez, T. and Grutzeck, M. W. Chemical stability of cementitious materials based on metakaolin, Cement andConcrete Research 199a, 29(7), 997-1004.

Palomo, A., Grutzeck, M. W. and Blanco, M. T. (1999b). Alkali-activated fly ashes: A cementfor the future, Cement and Concrete Research, 29(8), 1323-1329.

Papa, E.; Landi, E.; Miccio, F.; Medri, V. K2O-Metakaolin-Based Geopolymer Foams: Production, Porosity Characterization and Permeability Test. Materials 2022, 15, 1008.

Parker, C. D. The corrosion of concrete, The Australian Journal of ExperimentalBiology and Medical Science 1945, 23, 81-97.

Pauling L. and Hendricks Sterling B., 1925.

Pławecka K., Kinga Korniejenko and Patrycja Bazan. Effect of corundum sand proportion on strength properties geopolymer mortar based on fly ash. IOP Conference Series: Materials Science and Engineering. 2021, 1190.

Pavlik, V. Corrosion of hardened cement paste by acetic and nitric acids part I: Calculation of corrosion depth, Cement and Concrete Research 1994a, 24(3), 551-562.

Pavlik, V. Corrosion of hardened cement paste in acetic and nitric acids part II: formation and chemical composition of the corrosion products layer, Cement andConcrete Research 1994b, 24(8), 1495-1508.

Podolsky Z., J. Liu, Dinh H, J.H. Doh, M. Guerrieri, S. Fragomeni. State of the art on the application of waste materials in geopolymer concrete. Case Studies in Construction Materials 2021, 15.

Provis J.L., J.S.J Van Deventer, Geopolymers: Structure, Processing, Properties and Industrial Applications, Woodhead Publishing, Cambridge, UK 2009.

Rahier, H., van Mele, B., Biesemans, M., Wastiels, J. and Wu, X. Low-temperature synthesised aluminosilicate glass: Part I low temperature reaction stoichiometry and structure of a model compound, Journal of Materials Science 1996a, 31, 71-79.

Rahier, H., van Mele, B. and Wastiels, J. Low-temperature synthesised aluminosilicate glass II: rheological transformation during low-temperature cure and high temperature properties of a model compound, Journal of Materials Science 1996b, 31, pp.80-85.

Ren B, Zhaoo Y, Bai H, Kang S, Zhang T, Song S. Eco-friendly geopolymer prepared from solid wastes: A critical review. Chemosphere 2021, 267, 128900.

Ren, X.; Zhang, L.; Ramey, D.; Waterman, B.T.; Ormsby, S.T. Utilization of aluminum sludge (AS) to enhance mine tailings-based geopolymer. J. Mater. Sci. 2014, 50, 1370–1381.

Ribeiro, R.A.S.; Ribeiro, M.G.S.; Kutyla, G.P.; Kriven, W.M. Amazonian Metakaolin Reactivity for Geopolymer Synthesis. Adv. Mater. Sci. Eng. 2019, 2019, 8950764.

Riahi, S.; Nemati, A.; Khodabandeh, A.R.; Baghshahi, S. Investigation of interfacial and mechanical properties of alumina-coated steel fiber reinforced geopolymer composites. Constr. Build. Mater. 2021, 288, 123118.

Rowles, M., & O'Connor, B. Chemical optimisation of the compressive strength of aluminosilicate geopolymers synthesised by sodium silicate activation of metakaolinite. Journal of Materials Chemistry 2003, 13(5), 1161-1165.

Rosper DS, Kutyla GP, Kriven WM. Properties of Cork Particle Reinforced Sodium Geopolymer Composites. Developments in Strategic Ceramic Materials II: Ceramic Engineering and Science Proceedings Volume 37, Issue 7, XXXVII: Chapter 8. 2017.

Rozière E., A. Loukili, Cem. Concr. Compos. 2011, 33, 451-456.

Ruiz-Santaquiteria, C.; Fernandez-Jimenez, A.; Palomo, A. Quantitative determination of reactive SiO_2 and Al_2O_3 in aluminosilicate materials. In Proceedings of the XIII International Congress on the Chemistry of Cement, Madrid, Spain, 3–8 July 2011.

Samuel, D.M.; Inumerable, N.; Stumpf, A.; Kriven, W.M. Thermal conductivity of several geopolymer composites and discussion of their formulation. Int. J. Appl. Ceram. Technol. 2022, 20, 475–486.

Scherb, S., Köberl, M., Beuntner, N., Thienel, K.-C., Neubauer, J., Reactivity of metakaolin in alkaline environment: Correlation of results from dissolution experiments with XRD quantifications, Materials 2020, 13(10), 2214.

Shvarzman K. Kovler, G. S. Grader and G. E. Shter, Cement and Concrete Research 2003, 33, 405-416.

Siddiqui, K. S. Strength and Durability of Low-Calcium Fly Ash-based Geopolymer Concrete. Final Year Honours Dissertation. 2007, University of Western Australia, Perth.

Sudagar, A.; Andrejkovicova, S.; Patinha, C.; Velosa, A.; McAdam, A.; Ferreira da Silva, E.; Rocha, F. A novel study on the influence of waste corkresidue on metakaolin-zeolite based geopolymers. Appl. Clay Sci. 2018, 152, 196–210.

Sudagar, A.; Andrejkovicova, S; Rocha F; Patinha C.; Velosa, A; Ferreira da Silva, E. Compressive strength and heavy metal adsorption of cork residue, natural zeolite, and low-grade metakaolin-based geopolymers. Construction and Building Materials 2023, 366, 22.

Ukrainczyk N., O. Vogt, RILEM Tech. Lett. 2020, 5, 163-173.

van Deventer, J. S. J. Opportunities and obstacles in the commercialisation of Geopolymers, Geopolymer 2002. Melbourne, Australia.

van Deventer, J. S. J., Provis, J. L, Duxson, P., & Brice, D. G. Chemical research and climate change as drivers in the commercial adoption of alkali

activated materials. Waste and Biomass Valorization 2010, 1(1), 145-155.

Van Oosten, T. PUR Facts: Conservation of Polyurethane Foam in Art and Design; Amsterdam University Press: Amsterdam, The Netherlands, 2011.

Vieira C.M.F., R. Sànchez, S.N. Monteiro. Interceram 2005, 54-4, 268-271.

Vogt O., Ballschmiede C., Ukrainczyk N., Koenders E. Materials 2020, 13, 4522.

Wan H., L. Yuan, Y. Zhang, Front. Mater. Sec. Computational Materials Science 2020, 7.

Wallah, S. E., Hardjito, D., Sumajouw, D. M. J. and Rangan, B. V. Sulphate resistanceof fly ash based Geopolymer concrete, the Concrete in the third Millennium, the 21st Biennial conference of the Concrete Institute of Australia 2003, 17-19 July, Brisbane, Queensland, Australia, 205-212.

Wallah, S. E., Hardjito, D., Sumajouw, D. M. J. and Rangan, B. V. Sulphate and acid resistance of fly ash based Geopolymer concrete, Australian Structural Engineering Conference 2005, 11-14th September, Newcastle, Australia.

Xu, H. and van Deventer, J. S. J. The Geopolymerisation of alumino-silicate mineralsInternational Journal of Mineral Processing 2000, 59(3), 247-266.

Zaid, O., Martínez-García, R., Abadel, A.A., Fraile-Fernández, F.J., Alshaikh, I.M.H., Palencia-Coto, C. To determine the performance of metakaolin-

based fiber-reinforced geopolymer concrete with recycled aggregates. Arch. Civ. Mech. Eng. 2022, 22, 114.

Zhao Q., Nair B., Rahimian T. and Balaguru P. Novel geopolymer based composites with enhanced ductility. Journal of Materials Science. 2007, 42, 3131–3137.

Appendices

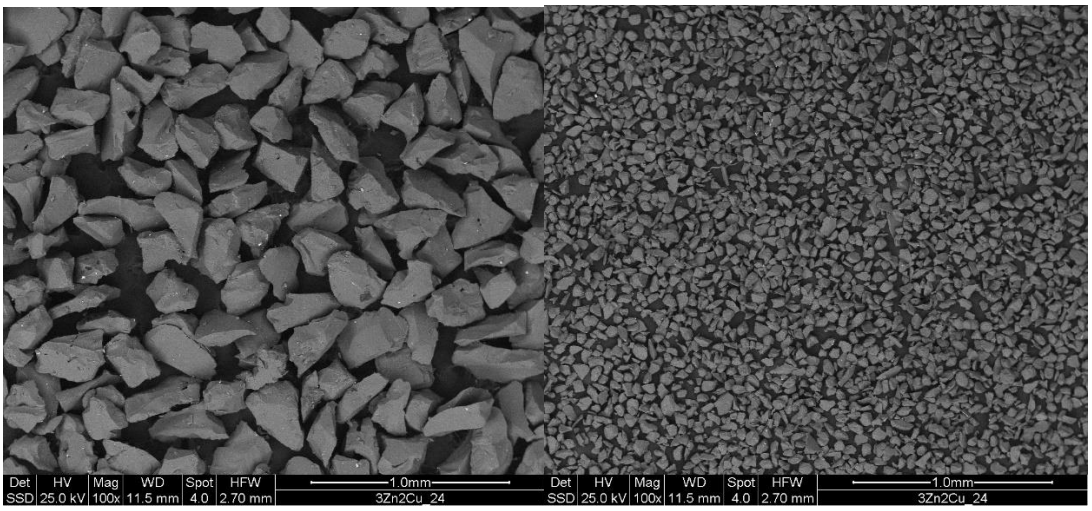

Fig.A1 Comparison between SEM picture of RC abrasive (left) and RC after erosion (right).

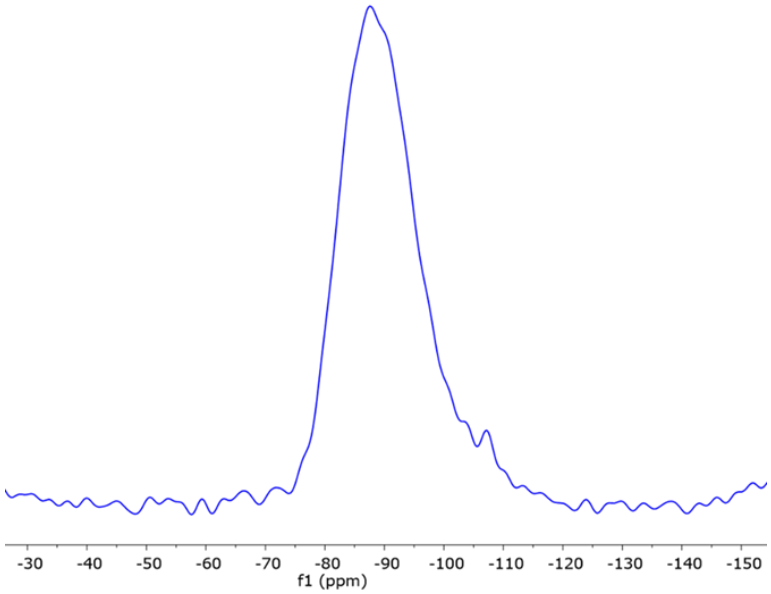

Fig.A2 ^{29}Si MAS-NMR Spectra GP-20RC.

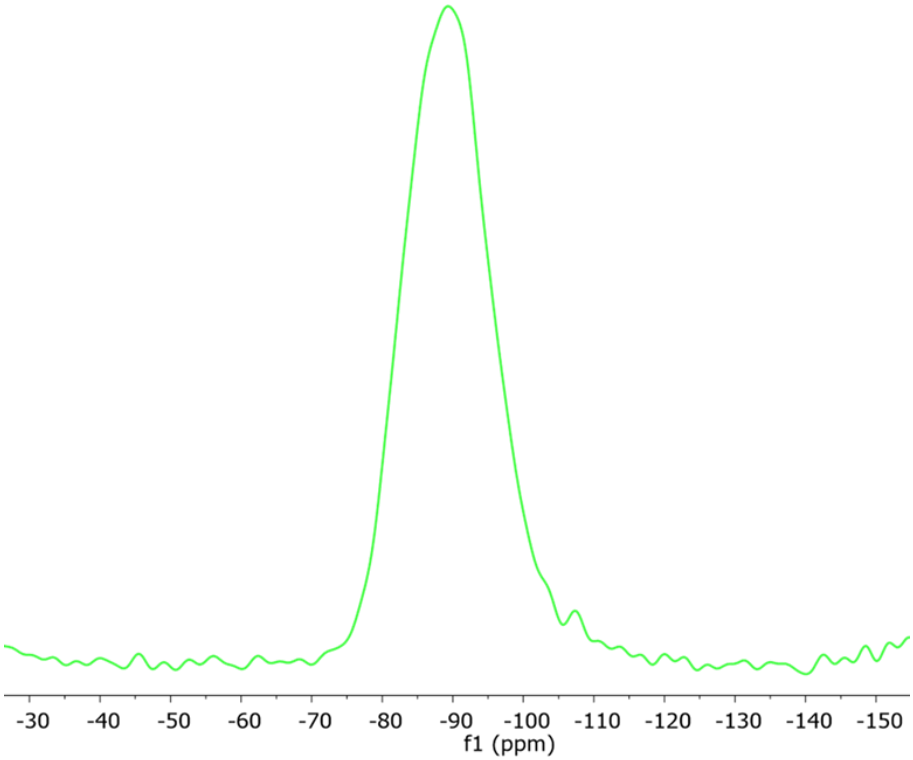

Fig.A3 ^{29}Si MAS-NMR Spectra of GP-50RC.

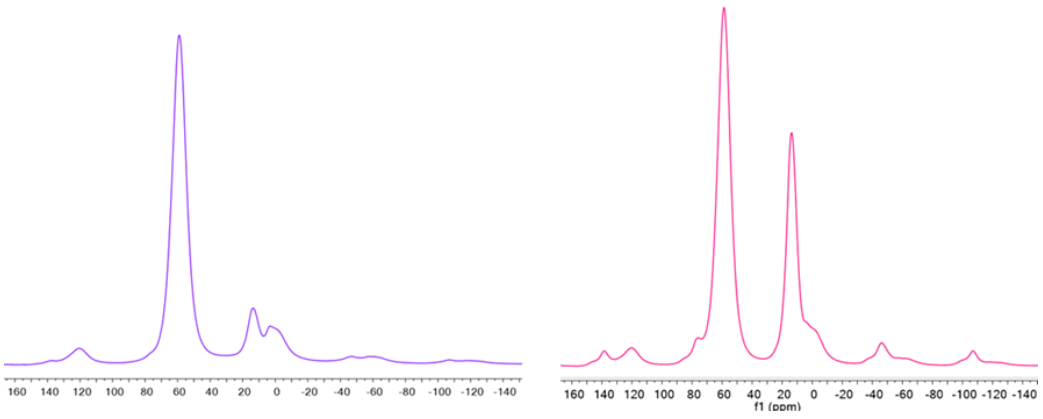

Fig.A4 ^{27}Al MAS-NMR spectra of GP-20RC (Left) and GP-50 (right).

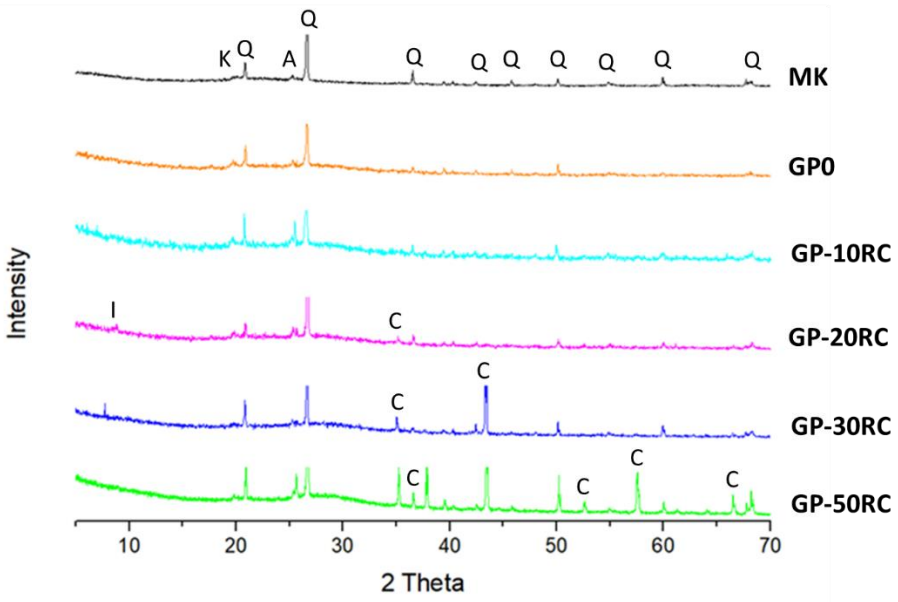

Fig.A5 XRD spectra of MK, GP0, GP-10RC, GP-20RC, GP-30RC, and GP-50RC.

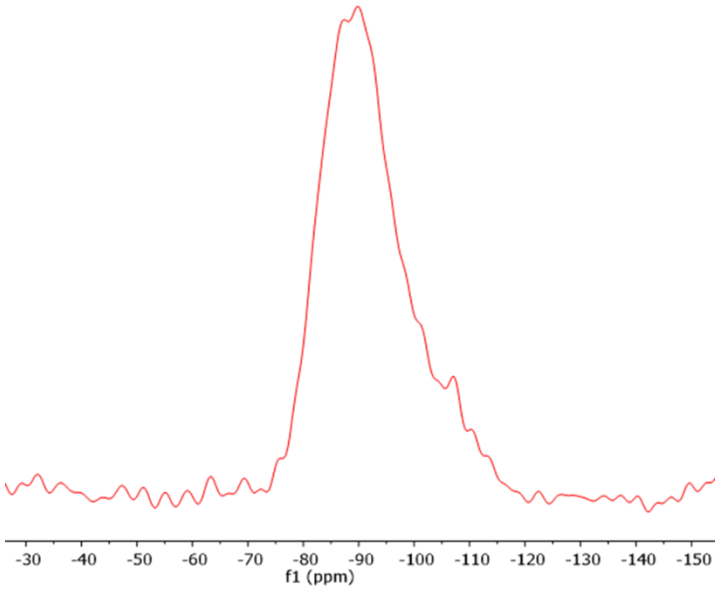

Fig.A6 ^{29}Si MAS-NMR spectra of 80GP0-20RC.

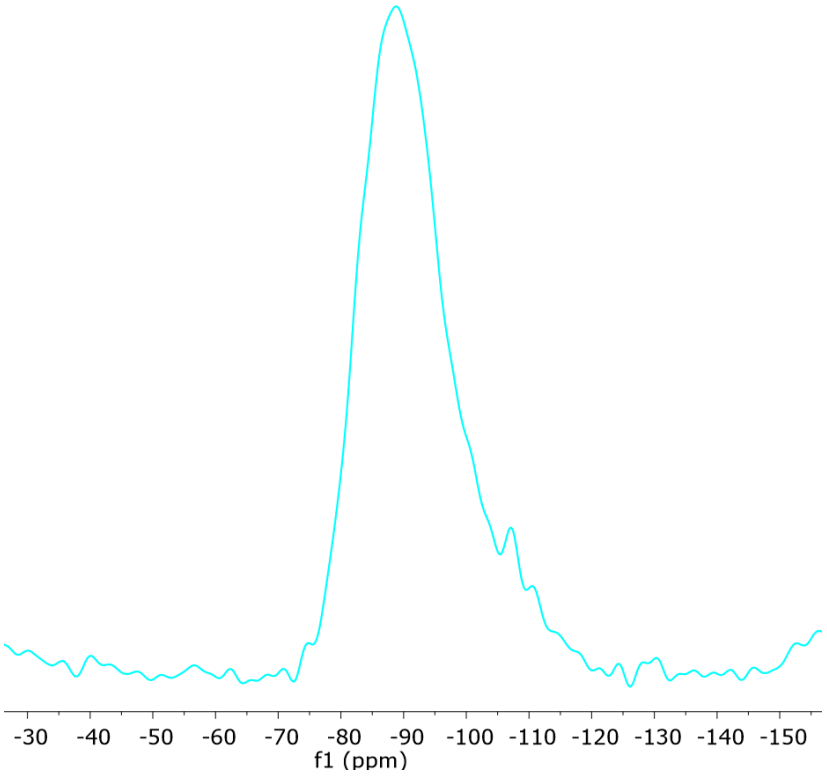

Fig.A7 ^{29}Si MAS-NMR spectra of 50GP0-50RC.

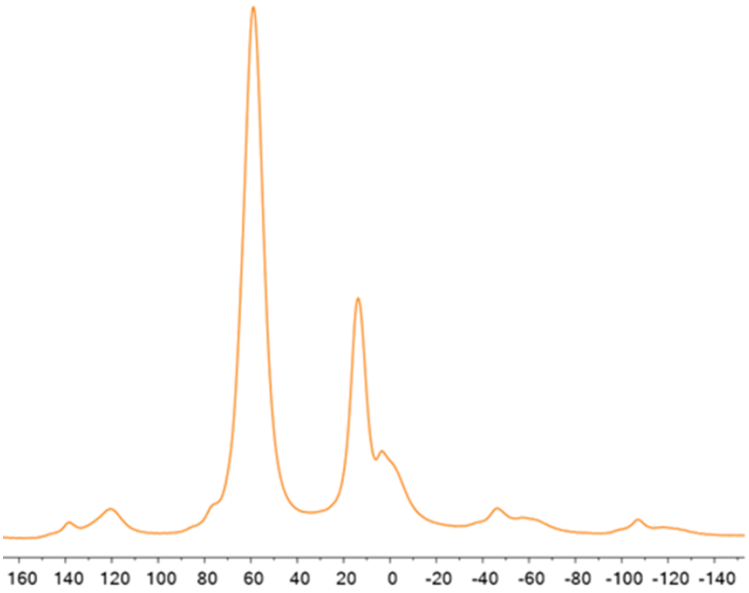

Fig.A8 ^{27}Al MAS-NMR spectra of 80GP0-20RC.

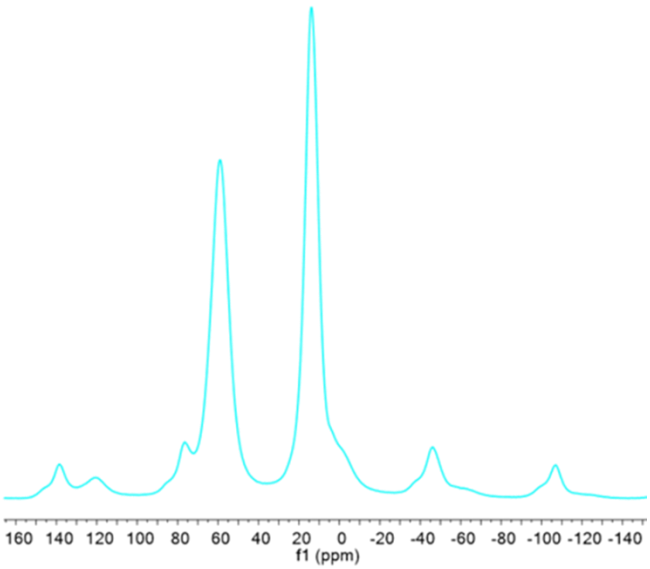

Fig.A9 ^{27}Al MAS-NMR spectra of 50GP0-50RC.

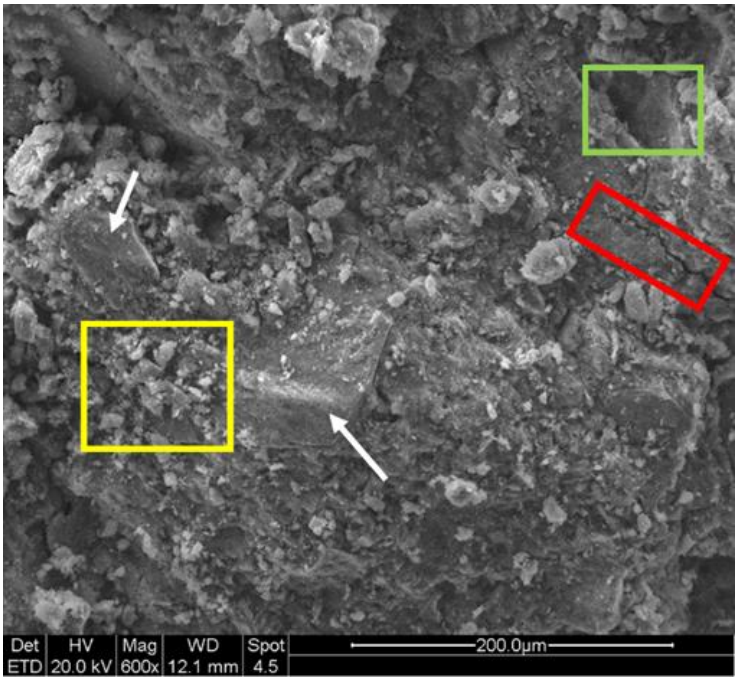

Fig.A10 Scanning electron microscopy images taken at low magnification (600x) of 70GP0-30RC.

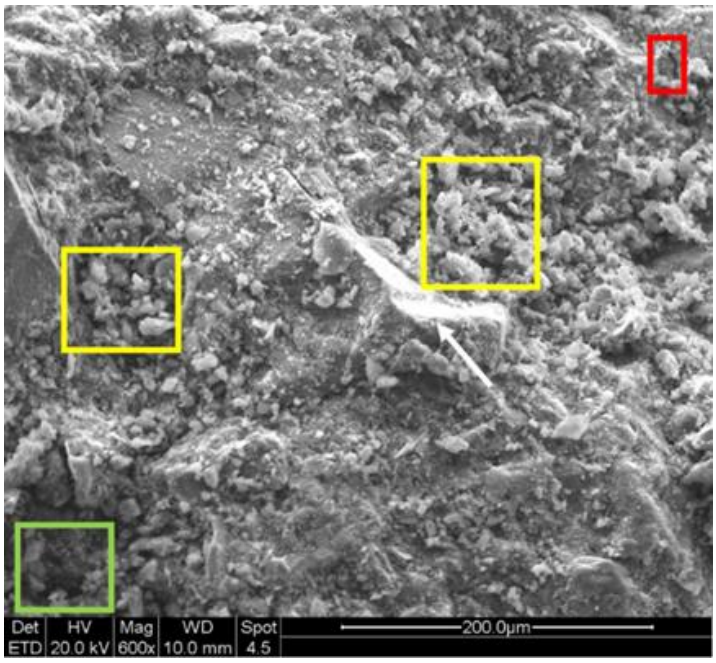

Fig.A11 Scanning electron microscopy images taken at low magnification (600x) of 60GP0-40RC.

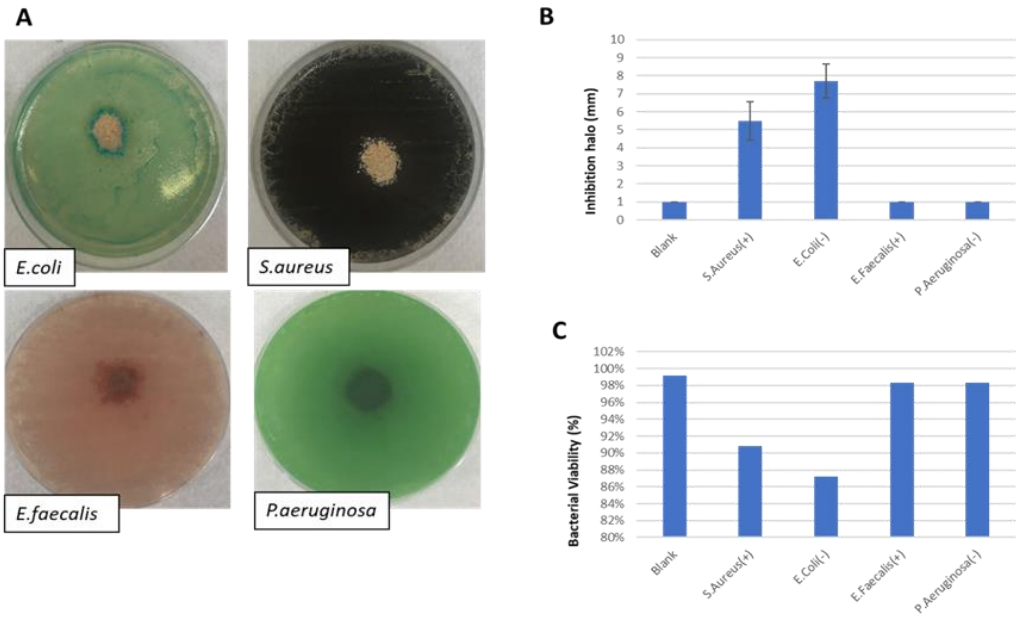

Fig.A12 Antibacterial properties of 70GP0-30RC.

List of original publications

Dal Poggetto G.*, D'Angelo A., Catauro M., Barbieri L. and Leonelli C. Recycling of Recycled corundum Abrasive Powder in MK-based geopolymers, Polymers 2022, 14(11), 2173.

Dal Poggetto G.*, Kittisayarm, P., Pintasiri, S., Leonelli, C., Chaysuwan, D. Chemical and Mechanical Properties of Metakaolin-Based Geopolymers with Recycled corundum Powder Resulting from Erosion Testing, Polymers, 2022, 14(23), 5091.

Dal Poggetto G.*, Fortunato, M., Cardinale, A.M., Leonelli, C*. Thermal, chemical and mechanical characterization of recycled corundum powder in metakaolin-based geopolymer binder Applied Clay Science, 2023, 237, 106875.

Dal Poggetto G.*, Marchetti, R., Lancellotti, I., Leonelli, C., Barbieri, L. Waste Cork in Metakaolin–Geopolymer Matrix: Physico-Mechanical Characterization, Applied Sciences (Switzerland), 2023, 13(3), 1804.

Dal Poggetto G.*, Leonelli, C.*, Barbieri, L., Altimari, F. Investigation on the effect of inorganic acid attack on composite prepared with MK-based geopolymer and waste cork dust. Ceramics International 2024.

Dal Poggetto G., Leonelli, C., Spinella, A. Influence of silica anionic forms in clear sol precursors on metakaolin reticulation via ^{29}Si and ^{27}Al MAS-NMR and microstructural investigation. Under Review manuscript to Journal of Materials Science (January 2024).

Dal Poggetto G., Leonelli, C. Barbieri, L., Zambon A. Study on Long-Term Durability of Discarded Cork-based Composites. *Submitted Environmental Science and Pollution Research (February 2024).*